LEVEL

DEVELOPMENT OF A SELF POWERED VEHICLE DETECTOR

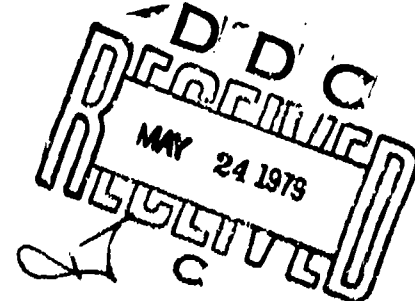BY J. F. SCARZELLO D. S. LENKO A. D. KRALL R. E. BROWN

RESEARCH AND TECHNOLOGY DEPARTMENT

OCTOBER 1978

D D C
RECEIVED
MAY 24 1979
C

NSWC

NAVAL SURFACE WEAPONS CENTER

Dahlgren, Virginia 22448 ● Silver Spring, Maryland 20910

79   05   2   007

UNCLASSIFIED

REPORT DOCUMENTATION PAGE		READ INSTRUCTIONS BEFORE COMPLETING FORM
1. REPORT NUMBER NSWC/WOL/TR-78-177	2. GOVT ACCESSION NO.	3. RECIPIENT'S CATALOG NUMBER
4. TITLE (and Subtitle) DEVELOPMENT OF A SELF POWERED VEHICLE DETECTOR		5. TYPE OF REPORT & PERIOD COVERED R&D, Nov 1976 - Sept 1978
		6. PERFORMING ORG. REPORT NUMBER
7. AUTHOR(s) J. F. Scarzello, D. S. Lenko, A. D. Krall R. E. Brown		8. CONTRACT OR GRANT NUMBER(s) FHWA/DOT Order No. 6-3-0180
9. PERFORMING ORGANIZATION NAME AND ADDRESS Naval Surface Weapons Center White Oak Silver Spring, Maryland 20910		10. PROGRAM ELEMENT, PROJECT, TASK AREA & WORK UNIT NUMBERS 0; 0; 0; WR43KA
11. CONTROLLING OFFICE NAME AND ADDRESS Final rept. Nov 76-Sep 78		12. REPORT DATE October 1978
		13. NUMBER OF PAGES 228
14. MONITORING AGENCY NAME & ADDRESS(if different from Controlling Office)		15. SECURITY CLASS. (of this report) UNCLASSIFIED
		15a. DECLASSIFICATION/DOWNGRADING SCHEDULE

16. DISTRIBUTION STATEMENT (of this Report)

Approved for public release; distribution unlimited.

17. DISTRIBUTION STATEMENT (of the abstract entered in Block 20, if different from Report)

18. SUPPLEMENTARY NOTES

This research was sponsored by the Federal Highway Administration, Office of Research, Traffic Systems Division, Washington, DC 20590

19. KEY WORDS (Continue on reverse side if necessary and identify by block number)

Vehicle Detection System, Magnetometer, Two-axis Magnetometer, Low Power RF Telemetry Link, Audio Tone Encoder/Decoder, Omnidirectional Microstrip Antenna, RF Oscillator, RF Transmitter, Battery/Solar Cell Tests Digital Nulling Loop, Voltage Controlled Crystal Oscillator

20. ABSTRACT (Continue on reverse side if necessary and identify by block number)

A battery operated motor vehicle detection system has been developed which detects a vehicle's magnetic signature, processes it and then transmits vehicle presence information from its roadway position to a nearby receiver control unit. The Self Powered Vehicle Detector (SPVD) is an advanced vehicle detector concept which requires minimum installation time and cost, little maintenance, and is capable of detecting vehicles on any standard roadway surface.

DD FORM
1 JAN 73 1473 EDITION OF 1 NOV 65 IS OBSOLETE
S/N 0102-LF-014-6601

UNCLASSIFIED

20. (Cont'd).

The SPVD system consists of two units, the roadway implanted sensor and a control unit which is located inside a traffic instrumentation enclosure less than 500 feet away. The SPVD sensor unit is placed in a standard roadway bore hole located in the center of the lane just beneath the surface. The estimated lifetime for a traffic flux of 20,000 vehicles/day is greater than one year. Twenty SPVD systems have been fabricated for FHWA evaluation.

PREFACE

NSWC/WOL TR 78-177

This final report describes all the research, development, design and fabrication work done by the Naval Surface Weapons Center on the Federal Highway Administration Program, "Development of the Self Powered Vehicle Detector," Intra-Government Order No. 6-3-0180 from November 1976 to September 1978. Twenty Self Powered Vehicle Detection (SPVD) Systems have been built, tested and delivered to the Federal Highway Administration on 1 September 1978. The SPVD System appears to meet or exceed all program design goals based on extensive simulated laboratory and roadway tests. All required program documentation is provided herein.

Paul R. Wessel

PAUL R. WESSEL
By direction

CONTENTS

LIST OF FIGURES

(Figures Continued)

(Figures Continued)

(Figures Continued)

(Figures Continued)

LIST OF TABLES

INTRODUCTION

The purpose of the Self Powered Vehicle Detector (SPVD) is to reliably detect vehicles passing through a desired surveillance zone (traffic lane) in all environments associated with its fixed location beneath the roadway. The detected vehicle magnetic signature information is then telemetered via an RF link to a roadside traffic instrumentation enclosure for the purpose of vehicle counting or traffic control. Desirea SPVD sensor unit operational life is to be greater than one year utilizing its self-contained batteries.

The Naval Surface Weapons Center, White Oak Laboratory, was introduced to the Federal Highway Administration's vehicle detection problem in August 1975 when personnel of both facilities met to discuss the Self Powered Vehicle Detector Concept (SPVD) and its initial hardware. During Phase I of FHWA program, done under outside contract as documented in Reference (1), three engineering prototypes were developed which did not meet several of desired system concept design goals. However, the Phase I effort demonstrated that if state-of-the-art improvements could be made in the magnetic sensor and the RF telemetry link components, such a system would be possible. In January 1976, a modest program was established at NSWC/WOL to optimize the SPVDs' magnetic sensor. The program's scope had these objectives: (a) determine the suitability of the low power two-axis Brown Magnetometer for the SPVD, (b) examination and optimization of the existing sensor described in Reference (1), and (c) briefly explore single and two-axis low-power magnetic gradiometers. These objectives were directed at solving the stopped vehicle detection problem in all anticipated roadway environments. Efforts on this

8

initial program (DOT #6-3-0063, January 1976 to June 1976) provided engineering data and the design approach for the sensor module.[2,3]

In November 1976, a research and development program was established at NSWC/WOL to complete the necessary component research on the magnetic sensor and sensor electronics, battery evaluation and the design testing and fabrication of twenty SPVD magnetic sensor modules and housings. The program was subsequently modified to include additional component research in a newly invented omnidirectional microstrip antenna, RF oscillator and transmitter, telemetry link encoder and decoder, and development problems and associated underestimates incurred during the fabrication of the twenty SPVD systems.

This final report covers all SPVD component research and development and is divided into seven major areas of investigation: (1) magnetometer development, (2) sensor system electronics development, (3) telemetry link encoder/decoder development, (4) telemetry link oscillator/transmitter development, (5) antenna development, (6) telemetry receiver and battery evaluations, and (7) mechanical component design and development.

In addition to the above documentation, detailed drawings, diagrams, test procedures and engineering data are provided which should be adequate to reproduce the prototype SPVDs. A hard-wired version of the SPVD electronics has also been fabricated and is described. In the Discussion section, several system improvements and options are discussed which should be considered for the development or procurement of next generation SPVD Systems.

Additional documentation generated by this program or related to it may be found in References (4), (5), (6), (7), and (8).

Key NSWC personnel actively associated with the SPVD program are: John F. Scarzello, Principal Investigator/Research Engineer; Daniel S. Lenko, Principal

Electronics Engineer, Telemetry Link Components; Albert D. Krall, Research
Physicist, Antenna Research; Dr. Robert E. Brown, Research Physicist, Magnetometer
Development; Wayne R. Grine, Mechanical Design and Fabrication; Chester W. Purves,
Mechanical Design and Fabrication; Albert M. Syeles, Antenna Design and Fabrication;
and George W. Usher, Jr., Electronics Design.

I. SPVD SYSTEM DESCRIPTION

This section consists of two parts, a general system information summary and operating instructions and then a brief system functional description.

General:

The Self Powered Vehicle Detector (SPVD) system is a motor vehicle detection system that detects a vehicle's presence by measuring its magnetic field beneath the roadway surface. A radio frequency (RF) telemetry transmitter conveys the roadway implanted SPVD's vehicle presence and device status information to a road-side control unit, which may be interfaced to other traffic control systems. Figure 1 is a drawing of the SPVD system concept for a typical traffic controlled intersection.

The SPVD system consists of two components, the SPVD (sensor unit) and the SPVD Control Unit shown in Figure 2. The SPVD sensor unit is a 4 1/2" diameter, 15" long cylinder which is implanted in the center of a traffic lane by boring a 4 1/2" diameter hole (minimum) using a standard core sample drill. When a vehicle passes directory over the implated SPVD sensor unit, it transmits a coded leading and trailing edge pulse which is received and decoded by the SPVD control unit located in a nearby (500 feet) existing weatherproof traffic instrumentation enclosure. An external receiving antenna is required for the control unit and may be mounted either on or near the traffic instrumentation enclosure and connected to it by a coaxial cable. The SPVD sensor unit is implanted approximately 1" below the roadway surface and oriented with case arrows pointing in the direction of traffic flow. The vehicle presence detection time of the SPVD sensor unit is set internally to approximately 15 minutes. After this time the SPVD rezero's its sensor digital nulling loops and again becomes active.

The SPVD control unit (Figure 2) contains a standby battery which can operate the SPVD control unit with interface relays for 24 hours when fully charged. The
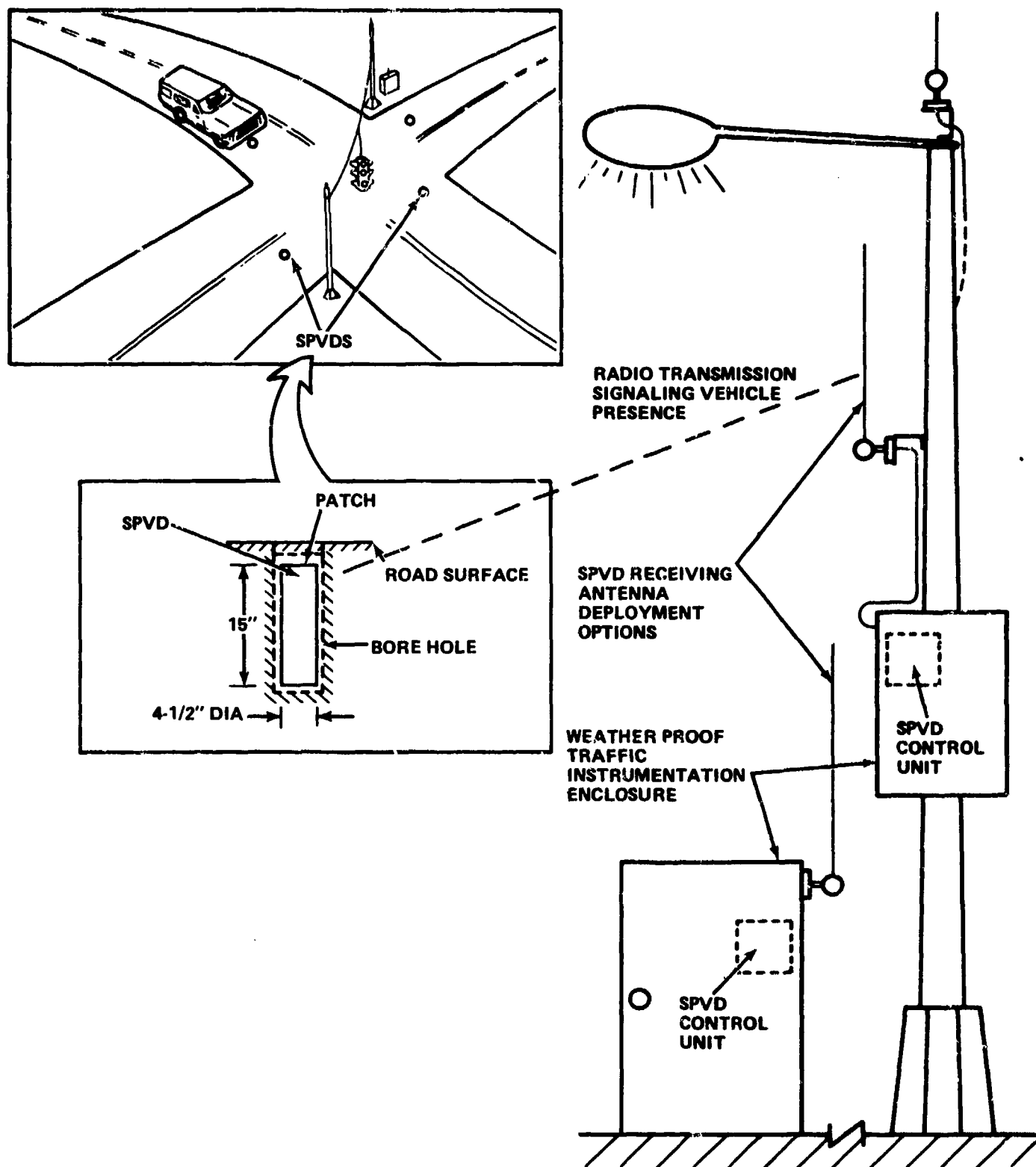
FIGURE 1. SPVD SYSTEM CONCEPT
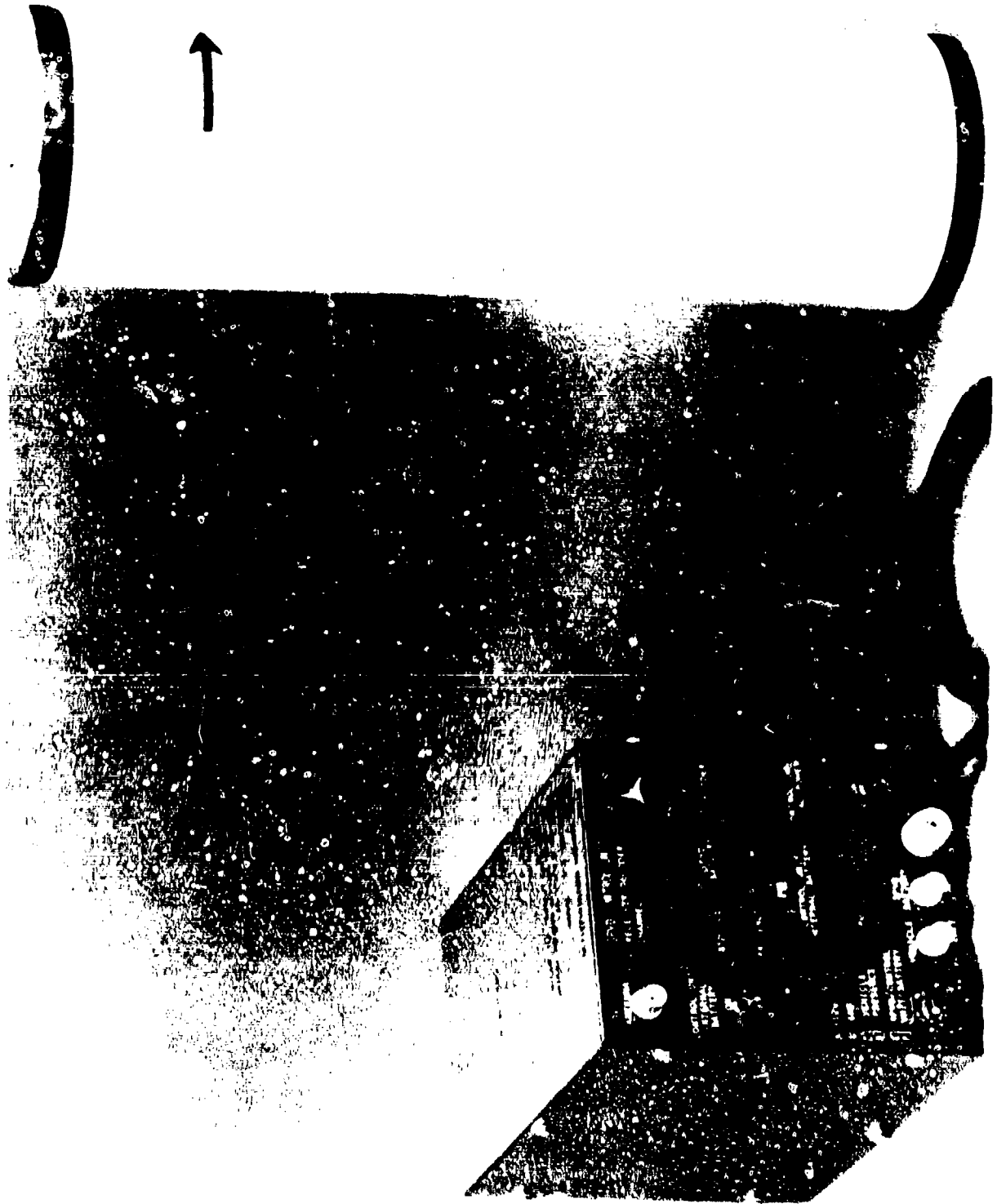
FIGURE 2. THE SPVD SYSTEM COMPONENTS.

SPVD sensor unit has approximately a two-year operational life before battery replacement is required. Low SPVD sensor battery is indicated by a distinct coded radio signal and will activate the undervoltage light and relay in the SPVD control unit.

Detection of most types of motor vehicles passing over the SPVD sensor with nearly zero miss and false alarm rates is anticipated except for motorcycles, especially 350cc displacement and under.

A six pin interface connector is supplied and may be used to activate other traffic control instrumentation. The relay contacts are normally open, i.e., for no vehicle presence or normal voltage conditions. BNC connector outputs are for testing and high input impedance devices only.

SPVD system component specifications are tabulated in Table I.

The inspiration behind the SPVD development effort is two-fold; reducing the high cost of installing or repairing hardwired automatic traffic control sensors in modern highways and streets by using an easily implanted sensor; and to improve the SPVD design by developing improved components, specifically to increase vehicle presence time and improve the telemetry link.

The SPVD system is functionally divided into two sections, the magnetic sensor module and the telemetry link. The telemetry link consists of the SPVD sensor units' transmitter/encoder module and omnidirectional microstrip antenna/housing, and the control unit which includes the receiving antenna, receiver module, decoder and interface electronics.

Figure 3 is a block diagram of the magnetic sensor module. A low power two-axis magnetometer measures the vertical and horizontal (parallel to road direction) components of the vehicle's magnetic field. The resulting magnetic field with respect to vehicle position over the sensor, is processed by determining the

14

Table 1. SPVD System Specifications

SPVD (Sensor Unit)

DETECTION RANGE SPEED: 0 to 128 KM/HR (0 to 80 MPH) 35.6 M/SEC. (117 FT/SEC)

DETECTION OUTPUT: Positive output vehicle presence

DETECTION RANGE: (Lateral from lane centerline)

Cars: ±1.2M (±4 FT)

Trucks: ±1.2M (±4 FT)

Buses: ±1.2M (±4 FT)

Motorcycles: ±.6M (±2 FT)

OPERATING TEMPERATURE: -34° to + 76°C(-30°F to +170°F)

MAXIMUM VEHICLE COUNTS: 20,000/Day

OPERATING LIFETIME: Greater than 1 Year (2 Years Estimated)

DIMENSION: 11.43cm (4½") DIA x 38.1cm(15") LONG (Sensor)

SPVD CONTROL UNIT

SIZE: 5" x 6" x 9"

POWER REQUIREMENTS: 115 Volt 60Hz

INTERFACE: MS-3116E-10-6P Six Pin Connector (Supplied); Vehicle Presence
Pins C and D Normally Open, i.e., No Vehicle Present; Undervoltage
Pins E and F, Normally Open Indicates Normal Condition.

ANTENNA: Requires custom length of RG-58C/U cable connecting the supplied
quarter wave whip antenna and antenna input BNC.

FUSE: 3A-250V Type FO Cartridge Fuse

STANDBY BATTERY: GEL CELL GC-1245-1, 12 Volt 4.5 A.hr. Operates unit for
minimum of 24 hours when fully charged.
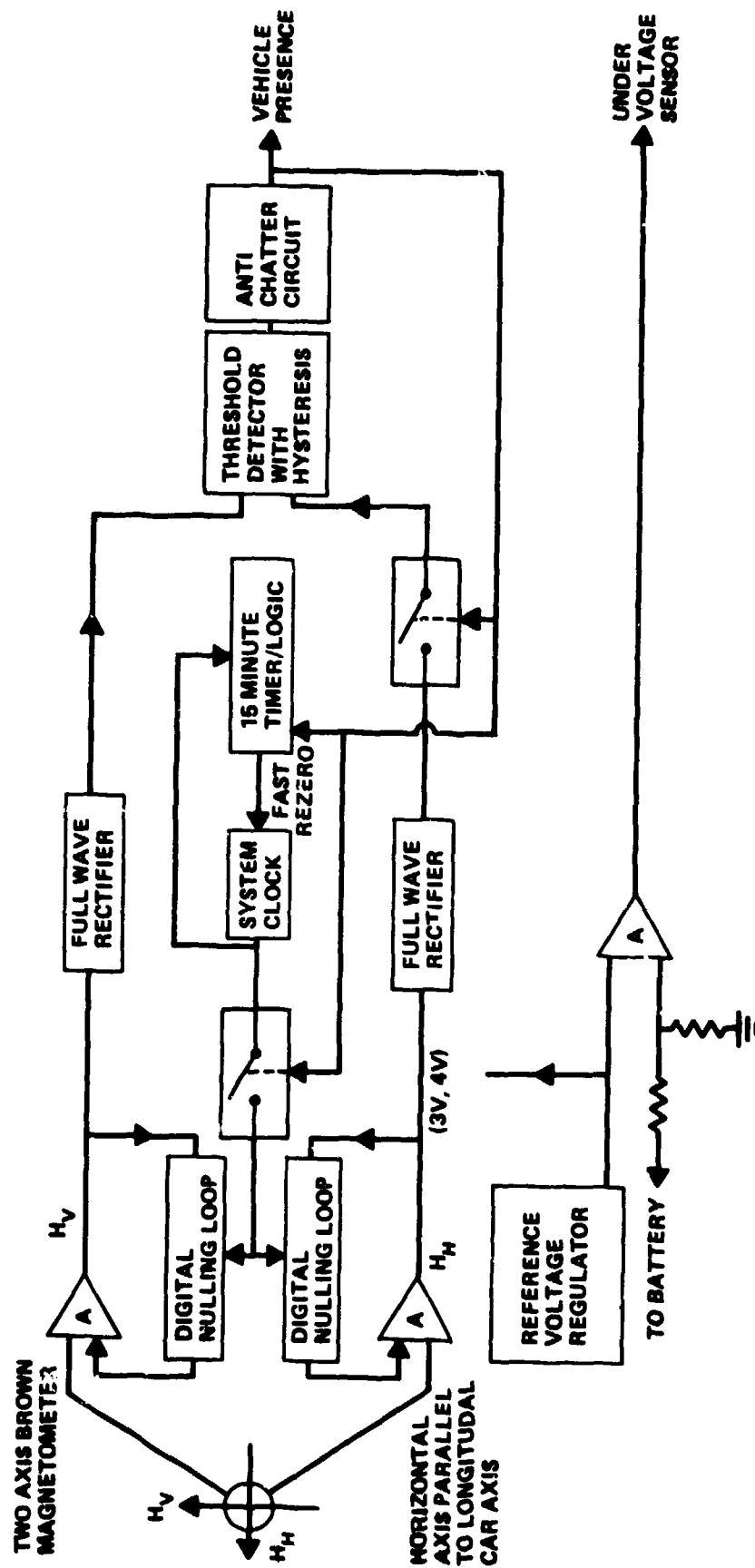
FIGURE 3. SPVD MAGNETIC SENSOR MODULE

vertical signal amplitude and deciding if it is sufficient to be a vehicle rather than background noise.

The extremely low power required of the magnetometer transducer (120 μ watts) has forced some system tradeoffs which necessitate electronics stabilization circuitry to increase magnetometer performance with respect to temperature and the resulting DC offset drift. Two digital nulling loops are required to null out the magnetometer offset with respect to time and temperature. There is much thermal inertia in the sensor module after the unit is implanted which produces gradual temperature changes despite the rate of ambient temperature change. The digital nulling loop electronics facilitate performing certain logic functions, specifically implementing the 15 minute vehicle presence and reset functions. The reset function occurs when a vehicle is stalled over the sensor for longer than 15 minutes, i.e., becomes operational after that time.

The basic logic is very similar to that developed in the Phase I effort[1]. The only major change was to reduce the threshold sensitivity in order to detect a variety of small vehicle types. Although several vehicle signature measurements were made during prototype evaluation, comprehensive measurements are beyond the program's scope and resources. A detailed explanation of sensor module functions is found in the sensor module section.

The SPVD RF telemetry link block diagram is illustrated in Figure 4. The SPVD sensor unit contains a transmitter/encoder module and omnidirectional microstrip antenna/housing which transmits 100mw leading and trailing edge transmission signals when the sensor module detects a vehicle presence. Within 500 feet of the roadway implanted SPVD sensor is a receiving antenna and control unit. The SPVD transmitted signal is received by a FM receiver and then signal conditioned for the decoder electronics. The decoder electronics detects the encoded tone code,

17
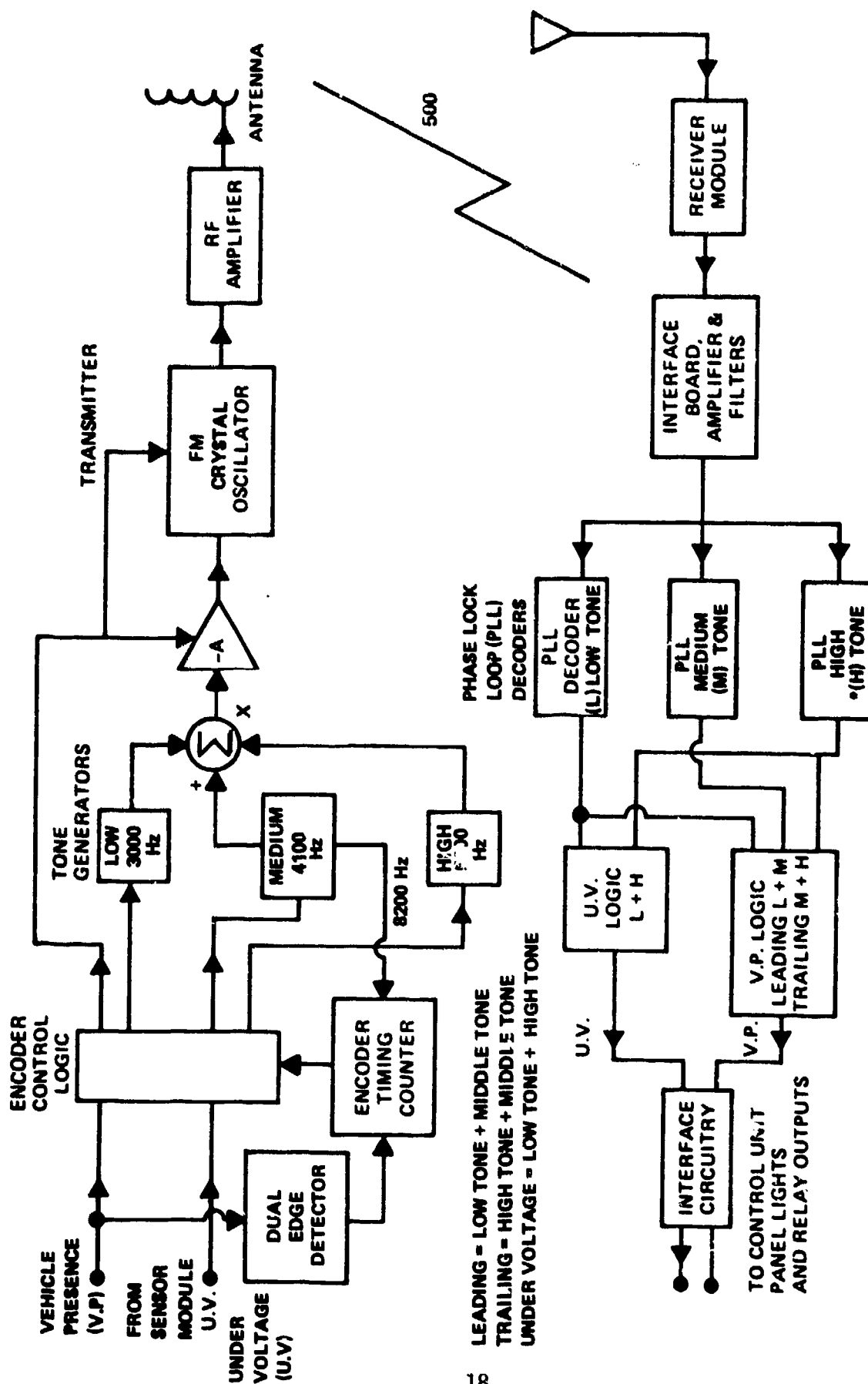
FIGURE 4. SPVD TELEMETRY LINK BLOCK DIAGRAM

LEADING = LOW TONE + MIDDLE TONE
TRAILING = HIGH TONE + MIDDLE TONE
UNDER VOLTAGE = LOW TONE + HIGH TONE

that is recognizes a combination of two tones, either a low and middle tone (leading edge), medium and high tones (trailing edge) or low and high tones (trailing edge/undervoltage condition in the SPVD). The following logic activates the interface circuitry to indicate the detected condition.

The entire SPVD sensor unit electronics consumes about 2 milliwatts continuously at 6.75 volts and with the 26 ampere-hour battery, a two year operational life is estimated based on detecting 20,000 vehicles per day. Even longer life is possible with improved lithium batteries only now becoming available.

All SPVD system design goals appear to be met, although survival in a variety of roadway environments is the crucial measure of SPVD performance. NSWC has operated a prototype unit for approximately one month in the "wet" roadway test hole and continuously operated the system electronics for over one year.

The system described in this report has been documented in the disclosure of Reference (8).

OPERATING INSTRUCTIONS

1. Turn on the SPVD control unit, either AC power or battery (see Figure 2).
Check internal battery condition by pushing front panel switch. If normal, the
meter needle will be in the center or to the right side of the scale (see Figure 2).
If to the left, charge the internal battery, i.e., plug into 115V 60 Hz AC and turn
both AC and control unit internal battery switches to on. Recheck after 24 hours.

2. Turn on the SPVD (see Figure 5). Remove the top cap with a 3" spanner
wrench. Plug the red and black wires into the appropriate terminals of the black
battery housing. Then put tape over the terminals to insulate them (supplied with
the SPVD). Reinsert the electronics/battery housing into the antenna/housing and
line up the arrows. Retighten the cap after cleaning the O-ring sealing surface.

3. After the presence time (≈ 15 minutes) check the system by moving a large
wrench or pliers over the SPVD sensor. If a vehicle presence is detected, shut
off the SPVD control unit and prepare to travel to implant site.

4. Items required for SPVD system installation:

    a. SPVD and SPVD Control Unit

    b. SPVD receiving antenna with appropriate length of RG-58 cable

    c. Misc. brackets for mounting the control box

    d. 4 1/2" dia. min. (6" max) core drill ≈ 17" long

    e. Output interface plug wired for appropriate instrumentation (see Figure 2
for pin out)

5. Drill core hole for the SPVD in the center of desired traffic lane. Use
4 1/2" dia. minimum size core drill bit (maximum size 6") approximately 17" deep.
(See Figure 6).

6. Insert SPVD with arrows in direction of traffic flow. (See Figure 5).
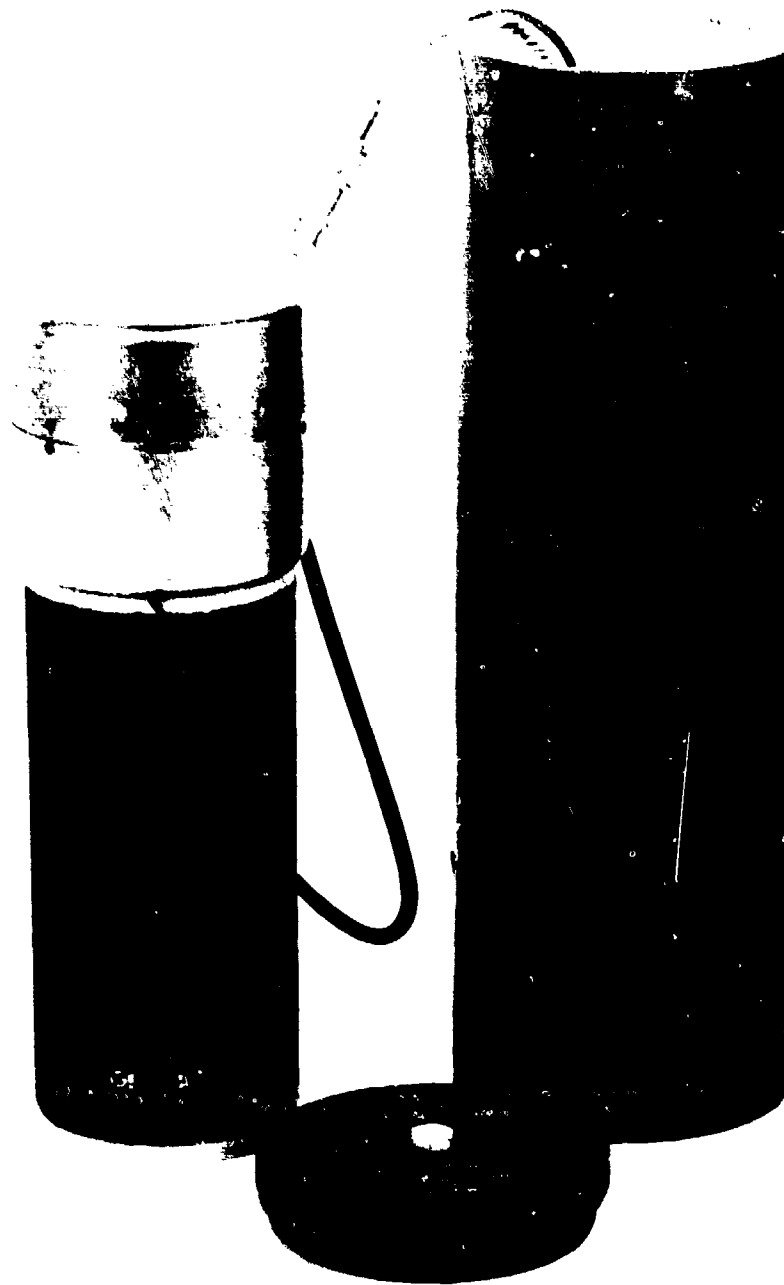
FIGURE 5. SPVD UNIT ELECTRONICS REMOVED FROM HOUSING.

IMPLANT DIRECTIONS:
- DRILL CORE HOLE (4-1/2" DIA MIN) IN PAVEMENT ≈17" DEEP, IN THE CENTER OF THE TRAFFIC LANE
- INSERT SPVD WITH ARROW IN DIRECTION OF TRAFFIC FLOW (1" BELOW ROAD SURFACE)
- CHECK OPERATION AND COVER WITH HOT PATCH

TRAFFIC FLOW

1"

15-1/2"

SPVD

9" PAVEMENT

GRAVEL

4-1/2"

EARTH
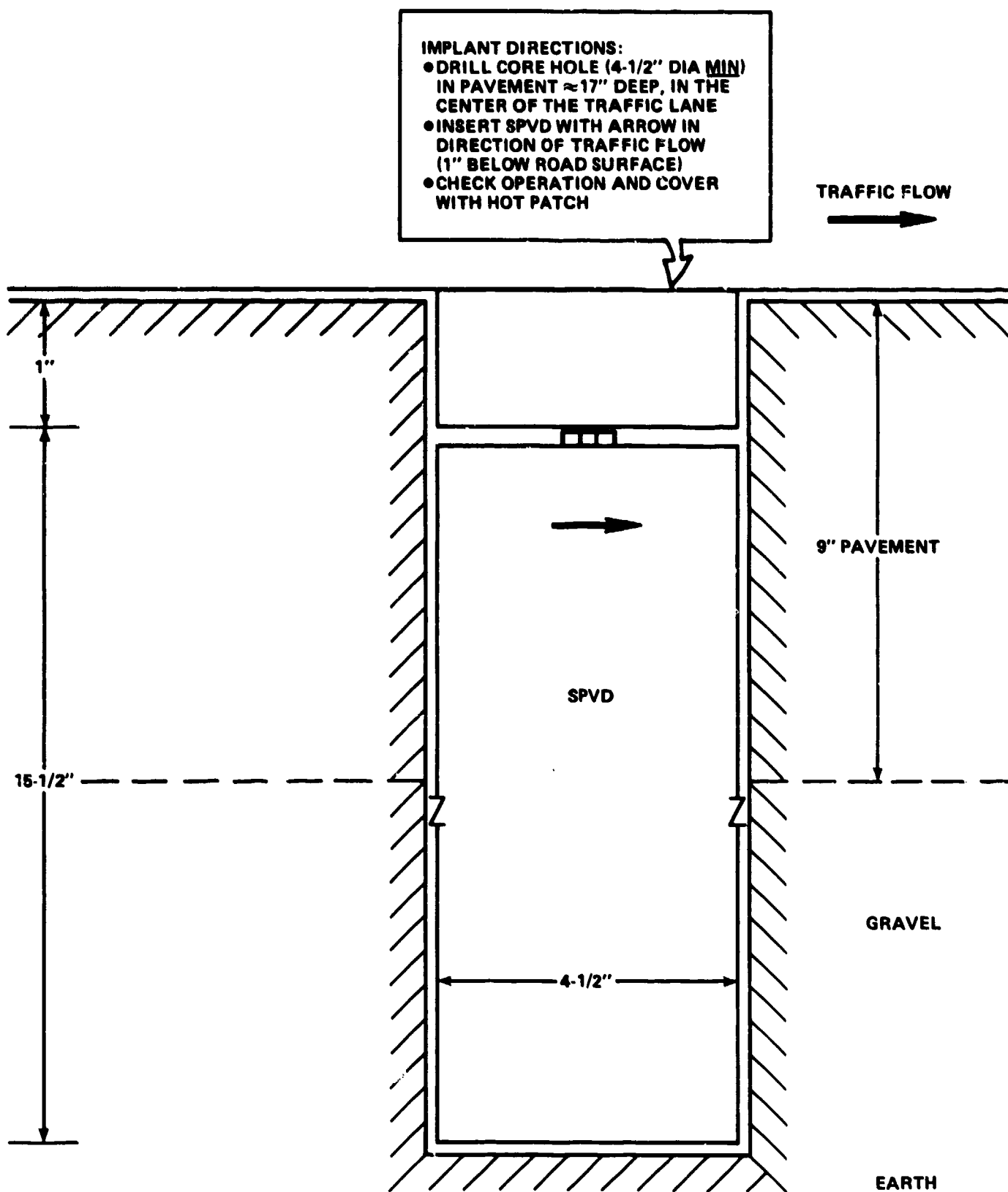
FIGURE 6. DRAWING OF SPVD ROADWAY IMPLANT

22

After insertion, check with SPVD control unit having either a short (2' long) wire antenna (Figure 7) or with the supplied receiving antenna. Move a magnet or large wrench over it to check system operation.

7. Space SPVD so it is about 1" below the road surface and cover with hot patch.

8. Check unit operation with a vehicle.

9. To remove the SPVD from the roadway, remove the hot patch with a hand chisel. Grab the nylon bolt and pull up with pliers. If the unit does not move, insert a 3" long 3/8"-16 steel bolt and pull straight up.

10. The undervoltage light on the SPVD control unit indicates the condition of the battery in the SPVD. Remove the SPVD only if it stays on after several vehicles have passed.

11. Install the receiving antenna either on the traffic control box or on a closeby lamp post. The spring mount is not required for installation on a traffic control box. With a simple bracket it may be mounted on a pole and soldered to an appropriate length of RG-58 cable to the SPVD control unit antenna input BNC connector. (See Figure 1). Installation of the receiving antenna and location of the SPVD will be quite important to system performance. Therefore it is suggested that several antenna locations be tried for optimum location before fabricating an antenna bracket.

12. To replace SPVD batteries, refer to the battery housing mechanical design section of this report.

FIGURE 7. PHOTOGRAPH OF SPVD IMPLANT IN NSWC "WET" HOLE.

II. DEVELOPMENT OF THE SPVD MAGNETOMETER SENSOR

Selection of a magnetic sensor proceeded through three stages: (1) evaluation of the Honeywell sensor; (2) modification of a pulse-driven fluxgate sensor previously used in Navy intrusion detectors; (3) development of a new pulse-driven fluxgate sensor optimized for the specific noise-sensitivity-cost-power requirements of the SPVD. The first two stages in the selection process have been reported upon previously[2,3]. Briefly the Honeywell sensor was found to be deficient in stability and the modified intrusion-detector sensor consumed too much power.

A properly designed ring-core fluxgate magnetometer has many advantages, including the power saving feature of measuring both the vertical and horizontal vehicle signal with a single sensor. The main deficiency in our existing design was a power demand considerably higher than desired. This power requirement is partially a design limitation and partially linked to the very low noise performance of the sensor, which was necessary for its intrusion-detector applications. In the SPVD the sensor noise may be an order of magnitude larger, and relaxation of this specification allows a re-examination of the design criteria previously imposed on our fluxgate sensor development efforts.

Fluxgate magnetometers in general require that electrical current be supplied periodically to a winding to magnetically saturate one or more magnetic cores. The presence of an applied magnetic field such as earth's field or the field of a magnetic body like a motorized vehicle is detected by an extra signal produced on core windings as the magnetic material of the core cycles in and out of saturation and exhibits non-linear magnetic permeability. A certain energy E must be supplied in each cycle to bring about saturation of the magnetic material. Material volume and other material parameters as well as core geometry and drive circuit efficiency

25

control the magnitude of this energy. Expenditure of energy E permits one sample of the ambient magnetic field to be taken and a numerical value assigned to it through a calibration procedure. This numerical value varies from cycle to cycle because of fluctuations in the magnetic material parameters and in the circuitry supplying the saturating drive current. If n samples per second are taken and averaged, a more stable value for the field measurement is obtained in some desired bandwidth. For a specified bandwidth and field measurement stability (noise) some power nE must be continuously expended to operate the fluxgate magnetometer. For the value of nE to be a minimum it is important to select an appropriate magnetic core and to optimize drive circuitry efficiency and stability. It is also necessary for feasible design realization to provide means to control selection of n and E independently.

We have found that a simple magnetically-coupled pulse generating circuit (Figure 8) is a stable and efficient current source for driving fluxgate magnetometers. For low-noise performance this has always been operated in the "flyback" mode, i.e., the ON interval, during which the core saturates, is substantially longer than the OFF interval. Experience has led us to select a specific molypermalloy tape wound bobbin core as the magnetic element of simple fluxgate magnetometers. It appears to have material parameters and a geometry yielding a useful range of sensitivity-noise-power consumption combinations as other circuit components are varied. The selection of this magnetic core and an efficient pulse drive largely fixes E in the above analysis to a value of about one erg. Thus one may anticipate that power reduction can best be realized by decreasing n. This decrease in n is acceptable because of the higher noise specification of the SPVD sensor.
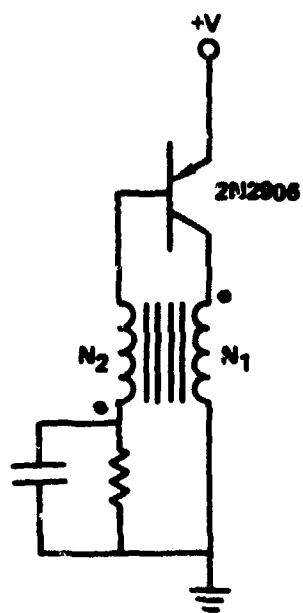
FIGURE 8. LOW-NOISE FLYBACK OSCILLATOR.
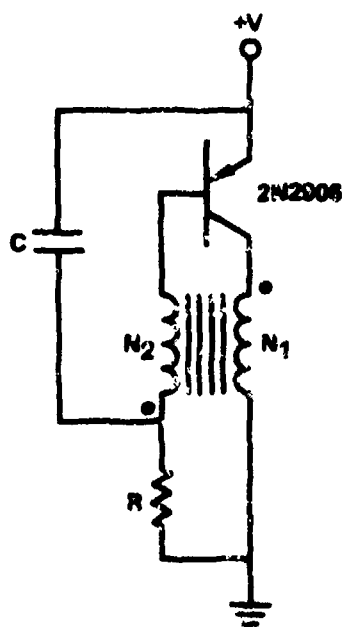
FIGURE 9. TYPICAL BLOCKING OSCILLATOR CIRCUIT.

For a given value of supply voltage V in Figure 8, the pulse repetition rate of the flyback oscillator, and thus n above, is largely determined by the inductance L_1 of the winding N_1. The initial attempt (stage 2) to produce a magnetometer consuming very low power consisted of efforts to increase L_1. Increasing L_1 increases both the length of the ON interval and the OFF interval while their ratio retains a similar value. Unfortunately the number of turns required for N_1 becomes quite large and forces inconvenient adjustments elsewhere in the magnetometer circuitry. The increased winding resistance and capacitance begin to degrade oscillator efficiency and stability. It was clear that another approach was necessary to lower the repetition rate of the pulse oscillator.

Features of a driving oscillator that were deemed necessary for fluxgate magnetometer operation at very low power expenditure are (1) a repetition rate controllable independent of core winding inductances and (2) a current-ON interval terminated only by core saturation. A desirable feature of the flyback oscillator of Figure 1 is its automatic achievement of condition 2 since core saturation generates the signal initiating turn-off. A potential candidate to replace it is the form of blocking oscillator shown in Figure 9. A blocking oscillator offers the possibility of controlling the length of the OFF interval independently of the magnetic core. But causing the ON interval termination to meet condition 2 requires a careful examination of the way the oscillator traverses its cycle.

When current starts to flow through N_1 in the circuit of Figure 9, a signal appears across N_2 of proper polarity to cause base current to flow charging C and driving the transistor into the saturation region. As the voltage across C approaches the voltage developed across N_2, base current ceases and the transistor turns off. It will turn on again after C discharges through the high resistance R. Thus the length of the OFF interval is controllable by the RC time constant,

and the ON interval length is determined by the duration of appreciable base current flow through C. Core saturation may participate in pulse termination, but in general it is achieved solely through the base-current "blocking" action of C. Calling L_2 the inductance of the N_2 winding, the L_2C circuit is generally configured to have a high Q in a blocking oscillator designed to produce fast rise-time pulses. Within the constraints imposed by magnetometer design it was found that appreciably lowering the Q of the L_2C circuit would lengthen the pulses until their termination could be controlled by the effect of core saturation on the signal developed on N_2. This was done by adding a resistor R' to the circuit (Figure 10). If I_s is the collector current required in N_1 to saturate the core, then core saturation is possible as long as base current $I_b > I_s/\beta$. Figure 11 shows the time behavior of I_b in the two cases R' = 0 and R' $\neq$ 0 to indicate how pulse length can be increased until the declining time rate of change of magnetic flux $d\phi/dt$ in the core at saturation can terminate it. For a particular minimum base current the achievable value of I_s is dependent on transistor β. Thus it is desirable to select R' to match each transistor.

Because R' has limited control in lengthening the base current pulse, it is necessary to keep L_1 low to limit the time required for core saturation. Referring to Figure 10 the circuit values for the SPVD sensor drive circuit are: N_1 = 400 turns, N_2 = 100 turns (#36 wire), R = 1 megohm, R' $\cong$ 300 ohms (selected to set average current at 30 microamps), C - .01 mfd, C' = 10 mfd, and V = 4 volts. Both N_1 and N_2 windings are equally distributed around the bobbin core. The capacitor C' keeps supply impedance low so that core saturation time is not lengthened by this quantity. The duration of the driving pulse is about 4 microseconds and the repetition frequency about 800 Hz with these circuit values. Specific magnetometer drive circuit waveforms are shown in Figures 12 and 13 for R' = 0 and R' $\approx$ 300 ohms.
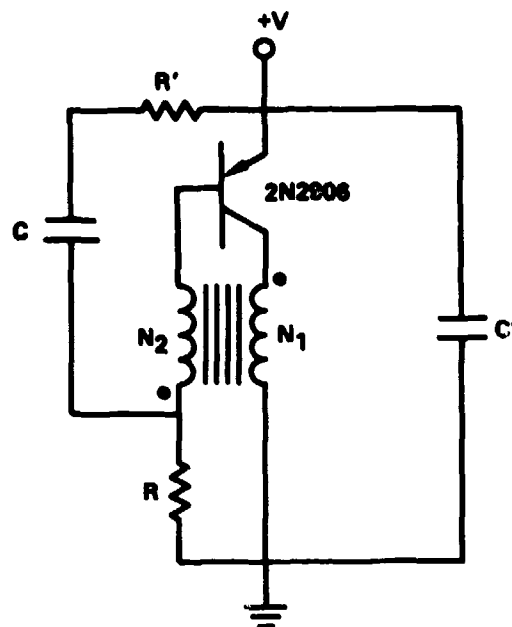
FIGURE 10.   MICRO–POWER PULSE CIRCUIT SUITABLE
FOR DRIVING FLUXGATE MAGNETOMETER.
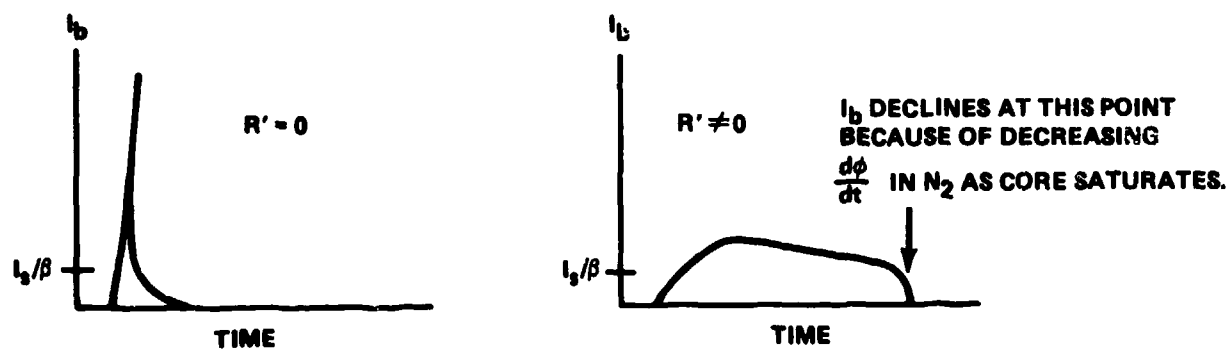
FIGURE 11.   BASE CURRENT DURING ON INTERVAL
OF CIRCUIT OF FIGURE 10.
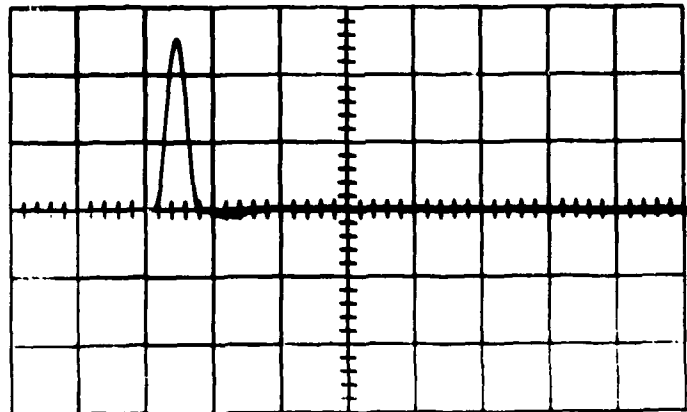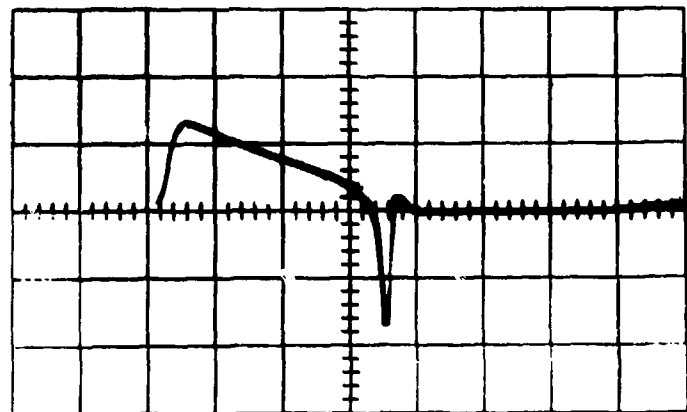
30

FIGURE 12. MAGNETOMETER TRANSISTOR BASE CURRENT
(R' = 0, R' ≠ 0).

Ic

R' = 0
20 ma/div.

1 μsec/div.

R' ≠ 0
20 ma/div.
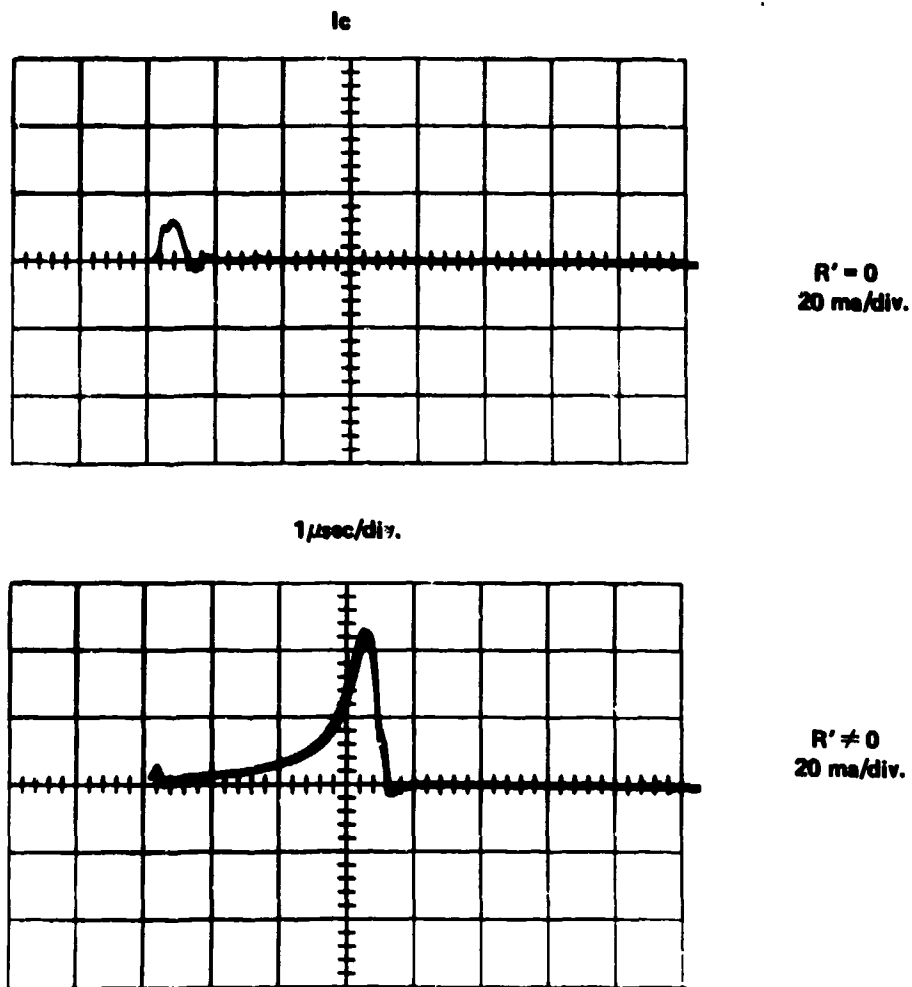
FIGURE 13.   MAGNETOMETER TRANSISTOR COLLECTOR
CURRENT (R' = 0, R' ≠ 0).

As in prior designs, detection of the ambient magnetic field dependent signal is done with additional windings on the core connected to a balanced pulse-average difference detector. Figure 14 shows how the difference between the averaged signals from windings on opposite sides of the ring-core is measured. The diodes have polarity to conduct during the drive current OFF period. The detection circuit is operated, in effect, by the energy stored in the magnetic core during the ON interval, producing high output with no additional power supply.

As core magnetization collapses, equal signals are generated in N_3 and N_4, for example, N_3 and N_4 being connected so that equal signals cancel in the detection circuit. If an external magnetic field is present parallel to the axes of N_3 and N_4, extra signals appear on these windings as the core permeability changes from near unity at saturation to a high value at remanence. These signals are added in the detection circuit. The R C combinations provide running pulse averages over times depending on the bandwidth desired. For this particular application R = 100K and C = 0.1 μfd for a 40 Hz bandwidth and output impedance of ~ 100K.

Another pair of windings, N_5 and N_6, with axes perpendiuclar to the N_3, N_4 axes yields measurement of the perpendicular magnetic field component at no additional expenditure of power. N_3, N_4, N_5, and N_6 are 200 turns of #36 wire distributed on 90° segments of the bobbin core. The circuit produces 0.7 volts per oersted of applied field with noise in a 1 Hz bandwidth varying from 5 to 30 gammas over the range of applied fields of ±1 oersted and at temperatures from -40°C to +70°C. The spectral amplitude of the noise is constant for frequencies below 40 Hz. Current drain is 30 microamperes from a 4 volt supply for the two axis magnetometer. Prior similar magnetometer designs have survived shock equivalent to unretarded air-drop. The noise amplitude cannot be accounted for solely by the decrease in $\underline{n}$. Evidently the pulse circuit of Figure 10 is somewhat inferior in stability to the circuit of

33
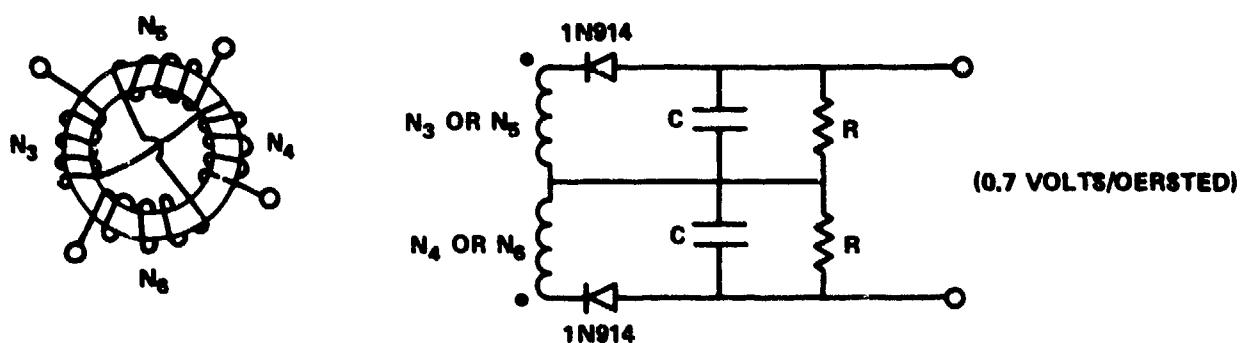
FIGURE 14. AMBIENT MAGNETIC FIELD DETECTOR (PULSE-AVERAGE DIFFERENCE DETECTOR).

Figure 8. Several moly-permalloy tape-wound cores are suitable for the magneto-
meter. They are Infinetics, Inc. (Wilmington, Delaware), Part No. S625C31-HC-2074C,
Arnold Engineering Company (Marengo, Illinois), Part Number 25538P-500-010 and
Magnetics, Inc. (Butler, PA), Part Number 80656-1/2D-025-1. Each manufacturer's
core and batch may require a different range of values of R' to obtain the proper
magnetometer operating point. Changing other component values is unlikely, but
may be necessary if other core types are used.

Figure 15 is a winding diagram for the complete core. Winding instructions
are listed below.

Magnetic Core Winding Instructions

1. Wrap cores with teflon tape ($\approx$4 mil thick) or mylar tape to insulate the
stainless steel bobbin from the windings.

2. Put the windings N_1, N_2, N_3, N_4, N_5 and N_6 in order, with N_1 first.

3. The winding sense must be maintained; that is, the core is not turned over
during winding or between windings.

4. Number 36 HF (Heavy Formvar) copper magnet wire is used on all windings.

5. Windings are layered on at about 400 turns per 360° layer. A winding or layer
requiring less density is distributed over the 360° winding space.

6. Numbered tags mark the beginning and end of each winding, the lowest number
tag for start of winding N_1 to the highest number tag marking the end lead of wind-
ing N_6.

7. There are six windings required: the first, N_1 = 400 turns is distributed around
the core 400 turns per layer for one layer. Leave a 5-inch length or wire on each
end of the winding and on the starting wire put tag #1. At the end of this winding
twist the wires together opposite the mark on the core where the winding was started,
and mark with tag #2.
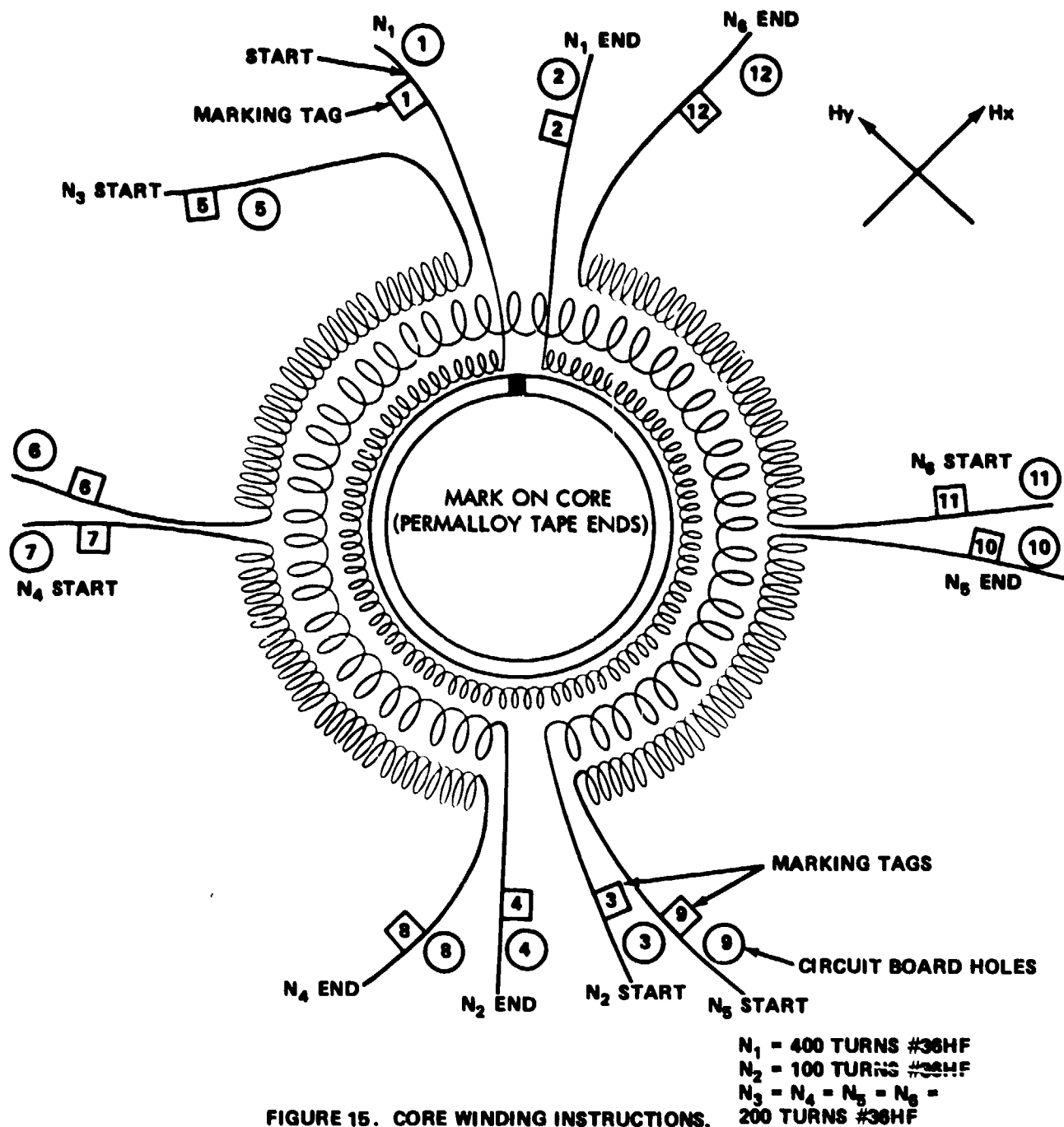
FIGURE 15. CORE WINDING INSTRUCTIONS.

N_1 = 400 TURNS #36HF
N_2 = 100 TURNS #36HF
N_3 = N_4 = N_5 = N_6 = 200 TURNS #36HF

8. The second winding N_2 = 100 turns is started 180° opposite the start of winding N_1. Mark the start lead (tag #3) and distribute the 100 turns evenly 360° and twist the wires together at the end of this winding. Mark the lead starting this winding with tag #3 and its end with tag #4

9. N_3 is a 200-turn winding distributed evenly over one quarter (90°) of the core on one quarter of the side between the termination of windings N_1 and N_2. Again mark the starting lead with a number tag (#5) and finish lead with tag #6.

10. N_4 is another 200-turn winding located on the other quarter of the core in an opposite 90° segment. Again, mark the start with a number tag (#7) and distribute the wire on the 90° segment. Mark the end of this winding with tag #8. Winding N_3 and N_5 together define one axis.

11. N_5 and N_6 are wound as N_3 and N_4 on the two remaining 90° core segments. Tag numbers, 9, 10, 11 and 12 mark the start and finish of winding N_5 and N_6 respectively. Figure 16 is a schematic diagram of the optimized SPVD Brown Magnetometer with a photograph of the sensor in Figure 17. Detailed circuit board layout is discussed in the mechanical section. Figures 16 and 17 depict two potentiometers (200K) used on the magnetometer's detection circuits. Since there will be variations in core winding and circuit component values, the DC offset with field can be modestly adjusted in this way without severely affecting sensor performance. The dynamic range of a typical magnetometer is shown in Figure 18. Other sensor specifications are tabulated in Table II. Reference 7 also describes the SFVD low power Brown magnetometer discussed herein.

To evaluate sensor performance a simple test set up is drawn in Figure 19. The magnetic shield contains internal Helmholtz coils that are used to apply a calibrated magnetic signal with a current source. The shield and coils must be large enough to surround a glass dewar which houses the magnetometer if temperature tests are desired. Hot air and cold nitrogen gas (from boiling liquid N_2) can be
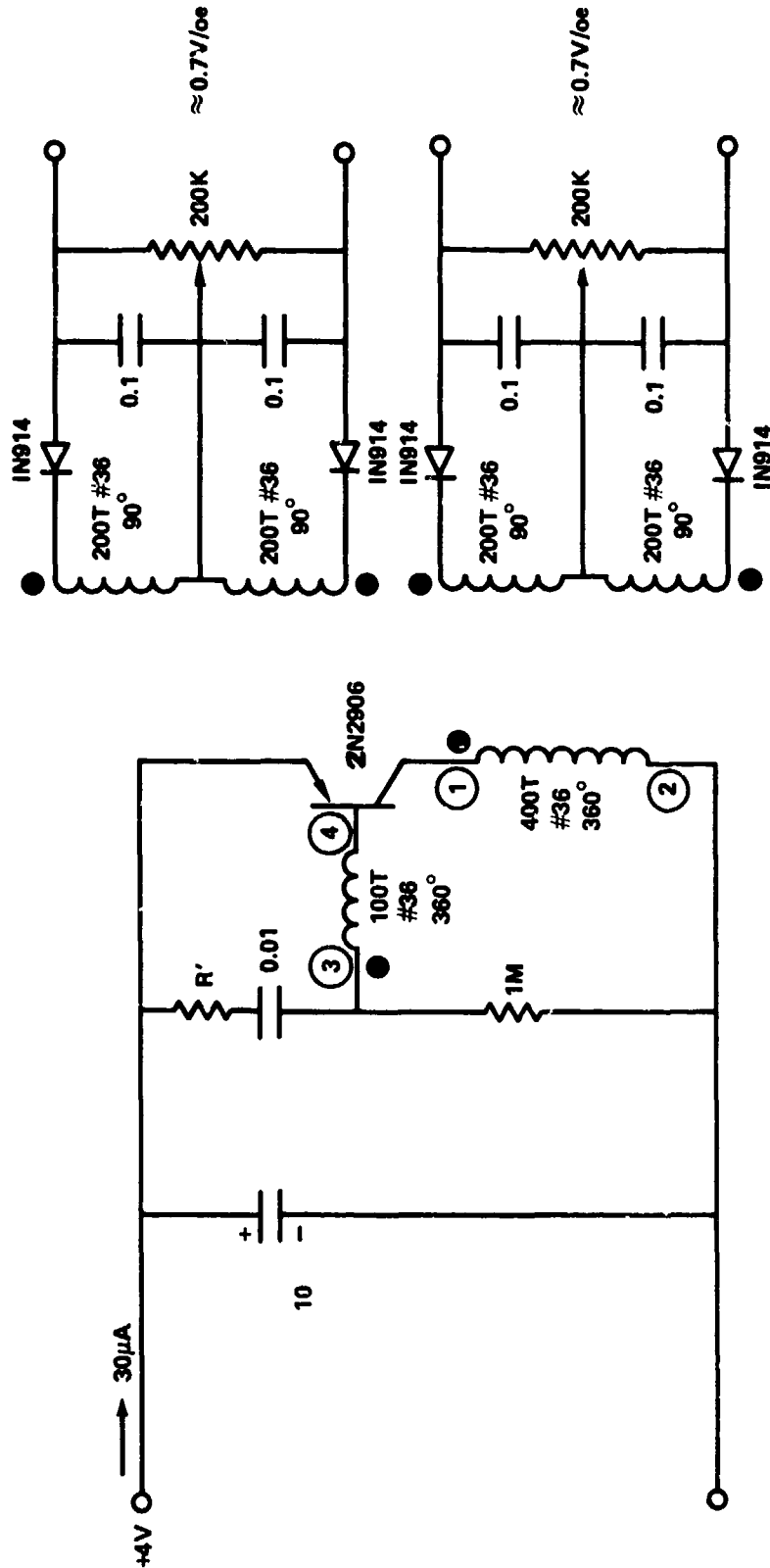
FIGURE 16.   LOW POWER BROWN MAGNETOMETER SCHEMATIC DIAGRAM.
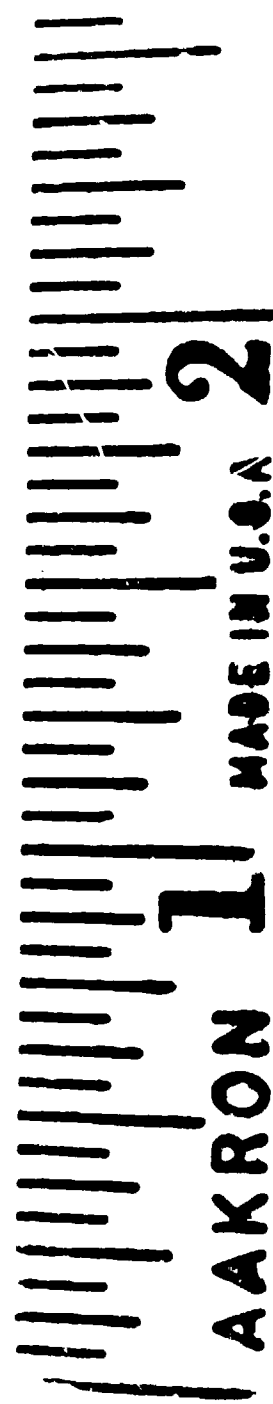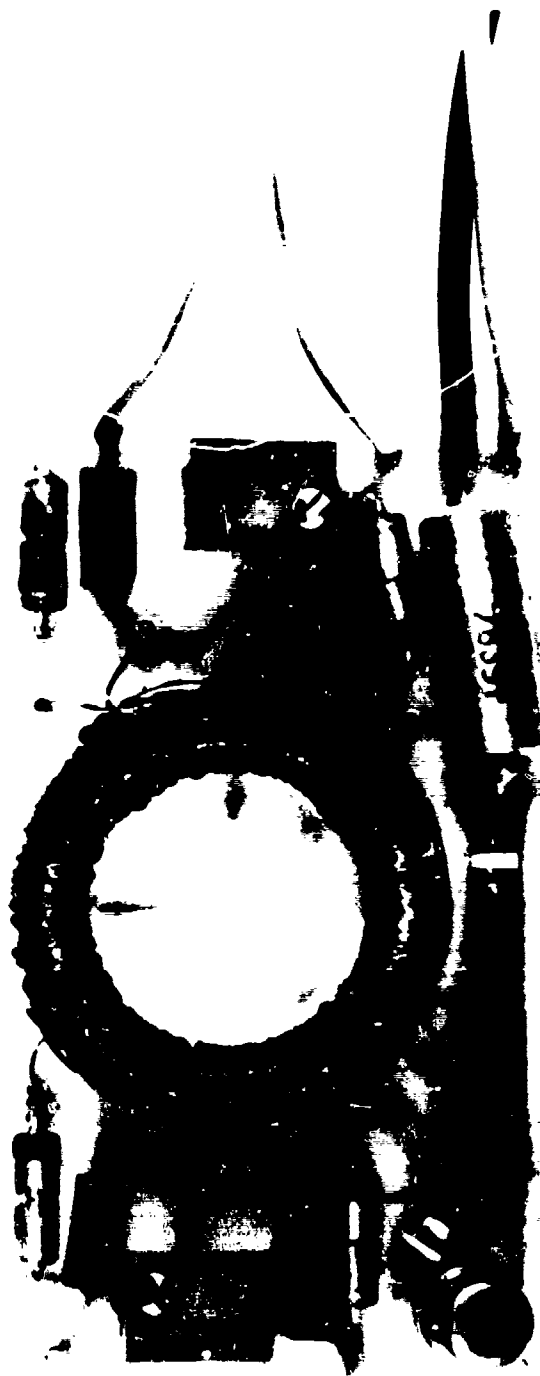
FIGURE 17. PHOTOGRAPH OF THE SPVD TWO AXIS BROWN MAGNETOMETER.
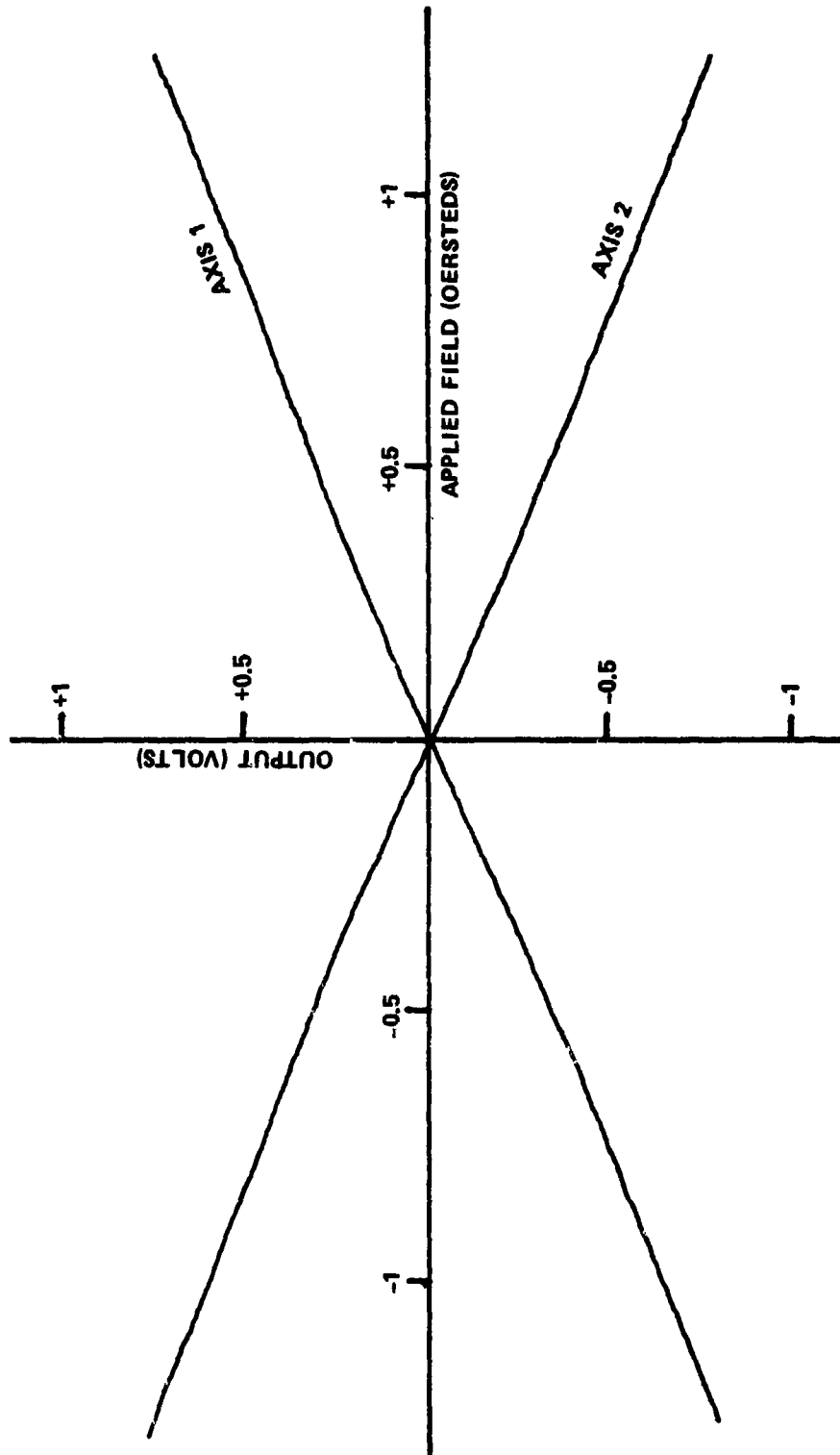
FIGURE 18. DYNAMIC RANGE PLOT OF TWO AXIS BROWN MAGNETOMETER

Table II. Low-Power Two-Axis Brown Magnetometer Specifications.

Sensitivity: ~ 7 microvolts/Nanotesla* (.7 volts/Oersted)

Noise: ≈ 5 to 30 nT p-p (1 Hz Bandwidth), 30 to 200 nTp-p (DC → 40 Hz)*

Dynamic Range: ± 1 x 10^{-4} tesla (± 1 Oersted)*

Linearity: ≈ 10% (± 1 x 10^{-4} tesla)*

Power Consumption: 120 microwatts @ 4 volts

Operating Temperature: -40°C to +70°C (-40°F → +158°F)

Size: 4.76 cm x 2.54 cm x 1.27 cm (1 7/8" x 1" x 1/2")

Weight: 15 grams (.53 oz)

*Same for both x and y axes.
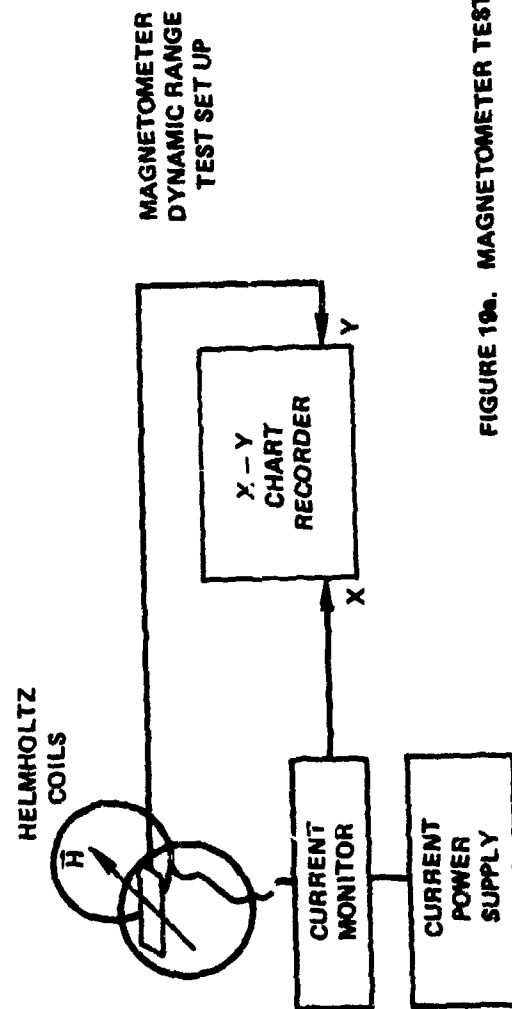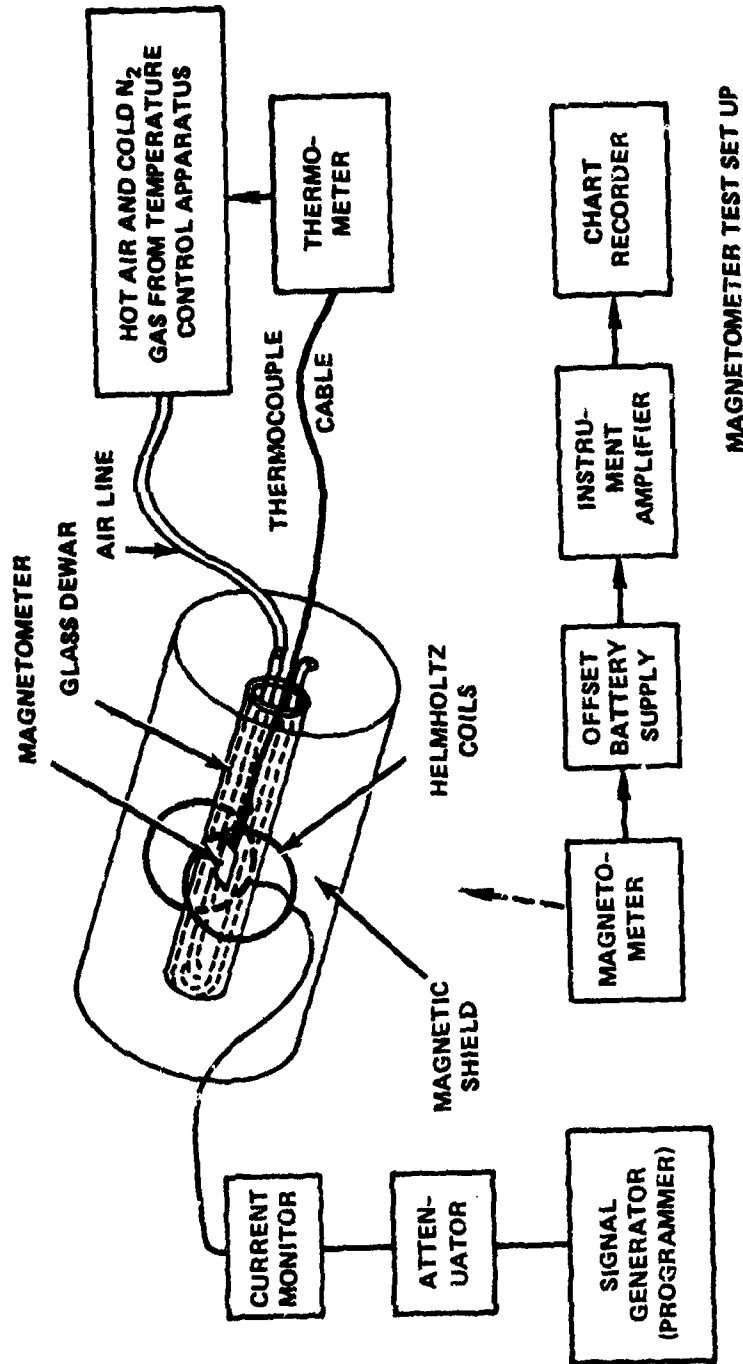
FIGURE 19a. MAGNETOMETER TEST SETUP.

used to heat and cool the sensor under test while monitoring the temperature using a thermocouple. The magnetometer output is amplified by an instrumentation amplifier (PAR-113) and connected to a strip chart recorder (Sanborn 320). Sensor offsets are biased out at the input with an isolated and stable battery power supply. Dynamic range can be obtained by attaching an x-y recorder to the sensor output varying the current supplied to a calibrated Helmholtz coil as shown.

III. SENSOR SYSTEM AND ELECTRONICS DEVELOPMENT

The SPVD sensor system module contains a two axis Brown magnetometer transducer and signal processing electronics necessary to meet the following technical requirements derived from the overall system specifications in Table I. They are:

- System Frequency Response: $0 \rightarrow 40$ Hz $(0 \rightarrow 80$ mph)

- System threshold for the magnetometer located 3" to 5" below the road surface: ≈ 5500 nT vertical field to produce a vehicle presence; below 3000 nT no vehicle presence; produces a positive output for a vehicle presence.

- Vehicle presence hold time: Internally set to ≈ 15 minutes

- Ambient field operating range: $\pm 1 \times 10^{-4}$ Tesla (± 1 oersted)

- Sensor Module Power Consumption: <2mw @ 6.75v

- Operating Temperature: $-40°C$ to $+76°C$ ($-40°F$ to $+170°F$)

- Must have EMI/RFI Immunity

The logic and magnetic detection criteria developed in the Phase I program[1] was used with some modifications in the present SPVD. Shown in Figure 6 is a block diagram of the sensor system and illustrates the following sensor module functions: (a) amplifies the magnetometer transducer output signal, (b) automatically nulls out the DC offset changes in the magnetometer caused by time and temperature with a digital nulling loop (DNL), (c) performs vehicle presence logic functions by controlling and timing the DNL, (d) senses the amplitude of the vertical magnetic signal and detects two thresholds (hysteresis threshold detector), one for the peak vertical field amplitude and then a minimum vehicle presence sustaining threshold from either the horizontal or vertical axis, and (e) incorporates logic which discriminates against sudden short EMI/RFI bursts which could increase the vehicle detector's false alarm rate.

In Figure 90 (Section X) is a schematic diagram of the SPVD sensor module. Refer to it for the following detailed functional circuit description.

The Brown magnetometer has two 200K ohm potentiometers for DC offset adjustment. After the magnetometer is turned on for about five minutes, it is put into a magnetic shield with zero magnetic field and its outputs (both x and y) are set as close to zero volts by adjusting the potentiometer and measuring the magnetometer output with a digital voltmeter. The magnetometer is then connected to an input filter consisting of two 20 KΩ resistors (either metal film or high quality carbon) and a parallel .03 ufd capacitor. This filter network removes much of the magnetometers drive signal. The signal is then amplified by an 8021C operational amplifier to the desired threshold level. The Intersil 8021C's were used in the Phase I effort and although several low power operational amplifier types are adequate (i.e., μA 776, UC 4250, etc.) the 8021C's gained our confidence after extensive temperature tests. They are used throughout the SPVD. Also the commercial grade (i.e., 8021C) performed well over the military temperature range in all tested units and are not as expensive.

Since the magnetometer output voltage is linearity related to the measured ambient magnetic field, in most cases there will be a DC offset in both horizontal and vertical axes corresponding to the ambient earth's magnetic field. The long vehicle presence time, >15 minutes (900 sec) requires that the magnetometer system be DC coupled so that the vehicle's magnetic signature would not be changed by the sor/amplifier coupling over the 15 minute period. An early attempt was made to develop an analog nulling loop (ANL) with a storage capacitor, but because of the "low" impedance (70 mΩ) of low power op amps about 5 - 10 minutes was the longest obtainable period. Temperature variations also affected ANL system

performance. If power consumption of extremely high input impedance amplifier decreases to the microwatt level and capacitor leakage improved in next generation capacitors, it may be possible to use an ANL. For presence times less than 2 minutes, the ANL is adequate and consumes less power, is lower in cost, contains fewer parts and could be used as a speed sensor. The Digital Nulling Loop (DNL) is significantly more complex. Basically it is a digital to analog converter which senses the magnetometer signal amplifier output and if outside specific limits, develops an appropriate reverse polarity nulling voltage which is connected to the magnetometer signal amplifier's non-inverting input.

If the amplified signal voltage is positive, the Comparator (8021C #V of Figure 90) switches the 12 bit counter consisting of three CD 4029 BE 4 bit up/down binary counters to count down or provide a positive nulling voltage. A low frequency system clock (CD 4093) provides a sharp clock pulse of short duration approximately every 1.7 seconds to the three up/down counters. This short duration system clock pulse is required in order to eliminate any residual offset buildup which could occur for a constant stream of vehicles passing over the sensor.

The outputs of the up/down counters are then connected to a 12 bit R-2R resistive ladder network (R = 50K) which produces the analog output voltage which is scaled and connected to the magnetometer signal amplifier (OPAMP #VII).

For any change in DC signal level, the nulling loop will attempt to compensate for it, until threshold is reached, at which time the system clock is inhibited to the up/down counters. Instead it goes to the CD 4040 12 stage binary counter which counts the number of system clock pulses until the preset vehicle presence time is reached (pin 14 = 15 min., pin 4 = 1.75 min. test position). After the 15 minutes, the CD 4040 activates several CD 4066 CMOS switches which speed up

46

the system clock (CD 4093) for a fast DNL rezero, and the system becomes active again. If the vehicle leaves prior to the 15 minutes, the DNL clock pulses are restored to the up-down counters and it resumes its slow nulling of any ambient magnetic field or sensor changes with time and temperature.

Two digital nulling loops are required, one for the vertical axis and one for the horizontal axis. Each output is then rectified to obtain an absolute value of signal amplitude (OP AMPS I & II) and then connected via diodes to the hysteresis threshold detector. The threshold detector then activates an anti-chatter circuit which discriminates between real vehicle detection signals and short-high amplitude pulses associated with RFI/EMI. One antichatter circuit output controls the reset function for the CD 4040 vehicle presence timer while the other output is the vehicle presence signal which also opens the horizontal signal gate so that either a vertical or horizontal signal in excess of 3000 nT will result in a vehicle presence signal.

An 8 bit DNL was designed, fabricated and analyzed in the initial NSWC task described in Reference 2. The DNL was expanded to 12 bits thereby providing a larger dynamic range, i.e., ± 2 oersteds for each step corresponding to $\approx 100\gamma$. The remaining signal processing logic consisting of a signal full wave rectifier, threshold detector with hysteresis, and the antichatter circuits which are fully described in Reference 1 and only modified slightly in the present SPVDs.

Several prototype sensor modules were temperature cycled numerous times. For the first prototype sensor module, temperature data is tabulated in Table III. As is clearly shown, the threshold level is quite temperature dependent varying by as much as 40% from one extreme to the other. Some effort was made to compensate for this threshold change, mainly by diode selection and compensation circuits.

TABLE III

SENSOR MODULE THRESHOLD VARIATION WITH TEMPERATURE

TEMPERATURE	ACTIVATION THRESHOLD (gamma = nanotesla)	SUSTAINING THRESHOLD
+25°C	4400	2400
+50°C	4000	2000
+76°C	4000	2000
+25°C	4400	2400
+0	4900	2900
-20°C	5800	3800
-30°C	6100	4100
-40°C	6400	4400
+25°C	4400	2400

After examining the magnetic signatures obtained in Reference 9 it was felt that such variations could be tolerated on the great majority of vehicles if the room temperature threshold value was lowered to a range of 5000 to 6000 gamma rather than the 7000 gamma used in Phase I as vertical field activation threshold level. At temperatures below -10°C, there will probably be a higher detection miss rate for small vehicles (Volkswagon).

The sensor module is isolated from its battery power supply by a diode with an R-C filter to help eliminate any surges and drops in system voltage resulting from transmitter activation. This RC/diode filter network prevents free running with extremely low battery voltage and results in transient immunity. An efficient self-starting low power regulator has been developed[10] which supplies both 4 volts as a reference voltage and the magnetometer power supply, and 3 volts for the analog electronics system ground. This low power regulator designed and optimized by George W. Usher, Jr.,[10] consumes less than 60μw of power under no-load conditions and has a typical 90% efficiency for load currents in excess of 100μa. Chief voltage regulator assets include voltage changes less than 2% over the SPVD temperature range, no component selection is required, self-starting, simplicity and low cost. An undervoltage sensor which uses the 4 volt reference provides an output to the transmitter encoder module when the system voltage is 20% less than normal.

The complete sensor module is housed in an aluminum container with EMI filters on the +6.75v, vehicle presence and undervoltage outputs. The large aluminum plate and isolated circuit board mounting provides some thermal inertia for the magnetometer thereby eliminating rapid changes in sensor characteristics due to temperature variations.

Magnetics Surveillance Considerations

Characterizing the close-in field from an irregularly shaped ferromagnetic motor vehicle is quite difficult to model. For this reason, magnetic field[2,9] and gradient[2] measurements were made on various motor vehicles in order to develop detection logic. A vehicle may be considered as a magnetic dipole in its far field (is greater than a car length away) and typical magnetic moment strengths for an American-made car and bus are 2×10^5 cgs (gauss-cm^3) and 2×10^6 cgs respectively. However, fields measured near a vehicle require a model to consider higher order moments which more accurately represent the magnetic state of the vehicle. Basically, it is necessary to determine (a) the minimum detectable magnetic signal from a valid vechicle, and (b) the maximum adjacent lane vehicle magnetic field produced at the SPVD location. For the most part, this information has been determined experimentally by Reference 9. From that data, vehicle fields from several hundred gammas to 80000γ (.8 oersted) require the magnetic surveillance system to have a very large dynamic range, i.e., $\approx \pm 2$ oersteds.

The ambient magnetic field in the U.S. varies from .55 Oe to .40 Oe Vertical field intensity and .14 to .26 Oe horizontal field intensity. However, in the roadway environment, steel reinforcing rods may also add an additional field which may enhance or attenuate the ambient magnetic field.

In order to test the sensor module for a variety of magnetic field and temperature conditions, a test setup shown in Figure 19b is used. It consists of a two-axis helmholtz coil which may be positioned inside a mumetal magnetic shield, and a sensor module readout device, in this case a chart recorder. Each axis of the two-axis helmoholtz coils contains two windings, one to produce a bias field to simulate the ambient earth's magnetic field while the other winding when powered by a signal
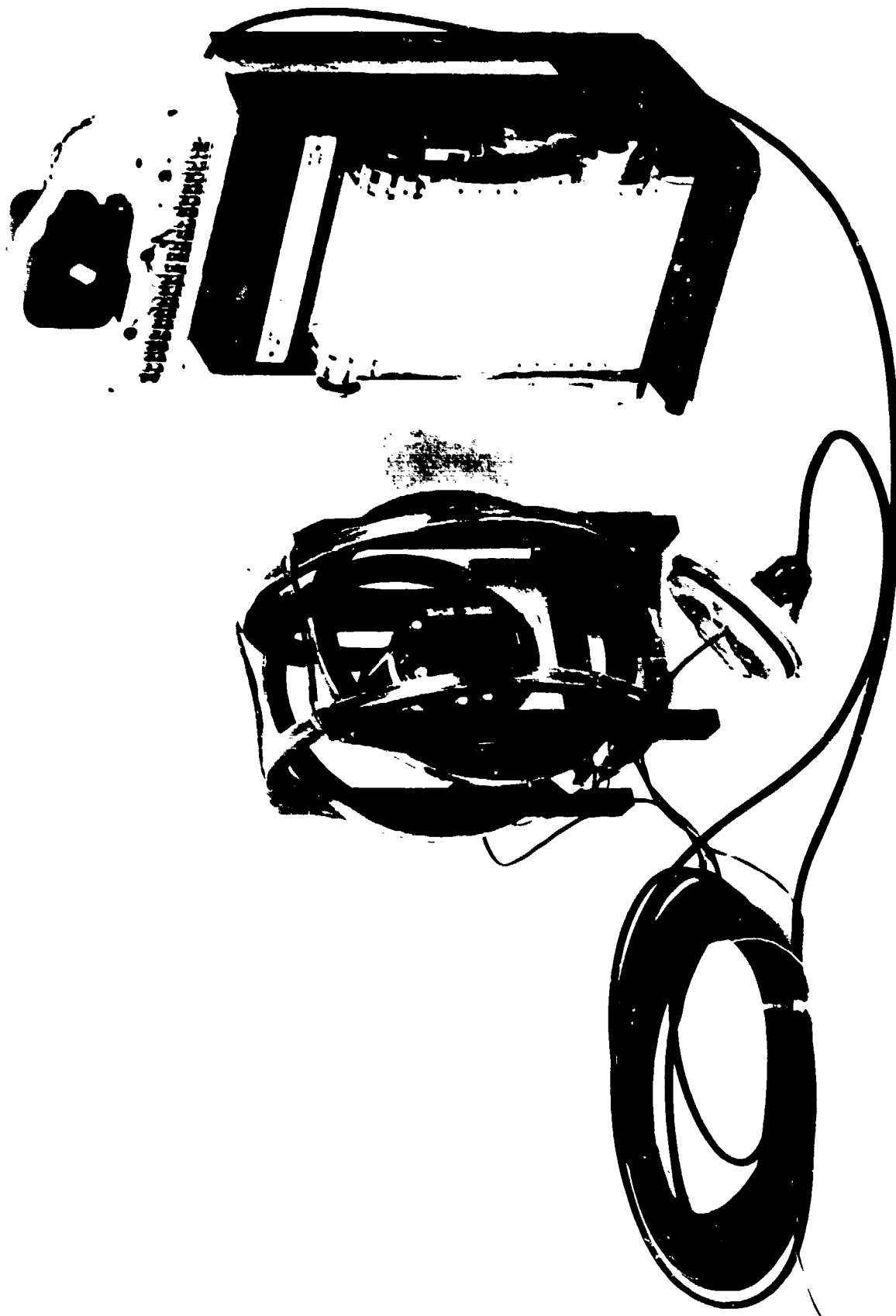
FIGURE 19B. SENSOR MODULE TEST SET UP.

generator produces the required vehicles magnetic signature. The sensor module checkout procedure requires (a) the SPVD activate for a 6000 gamma peak vertical signal in an ambient field of ±.5 Oersted, (b) determination that the horizontal threshold and gate are operable, (c) determination of the minimum threshold, and (d) determination of rise and fall times of the system for a vehicle presence.

If a line of vehicles is traveling at 60 mph (88'/sec) and are separated by one car length (17'), then a single cycle field of 2.58 hz can be used to simulate this situation if the sum of the system rise time and fall time is $\leq$ .386 seconds. To check the sensor modules rise and fall times, a square wave of 10000 gamma is applied to the vertical axis and typically T_{rise} = 10 msec and T_{fall} = 3 50 msec result.

After the rise and fall times are measured, a low frequency (.1 Hz) single cycle 10,000 gamma peak 1/2 of a sine wave magnetic field is applied to the vertical axis. The vehicle presence output and signal generator current (magnetic field intensity) are simultaneously monitored on a strip chart recorder and the activation and sustaining thresholds can then be determined by compensating for the system rise and fall times.

Since the vertical magnetic field in CONUS may be quite high in some locations, magnetometers' vertical axis was offset somewhat to expand this axes dynamic range. Detailed sensor module data may be found in Table XVI Section X.

IV. TELEMETRY LINK ENCODER AND DECODER DEVELOPMENT

SPVD Encoder

The SPVD sensor module generates three information items for use by the roadside control unit. These are: (1) the leading edge occurrence of the Vehicle Presence signal (V.P.) indicating the arrival of a vehicle, (2) each trailing edge transition of the V.P. signal (vehicle departing), and (3) the existence of an Under Voltage SPVD battery condition. Each of the items above are conveyed by the generation of two simultaneous tones which are added together for transmission lasting 30 ms. This short transmission time prolongs the operational lifetime of the unit to over a year. Below is table IV portraying the 3 combinations of the 3 tones taken two at a time and the information encoded on each combination.

TABLE IV. SPVD ENCODER TONES

Tone Combination	Information
3000 Hz, 4100 Hz	V.P. Leading Edge (LE)
4100 Hz, 5500 Hz	V.P. Trailing Edge (TE)
3000 Hz, 5500 Hz	V.P. Trailing Edge/Under Voltage

The SPVD encoder optimization began with a review of the existing Honeywell Phase I SPVD[1] design for possible component reduction. The realization incorporates SSI CMOS devices for both control and tone generation in the encoder (possibly because the more complex MSI CMOS chips were not available at that time). By using the CMOS 4047BE gated-astable multivibrators, an increase in tone frequency stability and reliability, in addition to a reduction package count, is realized. The Phase I sensor module generated a 1ms pulse both for the leading edge (L.E.) of the V.P. signal and the V.P. trailing edge (T.E.); however, in the revised encoder, only the

53

V.P. output from the antichatter circuit and the U.V. signal are needed to adequately direct the encoder.

Two encoder designs were formulated, each using three 4047 packages to generate the 3 tones. Reiterating, these units have excellent frequency stability versus temperature and battery voltage variations while dissipating less power than discrete CMOS oscillators. The tones generated are actually square waves which are added and attenuated with an 8C21 OP-AMP. The two encoder designs differed in the gating and control logic. The first approach incorporated a dual monostable multivibrator to produce a 30ms pulse (transmission duration) with each transition of the V.P. signal. The second encoder design, shown in block diagram form in Figure 20, which was selected for the SPVD production, derives the 30ms pulse by means of a 12 stage binary counter. The clock input of the counter is fed by the oscillator output (pin 13, IC 4047BE) of the 4100 Hz tone generator. Pin 13 outputs a pulse train which is twice the frequency of the 4047BE Q outputs. Thus by counting 256 cycles of an 8200 Hz signal, a 31ms duration is defined.

This implementation requires the 4100 Hz multivibrator be activated during every transition of the V.P. signal; however, Table IV indicates that no 4100 Hz tone should exist when the SPVD unit is transmitting T.E./U.V.. Fortunately, the 4047BE has an oscillator output and $Q/\overline{Q}$ outputs which are derived by dividing the oscillator signal by two. The Astable/$\overline{\text{Astable}}$ gate inputs control the oscillator operation; also, the Reset input clears the $Q/\overline{Q}$ outputs but allows the oscillator to function under the direction of the Astable/$\overline{\text{Astable}}$ inputs. Therefore, the Q output provides the 4100 Hz tone that is summed, along with the two other tones, by the 8021 OP-AMP.

54
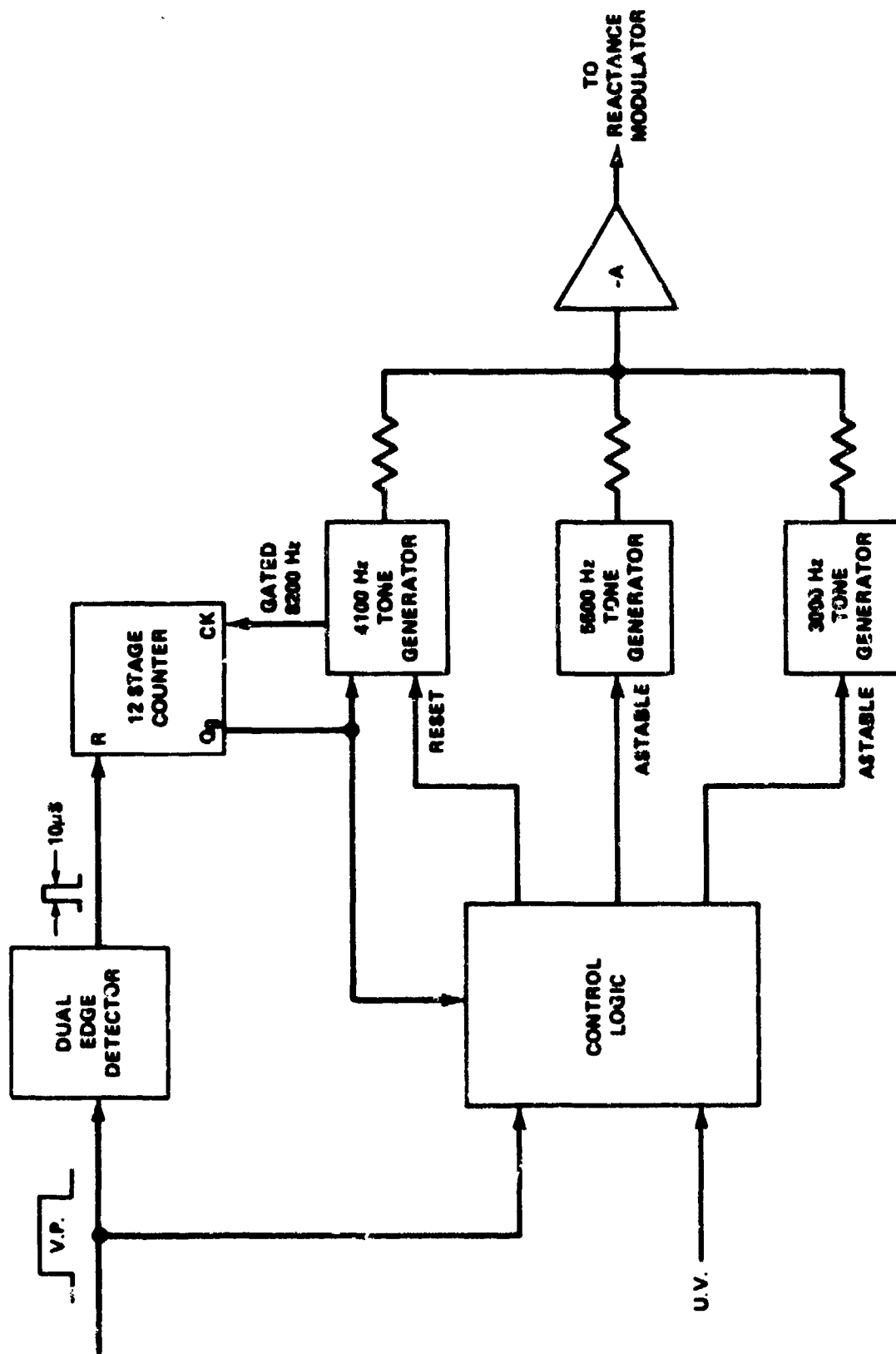
FIGURE 20. SPVD ENCODER BLOCK DIAGRAM.

A typical sequence of circuit operation is now presented assuming a vehicle is about to be detected. The V.P. line goes high which causes the dual edge detector (1/4 of 4070) to emit a 10 μs pulse which clears the 4040 counter. Q_9 output is now low gating on the 4100 Hz tone multivibrator. The oscillator pulses (8200 Hz) increment the 4040 counter until state 256_{10} (31 ms) is reached; at this point, Q_9 goes high which inhibits the Middle Tone oscillator. The circuit is now again in an inactive state. As the vehicle departs, the V.P. signal goes low causing the dual edge detector to output a pulse resulting in action identical to that described above.

The logic that determines which tone generators are enabled during each 31 ms transmission is realized with a 74C157 CMOS I.C. The 74C157 is a Quad 2 to 1 Multiplexer with strobe and is used here as an 8x3 ROM. The 3 "address" inputs to this ROM-like configuration are Q_9 ($\overline{31\ ms}$), V.P., and the U.V. signals. Below in Table V is depicted the memory listing for this equivalent ROM.

TABLE V.   74C157 8x3 MEMORY LOGIC LISTING

	Address			Data		
	Q_9 ($\overline{31\ ms}$)	V.P.	U.V.	5500Hz Tone	4100Hz Tone (Reset)	3000Hz Tone
TE	0	0	0	1	0	0
TE/UV	0	0	1	1	1	1
LE	0	1	0	0	0	1
LE/UV	0	1	1	0	0	1
	1	0	0	0	0	0
No	1	0	1	0	0	0
Trans-	1	1	0	0	0	0
mission	1	1	1	0	0	0

It should be noted that the 4100 Hz tone generator is controlled by both the Q_9 output of the 4040 counter and output D_3 of the 74C157. The oscillator portion is functioning as long as Q_9 is low while a 4100 Hz tone is outputed during $\overline{Q_9}$ ($\overline{V.P. \cdot U.V.}$).

As stated before, the Q outputs of the three 4047BE tone oscillators are summed and attenuated by an inverting OP-AMP configuration. The current-setting resistor is set at 2.2 mΩ to lessen the slew rate of the amplifier providing some reduction in the higher harmonics of the summed tones which are square waves. It was first envisioned that the OP-AMP output would be AC coupled to the modulator section of the SFVD FM transmitter. However, it was decided to DC-couple the two together so the OP-AMP not only provides the necessary tone modulation but also supplies the bias for the varactor diode in an effort to reduce start-up transients.

Looking ahead for a moment, it was determined that a good value for the varactor diode bias was 4.2 volts on which a 1.2v p-p baseband signal was added to give the desired ±5 KHz deviation at each channel frequency. The gain (attenuation) of the stage is calculated by finding the input conditions which give the maximum and minimum values on the OP-AMP output. Shown below (Figure 21) is a partial schematic of this circuit using 100KΩ resistors on each input tone signal.

During normal operation assuming transmission is taking place, one tone will be inhibited (0 v) while the other two oscillate between +6.7 v and ground. Therefore, the input conditions which cause the maximum and minimum output values are both remaining tones "low" or both tones "high," respectively. The output equation is

$$V_1/100K + V_2/100K + V_3/100K = -\frac{V_{out}}{R_F}$$

$$\Delta V_{in} \frac{R_F}{100K} = -\Delta V_{out}$$
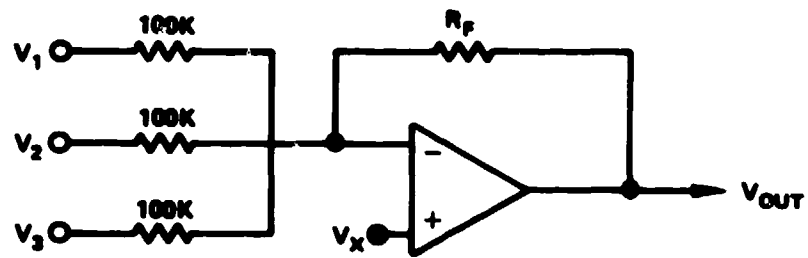
FIGURE 21. TONE MIXING AMPLIFIER.
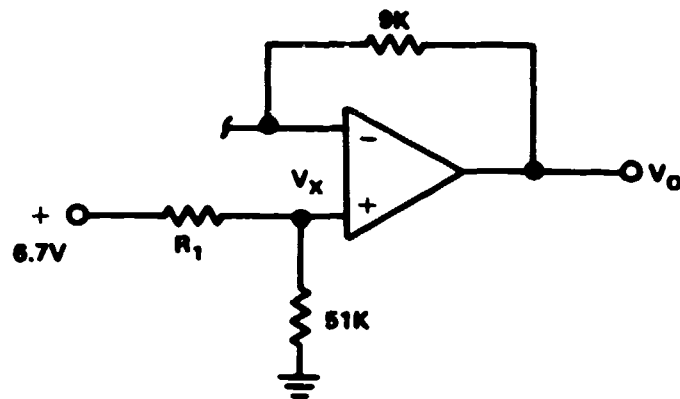
FIGURE 22. BIAS CIRCUIT OF TONE MIXING AMPLIFIER.

Given: $\Delta V_{out} = \pm.6v$

$\Delta V_{in} = \pm 6.7v$

$$R_F = \frac{.6v}{6.7} \times 100K$$

$$R_F \approx 9K\Omega$$

Now that the feedback resistor is defined V_x must be found so that a no-modulation bias of 4.2v exists.

Going back to the partial schematic of the OP-AMP stage (Figure 21) when two inputs are low and one is high, the unmodulated bias point is obtained. Using Kirchoff's Current Law, the current equation at the inverting input terminal is:

$$\frac{6.7 - V_x}{100K} + \frac{0 - V_x}{100K} + \frac{0 - V_x}{100K} + \frac{4.2v - V_x}{9K} = 0$$

Solving for V_x:

$$V_x \approx 3.78v$$

Now assuming a voltage divider configuration on the noninverting terminal as shown below (Figure 22), the unknown resistance R_1 is calculated.

$$\frac{6.7 (51K)}{51K + R_1} = V_x = 3.78v$$

$$R_1 \approx 39K$$

The transmitter alignment began by first setting the tone oscillators to the desired frequencies. A series combination of two fixed film resistors and 5KΩ potentiometer was used to fine tune the 3 frequencies. After the oscillator/ transmitter were coarsely tuned the frequency deviation had to be adjusted to ±5KHz. This was accomplished by varying the gain of the OP-AMP slightly and also realigning the tuning coil of the oscillator. It is suggested that a 7KΩ fixed film resistor be connected in series with a 5KΩ potentiometer to provide an easily adjustable R_F. Table VI presents typical data taken of the 4047BE Multi-vibrators as the ambient temperature was varied from +70°C to -40°C.

TABLE VI. 4047 Oscillator Temperature Stability Data

Temp °C	High Tone	Mid-Tone	Low Tone
25	5535	4124	3015
70	5506	4092	3023
25	5539	4127	3044
-40	5575	4167	3063
25	5540	4128	3043

The data in Table VI indicates that the worst case temperature drift was about ±.95%. From the RCA CMOS data book we can expect a 1.5% drop in tone frequency due to a battery voltage decrease from 6.7v (new) to 5v. The above figures indicate that the 4047BE are quite stable in frequency leading to a better system reliability.

Figure 23 is a complete encoder schematic diagram. Note that this encoder has the capability of controlling two transmitters for 15ms transmissions and was originally designed for an SPVD having two transmitters each powering two orthogonal loop antennas. For the present single transmitter with the Omnidirectional Microstrip Antenna, this is not used.
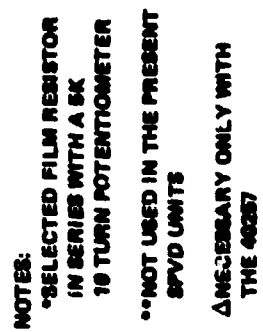
FIGURE 23. SPVD ENCODER SCHEMATIC DIAGRAM.

NOTES:

*SELECTED FILM RESISTOR IN SERIES WITH A 5K 10 TURN POTENTIOMETER

**NOT USED IN THE PRESENT SPVD UNITS

△NECESSARY ONLY WITH THE 40257

61

Tone Recognition and Decoding Logic

Once the encoded tone information transmitted from the SPVD unit is demodulated by the roadside receiver, it is fed to an interface board. The purpose of this circuitry is to bandpass the receiver output for a reduction of out-of-band noise. More specifically, the Interface circuit consists of a 1 pole Low Pass filter (break frequency is 8.8 KHz) followed by a 2 pole high pass filter (break frequency is 2.7 KHz). Finally the signal is amplified in a variable gain OP-AMP stage. Because the Radio Shack receiver (see receiver section) does not provide a flat frequency response in the vicinity of the SPVD tones favoring the lowest tone, the interface circuit compensates partially for this by attenuating lowest tone relative to the others. The filtered tone information is adjusted to an amplitude of 2v p-p before entering the tone decoding section.

A functional description of the Tone Recognition and Decoding Logic is now presented and the corresponding block diagram is shown in Figure 24.

The filtered/amplified receiver audio signal is directed to three XR567 Phase-Locked-Loop Tone decoders. Each is set up to recognize one of the three tones generated by the SPVD Encoder unit; the PLL output goes low whenever the incoming signal contains sufficient spectral energy that is within the detection band of the tone decoder. The output of the PLL's are each sent to a minimum pulse width discriminator which provides additional noise immunity. Being an "active low" signal, the tone decoder output must remain logical zero for a minimum preset time duration before a valid tone reception is indicated. Due to the nature of the pulse width discriminator output, a latch is needed to store a valid tone reception until the PLL loses lock on the tone.

The three latches control the decoding logic which is responsible for determining what information was transmitted by the SPVD unit encoded on the
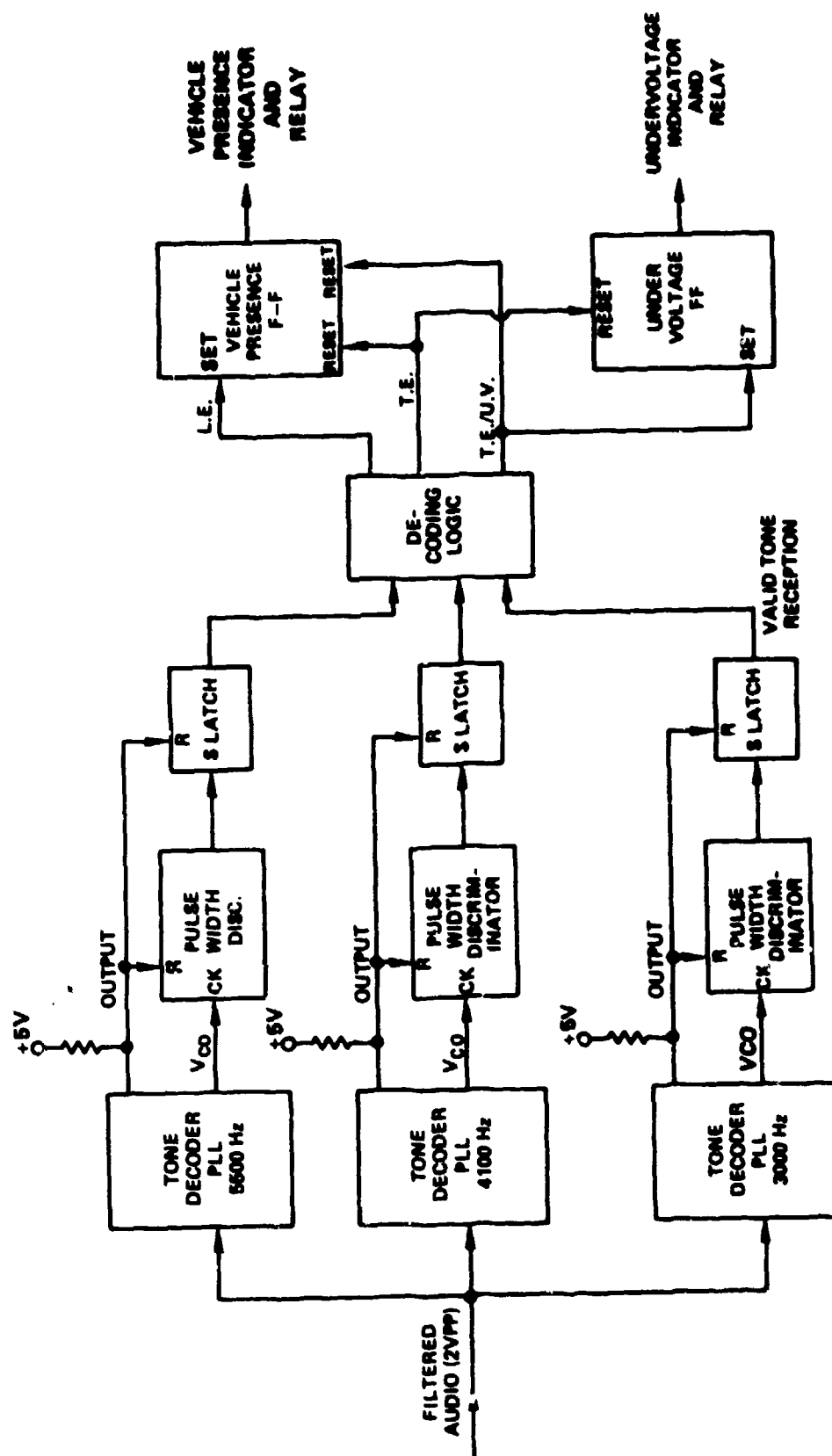
FIGURE 24. TONE RECOGNITION AND DECODING BLOCK DIAGRAM.

combination of valid tone receptions. The three outputs of the Decoding Logic are Vehicle Presence Leading Edge, Vehicle Presence Trailing Edge and Trailing Edge/Under Voltage. These three data lines in turn, control the V.P. Flip-Flop(F-F) and the SPVD Under Voltage F-F. Finally the two F-F outputs drive the associated indicators and relays via transistor buffers.

Having presented a general operational description of the Tone Recognition and Decoding Logic section, more specific design details are spelled out below. The reader may wish to refer to the schematic diagram of this circuitry in Figure 25. The XR 567 Tone decoders are configured with the following objectives in mind: (1) the transmitted tones exist only 31ms and therefore lock time must be minimized and (2) since the ambient temperature will vary widely, a shift in PLL center frequency and SPVD Tone frequency must be tolerated. Consequently, these PLL Tone decoders are set to have the largest detection bandwidth possible (14%) implying a higher loop natural frequency. To minimize responses due to transient signals, the quadrature phase detector filter capacitor is larger in value than usual. The low pass filter capacitor was given the value according to the relationship $C = \frac{130}{f_o} \mu F$ to minimize lock time. It was found that the Detection Bandwidth Skew worsened by d.c. coupling the 3 PLL inputs together which explains the usage of capacitors on the inputs of the tone decoders.

The XR 567 PLL Tone Decoder is designed to operate over the military temperature range; various temperature cycling tests were conducted to determine how the center frequency stability, sensitivity, and detection bandwidth were affected by temperature changes. Sensitivity to input signal amplitude, and detection bandwidth varied slightly. Best frequency stability was obtained by using 200v mylar capacitors in the timing circuit of the current controlled oscillator. Table VII presents temperature data of three tone decoders, one
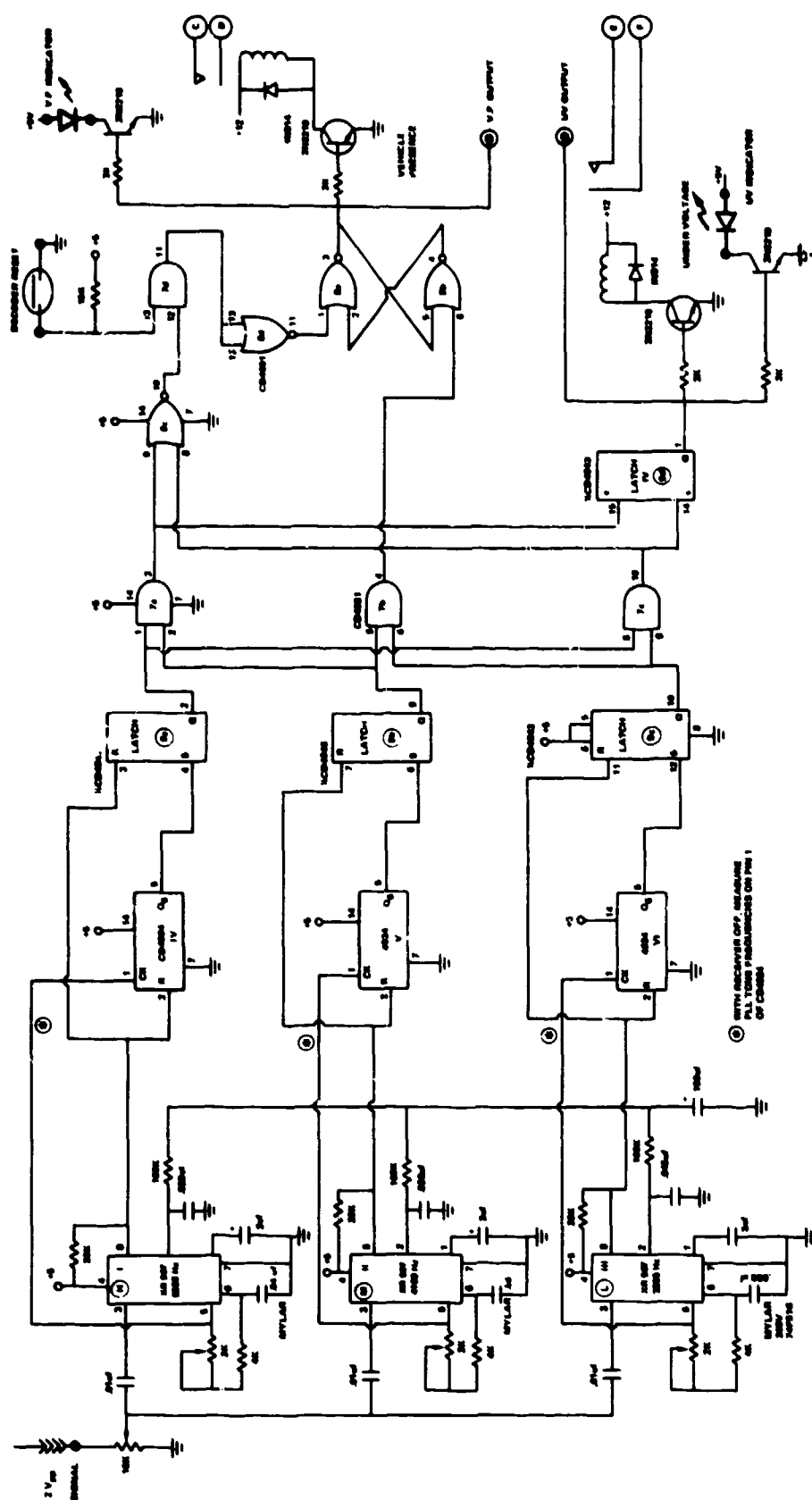
FIGURE 25. SPVD DECODER SCHEMATIC.

corresponding to each of the SPVD tones.

TABLE VII. SPVD DECODER PLL OSCILLATOR TEMPERATURE STABILITY
(With 200v Mylar Capacitors)

Temp. (C°)	High Tone (Hz)	Middle Tone (Hz)	Low Tone (Hz)
26	5529	4144	3032
70	5511	4139	3028
26	5520	4141	3022
-40	5531	4158	3028
26	5522	4141	3023
26	5525	4142	3030
70	5513	4137	3031
26	5520	4138	3028
-40	5531	4161	3034
26	5521	4142	3028

The data above indicate these tone decoders have good temperature stability; in fact, they drift in the same direction as the tone generators in the SPVD unit but to a lesser amount for an equal temperature variation. To further improve frequency stability, the power supply which feeds the tone decoders is well regulated and bypassed minimizing supply voltage variations due to load and temperature fluctuations.

Two realizations of the minimum pulse width discriminator were devised. The first is shown schematically in Figure 26 and uses a monostable multivibrator to generate the minimum time reference ($\sim$10ms). As can be seen, actually two one-shot's are needed in addition to a latch (D-FF); the 10ms monostable multi vibrator must provide an output pulse of fairly good period stability over the operating temperature extremes.

Approach II which was selected for SPVD usage, consists basically of a 7 stage binary counter whose clock input is fed by the PLL Current Controlled Oscillator (CCO) signal (pin 5). The counter reset input is controlled by the
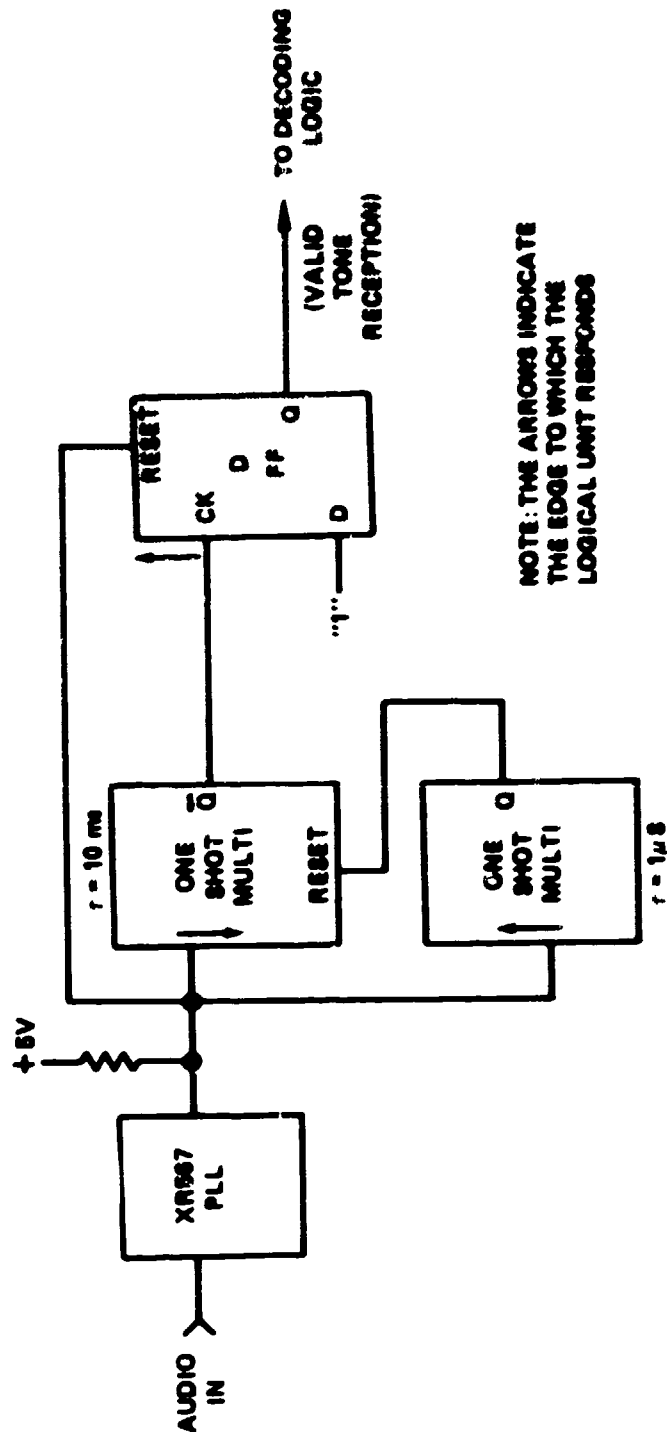
NOTE: THE ARROWS INDICATE
THE EDGE TO WHICH THE
LOGICAL UNIT RESPONDS

FIGURE 28. PULSE WIDTH DISCRIMINATING CIRCUIT IMPLEMENTED WITH MONOSTABLE MULTIVIBRATORS.

PLL active low output. As the Tone decoder lock time is specified in terms of cycles instead of time, it is actually a function of Tone decoder frequency. Thus utilization of a binary counter to count CCO cycles is a more realistic and also economical means of determining whether the PLL has been locked on a signal for a minimum time duration. The schematic diagram in Figure 25 illustrates this type of pulse width discriminator. Whenever the Tone decoder locks onto an input signal, its output goes low removing the reset condition on the counter. At the occurrence of each falling edge of the CCO output, the counter increments by one. Should 32_{10} cycles be counted a valid tone reception is assumed to have occurred and this event is stored by an R/S Latch (1/4 of 4043). The latch is necessary because the Q_6 counter output will go low if more than 63_{10} cycles are present during a continuously locked PLL condition. It should be pointed out that the lock time varies randomly according to the initial phase difference of the incoming tone and the internally generated CCO signal. We cannot expect that with the reception of two simultaneous tones, each corresponding tone decoder to lock after the same number CCO cycles or remain locked for an identical length of time.

Once the R/S Latch is set by the counter reaching a state of 32_{10}, the Latch output remains high until the PLL loses lock and its output goes high. This logical 1 clears the latch and also the counter removing the valid tone reception signal from the decoding logic. In summary, the use of a binary counter/latch combination for the pulse width discriminator eliminates the need of 3 critical timing circuits and effects a reduction in package count.

The valid tone reception latches feed into the decoding logic which determines what information if any is being received from the SPVD unit in the roadway. This logic simply consists of 3 2-input AND gates (1/4 of 4081); the three outputs indicate the transmission of the V.P. Leading Edge, V.P. Trailing Edge, and

and also directly connects to the U.V. BNC with a CMOS compatible output. The U.V. relay may also be energized by a low control box battery voltage condition. The voltage sensing circuit is located on the Interface board mentioned earlier in this report. (See Receiver Section). Thus control box connector pins E & F will be shorted together whenever the SPVD battery or the control box battery is too low in voltage.

During the SPVD Phase I effort, there was a very significant false alarm problem with the tone decoder in urban areas. Therefore extensive tests were made on the prototype decoder design. A sensitive receiver (AN/URR-52B - Watkins Johnson RS-111B) attached to an outside antenna provided signals for the decoder whose output was then recorded on a Rustrak strip chart recorder. No false alarms were recorded for the 500 hour test period despite noted RFI/EMI, i.e., occasional voices in our Maryland-Washington, DC location.

One accidental observation, that of locating the control box (receiver/decoder) near ($\approx$ 50 feet) an electric arc welding shop, produced a very high miss rate effectively disrupting the telemetry link. Removing the control box from the building (i.e., 100 feet) eliminated the problem.

V. TELEMETRY OSCILLATOR/TRANSMITTER DEVELOPMENT

Introduction

The original SPVD in-house effort[2] was primarily involved with the magnetic sensor module improvement and upgrading of the tone encoding/decoding schemes. In final form our responsibilities included optimization of the RF section in the SPVD unit. Not having in-house RF designers, attempts were made to contract that portion of the project to someone who would not have to spend most of his efforts while on the learning curve. This proved futile; however, expert advice was obtained from Mr. Philip J. Lizzi, who made several recommendations regarding the oscillator and transmitter designs. The SPVD transmitter (RF power amplifier) is, in fact, the basic circuit that he suggested with a few modifications. It is felt that this SPVD transmitter circuitry is not the ultimate in RF realizations but it is an improvement over the previous hardware and appears to satisfy system requirements.

The same general telemetry configuration as devised by the Phase I SPVD effort is employed here. However to reduce false detections, vehicle leading edge, trailing edge, and SPVD battery undervoltage are now encoded for tranmission by means of two simultaneous tones (a combination of 3 tones taken two at a time). Again the radiated signal duration is 30 ms. The tones are frequency modulated onto a 41 MHz carrier with approximately 100mw of RF energy being delivered to the antenna. This low power level not only extends battery lifetime, but eliminates the need for FCC type approval. The areas of probable SPVD improvement were circuit stability, wider frequency deviation, and transmitter efficiency. Because the signal to noise ratio of an FM system increases with larger deviations (requiring a larger bandwidth), the maximum deviation desired was determined by the bandwidth

and deviation acceptance of the SPVD Receiver. The SPVD receiver selected for this system was specified as having an I.F. selectivity of ±13 KHz @ -6db and a modulation acceptance of ±7 KHz. Allowing for center frequency drift due to long-term aging, temperature, and voltage variations, the oscillator deviation extremes were selected to be ±5 KHz. Frequency stability and deviation were given a higher priority than oscillator energy consumption and thus no quantitative efficiency goals were set.

The use of the newly-designed single $\lambda/4$ omnidirectional microstrip antenna permitted a markable reduction in the RF amplifier complexity and higher circuit efficiencies. Now only one RF amplifier is required and an additional battery can be accommodated within the SPVD unit thereby doubling the energy available to power a less efficient oscillator/transmitter if necessary.

Before proceeding with an outline of what will be covered in this section of the report, the term oscillator when referring to a circuit assembly of the SPVD is to be understood to include the modulator, oscillator, and doubler components. The first item to be discussed will be SPVD oscillator design and performance goals. Next follows a general presentation of the two possible oscillator realizations noting the advantages and drawbacks to each in light of the SPVD program. Then the Phase I SPVD oscillator is analyzed regarding its performance characteristics. Several theoretical concepts are reviewed regarding wider-deviation Voltage Controlled Crystal Oscillators (VCXO) and, finally, the development of the present SPVD oscillator is documented.

SPVD Oscillator Technical Objectives

The oscillator design and performance goals are defined by the overall SPVD system objectives namely: (1) SPVD operational lifetime is one year, (2) volumetric

constraints of a cylinder 4 1/2" in diameter and 12" long, (3) wide operating temperature range of -30°F to +170°F and (4) low cost due to possible widespread utilization of SPVD systems. The SPVD oscillator technical objectives are listed below in a descending order of priority.

Because of the nature of this project, these goals are often expressed in qualitative form.

1. Oscillator Frequency Stability - ±2 KHz of preset channel frequency: 41.41 MHz or 41.37 MHz.

2. Frequency Modulation Characteristics - 0 to ±5 KHz deviation

3. Physical Size - minimal

4. Power consumption - minimal

5. Cost - minimal

Frequency Modulation Generation

The generation of an FM signal may be accomplished in one of two ways, the direct or the indirect method of frequency modulation. Indirect frequency modulation is implemented by means of a narrowband phase modulator whose carrier frequency is supplied by a stable source, usually a crystal-controlled oscillator, ensuring good stability. The baseband signal is integrated before its application to the modulator so that the frequency rather than the phase is proportional to the modulation. To increase the frequency deviation of the narrowbanded FM signal, frequency multiplication is employed. Here the carrier frequency and frequency deviations are increased without affecting the modulating frequency. Because it may be necessary to have many stages of multiplication before the desired deviation is achieved, heterodyning is required to translate the spectrum intact to the proper location using a second crystal-controlled oscillator. As can be surmised

indirect frequency modulation, while providing very good frequency stability suffers from high cost, complex realizations (large size), and high power consumption.

The direct method of frequency modulation (parameter variation method), on the other hand, is characterized by low cost, small size, and low power dissipation at the expense of a degradation in frequency stability. Conceptually this type of FM generation is straightforward and requires nothing more than a Voltage Controlled Oscillator (VCO) whose oscillation frequency has a linear dependence on an applied voltage. The generation of an RF carrier is usually provided by a tuned circuit oscillator. The frequency of oscillation is principally determined by an inductance-capacitance combination in resonance and is described by the relationship

$$F = \frac{1}{2\pi \sqrt{LC}}$$

F = frequency of oscillation (Hz)
L = henries
C = farads

If either the inductance or capacitance were to be made voltage-dependent, then the frequency of oscillation would be a function of voltage (in this instance, the baseband signal). A varactor diode serves as a voltage-variable capacitor when reverse biased as the magnitude of the reverse bias determines the terminal capacitance. Thus a quite simple and inexpensive VCO can be realized using a varactor diode as the variable reactance element. Significant frequency deviations may be achieved without the need of additional operations (multiplication and heterodyning) but frequency stability will be poor.

A quartz crystal resonator when introduced as the frequency-determining element greatly improves stability of an oscillator by at least several orders of magnitude. However, frequency modulation of a crystal-controlled oscillator is

74

difficult and therefore limited due to the stable nature of the crystal. This dilemma is summarized as follows: there is a measure of inconsistency in requiring an oscillator to have long-term frequency stability and yet be able to respond readily to frequency shifts caused by a modulating signal. We expect therefore an inverse relationship exists between a VCO's deviation and its long-term stability. A compromise condition must be reached whereby an acceptable deviation is obtained with satisfactory frequency stability performance.

Due to the simplistic nature of direct frequency modulation, the SPVD oscillator is, in both the Phase I SPVD and the present system, a Voltage Controlled Crystal Oscillator (VCXO) incorporating a varactor diode as the reactance modulator. The Phase I approach was characterized by good frequency stability but insufficient deviation. The present SPVD oscillator widens the deviation extremes with the addition of several components that alter slightly the crystal resonator charac- teristics. The frequencies allocated to the SPVD system are 41.41 Mhz and 41.37 MHz which requires that either a fundamental mode crystal be used followed by a frequency doubler or a 3rd overtone crystal oscillator be incorporated without subsequent multiplication. The fundamental crystal/doubler technique was chosen for the SPVD system since a frequency doubler is easily realized, it doubles the deviation, and provides isolation between the oscillator and the RF amplifier. Also overtone crystal operation does not permit as wide a frequency deviation and generates more distortion than a fundamental mode crystal oscillator.

The Phase I SPVD Oscillator

The Phase I VCXO is a parallel mode crystal oscillator of the Colpitts configuration that is frequency modulated by means of variable-capacitance loading of the quartz resonator. As stated before, the crystal ($f = 1/2f_o$) is operated in the fundamental mode and is doubled by the collector tank circuit.

The encoded tones control the reverse bias of the varactor diode in series with the crystal generating the desired frequency modulation. Reference 11 provides an explanation of the Colpitts parallel mode crystal oscillator. Reference 12 describes the variable-capacitance loading of quartz resonators and gives the mathematical derivation that predicts the frequency pulling range for such an oscillator. In Figure 27 is shown the Phase I SPVD oscillator and the equivalent resonator circuit assuming C24 and C25 are large enough so that the load seen by the crystal is almost totally dependent on the varactor diode circuit.

Table IX presents the varactor capacitance and associated crystal load capacitance for various varactor diode bias conditions.

TABLE IX. VARACTOR DIODE CHARACTERISTICS

Varactor Rev. Bias (volts)	Varactor Cap (pF)	Crystal Load Cap * (pF)
4	48	41
5	30	32
6	20	26
7	15	22
8	13	20.5

Varactor = Motorola MV1404

*Trimmer is set at 9pF

With 6 volts as the unmodulated bias point, a two volt P-P signal would create a crystal load minimum and maximum capacitance of 22pF and 32pF respectively. Thus the pulling range (KHz) derived from Equation 14 of Reference 12 is shown below:

$$\frac{B \ (KHz)}{f_o \ (MHz)} = \frac{500}{r_o} \left[\frac{1}{1 + \frac{C \ min}{C_o}} - \frac{1}{1 + \frac{C \ max}{C_o}} \right]$$

76

SCHEMATIC DIAGRAM

$Q_1 - 2N2369$

X TUNED FOR f_o
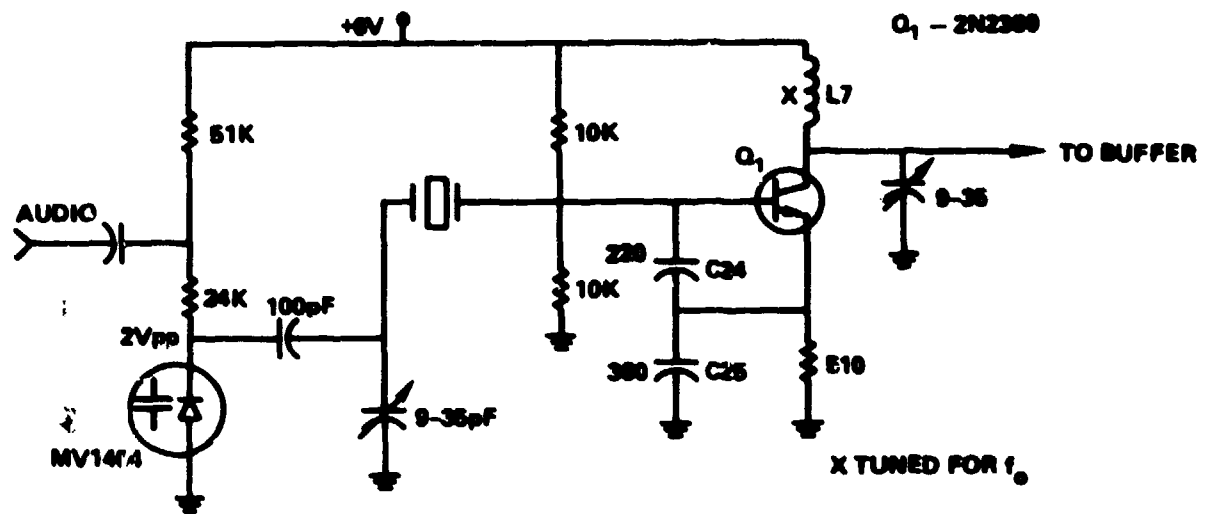
EQUIVALENT RESONATOR CIRCUIT

FIGURE 27.   PHASE I SPVD OSCILLATOR.
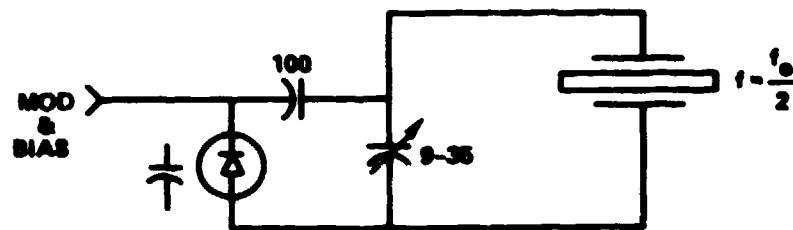
$$r_u \approx \frac{C_o}{C_1} \approx 200 \qquad C_o \sim 5pF$$

$$B = 2.5 \text{ KHz}$$

After doubling the deviation would be 2.5 KHz. Reference 13 does a computer analysis of a similar VCXO at 20 MHz using the AC-Coded circuit analysis program. As the load capacitance is varied from 22pF to 32pF a frequency deviation of about 2.4 KHz occurs; subsequent doubling would result in ±2.4 KHz deviation. Even though the analysis approach taken in Reference 12 and Reference 13 differ, the expected deviation of ±2.4 KHz is substantiated by both.

If the modulation were increased to 4v pp, C min and C max loading on the crystal would be about 20.5 and 41pF respectively. Application of Equation 14 (Reference 12) gives a deviation of 4.37 KHz which after doubling becomes ±4.37 KHz. Reference 13 for the same capacitive loading limits on the crystal identifies a ±5 KHz deviation after doubling.

Although the above results predict satisfactory deviation performance with a modulating signal of 4v pp on the varactor, the actual SPVD oscillator had much less deviation, in the order of ±500 Hz. This may have been due to the particular quartz resonator and/or stray and other circuit capacitance which were not taken into account during the preceeding theoretical analysis. It was quite apparent that another approach to the VCXO was needed.

Present SPVD Oscillator

Additional research revealed that a VCXO may be implemented in a way which permits rather large frequency deviations at a moderate loss in stability. Having numerous sonobuoys available and knowing acoustic information was frequency modulated, investigations began on the VCXO techniques used. The Spartan

Electronics Corporation AN/SSQ-57, although having a final transmitting frequency of 160 MHz, employed a 20 MHz VCXO that was frequency multiplied by a factor of 8. Closer inspection revealed the oscillator was a series-tuned Colpitts oscillator using a fundamental mode crystal, a reactance modulator (varactor diode), and a collector tank circuit tuned to the second harmonic. The modulator-oscillator-doubler stage was extracted from a sonobuoy to get a feel for its deviation, stability, and the feasibility of interfacing it to the RF amplifier described later in this report. The oscillator was powered by the 6.7v SPVD battery, and the current drain was about 16ma. Very large deviations were observed and the oscillator provided sufficient power at 41 MHz to drive the RF amplifier at a 100 mw level into 50Ω. In fact with everything peaked, 200 mw was delivered into 50Ω at a combined oscillator/RF amplifier current of 67ma. Several temperature performance tests were conducted cycling the oscillator from -30°C to +70°C; the corresponding frequency drift totaled about 6 KHz maximum. Later when the spectrum analyzer became available, it was found that the tuning procedure used up to that point caused the oscillator to operate in a mode generating amplitude modulation of significant proportions. This led to poorer frequency stability than the circuit is capable of.

The initial VCXO derived from the sonobuoy circuit is shown schematically in Figure 28. Much of the work done on this oscillator was experimental. A literature search surfaced several papers discussing this type of VCXO. The basic Colpitts oscillator equivalent circuit is shown in Figure 29 having a collector tank tuned to the 2nd harmonic of the oscillator. X_L represents the series connection of the varactor diode C_S, series inductance L_S, and the quartz crystal unit. Figure 30 demonstrates the effect of a series reactance element on a crystal assuming the reactance of the capacitance and
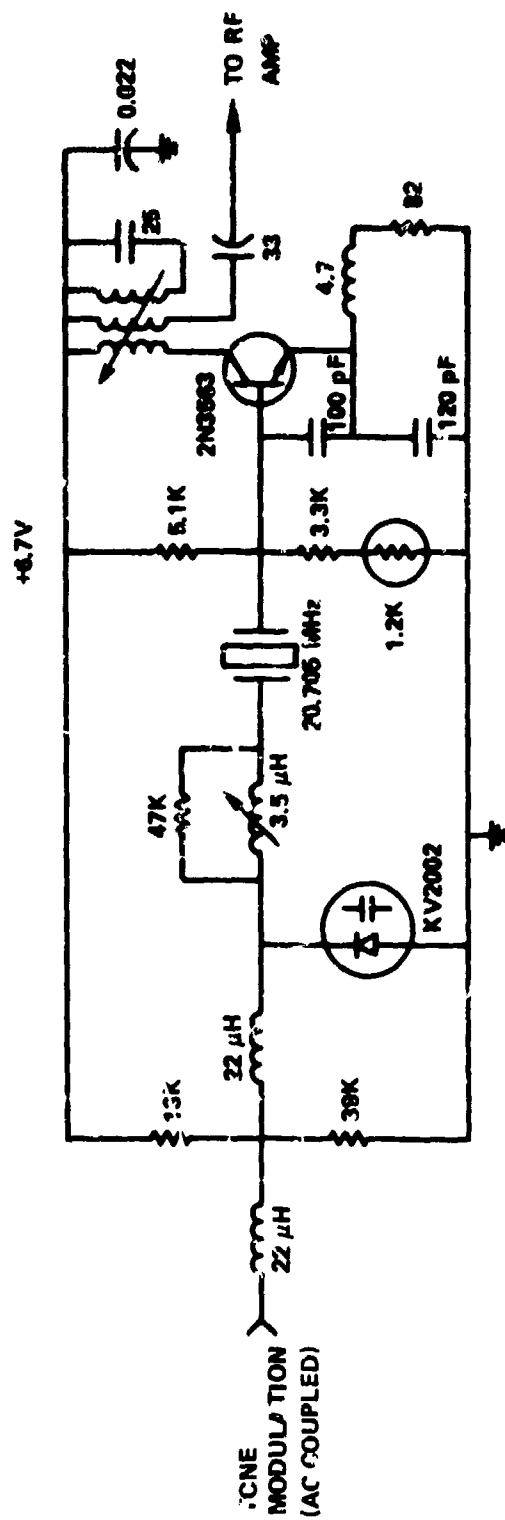
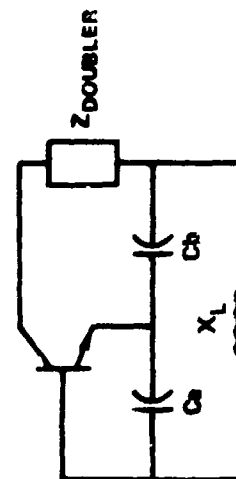FIGURE 28. VOLTAGE CONTROLLED CRYSTAL OSCILLATOR SCHEMATIC.
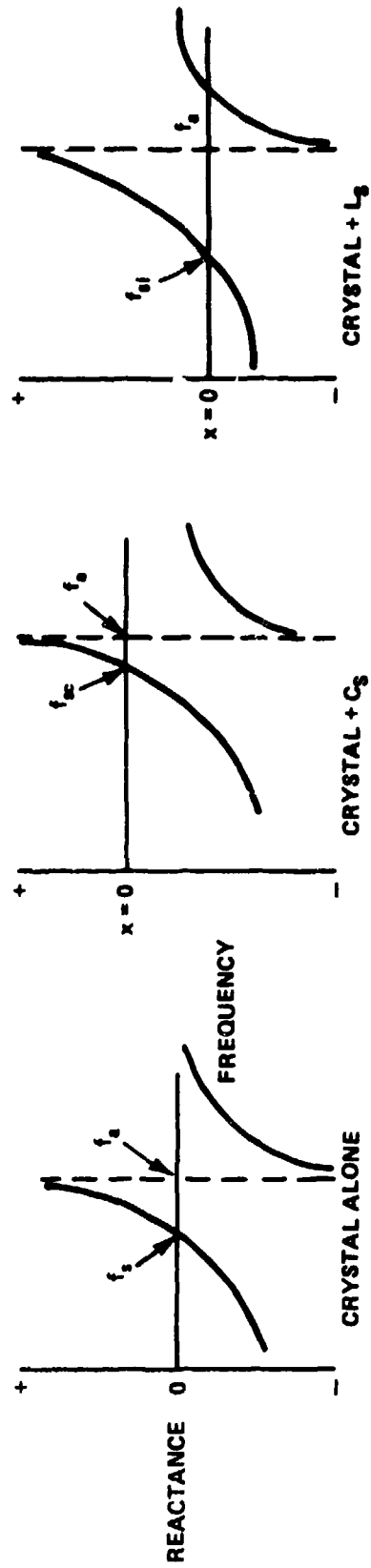

FIGURE 29. BASIC COLPITTS OSCILLATOR CIRCUIT.

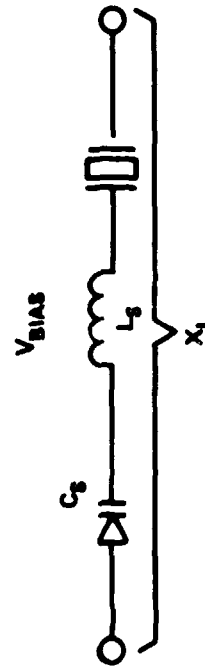FIGURE 30. EFFECTS OF SERIES REACTANCE TUNING OF A COLPITTS CRYSTAL OSCILLATOR.

FIGURE 31. CRYSTAL WITH SERIES REACTANCE.

81

inductance is constant over this narrow frequency range. Essentially the series reactance/crystal combination results in a reactance vs frequency relationship which is that of the crystal itself but shifted up or down relative to the X = 0 line. In the case of series capacitance, the series resonant point is raised above the series resonant frequency of the crystal alone. The inductance on the other hand, displaces the series resonant point away from the anti-resonant crystal frequency.

Because frequency stability is greatest when we have achieved the highest $\frac{dz}{df}$, the crystal oscillator frequency may be deviated more easily as the circuit is operated where the reactance vs frequency slope is more shallow. For the Colpitts oscillator to function, X_L must appear inductive to the circuit requiring oscillator operation somewhere between the series resonant point and the anti-resonant point of the crystal/series reactance combination. As seen in Figure 30, a series inductance lowers fs while $\frac{dz}{df}$ above f_{SL} is more shallow. In summary, the

series resonant frequency is lowered by the addition of a series inductance which increases the total equivalent circuit inductance. Because the reactance vs frequency curve is more shallow in the vicinity of f_{SL} , the oscillator frequency

is able to be pulled more easily, but stability suffers proportionately.

If both a voltage-controlled capacitance and an inductance are connected in series with the crystal as shown in Figure 31, a wide deviation VCXO is realized.

By making X_{LS} larger than X_{CS}, the resultant resonant frequency is lowered;

as X_{LS} is increased the tuning effect of the varactor diode becomes greater

$\left(\frac{dz}{df} \text{ at the operating point is lower} \right)$. A qualitative measure of frequency

instability in the above series combination can be obtained by comparing the magnitude of L_S to the crystal-unit effective inductance.

The specifications of the SPVD crystal unit were determined to be the following:

1. Channel 1: 20.690000 MHz, Channel 2: 20.710000 MHz

2. Temp. Tolerance -30° to 60°C ±.003%

3. Calibration Tolerance .0025% @ 25°C

4. Holder HC-32/U

5. Series Mode

The crystal frequency was specified after several circuit parameters were defined. First, the bias on the varactor diode is made as large as possible to reduce temperature-induced effects on the diode capacitance. Originally the tone-summing OP-AMP was AC coupled to the varactor diode modulator, but subsequently DC coupling is employed to reduce startup transients. The OP-AMP output is limited to about 6v max (V_{DD} = 6.7v) before saturation occurs; by selecting a center frequency bias of about 4.5 volts, a maximum modulation of ±1.5v is permitted. Since the OP-AMP now supplies the center frequency biasing, the 13K and 39K biasing resistors are no longer required in the circuit.

In an effort to achieve reasonable linearity of the frequency modulated tones, the target modulation sensitivity of .5v/5 KHz deviation (@ f_o) was chosen. Because the log-log plot of varactor reverse bias vs varactor capacitance is not linear, a smaller voltage swing impressed across the varactor was assumed would produce less nonlinearity in the modulated tones. Series inductor L_S was increased until the desired modulation sensitivity resulted; at this point, the oscillator operated 5 KHz below the marked crystal frequency. Thus the specified crystal frequency became 5 KHz higher than the actual desired channel frequency (divided

by 2).

The temperature crystal tolerance is certainly not typical of a precision quartz resonator unit since the temperature drift of L_S and C_S will be rather large in comparison to the crystal.

The final circuit configuration is shown in Figure 32. Parasitic oscillations resonated by the varactor diode (C_S) and the series inductance (L_S) are suppressed by the 47 KΩ resistor shunting L_S. To prevent oscillator moding, (circuit operation at a higher frequency determined by the series coil and the shunt capacity of the quartz crystal), the series combination of the .02 µF capacitor and the 3.9 KΩ resistor shunts the crystal. It was noticed that when using a wideband receiver (100 KHz) the demodulated tones contained a damped sinusoid following each first derivative discontinuity of the baseband signal. Using fourier analysis, complex modulating waveforms when frequency modulated generate high sidebands; should sidebands coincide with an undesired crystal mode, spurious responses occur. Even though these higher sidebands exist, they are ignored by the fairly narrowband SPVD receiver eliminating the need to generate and sum sinusoids instead of easily produced square waves for the tones.

Numerous attempts were made to alter the oscillator configuration for the purpose of obtaining higher stability and/or greater efficiency. However, temperature cycling tests revealed a general lack of improvement over the basic oscillator design. The frequency drift characteristics due to temperature variations are listed in the RF amplifier section of this report while the oscillator tuning steps are described in the SPVD Transmitter Tuning Procedure section.

Several circuit improvements seem at least conceptually plausible. After temperature vs frequency data is taken on a number of units, temperature compensating
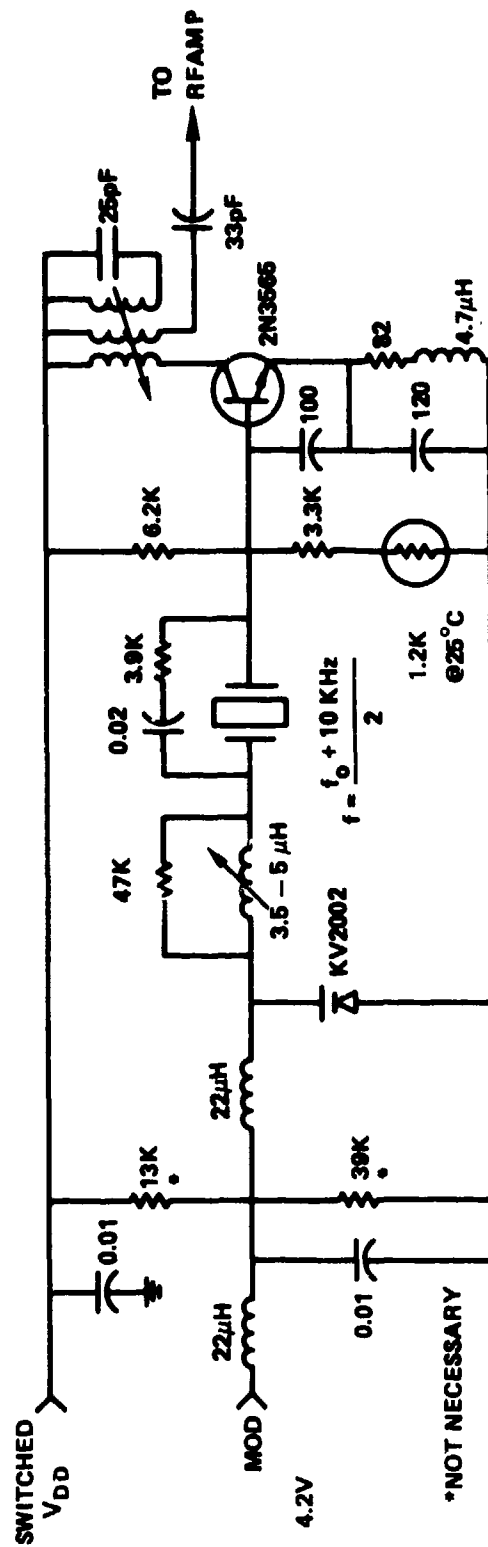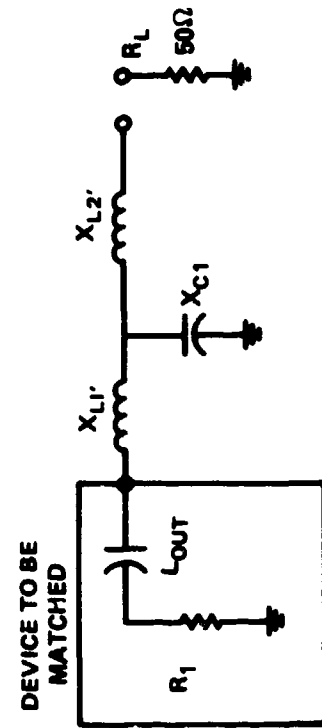
FIGURE 32. OSCILLATOR SCHEMATIC.

FIGURE 33. MATCHING NETWORK D (EQUIVALENT CIRCUIT).

components could be utilized to improve frequency stability. For example, a thermistor might be inserted in the bias circuit for the varactor diode, or capacitors with certain temperature coefficients could be used in the base/emitter circuit of the oscillator. To reduce frequency drift due to battery voltage changes, the 4 volt regulator may somehow be tied into the varactor bias circuit. Also, oscillator efficiency could see improvement through the use of a field effect active element instead of the bipolar transistor; however, it is anticipated that a high battery voltage would be necessary. With such a device, the oscillator configuration of References 11 and 12 may be applied leading to both greater frequency stability and efficiency.

Transmitter Design

The transmitter (RF power amplifier) supplied with the original SPVD suffered from temperature instability and had a high frequency amplitude modulation superimposed on the carrier. Mr. P. J. Lizzi, an FAA engineer, suggested that the transmitter be designed in accordance with Motorola Application Notes AN-267 (Matching Network Design with Computer Solution)[13] and AN-282A (Systemizing RF Power Amplifier Design).[14] Reference 14 describes the means to determine the large signal input and output impedance of the transistor while Reference 13 provides a solution for various matching networks. It was assumed that the RF Amplifier would be driving a 50Ω antenna (the 20 production SPVD antennas were not 50Ω as originally expected but varied from several ohms to about 30 ohms depending on the hole environment). A later discussion will indicate how this discrepancy was treated.

The first parameter needed to design the RF amplifier output matching network is the parallel equivalent load resistance at the desired power level. Using equation 2 of Reference 14

$$R_L' = \frac{(V_{CC} - V_{CE}(sat))^2}{2P}$$

Power = .1 watt

V_{CC} = 6.7 volts

$V_{CE}(sat)$ = 1.5 volts

$R_L' \approx 135\,\Omega$

From the data sheet for the 2N3866, the parallel equivalent output capacitance is about 7pF.

Using the formula below, we convert the equivalent parallel resistance and capacitance into their series equivalents.

$$R_S = \frac{R_p}{1 + \left(\frac{R_p}{X_p}\right)^2} \quad \text{and} \quad X_S = R_S \frac{R_p}{X_p}$$

$$X_p = \frac{1}{(2\pi)(41\times10^6)(7\times10^{-12})}$$

$$R_S = \frac{135}{1 + \left(\frac{135}{554}\right)}$$

$$X_p = 554\,\Omega$$

$$X_S = \frac{108 \cdot 135}{554}$$

$$R_S = 108\,\Omega \qquad X_S = 26.4\,\Omega$$

Of the four matching networks presented in Reference 13, Network D was recommended by Mr. Lizzi as yielding the highest collector efficiency. It also is useful when matching impedance of less than or greater than 50 ohms. Figure 33 below illustrates network D.

Assuming a Q of 10, the computer solutions indicate that:

$$X_{L1} = 1100\Omega \qquad \text{and} \quad X'_{L1} = X_{L1} + |X_{cont}|$$

$$X'_{L1} = 1126\Omega$$

$$X_{L2} = 730\Omega$$

$$X_{C1} = 430\Omega$$

Converting these impedances to component values, we have

$$L_1 \approx 4.37 \ \mu H$$

$$L_2 \approx 2.83 \ \mu H$$

$$C_1 \approx 9pF$$

Reference 13 states that tuning of the matching network may be accomplished by using a variable capacitor for C1. In the SPVD units L1, L2, and C1 are variable since several unknowns still existed, i.e., antenna characteristics and adjustment of transmitter power. Applying the coil winding formula below, L1 and L2 were fabricated.

$$L \ (\mu H) = \frac{n^2 \ r^2}{9r + 10\ell} \times 10^{-6}$$

r = radius of winding
n = no. of turns
ℓ = coil length

L1 - 5/16 dia. form, 23T, #28 w/o slug L_1 = 3.3 μH

L2 - 5/16 dia. form, 17T, #25 w/o slug $L_2 \approx$ 1.8 μH

C1 - variable capacitor 4 to 24pF

The initial SPVD RF transmitter is shown schematically in Figure 34.

Capacitors C2 and C3 AC couple the oscillator stage to the RF amplifier and the matching network to the antenna, respectively. The 51Ω base resistor provides the necessary bias for proper Class C transistor operation, while the 100μH inductor effectively blocks the RF drive signal from being shunted to ground thru the 51Ω resistor. The 10μH RFC inductor supplies the DC energy to the collector circuit of the transistor while preventing the output RF signal from being shunted to AC ground. Two capacitors are inserted across V_{CC} and ground to insure good AC ground on V_{CC}.

The choice of coupling capacitor C2 was arrived at empirically. First a 220pF capacitor was used; this resulted in an uncontrolled AM spurious oscillatory mode. At 50pF the AM oscillations could be eliminated and when the matching network was peaked, the resulting power was 200mw @ 63ma (current includes about 16ma for the oscillator/doubler) yielding an efficiency of about 47%. However, adjusting the matching network to an output level of 100mw, overall efficiency dropped to 34%. The optimum value of C2 appeared to be 33pF, at this point the AM spurious oscillation was less of a problem and at an output of 100mw, efficiency was 38%. A value of 25pF resulted in slightly higher efficiency but at the expense of higher harmonic content at 3 and 4 times the fundamental frequency.

As expected the power output of the RF amplifier could be adjusted by detuning the matching network from the "peaked" condition. Much of the early experimentation in tuning and temperature tests were conducted without the use of a spectrum analyzer. It was later discovered that the AM spurious oscillatory mode could be induced by various tuning combinations. This degenerate oscillation, characterized by sidebands spaced 2 MHz apart, actually increased efficiency and worsened frequency stability. Most the early temperature tests were invalid because of this undetected
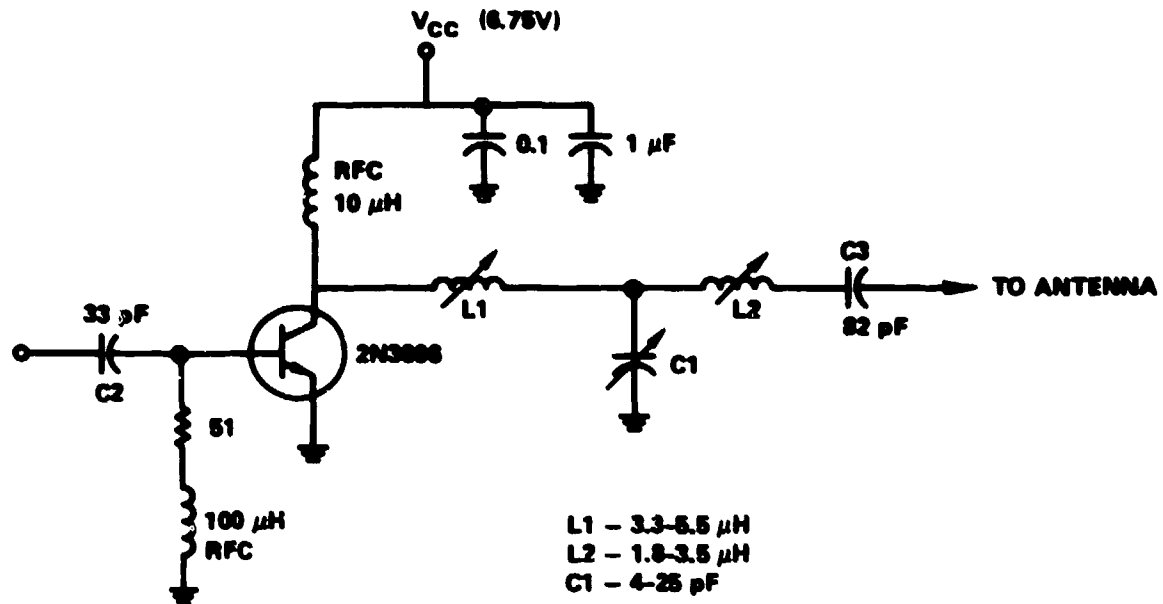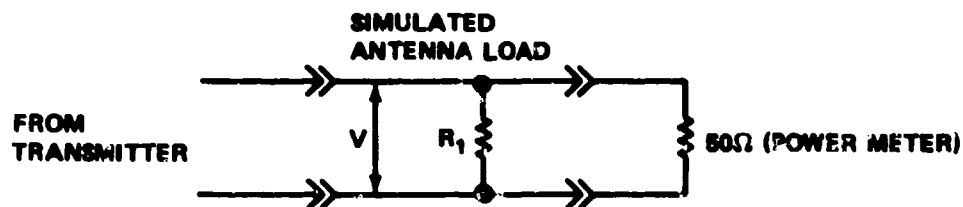
FIGURE 34. INITIAL SPVD RF TRANSMITTER.

L1 – 3.3-5.5 μH
L2 – 1.8-3.5 μH
C1 – 4-25 pF

FIGURE 35. POWER METER TEST SETUP.

anomally. The power meter cannot discriminate between various frequency signals and apparently the AM sideband was adding power in a manner that increased efficiency. Once the spectrum analyzer was available, the tuning procedure became one of getting maximum efficiency at 100mw and, at the same time, minimizing subharmonic and harmonic content of the RF signal.

At this point in time the transmitter alone was temperature cycled to determine the effects on the oscillator/doubler due to changing load conditions (input impedance variations of the RF amplifier) and also get a temperature vs power output profile of the transmitter. Table X summarizes the results, where the current and efficiency include both the oscillator/doubler and transmitter even though the transmitter was the only item temperature cycled.

TABLE X. SPVD RF AMPLIFIER POWER CHARACTERISTIC VS TEMPERATURE

T (°C)	Power (mw)	Current (ma)	Frequency (MHz)	Efficiency (%)
17	105	39.5	41.40020	40
60	98	39	41.40020	38
70	96	39	41.40020	37
-10	94	38	41.40020	37
-30	84	37	41.40020	34
-40	78	36	41.40020	32
20	104	39	41.40020	40

From the data in Table X, the power output of the RF amplifier dropped slightly as temperature increased and fell off more significantly at lower temperatures. This is no cause for alarm since the oscillator/doubler output increases below 20°C. It is worthwhile noting the oscillator/doubler frequency was not pulled due to temperature variations in the RF amplifier.

The trouble began when the transmitter, tuned for 100mw into 50Ω, was connected

to the SPVD antenna. The antenna did not present a 50Ω load to the transmitter as previously assumed. When placed in a dry hole, the antenna impedance was about 30Ω but it dropped to several ohms when submerged in a roadway hole filled with water. Once the transmitter was activated and the 30ms transmission was complete, the RF amplifier remained oscillating on its own. Because current consumption was about 20ma, the SPVD battery would be discharged in short order.

The first efforts in preventing this self oscillation resulted in the placement of ferrite shield beads in two locations. One replaced the 100μH RF choke in the base circuit of the 2N3866. The other was placed on the lead of the oscillator-transmitter coupling capacitor C2. This did not, however, eliminate the oscillation completely. The sustained oscillation involved the base circuit of the 2N3866 transistor and included the tank components of the oscillator/doubler but not the oscillator itself. Therefore it was not an "on-channel" signal, but centered several megahertz below the channel frequency.

The elimination of this problem seemed to point toward detuning the 2N3866 base circuit when transmission was not to occur. A varactor diode has a voltage dependent capacitance characteristic in which the greater the reverse-bias on the diode, the less capacitance appears at its terminals. Thus the varactor diode (identical to the one used in the modulator) was connected from the switched V_{CC} line that powers the oscillator/doubler to the base lead of the 2N3866 transistor. During the 30ms transmission the varactor diode capacitance is about 15pF but with the oscillator/doubler unpowered and a reverse bias of 1 volt the varactor capacitance rises to 35pF. With a reverse bias of .25 volts the capacitance is at least 80pF. Apparently, this additional capacitance during transmitter de-activation detunes the base circuit sufficiently to eliminate the sustained transmitter oscillation. Out of curiosity, the ferrite shield beads were removed from the

circuit leaving just the varactor diode in place. The transmitter did break into the degenerate sustained oscillatory mode indicating both the varactor diode and the ferrite beads are necessary in the circuit.

Next on the agenda was to determine how to tune the matching network of the transmitter so the large antenna impedance variation would be accommodated. Also a measurement technique was needed to get a figure of RF power reaching the antenna when inserted in various hole environments. To accomplish the latter, a 50ma current meter was connected in series with the SPVD battery to measure the DC current drawn by both the oscillator/doubler and the transmitter. Next, the meter was mounted to an antenna lid that was fitted with a plexiglas window. Thus the current could be read even though the SPVD unit was assembled as a watertight package. The entire RF section of the SPVD was powered for continuous operation.

A dummy antenna was fabricated (details are in the SPVD Transmitter Tuning Procedure), being a 22" length of RG-58 coaxial cable having male BNC's at both ends and the capability for shunting one end with a fixed resistor. The non-resistor end was connected to the transmitter output lead and the other end connected to a 50Ω power meter having a full scale setting of about 30mw. Assuming that both the fixed resistor and the 50Ω power meter appear resistive to the transmitter, a calculation could be made to determine the power dissipated in the fixed resistor at a particular current since we know the power dissipated in the 50Ω power meter. Illustrated in Figure 35 is the setup. The equation used to determine power into the fixed resistor is:

P_1 = power dissipated in fixed resistor (unknown)

P_2 = power dissipated by 50Ω power meter

$$P_1 = \frac{V^2}{R_1} \qquad P_2 = \frac{V^2}{50}$$

93

$$P_1 R_1 = P_2 \cdot 50$$

$$P_1 = \frac{50 \cdot P_2}{R_1}$$

The procedure now used was to tune up the transmitter to an assortment of fixed resistor values for 100mw and then place the SPVD unit in both the "dry" and "wet" holes. In each environment the d.c. current was recorded, the current being an indication of RF power dissipated by the antenna. In Table XI the results are summarized as the resistor was varied remembering that with each resistor tried the matching network was tuned for 100mw at about 40ma on the bench.

TABLE XI. TRANSMITTER CURRENT IN ROADWAY HOLE ENVIRONMENTS FOR VARIOUS TUNING CONDITIONS.

R$_1$ (Ω)	Hole Environment Current (ma)	
	Dry	Wet
33	42	20
10	>50	30
6.8	37	33
5.6	37	42
4.7	38	45
3.9	30	>50
2.7	24	>50

From the data in Table XI the best tuning resistance of R$_1$ was 5.6Ω for a balanced power dissipation.

The validity of this tuning approach was substantiated in the first several SPVD units assembled. Ranges were generally 600 to 700 feet for a dry hole environ-

ment and 450 to 600 feet with the SPVD unit submerged in water. However, not all remaining units were this balanced indicating that due to transmitter/antenna variations, a more personalized tuning technique might be employed if sufficient time and funds are available. Each of the 20 SPVD units did exhibit ranges of at least 500' in the dry hole environment meeting the design goal.

As a final temperature performance check, an SPVD RF module was operated from +70°C to -40°C and the results are summarized in Table XII.

TABLE XII. RF OSCILLATOR/TRANSMITTER TEMPERATURE PERFORMANCE

Temp (°C)	Freq MHz	RF PWR (mw)	Current (ma)	Total Power (mw)
32	41.410113	11.1	40	110
70	41.410137	9.6	40	95
10	41.411010	11.5	39.8	114
-15	41.411752	11.6	38.9	115
-30	41.412100	11.2	37.8	111
-40	41.412240	11.0	36.5	109
28	41.409948	10.8	39	107

In this test, the SPVD battery was external to the environmental chamber and the dummy antenna mentioned previously coupled the transmitter output to the power meter or the 50Ω frequency counter.

We observed,first of all, the RF frequency rose slightly as the temperature was increased to +70°C; the power, however, dropped about 14% with a corresponding drop in efficiency. At the low temperature extremes, output power increased slightly as efficiency rose also. The RF frequency gained about 2 KHz; this does not cause much concern since the battery terminal voltage will drop with lowering temperature and the frequency drift will be partially cancelled.

Possible areas of improvement seem to be contingent on a higher battery voltage. With such a case, a power FET or MOSFET could be employed requiring less input drive from the oscillator section. Also references 16a and 16b present techniques for higher efficiency if the appropriate drive signal could be generated.

Figure 36 is a complete schematic diagram of the SPVD Oscillator/Transmitter.
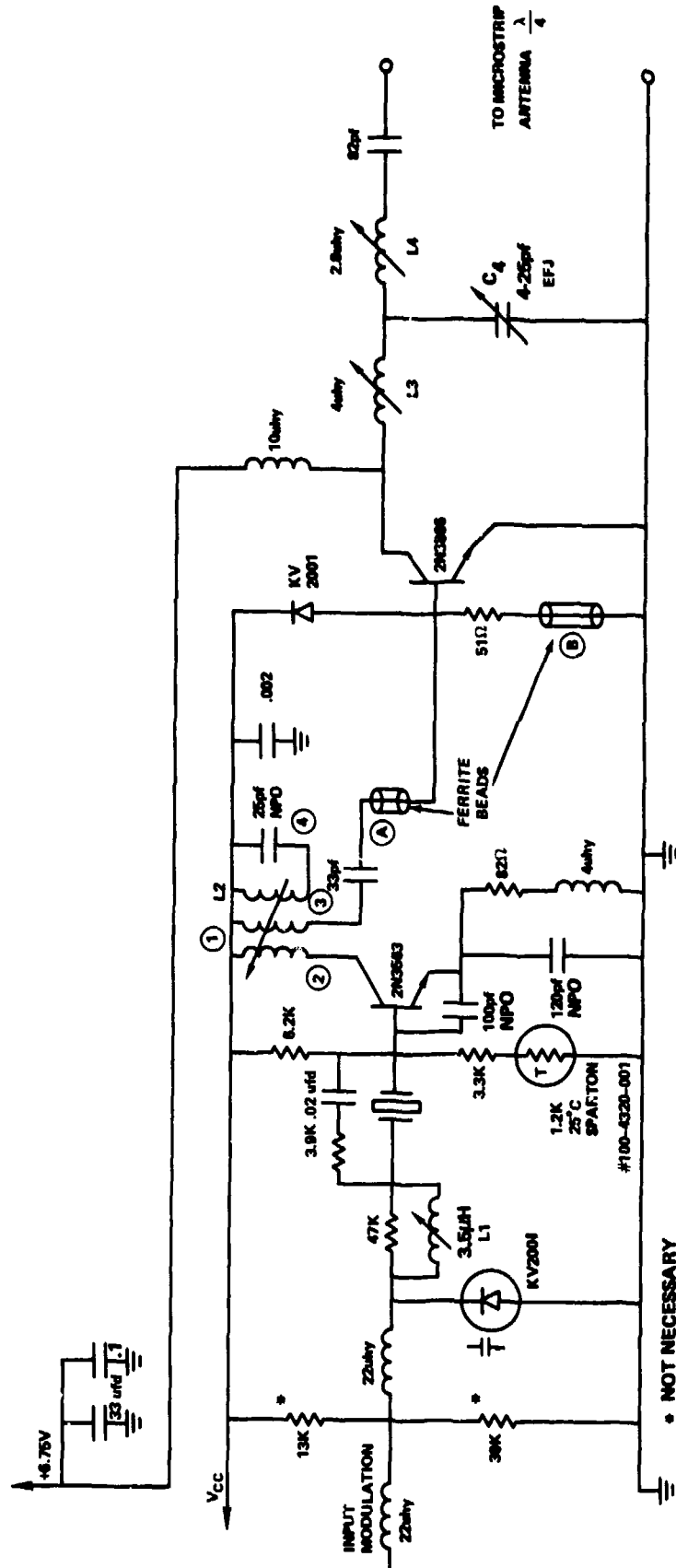
FIGURE 36. SPVD OSCILLATOR/TRANSMITTER SCHEMATIC DIAGRAM

97

SPVD Transmitter Tuning Procedure

A. Unit and Setup Preparation

    1. Make up a dummy antenna cable as follows:

        a. Cut a 50Ω coaxial cable to a length of 22".

        b. Install a male BNC connector to one end of the cable.

        c. To the other end, solder a 5.6Ω resistor from the inner conductor
to the shield.

        d. Solder a BNC (male) connector across the 5.6Ω resistor.

    2. Connect the dummy antenna (non-resistor end) to the coax cable of the
transmitter board using a barrel BNC connector.

    3. Couple the resistor end of the dummy antenna to a 50Ω RF power meter
which is set to indicate about 30mw full scale.

    4. Remove the transmitter/sensor assembly from the battery housing so that the
components on the transmitter board are accessible.

    5. Adjust the following inductors to these initial positions: L1 - minimum
inductance (slug screwed down as far as possible); L2 - adjusted to about 1/3 up
from the bottom of the form; L3 - minimum inductance; and L4 - maximum inductance.

    6. Power up the SPVD unit as shown in Figure 37 using a mercury battery
identical to the batteries of the SPVD.

    7. Place a DIP-CLIP on IC 4070BE and connect a clip lead to pin 6.
NOTE: An external battery is used almost exclusively for the tuning procedure
because the actual SPVD battery compartment is internally fused at 1 amp. Thus,
any inadvertent shorting of the battery will blow the fuse and necessitate a 15-30
minute fuse replacement endeavor.
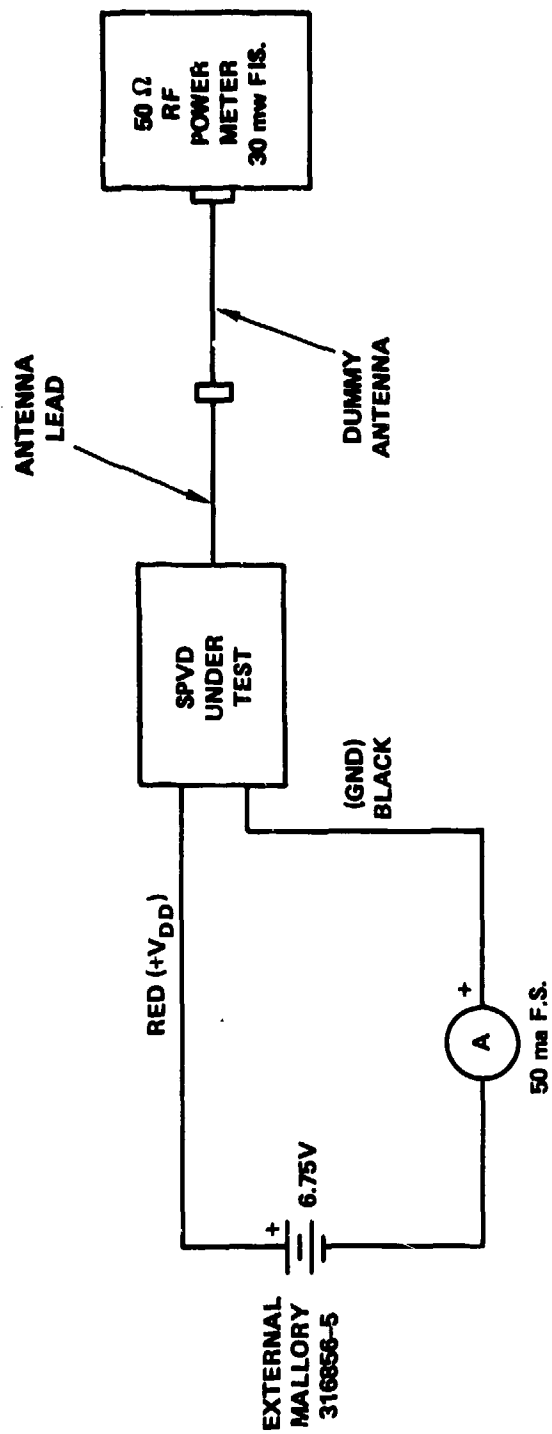
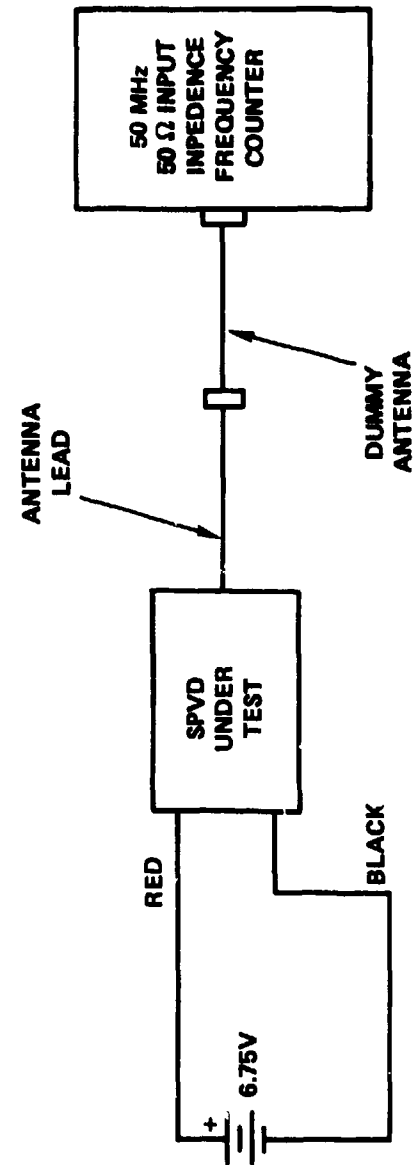FIGURE 37. TRANSMITTER TUNING SET UP I

FIGURE 38. TRANSMITTER TUNING SET UP II

8. Monitor the Vehicle Presence (V.P.) line from the sensor module. If V.P. is low (the sensor has nulled properly) connect the other end of the clip lead on pin 6 (4047BE) to V_{DD}(+). However, should V.P. be high (sensor not nulled) connect pin 6 to ground. This will activate two tone generators and power up the transmitter section. At this point the current drain should be at least 15ma which is required by the RF oscillator even if everything else is misaligned.

B. Power Output Adjustment (Initial)

9. Vary C4 to get a maximum deflection on the power meter.

10. Adjust L2 to get highest power meter indication.

11. Repeat 9 and 10 until power will not increase. A reading of at least 11mw should be observed at a minimum current of 40ma.

12. Slowly increase the inductance of L3 and adjust C4 for maximum power delivered to the power meter. The objective here is to obtain a reading of 11.5mw on the power meter with the largest inductance value of L3; the corresponding current will be about 40ma.

13. Repeat 12 until the objective is realized. If in adjusting C\, 11.5mw cannot be obtained, decrease the inductance of L3 and readjust C4 until 11.5mw is obtained.

14. Repeat step 10.

C. RF Frequency and Deviation Alignment

14. Remove the ammeter from the battery circuit and connect the resistor end of the dummy antenna to a 50Ω - input frequency counter capable of reading at least 50 MHz. The setup is depicted in Figure 38.

15. Adjust L1 until the proper frequency is obtained; for channel 1 it is 41.37 MHz and for channel 2, 41.41 MHz.

16. For the deviation checkout/adjustment, it is assumed that V.P. is low; if the sensor does not null in its current position, a temporary jumper from V.P.

to ground will simulate a nulled sensor condition. Now pin 6 (4047BE) is connected to V_{DD} and the 4100 Hz tone oscillator, the 5500 Hz oscillator, and the transmitter will be activated.

17. The frequency deviation limits are checked by inhibiting the tone oscillators in a particular output state condition. Table XIII summarizes the 4 possible output combinations for the two inhibited tone oscillators and the corresponding significance of the combination with regard to the modulation.

XIII.   Transmitter Output for Selected Tone States

Combination Number	4100 Hz Output Q	5500 Hz Output Q	Carrier Frequency Significance
1	L	L	Upper Frequency Deviation Limit
2	L	H	Center Frequency
3	H	L	Center Frequency
4	H	H	Lower Frequency Deviation Limit

Because the tone generators are prevented from oscillating the transmitted signal will be an unmodulated carrier.

18. To inhibit a tone oscillator, connect the node common to both fixed resistors in the timing circuit of the 4047BE to ground. The output of the 4047 will result randomly in a high or low state. Both the 5500 Hz and 4100 Hz tone generators must be jumpered to ground.

19. It is desired to realize a ±5KHz deviation. That translates for Channel 1 - to an upper deviation limit of 41.375 MHz and a lower limit of 41.365 MHz while for Channel 2 it is 41.415 MHz and 41.405 MHz respectively.

20. The frequency deviation is function of several parameters: (1) the bias point on the varactor diode, (2) the amount that the crystal is pulled below its natural resonant frequency (the farther the crystal is operated from its series resonant

point the greater its sensitivity to frequency modulation), and (3) the gain of the tone summing OP-AMP which directly controls the modulation amplitude. Since a change in the OP-AMP gain alters the bias point on the varactor diode, it is necessary to retune L1 to achieve the proper center frequency after a gain change has been made.

21. Insert a 20KΩ potentiometer (initially adjusted to about 12KΩ) between the inverting input of the OP-AMP (pin 2) and its output (pin 6), in place of the fixed resistor.

22. Apply Step 18 to the 4100 Hz and 5500 Hz oscillators to obtain combination #2 in Table XIII. Now adjust L1 for the proper center frequency for that channel.

23. Apply Step 18 to both of the above oscillators to achieve combination No. 1 in Table XIII. There should be a 5 KHz increase in RF transmitter frequency. If the frequency change is less than 5 KHz, increase the pot resistance until half of the frequency deviation deficiency is eliminated.

24. Repeat Step 22.

25. Repeat Step 23 and 24 as often as necessary to get the 5 KHz increase from the proper center frequency. As can be expected if the deviation is too large the pot resistance must be decreased sufficiently to where 23 and 24 can be applied.

25. With the positive going deviation appropriately adjusted, check the negative going deviation limit by applying step 18 to achieve combination 4 in Table XIII. It should result in a 5 kHz decrease in transmitter frequency. The frequency deviation limits will, in all likelihood, not be exactly symmetrical about the center frequency of the channel. The 20 SPVD units had deviations ranging from about ±5 KHz to ±5.25 KHz.

26. Once the proper frequency deviation is obtained at the specified channel

frequency insert permanently a fixed resistor of equal value to the potentiometer. It is recommended that a 7 KΩ fixed resistor and a 5 KΩ potentiometer be used as the feed-back element of the OP-AMP in any additional SPVD units that may be fabricated.

27. As a final check, repeat 18 for combinations 1, 2, and 4 to ensure that the fixed resistor is the proper value.

D. Adjustment of the Tone Frequencies

28. Connect a frequency counter to the output of an SPVD control box receiver.

29. Remove the shorting jumper from the 5500 Hz oscillator (4100 Hz oscillator still inhibited). Adjust the 5K potentiometer associated with the 5500 Hz oscillator until the frequency counter in 28 reads 5505 Hz.

30. Inhibit the 5500 Hz oscillator and remove the shorting jumper from the 4100 Hz oscillator. Adjust its corresponding pot to get a tone frequency of 4104 Hz.

31. Jumper the Under Voltage (U.V.) output of the SPVD sensor to $V_{DD}(+)$. This will activate the lowest tone generator (5500 Hz oscillator still inhibited). Now adjust the 3000 Hz oscillator pot for a tone frequency of 3003 Hz.

E. Final Adjustment of Transmitter Power

32. Reinsert the ammeter, remove shorting jumpers on all tone generators, and adjust L1 for the proper channel frequency.

33. Disconnect the dummy antenna from the frequency counter and connect it to the power meter which is set for 30mw f.s. The SPVD sensor should be positioned so that the sensor is nulled (V.P. is low). After sensor nulling is complete, the jumping of pin 6 to V_{DD} again activates the tone generators and transmitter.

34. Maximize power by adjusting L2. Tune for 11.5mw on the power meter with the largest possible value of L3 by alternately tuning L3 and C4 for maximum power.

103

The current should be about 40ma.

35. Now disconnect the dummy antenna from the power meter and adjust L4 for maximum current drain. If the maximum current is less than that of 34, reduce slightly the inductance of L3 until that current level is reached.

F. Final Channel Frequency Tuning and System Checkout

In the following steps, be extremely careful not to short V_{DD} to ground once the SPVD unit is powered by its own battery. Failure to heed the above warning will result in a fuse replacement effort.

36. Connect the SPVD power leads to its internal battery and link the dummy antenna to the frequency counter. Adjust L1 for a carrier frequency of about 500 Hz higher than the aforementioned channel frequencies (900 Hz higher if the SPVD has a new internal battery).

37. Remove the jumper on pin 6 (4070). Connect a pulse generator (0 to 6 volts output) to the V.P. wire. A square wave of 10 Hz is needed. An SPVD control box should have its V.P. indicator alternately flashing at the same rate.

38. If an oscilloscope is externally triggered by the pulse generator, the SPVD receiver output will be a 30ms burst of two simultaneous tones.

39. Momentarily, jumper the U.V. output to $V_{DD}(+)$. The U. V. indicator on the control box will flow as long as the U.V. is high.

40. Remove all temporary wires from the SPVD sensor/transmitter module and install it on the battery compartment.

41. A 0-1ma ammeter should be placed in series with the SPVD power leads and its own battery to determine the quiescent current drain of the entire unit. The current will be less than 400μA for a nulled SPVD (2.7mw).

42. Remove the ammeter and insert the power leads into the battery pos... Cover the terminals with several layers of heavy tape to prevent the terminals from shorting against the ground plane of the antenna.

43. Disconnect the dummy antenna and connect the antenna lead tc the SPVD antenna.

44. Carefully insert the SPVD battery/sensor assembly into the SPVD antenna housing and tighten down the lid with a spanner wrench.

VI. ANTENNA DEVELOPMENT

Introduction

The object of the antenna was to transmit information from the buried SPVD to a remote receiver located in the air. The initial constraints were:

1. Antenna must be contained within existing housing (PVC container ∿37.6 cm x 11.3 cm O.D.) and be compatible with batteries and electronics.

2. Antenna must operate on either/or both frequencies 41.37 MHz 41.41 MHz over a temperature range -30° to + 77°C.

3. Antenna is to be fed by a transmitter whose normal output impedance is 50 Ω and whose peak power is on the order of a few hundred milliwatts.

4. The far field signal is to be omnidirectional in a plane horizontal to the earth and of such amplitude as to be detectable in the existing noise environment and surface conditions of the continental United States.

The initial approach was to continue the reported development of the Phase 1 SPVD[1] where two RF amplifiers were switched to feed two vertically mounted ortnogonal loop antennas. Vertical mounting of the loops was necessary to achieve a vertically polarized far field whose ground wave suffers lower attenuation with distance than does horizontal polorization. The two orthogonal loops were then necessary to achieve omnidirectional patterns on the earth surface. A field test of the system at the FHA Fairbanks Research Center revealed problems with the expected range. Instead of 500 ft ranges predicted the output was barely detectable at much smaller ranges with the SPVD housing on the surface. A background investigation of the loop itenna was then initiated. The problem with loops whose dimensions are much smaller than the wavelength that excites them is two fold. First their efficiency is low because the radiation resistance is much less than the copper loss. Secondly, since the sum of these two resistances is also low, it is difficult to

106

transform power efficiently from the transmitter's output to the antenna. In dealing with the first problem, the loops were made as large as the internal housing would allow in an effort to maximize the radiation resistance. These loops were constructed of 10 skin depths thick conductor on epoxy glass laminate P.C. boards. (See Figure 39)   The width of the conductors was made wide to decrease the conductor loss. Those steps designed to increase the radiation resistance and lower the losses thus increased the antenna efficiency. The second problem was attacked by an analysis of various matching networks and the sensitivity of the resonance match to component changes. Very high Q capacitors were purchased to limit the losses of the matching networks. Although we did not accurately measure the efficiency of this system an estimate of <.1% efficiency through a narrow band of frequencies was the best that could be expected.

The problems of temperature compensation to keep the narrow band of frequencies at the operating frequency was considered when the problem of mutual coupling between the orthogonal loops arose. The plan was to operate one antenna with the other detuned and then reverse the roles, all this to eliminate the mutual coupling. In the face of these difficult engineering problems the decision was made to explore other antenna structures. The experience with the orthogonal loops took us in the direction of a single antenna that provides the omnidirectional vertically polarized pattern. This would eliminate the dual output amplifiers in the transmitter and the switching network needed to get around the mutual coupling problem.

Since the vertical whip had been previously ruled out because of serious detuning in the ground we tried a horizontal loop. The horizontal loop provides the omnidirectional pattern but produces a horizontally polarized electric field. This coupled with the insufficiency of the loop to matching network also made for a marginal communication system.

107
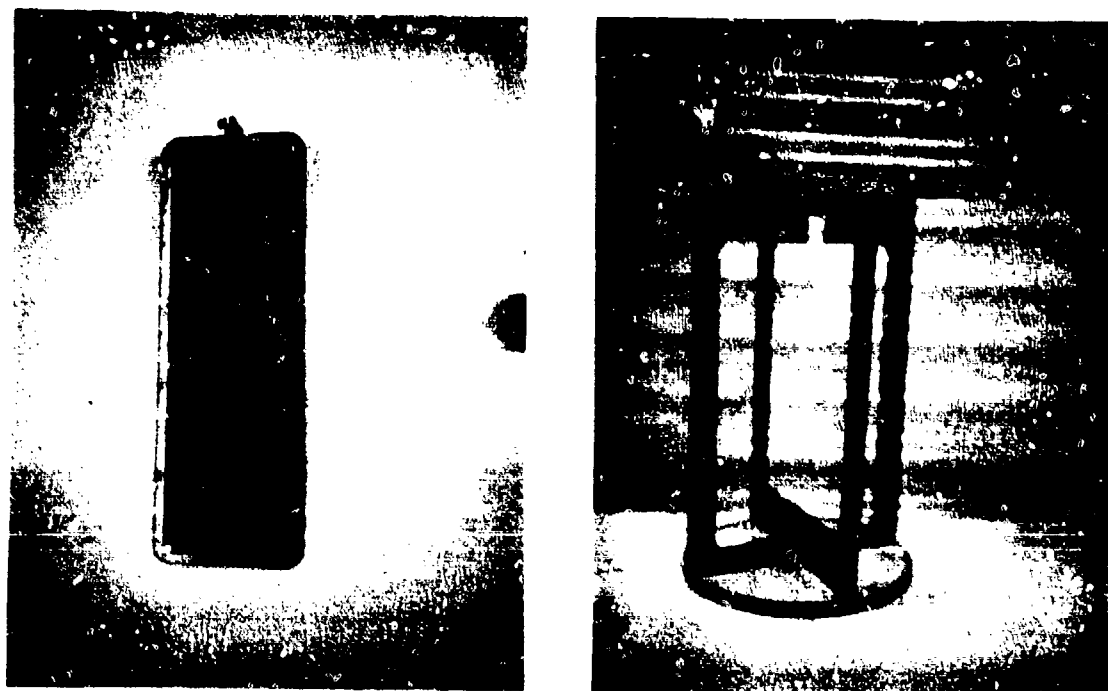
FIGURE 39. EXPERIMENTAL LOOP ANTENNA CONFIGURATIONS.

The antenna problem then became more precisely defined. What we needed was an antenna that had the following properties:

1. Omnidirectional pattern in the plane of the earth.

2. Vertical polarization.

3. High efficiency when combined with the matching network over a reasonable bandwidth.

There is such an antenna[17] under development at NSWC/WOL for use on missiles at microwave frequencies. The antenna called the Micropatch was a development of the microstrip transmission line commonly used in microwave integrated circuits (MIC). This micropatch antenna is fabricated opposite the ground plane of a thin dielectric substrate and is approximately $\lambda/2 \times \lambda/2$ in dimensions. While this would produce an antenna the size of 3.6m x 3.6m at the SPVD operating frequency, it had all of the other desired requisites. At microwave frequencies it is very efficient (>70%), produces an omni pattern with vertical polarization and can be matched directly with a transmission line. Unfortunately, little theory except for some empirical results are available. Fortunately, there exists a vast array of theory concerning the microstrip transmission line. The reason the latter seemed applicable was that we planned to change the $\lambda/2 \times \lambda/2$ dimensions of the micropatch antenna to something like $\lambda/2 \times \ll \lambda/2$ making it look like a microstrip transmission line half-wave resonator. It was felt this long thin line could be fit into the SPVD container through the shortening effects of high dielectric materials and spiraling of the line. The spiraling seemed reasonable because the fields of a microstrip occur at open ends. Simultaneously, some experimental models were built and a theoretical model was devised to explain the experimental results. Long linear resonators were fabricated and after probing the fields associated with these it was evident that the antenna could be structured as a shorted $\lambda/4$ resonator instead of an open ended $\lambda/2$ resonator used in the micropatch. The structures fit better

for the SPVD application because the open end of the resonator could be placed close to the surface of the ground where radiation would be directed outward. The shorted end facing into the earth no longer radiates. And of course, it was 1/2 the length of the $\lambda/2$ resonator. The first success of this approach appeared from microstrip line 1/2" wide cut from a long sheet of epoxy fiberglass PC board, spiraled inside the PVC cylinder and held with tape. This antenna had a vertically polarized omni-pattern, required no matching network for resonant feed and seemed to emit a stronger signal than the best of the previously tried loops. To decide what parameters would optimize bandwidth and efficiency of this structure the theoretical model was developed.

Theory of Development

The underlying philosophy behind the following approach is that we are dealing with a $\lambda/4$ shorted microstrip transmission line shown in Figure 40a and can therefore piece together relevant parts of previously developed theories. The only first order effect resulting from the spiraling of the transmission line shown in Figure 40b, is that the structure will become short compared to $\lambda/10$ and will be incapable of producing a highly directional pattern.

The microstrip guide wavelength is given by

$$\lambda_g = \frac{\lambda_o}{\sqrt{e_r'}} \ (m) \tag{1}$$

where λ_o is the freespace wavelength and e_r', the effective relative dielectric constant, is the result of the manner in which the field distributes itself around the line. In terms of the ordinary relative dielectric constant, e_r

$$e_r' = 1 + q(e_r - 1) \tag{2}$$
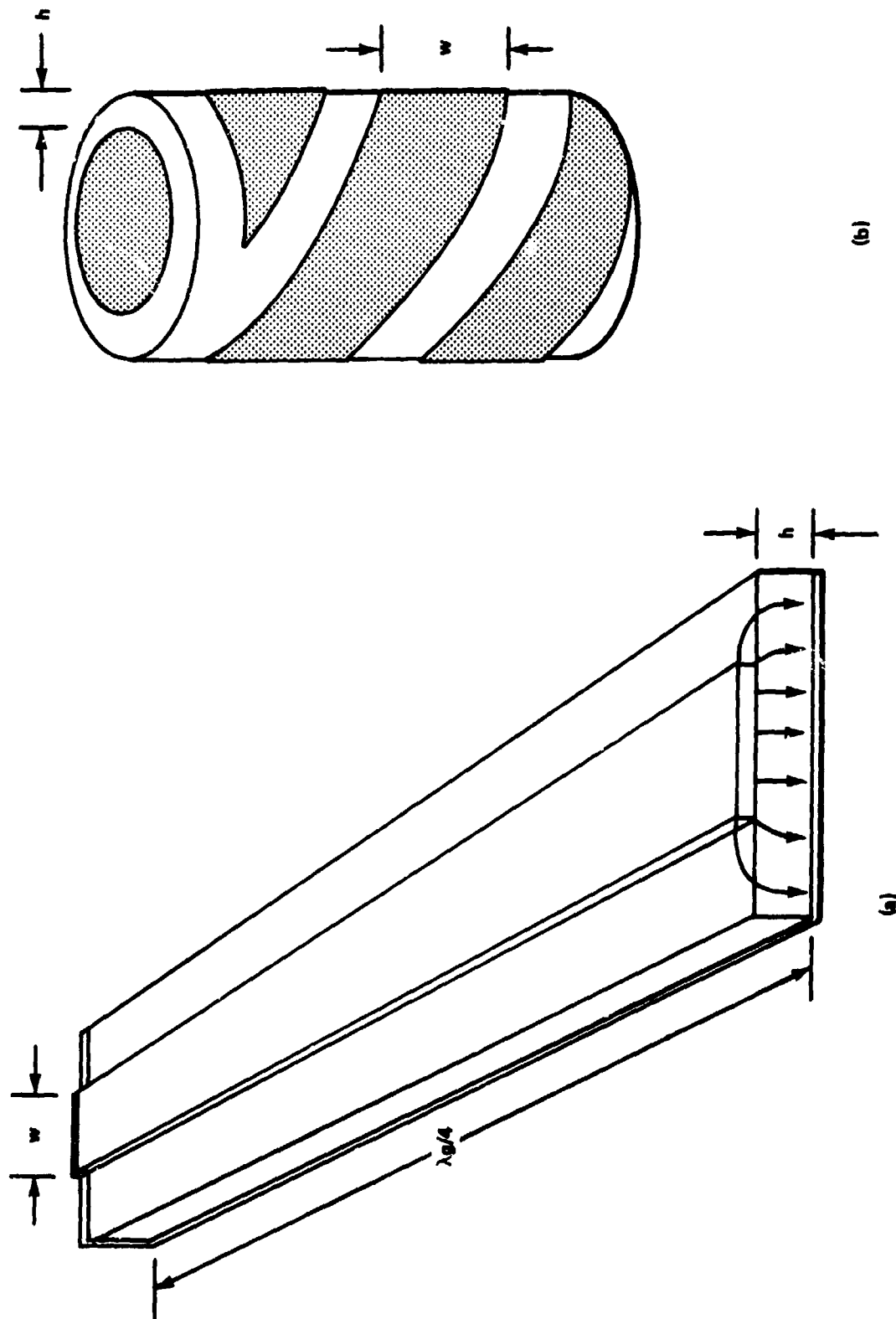
FIGURE 40. (a) LINEAR SHORTED λg/4 MICROSTRIP RESONATOR
(b) THE OMA, A CYLINDRICAL SHORTED λg/4 MICROSTRIP RESONATOR

The filling factor, q, was solved by Wheeler[18] and shown to be a function of the strip width (w) and the dielectric substrate thickness (h). An analytic expression[19] for the case of w > h is given as

$$q = \frac{1}{2} \left[1 + \frac{1}{(1 + 10\frac{h}{w})^{\frac{1}{2}}} \right] \qquad (3)$$

As an antenna the $\lambda_g/4$ shorted resonator will lose energy to three main sinks. They are the radiation into space, the resistive loss of the conductive currents flowing in the metal strips, and the dielectric loss of the displacement currents through the substrate. Expressing the loss factors in the form of Q values where in general

$$Q = \frac{2\pi \; (\text{Total energy stored})}{\text{Energy dissipated per Hertz}} \qquad (4)$$

The conductor loss (Q_c) is given by[20]

$$Q_c = \frac{1580 Z_0 \; w\sqrt{e'_r}}{\lambda_0 (f_0 \rho)^{\frac{1}{2}}} \qquad (5)$$

where Z_0 = characteristic impedance of microstrip line (Ω)

$\quad f_0$ = resonant frequency of the resonator (Hz)

$\quad \rho$ = resistivity of the resonator conductor (Ω-m)

The dielectric loss (Q_d) is given by (20, 21, 22)

$$Q_d = \frac{e'_r}{q e_r \tan \delta} \qquad (6)$$

where tan δ = loss tangent of the dielectric substrate. Combining equations 5 and 6 to yield an overall term for lossy materials yields

$$Q_M = \frac{Q_c \, Q_d}{Q_c + Q_d} = \frac{1580 \, Z_0 w e_r'}{1580 \, Z_0 w q e_r \tan\delta + \lambda_0 (e_r' f_0 \rho)^{\frac{1}{2}}} \tag{7}$$

The radiation from a microstrip line has been discussed by many authors[20, 23, 24, 25] and the radiation Q for a $\lambda/4$ resonator is given by

$$Q_R = \frac{Z_0}{960\pi \left(\frac{h}{\lambda_0}\right)^2 Fe_r'} \tag{8}$$

where

$$Fe_r' = \frac{e_r' + 1}{e_r'} - \frac{(e_r' - 1)^2}{2e_r' \, 3/2} \, \ln \frac{e_r'^{\frac{1}{2}} + 1}{e_r'^{\frac{1}{2}} - 1} \tag{9}$$

Equation 9 is rather cumbersome to carry along and a simple approximation has been found as

$$Fe_r' \simeq \frac{2.4}{e_r'} \tag{10}$$

Utilizing equation 10 in equation 8 the radiation Q becomes

$$Q_R = \frac{Zo \, e_r'}{2300\pi \left(\frac{h}{\lambda_0}\right)^2} \tag{11}$$

The fractional power (22) radiated by the antenna is the antenna efficiency,

$$\eta = \frac{Q_M}{Q_M + Q_R} = \frac{1}{1 + \frac{Z_0 q e_r \tan\delta}{2300\pi} \left(\frac{\lambda_0}{h}\right)^2 + \frac{(e_r' \, f_0 \, \rho) \, \lambda_0^3}{3.63 \times 10^6 \, \pi \, w \, h^2}} \tag{12}$$

The second term in the denominator represents the dielectric loss and the third

term is due to the resistive loss. Thus if these terms can be made negligible compared to 1, the efficiency will approach 100%. The term Z_o is the characteristic impedance of the microstrip line and is used in the form[36].

$$Z_o = \frac{120\pi h}{\sqrt{e_r} \; w \; [1 + 1.735 \; e_r^{-.0724} \; (\frac{w}{h}) - .836]} \qquad \frac{120\pi h}{\sqrt{e_r} \; w[A]} \quad (\Omega) \qquad (13)$$

where $1 < [A] < 2$

Substituting this expression into equation 12 helps to reveal the physical quantities that effect the efficiency.

$$\eta = \frac{.1}{1 + \dfrac{q e_r^{\frac{1}{2}} \tan \delta \; \lambda_o^2}{19.2 \; A \; h \; w} + \dfrac{e_r^{\prime\frac{1}{2}} \; \rho^{\frac{1}{2}} \lambda_o^{5/2}}{210\pi \; h^2 \; w}} \qquad (14)$$

Efficiency increases with frequency $(1/\lambda)$, thicker dielectrics (h), wider microstrip widths (w), and lower dielectric constants (e_r). It can also be seen that the ratio of losses (therefore heat) in the conductors and the dielectric can be changed by frequency and dielectric thickness. Increasing the efficiency is generally done at the expense of bandwidth which will now be considered.

The antenna is a $\lambda_g/4$ resonator whose total Q governs the bandwidth Δf.

$$Q_T = \frac{Q_M \; Q_R}{Q_M + Q_R} = \frac{f_o}{\Delta f} \qquad (15)$$

Inverting and substituting for Q_M & Q_R yields the fractional bandwidth

$$\frac{\Delta f}{f_o} = \frac{1}{Z_o} \left[\frac{2300\pi}{e_r^{\prime}} \left(\frac{h}{\lambda_o}\right)^2 + Z_o \; q \; \frac{e_r}{e_r^{\prime}} \tan\delta + \frac{\lambda_o}{1580w} \left(\frac{f_o \rho}{e_r^{\prime}}\right)^{\frac{1}{2}} \right] \qquad (16)$$

From this equation it can be seen that decreasing the values of tan δ and ρ (which increase efficiency) will decrease the bandwidth.

The bandwidth and efficiency are both functions of common factors making it reasonable to investigate a figure of merit based on their product.

$$\frac{\Delta f}{f_o} \times \eta = \frac{Q_M + Q_R}{\frac{Q_M}{Q_R}} \times \frac{Q_M}{Q_M + Q_R} = \frac{1}{Q_R} \tag{17}$$

$$= \frac{19.2 \; wh\sqrt{e_r} \left[1 + 1.735 \; e_r^{-.0724}(\frac{w}{h})^{-.836}\right]}{\lambda_o^2 e_r'}$$

The figure of merit increases as the square of the frequency. It is also very interesting that this product depends only on the inverse of the radiation Q and is independent of the dielectric loss tangent and the conductor resistivity. To get the most out of any design at a particular frequency, the strip should be as wide as possible, the dielectric as thick as possible and the dielectric constant as low as possible. Because of the underlying assumptions in the theory, the width is limited to be less than $\lambda_o/2$ and the thickness is limited below a value that allows higher order modes to exist. The dielectric constant, of course, has a lower limit of air.

In any design, equation 17 should be considered along with equation 1. Equation 1 allows the antenna to be small by increasing e but from equation 17 this will simultaneously decrease the figure of merit. Once these equations are compromised within the bounds of the design and the figure of merit is maximized, the bandwidth and efficiency can be determined. The maximum attainable efficiency given by equation 14 will then be determined by the lowest loss tangent ($\sim.0001$) and the lowest resistivity (1.7×10^{-8} Ω - m) that is available in materials.

115

The corresponding minimum attainable bandwidth is then given by equation 16 or simply dividing equation 17 by the efficiency. If the required bandwidth is larger than this miminum it can be adjusted by choosing a more resistive conductor or a lossier dielectric, at the expense of efficiency. The purpose of this procedure is to reduce the impedance variation of the antenna throughout the bandwidth thus making it a more reasonable load on an amplifier.

The antenna is excited by means of a coaxial line passed through the ground plane. The coaxial cable center conductor is connected to the middle of the strip width and the outer conductor is connected to the microstrip ground plane. At resonance this feed point presents a resistive impedance to the coaxial cable.

The problem of finding the position along the microstrip that presents a desired impedance has been solved[27] for a λ_4 resonant line. The input resistance R_d at a distance d from the short can be written as

$$R_d = \frac{4}{\pi} \frac{f}{\Delta f} Z_0 \sin^2 \left[\frac{360 d \sqrt{\varepsilon_r}}{\lambda_0} \right] \text{ (ohms)}$$

Antenna Design

The units of all equations are SI units. At this point in the project there was a preexisting well tested PVC cylinder to house the sensor, the signal processor, amplifier and batteries. The question became one of utilizing already crowded space in the interior of the existing cylinder or time to proof a new cylinder of different material. To avoid either of these choices the decision was made to utilize the PVC cylinder that existed as the dielectric and to fabricate the microstrip on it. This decision was based on expediency and not on the best choice of materials from the standpoint of building the best antenna.

The PVC tubing (4.5 OD x 1/4"(.0064m) wall thickness) was purchased in 20 foot lengths and cut to ~14" lengths. Of this, approximately 13" could be utilized by

the antenna, the nest reserved for the screw on cap allowing access to the housed electronics. Measurements were made of the dielectric constant and loss tangent and resulted in values $e_r' = 2.33$, tan $\delta = 0.01$. Equation 1 with e_r substituted for e_r' yields.

$$\lambda g = \frac{7.24}{\sqrt{2.33}} = 4.74 \quad \text{- 1}$$

and therefore a quarter wavelength strip is about 1.19m (47"). A simple geometric calculation of the cylindrical surface indicates that the antenna will have to spiral approximately 3.2x around to reach the height of 13" while extending 47". Figure 41 is a photograph of two prototype antennas, one $\lambda/4$ on the PVC while the other is a $\lambda/2$ internal antenna. The distance between the leading edge of consecutive wraps is 3.89". It was determined empirically that the antenna operates well if the open space between consecutive strips is at least one-half the strip width and not much more can be gained by trying to decrease this dimension. The width (w) of the antenna strip was then fixed at 2.5" (.064m) leaving a gap between strips of 1.4" (.036m). Equations 3, 2 and 1 can now be evaluated as

$$q = \frac{1}{2} \left[1 + \frac{1}{(1 + 10 \frac{0.25}{2.5})^{\frac{1}{2}}} \right] = 0.854 \quad \text{- - - - - - - - - - - - - - - - 3}$$

$$\varepsilon_r' = 1 + 0.854(2.33-1) = 2.14 \quad \text{- - - - - - - - - - - - - - - - - - - 2}$$

$$\lambda g = \frac{7.24}{\sqrt{2.14}} = 4.95 \text{ m} \quad \text{- 1}$$

The corrected value of the antenna length $\lambda g/4$ is 1.24m (48.7"), and was accomodated by narrowing the gap to 1.3" (0.03m). The only other parameter available for choice is the conductor material resistivity. Copper ($\rho = 1.72 \times 10^{-8} \Omega$ - m) was chosen when equation 16 revealed that the bandwidth would be appropriate. The tubes were first threaded to receive the top cap and then plated with 0.002" of copper on

117
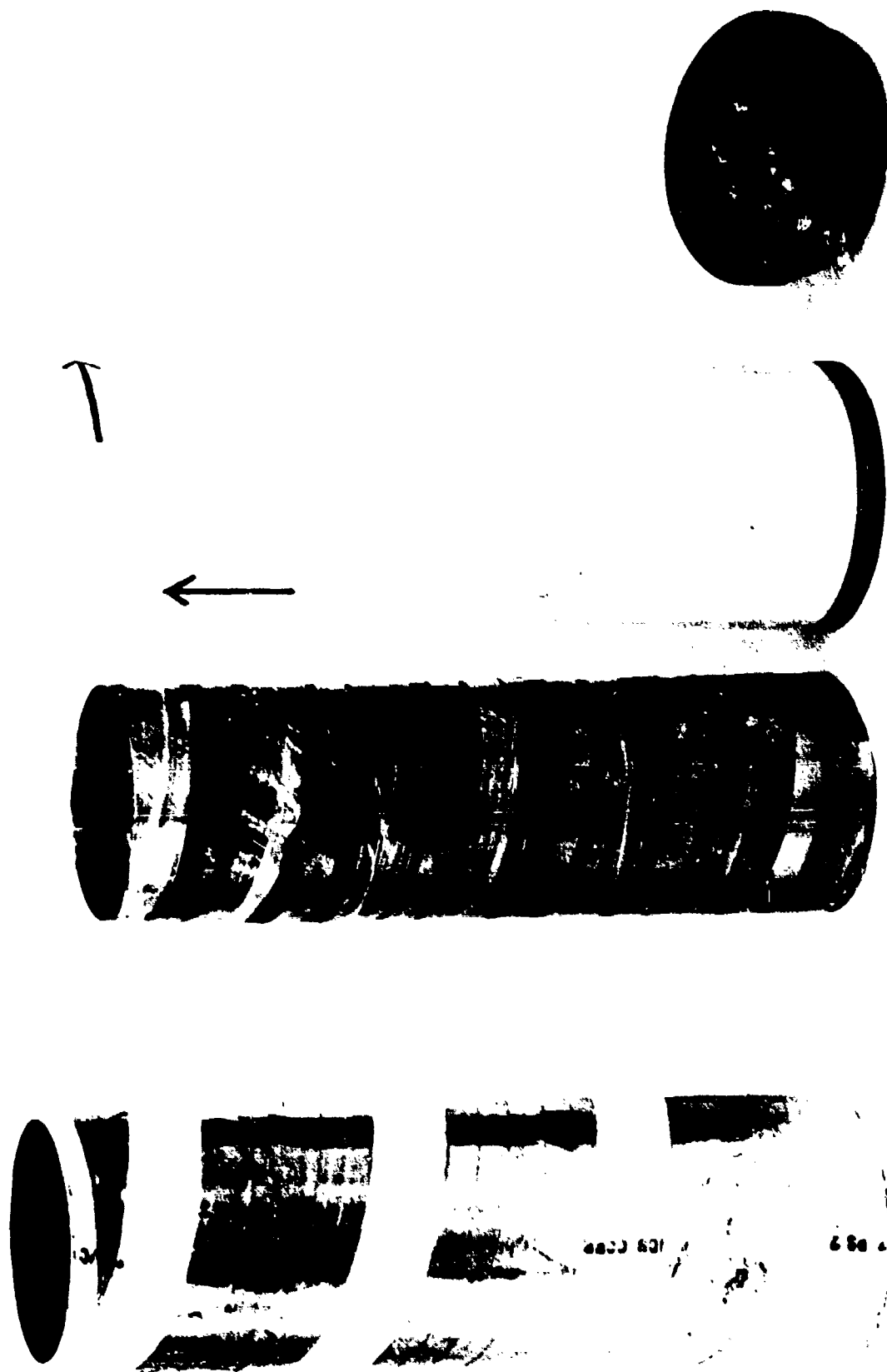
FIGURE 41. PHOTOGRAPH OF PROTOTYPE OMNIDIRECTIONAL MICROSTRIP ANTENNAS.

all sides. The cleaning, sensitizing and plating was done at the Harry Diamond Laboratories, Adelphi, Maryland. The copper on the threaded section of the tube was then removed by dipping that end in an etching solution of 300g $FeCl_2$ to a liter of water. The defining of the antenna strip on the spiral was handled either by masking and etching or by cutting through the 2mil copper with a blade and peeling the excess mechanically. Photo processing would have been preferred but limited resources precluded the development of cylindrical photo processing geometries.

The length of the strip was deliberately made 1/2" longer than the expected 48.7" length. The next step in the process was to insert a 50 Ω coaxial feed cable. To find the position of the cable insertion (the distance (d) from the shorted or bottom of the antenna strip) equation 18 must be evaluated. Since this requires the evaluation of other equations, all necessary equations will be calculated.

$$Zo = \frac{120\pi \ \ .25}{\sqrt{2.33} \ \ 2.5[1 + 1.735e_r^{-.0724}(10)^{-.836}]} \approx 19.9\ \Omega \ \text{---------} \ 13$$

$$\frac{\Delta f}{f} = \frac{1}{19.9}\left[\frac{2300\pi}{2.14}(\frac{.0064}{7.24})^2 + 19.9 \times .854\left[\frac{2.33}{2.14}\right].01 + \frac{7.24}{1580 \times .064}(\frac{41.39 \times 10^6 \times 1.72 \times 10^{-8}}{2.14})^{\frac{1}{2}}\right] \ \text{-----} \ 16$$

$$\frac{\Delta f}{f} = \frac{1}{19.9}\left[0.00264 + 0.185 + 0.0414\right] = .0116 \ \text{--------------------} \ 16$$

$$\Delta f = 0.48 \times 10^6 Hz$$

$$n = \frac{1}{1 + \dfrac{.854 \times 2.33^{\frac{1}{2}} \times .01 \times 7.24^2}{19.2 \times 1.24 \times .0064 \times .064} + \dfrac{2.14^{\frac{1}{2}}(1.72 \times 10^{-8})^{\frac{1}{2}} \ 7.24^{5/2}}{210\pi \times .0064^2 \times .064}} \ \text{-----} \ 14$$

$$n = \frac{1}{1 + 70.1 + 15.6} = 0.0115 \ \text{-----------------------} \ 14$$

$$d = \frac{\lambda o}{360\sqrt{\epsilon r^1}} \, Sin^{-1} \left[\frac{\pi R d \Delta f}{4 \, Z o f o} \right]^{\frac{1}{2}} \text{-- -- -- -- -- -- -- -- -- -- -- -- -- -- 18}$$

$$d = \frac{7.24}{360\sqrt{2.14}} \, Sin^{-1} \left[\frac{\pi \times 50 \, .0115}{4 \times 19.9} \right]^{\frac{1}{2}} = 0.119 \, m \, (4.69") \text{-- -- -- -- -- -- -- -- -- 18}$$

The value of d from equation 18 indicates the 50 Ω coax should be placed 4.69"
from the short. After a hole is drilled and the coax is soldered in place the antenna
is measured by a network analyzer. A typical Smith chart of the antenna terminal
impedence is shown in Figure 42. Here the antenna has been trimmed to resonate at the
proper frequency and the coax has been adjusted to provide a proper match. It can be
seen from the points $(.5 \pm j.5)$ that the 3dB bandwidth of the antenna is 0.51 MHz.
this agrees well with the evaluation of equation 16. The length of the trimmed
antenna agrees to within a few percent of the calculated length as does the position
of the 50 Ω input. The only parameter to be measured is the η of equation 14. The
measurement is the most difficult and probably the least accurate of all; thus two
different methods were utilized.

The first method called the radian sphere method was developed by Wheeler.[28]
An antenna operating in free space can be modeled as dissipating its energy in a
radiation resistance and a loss resistance. If it is then surrounded by a conductive
sphere of sufficient size to allow local fields to continue to exist, the previously
radiated fields will be reflected and its associated radiation resistance disappear.
By measuring the bandwidth of the antenna in these two states it is possible to sep-
arate the two resistive sinks of energy and therefore be able to compute the
efficiency. The computation is as follows. The total Q_t of the resonant antenna is
modeled as

$$Q_t = \frac{\omega L}{R_R + R_L}$$
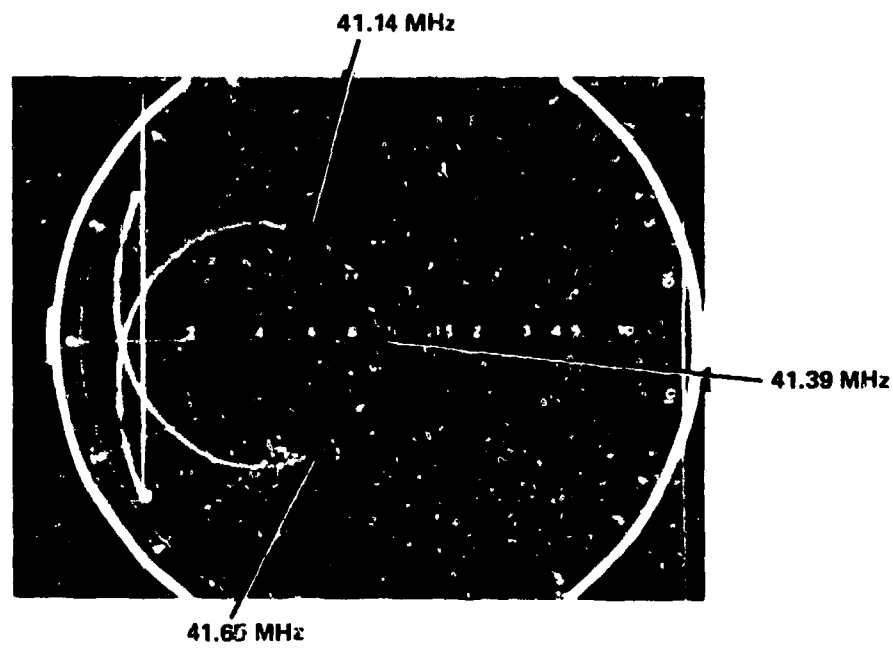
FIGURE 42. SMITH CHART PLOT OF THE SPVD OMNIDI-
RECTIONAL MICROSTRIP ANTENNA.

where Rr is the radiation resistance and $R\ell$ is the loss resistances. The bandwidth which can be measured at the antenna terminals by a network analyzer is related to Q_t by

$$\Delta f = \frac{fo}{Q_t} = \frac{fo(Rr+R\ell)}{\omega L}$$

If the measurement of bandwidth in free space is denoted Δf_1 and that within the radian sphere denoted Δf_2 then

$$\frac{\Delta f_1 - \Delta f_2}{\Delta f_1} = \frac{\dfrac{f_c(Rr + R\ell)}{\omega L} - \dfrac{f_0(0 + R_\ell)}{WL}}{\dfrac{f_0(R_r + R\ell)}{\omega L}} = \frac{Rr}{Rr + R\ell} = \eta ,$$

which is recognized as the antenna efficiency. A radian sphere 7 feet in diameter was constructed (see Figure 43) in the shape of an icosahedron. The antenna bandwidth was measured in the two states but the uncertainty in defining the 3dB points for the measurement only permits putting an upper bound on the efficiency. The factor $(\Delta f_1 - \Delta f_2)$ was nearly zero leading to the conclusion that the antenna efficiency was not greater than a few percent How much less than a few percent the efficiency is was undetermined by this method.

The second measurement for efficiency involved field measurements that were also utilized for pattern and polarization measurements. The antenna was placed upright in the middle of a large (150m x 150m) conducting ground screen. It was then measured to insure that it presented a 50 Ω matched impedance at resonance. Upon exciting the antenna with a known power the signal in the far field was detected. For an input power of -12.5dBm at a distance of 34.2m it was typical to detect -57dBm of vertically polarized power. The detection was made with the aid of a calibrated dipole, transmission line and spectrum analyzer, the gain of which was almost unity at the operating frequency. Horizontal polarized power was measured as less than -80 dBm at this distance, indicating a predominance of vertically polarized
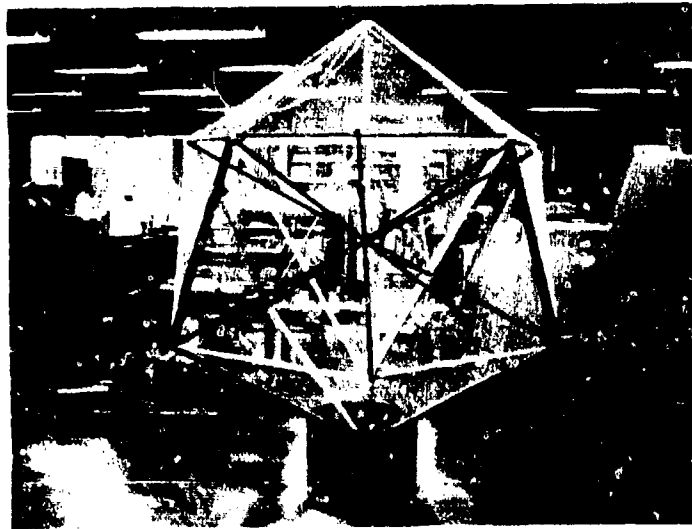
FIGURE 43. PHOTOGRAPH OF THE RADIAN SPHERE.

signal from the antenna. The antenna was then rotated 360° about its cylindrical axis and the received vertically polarized power remained -57 ± 1dBm. This pattern in the horizontal plane parallel to the earth is omnidirectional. The dipole was then raised in a circular arc over the test antenna and the signal power was observed to decrease more or less continously to a value of -77 dBm at the zenith. The radiation pattern is toroidal from the field measurements and resembles a $\lambda/4$ dipole above a conducting ground plane. A directive gain of 3.3 was assigned to it along with a power gain of 2 for the dipole above the ground screen. With these assignments the Friis transmission formula[29] can be used to calculate the efficiency. The Friis transmission formula can be written as

$$\frac{W_r}{W_t} = (\frac{\lambda}{4\pi r})^2 \; G_r \; \eta_t \; D_t.$$

Where W_r is the received power

W_t is the transmitted power

G_r is the power gain of the receiver

D_t is the directive gain of the transmitter

η_t is the efficiency of the transmitter

r is the distance between transmitter and receiver

Transposing and substituting yields

$$\eta_t = (\frac{4\pi r}{\lambda})^2 \; \frac{W_r 1}{W_t G_r D_t} = (\frac{4\pi \times 34.2}{7.24})^2 \; \frac{2.00 \times 10^{-6} mW}{.962 \; mW} \; \frac{1}{2 \times 3.3}$$

$$\eta_t = .019$$

To this point, antenna measurements have been made in the laboratory or above ground. The insertion of the antenna in a earthen hole causes approximately a -10dB change in field strength depending on the soil its moisture content, temperature, depth of immersion, local inhomogeneities and aging of the container in the environment. One could expect alkali, acids and highly conductive salts as part

of the environment. Many serious problems remain to be solved or investigated in this respect. The antennas were buried 3" from the surface in a reasonably moist soil which produced a measured change in the resonant frequency and a change in the terminal resistance. The resonance decreased from 40.39 by approximately 2 MHz and the terminal resistance changed from 50Ω to approximately 15Ω. These changes were well defined allowing us to cut the antenna in the laboratory at 43.38 MHz and match them to an input of 170Ω. In the ground they then resonate at the desired frequency of 41.39 MHz and present 50Ω impedance. Because of the extra loss factor in the ground, the bandwidth increases to approximately 1.9 MHz making the precise cutting of the center frequency not very critical. The required bandwidth to accomodate the two assigned frequencies is .04 MHz. A laboratory simulation of the antenna buried in a hole was devised. One section of an x-Band microwave absorber (carbon loaded foam) was fashioned to fit snuggly around the antenna cylinder and adjusted in height to produce the desired results. Utilizing the inside chamber of the antenna as a source or sink of heat, the temperature was varied from -30° to +77°C and the shift in center frequency and matching impedence was observed. While these remained within the limits of the 1.9 MHz bandwidth available, the test was not considered definitive for the actual environment. In the environment, soil moisture will change its dielectric constant and loss tangent with temperature especially at the ice phase change. Careful exhaustive field testing in different environments over closely monitored temperature ranges will be necessary to define and sort out the detailed effects.

It should be pointed out here that while P.V.C provides a low-cost suitable container to house the SPVD sensor and electronics, it is far from ideal as an antenna dielectric. At high temperatures (~100°C) it shrinks, presumably because of plasticizer loss. A 35 cm tube becomes 34 cm. In the long term this effect may occur at lower temperatures where time and temperature are interchangeable.

This could cause problems with the adhesion of the electroplated copper that forms the antenna conductors. From another point of view PVC is a lossy dielectric relative to a material such as Teflon or Polystrene. This loss term dominates the efficiency which could by a choice of a lower loss material aid in producing an order of magnitude improvement to the antenna efficiency. Increasing the efficiency could result in more range, higher detection probability or longer battery life time for the SPVD. A recommended material would be Teflon-fiberglass $e_r \sim 2.6$ and $\tan \delta \simeq 0.001$.

From a more optimistic point of view, field tests have indicated the system has greater than the 500 foot range detection capability even when the PVC transmitting antenna is tuned far beyond its bandwidth.

To protect the outside copper strip of the antenna several coatings were tried. A PVC cement roll-dip was applied but formed bubbles in the surface and was rejected. Scotch-Grip plastic adhesive #4693 also produced problems in providing a smooth continuous coating. The protective surface that proved most successful was two spray coats of Grey 100S DuPont Acrylic Lacquer Primer-Surface that were air dried and followed with two spray coats of DuPont Imron Polyurethane 500 S Clear Enamel also air dried. This coating was proported to be acid and alakai resistant and produces no noticable changes in the antenna except for a slight decrease (0.1 MHz) in the resonant frequency.

One final experimental variable that will be encountered is that of the depth at which the unit is buried below the surface and the asymmetry that may exist around the hole. In general the magnetometer sensor determines the depth (3") that the unit is to be buried. For the majority of cases tried, the deeper the antenna is buried the weaker the far field signal becomes. There were a few times when the reverse was true, always in very moist soil at temperatures between 5^0 - 10^0 C. The cause that produced this could not be isolated.

Also, if a hole is prepared that is larger in diameter than the antenna and the antenna is placed in the hole asymmetrically, i.e. touching one side and not the other, serious detuning can result. In a large hole the antenna should be centered by the use of polystrene foam spacers for proper operation.

Summing up the results of the experience gained in the antenna development it is recommended that any future development consider the following:

1. The dielectric should be changed to a material with:

    a. lower losses

    b. less temperature variation of e_r and tan δ

    c. more dimensional stability with temperature

2. The dielectric wall thickness should be increased.

3. The choice of transmission frequency should be reviewed in view of the fact that the figure of merit increases with frequency squared.

The above described antenna development work is also documented and disclosed in Reference 30.

Propagation of the Ground Wave

The electric field expressions for the Omnidirectional Microstrip Antenna (OMA) have not been derived and thus we have no way to solve exact equations for the expected field as a function of distance. Similiar equations for a vertical half-wave dipole have been written which can lead to a suitable approximation. If one takes the total electric field expression, which is a complicated formula, and reduces it for the case of low-angle vertical-field groundwave propagation[27], the magnitude can be written as

$$|E_{su}| = \frac{120I}{R} A \text{ volts/meter}$$

where I is the dipole current

R is the distance from the dipole to the field measurement

A is the attenuation factor because of the earth

If the antenna output is propagating across a perfect conductor the factor A becomes unity. The remainder of the equation is simply the field strength that reduces with distance. The OMA was measured as having a field strength of -57dBm at 34.2 m with -12.5 dBm input on a ground screen which in terms of electric field yields.

$$E = \frac{9.70\sqrt{P_{in}/50}}{R} \quad \text{volts/meter}$$

where P_{in} = input power to the antenna

If now the attenuation factor can be reinserted for the propagation across a dielectric path, then for the antenna above ground

$$|E|_{OMA} = \frac{9.7\sqrt{P_{in}/50}}{R} A \quad \text{volts/meter}$$

There is no known expression that allows the calculation to be made for a buried antenna. However, it was observed that a normal figure for the insertion of the antenna into the ground was 10dB power loss. If we can then assume that to be an average ground insertion loss, we arrive at an

128

expression for the far field from the buried antenna (3" below surface) as

$$|E|_{OMA} \quad \frac{9.7^{\sqrt{P}\text{in}/500}}{R} \quad A$$

The attenuation factor A can be approximated by the empirical formula

$$A \simeq \frac{2 + 0.3p}{2 + P + 0.6p^2} \quad - \quad \text{Sin } b\sqrt{\frac{P}{2}} \, e^{-(5/8)\,P}$$

where $P \simeq \frac{\pi R}{\lambda x} \text{ Cos } b$

$b \simeq \tan^{-1} \frac{e_r + 1}{x}$

$x = \frac{18 \times 10^3 \sigma}{f_{MHz}}$

e_r = relative dielectric constant of earth

σ = conductivity of earth in mho/m

Evaluating two kinds of earth that represent the extremes of conductivity commonly found in the contintental United States for a range R = 150m yields the limits to be expected for field strength. For mountainous regions where poor conductivity prevails let $\sigma = 10^{-3}$ mhO/m and e_r = 7 resulting in A = .065. For plains regions where good conductivity prevails, let $\sigma = 3 \times 10^{-2}$ mho/m and e_r = 30 resulting in (good) A = 0.14. Going back to calculate field strength at 150 m. for an input power of 100 mW results in

$$|E|_{\substack{OMA \\ poor}} = 59.4 \; \mu \text{ volts/meter}$$

$$|E|_{\substack{OMA \\ good}} = 128 \; \mu \text{ volts/meter}$$

The receivers that were purchased require 1μ volt signal for 20 dB quieting, and the $\lambda/4$ wave monopole receiving antennas have an efficiency of approximately 10% depending on how and where they are mounted above ground. Thus even for the poorest

129

ground conditions expected, the communication system should have an excess of 20dB

signal capacity available for shielding and pattern distortion caused by vehicles

near the antennas.

VII. TELEMETRY RECEIVER EVALUATION

The RF telemetry link used in the SPVD in a narrowband FM system having a modulation index ($B = \Delta f/fm$) less than 1.57. The SPVD FM transmitter is modulated with the encoded tones for approximately $\Delta f = 5$ KHz frequency deviation. The channel spacing in the 41 MHz band is 20 KHz, and a receiver which could provide this channel spacing and pass the 10 KHz signal deviation while demodulating the encoded tones was sought.

During the Phase I effort[1] an FM communications transceiver (E. F. Johnson Model 507) receiver was used as the SPVD telemetry receiver in the 30 MHz band. This double conversion FM receiver was quite sensitive and would probably function adequately in the 41 MHz band, however its cost and size could not meet the new SPVD receiver requirements.

Several domestic manufacturers were contacted and told of the SPVD telemetry receiver specifications and the desire for a low cost modular unit which would approach the performance of the following desired specifications:

Frequency Range: 41.41, 41.37 MHz

Type: Double Conversion

Sensitivity: .4μv for 12db SINAD*

Modulation Acceptance Bandwidth: ±10 KHz

Selectivity: $\geq$ 65 db (20 KHz channel spacing)

Antenna Impedance: 50 Ω

Spurious and Image Rejection: $\geq$ 85 db

Intermodulation Performance: > 60 db

Frequency Stability: ±.002% (-30°C → +60°C)

Output Voltage: 200mv < V_o < 12v @ 1 KΩ

Power Supply Voltage: $\leq$ 12 VDC

Cost: ≈ $100

131

(*SINAD sensitivity is minimum modulated RF signal input level required to produce a specified SINAD ratio at a designated audio output power; SINAD is the ratio of audio output of a receiver (db), equal to signal + noise + distortion to noise + distortion.)

Generally, the communications manufacturers were interested in large orders, development contracts (i.e., $50K for 20 receiver modules with above specifications), or modifying existing receiver designs (specifically, a production military field radio at high cost >$500/unit). Motorola Inc., however, modified their MINITOR monitor receiver to operate on the 41.41 MHz frequency. The MINITOR Alert Monitor Model HO1EAB1112-M (Cost $176) uses a 2.7 volt mercury battery and consists of two circuit boards neatly packaged in a 4.5" x 2.3" x 1.3" (11.4 x 5.8 x 3.3cm) plastic case. The entire double conversion receiver board was removed from the MINITOR housing which contains the speaker, decoder electronics and battery compartment. It was then placed in a plastic bag and subject to receiver performance tests over the required temperature range.

Several scanning receivers operating in the low VHF band were investigated. The Radio Shack REALISTIC Pocket-Scan Model PRO-6 scanning receiver was purchased and evaluated as the unit most likely to meet all SPVD receiver module requirements. It is a four channel scanner, operating in either the high or low VHF band and capable of being manually or automatically set to a desired channel. The miniature receiver is a dual conversion (10.7 MHz/455 KHz) receiver with specifications tabulated in Table XIV.

The PRO-6 battery compartment was removed. Power, output, and antenna leads were attached and the unit placed in a plastic bag for performance tests. The volume control was on the lowest setting; the squelch control was off as minimum attack time is required to permit reception of the short encoded RF transmissions;

TABLE XIV. SCANNING RECEIVER PRO-6

SPECIFICATIONS

CHANNELS OF OPERATION: Four--as determined by any one of
4 crystals operating in the frequency
range.

FREQUENCY RANGE: 30 to 50 MHz and 148 -- 174 MHz

FREQUENCY COVERAGE: (Lo) 6 MHz for maximum sensitivity
(40 MHz ±3 MHz)

(Hi) 8 MHz for maximum sensitivity
153 MHz ±4MHz)

SENSITIVITY: Better than 1 microvolt for 20 dB quieting

SELECTIVITY: ±13.5 kHz, -6 dB

±20 kHz, -50 dB

MODULATION ACCEPTANCE: ± 7 kHz

IF. FREQUENCY: 10.7 MHz and 455 kHz

FILTER: 10.7 MHz and 455 kHz Ceramic Filters

SQUELCH SENSITIVITY: Variable from less than 1 microvolt

SCANNING SPEED: 6 channels/second

DELAY TIME: 0.7 to 1.5 seconds

AUDIO POWER: 150 milliwatts

POWER REQUIREMENTS: ±6 volts DC (negative ground only)
Current drain: 40 to 11 mA (no signal/squelched,
to full volume)

SEMICONDUCTOR
 COMPLEMENT: 2 Integrated Circuits
27 Silicon Transistors
17 Diodes
4 Light Emitting Diodes (LED's)

SPEAKER: 2", 16 ohm, Permanent Magnet, dynamic type

ANTENNA: Built-in wire loop, plus external whip-type wire

CRYSTAL REQUIREMENTS: Standard HC-25/u 3rd overtone

and the desired channel was manually selected.

Both the Motorola and Radio Shack receiver modules were evaluated over the desired -40°C to +75°C temperature range by using a stable RF signal generator outside of the temperature chamber. Both units performed adequately, but a DC voltage offset and signal clipping was observed on the MINITOR receiver at low temperatures.

After two more temperature cycles and similar results with the system telemetry decoder connected, the Radio Shack PRO-6 was selected. The reasons are (a) temperature dependent output offset and clipping of the MINITOR, (b) somewhat more complex interface and power supply circuitry is required for the MINITOR receiver board, (c) the PRO-6 is easier to mechanically adapt to the SPVD control box, (d) added capability of more than one channel, conveniently selectable, (e) much lower cost of the PRO-6 ($80 vs $176), and (f) availability (short lead time).

Several minor modifications to the PRO-6 receiver were made. This consisted mainly of removing the battery compartment by milling off the receiver's bottom plastic battery compartment and then soldering power and signal leads to the receiver circuit board. The schematic diagram of the receiver and interface circuitry comprising the receiver module is shown schematically in Section X. An antenna lead is fabricated from a length of RG-174/U coaxial cable with a BNC female chassis mount connector on one end and a modified earphone plug on the other. The crystals are inserted in the crystal sockets of the crystal compartment. Even though each SPVD receiver has one operating frequency, an extra set of crystals was ordered to provide each control box with the capability of operating on either of the two assigned frequencies. In the control units provided, Channel No. 1 is 41.37 MHz and Channel No. 2 is 41.41 MHz.

Twenty-four Radio Shack PRO-6 receivers were purchased. Two receivers failed to operate satisfactorily. The sensitivity of both rejected units was low and one unit provided no signal output.

In order to eliminate receiver noise outside the SPVD encoder tone frequency band (2000 → 6500 Hz) and provide proper signal level to the tone decoder electronics, an interface electronic board is required. The interface board consists of several operational amplifier circuits designed to provide gain and filter (bandpass) the receiver output.

The interface board also has a 6 volt regulator (7806) to power the PRO-6 receiver and circuitry to sense the condition of the control units standby battery. The schematic diagram of the interface board is illustrated in Section X.

The power supply module selected is a Power Mate Corp. Model EMA-12/15B which has passed all temperature performance tests. The prototype control box power supply has been operating for more than one year. The power supply schematic diagram appears in Section X and is the Power Mate Corporation data sheet which also lists all parts. All modules have functioned well except for one, which required a new μA 723 voltage regulator IC after about 100 hours of operation.

VIII. BATTERY EVALUATION

During the previous SPVD development[1] a battery evaluation was conducted on several available electrochemical energy systems. Our approach was to resurvey the current batteries and perform tests over a longer period of time. This investigation's objective was to select a electrochemical system and battery which could supply the required energy to the SPVD for one year with a traffic flux of 20,000 vehicles per day and at all expected CONUS ambient temperatures.

Specifically, the tasks performed were:

• Establish realistic worse case SPVD energy requirements;

• Obtain several sample batteries of different electrochemical energy systems and conduct a long term test at ambient temperatures with a programmed constant and pulsed load simulating an SPVD.

• Conduct accelerated drain cycles at high and low temperatures on promising battery types;

• Investigate solar cell array charging rates and capacity in a roadway for a significant period;

• Select a suitable standby battery for the SPVD control unit; and

• Investigate related parameters as environmental, safety, cost and system performance effects.

Required Battery Capacity

> The SPVD system operational lifetime design goal is one year at ambient roadway temperatures (-30°C to +75°C, i.e., -22°F to +167°F) for a vehicle traffic flux of 20,000 vehicles/day. For a system voltage of nominally 6 volts, the sensor module will have a constant quiescent drain of .5ma (3mw) or for one year require 4.38 A-hrs. The transmitter is designed to operate for 30msec with a 40ma drain, for both the leading edge and trailing edge transmissions, or 40,000 transmissions a day.

Therefore .060sec/vehicle x 20000 vehicles/day = .33 hrs/day; and .33 hrs/day x

.04 amperes x 355 days leads to an additional 4.8 A-hr required battery capacity

for the transmitter. The total required battery capacity for the design goal is

then 9.18 A-hrs/year.

Since we were just starting sensor module development, a conservative worse case

test was planned as:

Sensor Module

6.75v x .5ma (goal < 2mw) = 3.37mw; 4.4 A-hr.

Transmitter

6.75v x 40ma (goal 236mw)=270mw

(per 30msec transmission for 100mw R.F. power)

80,000 transmissions/day instead of 40,000

.060 sec/vehicle x 40,000 vehicles/day x .040 Amps x 365 days x

$$\frac{1}{3600 \text{ sec/hr}} = 9.7 \text{ A-hr}$$

Total = 14.1 A-hr worse case

To simulate "worse case" SPVD operation a programmer was designed and

fabricated as shown in Figure 44. Also illustrated in Figure 44 is the Battery

Evaluation Instrumentation Block diagram. Figure 45 is a photograph of the

Ammunition Box housing the test batteries at ambient temperature. Also notice

the SPVD receiving antenna mounted on it and the roof mounted antenna used to

determine the decoder false alarm rate for the Maryland/Washington, DC urban area.

As reported in Reference 1, extensive tests had been conducted on several

electrochemical battery systems resulting in the selection of Union Carbide's

Eveready No. 1209 cell (Heavy Duty LeClanche Lantern Battery). We included

several types of lantern batteries in order to confirm the performance with a
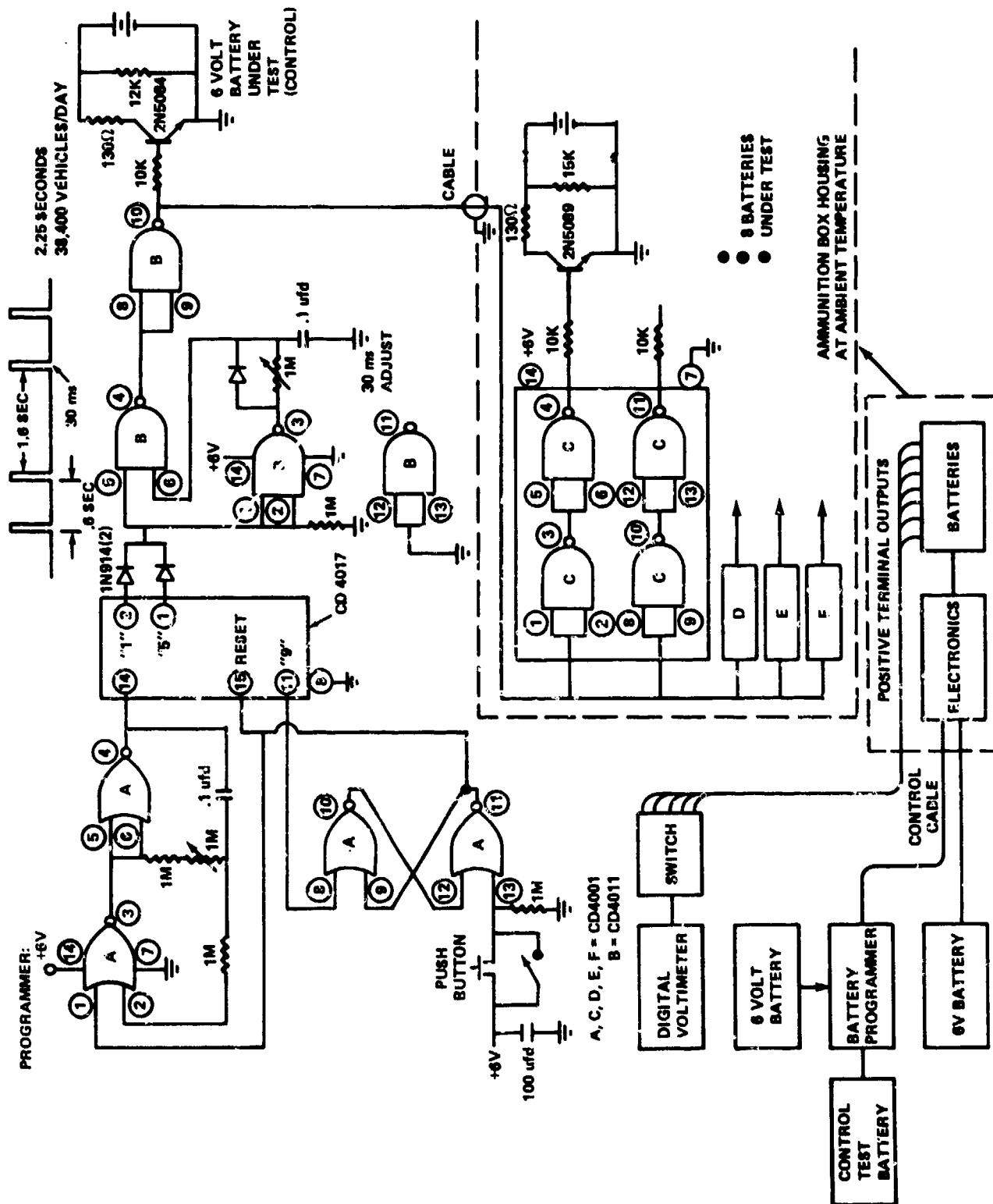
FIGURE 44. SPVD BATTERY TEST INSTRUMENTATION.

FIGURE 45. PHOTOGRAPH OF BATTERY TEST CONTAINER.

more typical SPVD load (i.e., without accelerated discharge cycles).

Battery Systems Tested:

The electrochemical battery systems considered are Carbon-Zinc (LeClanche), Carbon Zinc (Zinc Chloride), Alkaline - Manganese Dioxide, Mercuric Oxide (Zn/HgO), Nickel Cadmium, Sealed lead acid, Lithium (Organic electrolyte). Table XV lists the various electrochemical battery systems, assumed chemical reaction and energy densities that were considered.[31,32]

The following batteries were selected for test: Lantern battery types Eveready 1209, Ray-O-Vac 944, Mallory M908, BA-200/U, Bright Star #646, BA-803/U; Lead Acid (sealed secondary) Gates #0810-0005; Lithium, Eagle Picher D Cells; Alkaline, Mallory #MN1300; and Mercury Mallory types RM-42R(BA-1030/U) and Mallory #316856-5 (RM-2550R).

Numerous lantern cells were tested because of their potential low cost $\approx$ \$1.20 ea/1000 and Phase I test results. In Figures 46 to 50 are plotted the open circuit voltage of the lantern battery types with respect to time and temperature. Clearly the Eveready #1209 has better performance for the programmed load.

The Gates Sealed Lead Acid cell discharge curve is plotted in Figure 51. Two of the three series cells had failed.

Two series Lithium batteries, Eagle Picher D-cell types were tested and the results plotted in Figure 52. One very notable characteristic is the batteries low internal impedance. The Mallory Alkaline Duracell battery discharge curve is plotted in Figure 53.

Five RM-42R mercury batteries (BA-1030/U) were tested and its discharge curve plotted in Figure 54. Although its low temperature performance was suspect, this electrochemical system performed very well for the moderate temperatures experienced over the measurement period (15°F). However, to confirm our results shown in

140

TABLE XV. BATTERY ELECTROCHEMICAL ENERGY SYSTEMS

System	Chemical components	Open circuit cell voltage	System type/recharge capability	Energy density watthour/lb.	-watthour/in^3	Operating Temperature range	Shelf life less % year.	Comments
Carbon zinc (Leclanche)	C.../NH$_4$Cl, H$_2$O/Zn	1.5v	primary/poor	30	2	200°F→130°F (-6.7°C→54.4°C)	20%	
Carbon zinc (zinc chloride)	C-MnO$_2$/NH$_4$Cl, ZnCl,H$_2$O/Zn	1.5v	primary/poor	35	3	0°F→160°F -17.8°C→71.1%	15%	
Alkaline manganese dioxide		1.8v	primary/yes	40	3	-20°F→130°F (-28.9°C→54.4°C)	5%	
Mercuric oxide	HgO/KOH,H$_2$O/Zn	1.35v	primary/no	45	6	32°F→130°F (0°C→54.4°C)	5%	poor low temp. depends on construct.
Nickel-Cadmium	Ni(HO$_3$)$_2$/Cd	1.2v	secondary/yes 300→2000 cycles	12	1.2	-4°F→113°F (-20°C→45°C)		memory problem poor at Hi temp.
Sealed lead acid	PbO$_2$/H$_2$SO$_4$, H$_2$O/Pb	2.0v	secondary/yes	22	.96	(-30°C60°C)	30%	
Lithium (organic electrolyte) Li/methyl acetate, LiAsF$_6$/CF or Li/propylene carbonite, LiBr/SO$_2$		2.2→3.6v	primary/no	150→300	10→20	(-40°C→+70°C)	1%	
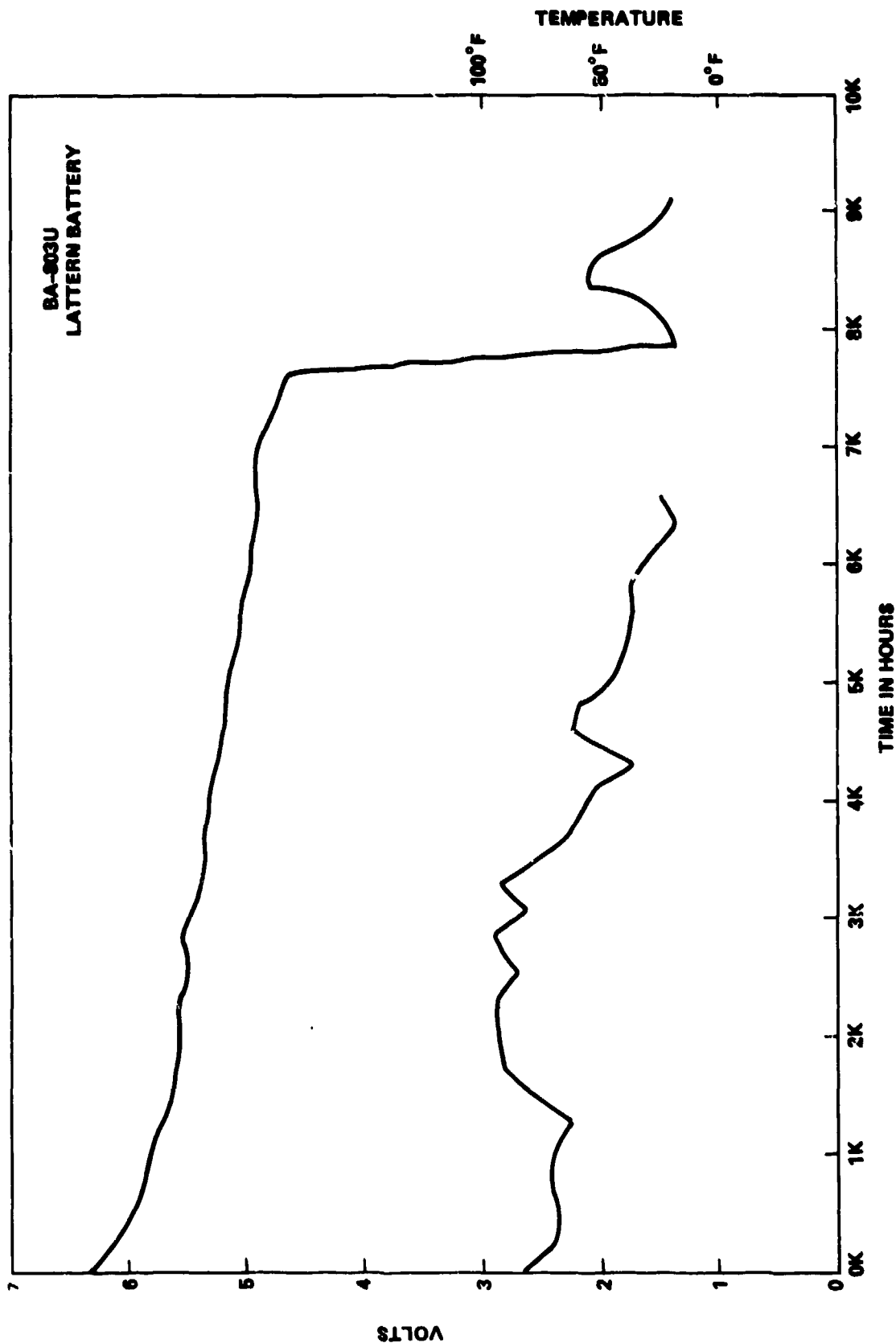
FIGURE 46. BATTERY DISCHARGE CURVE, BA-903/U.

142
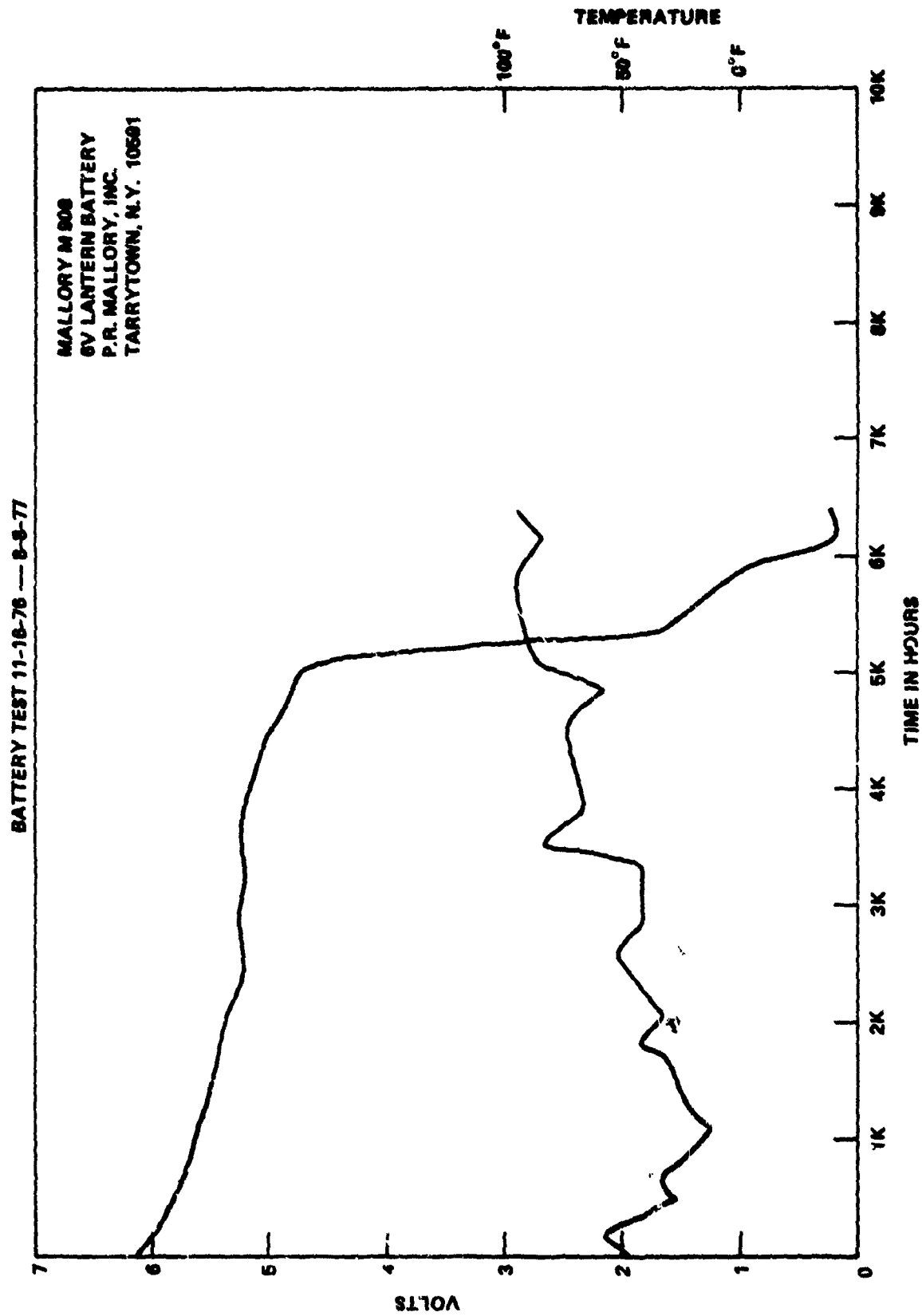
FIGURE 47. BATTERY DISCHARGE CURVE, MALLORY M 908.

143
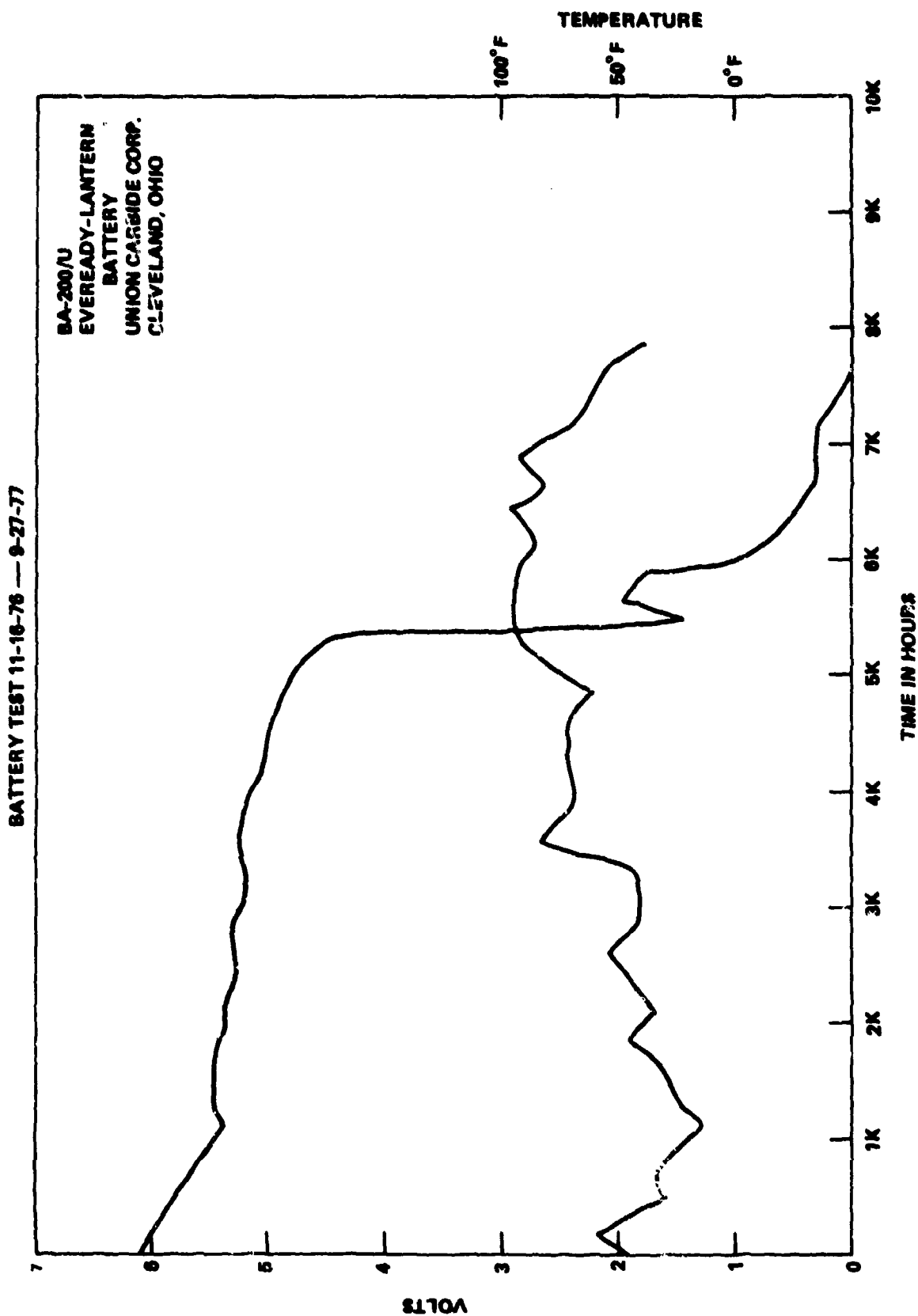
FIGURE 48. BATTERY DISCHARGE CURVE, BA-200/U.
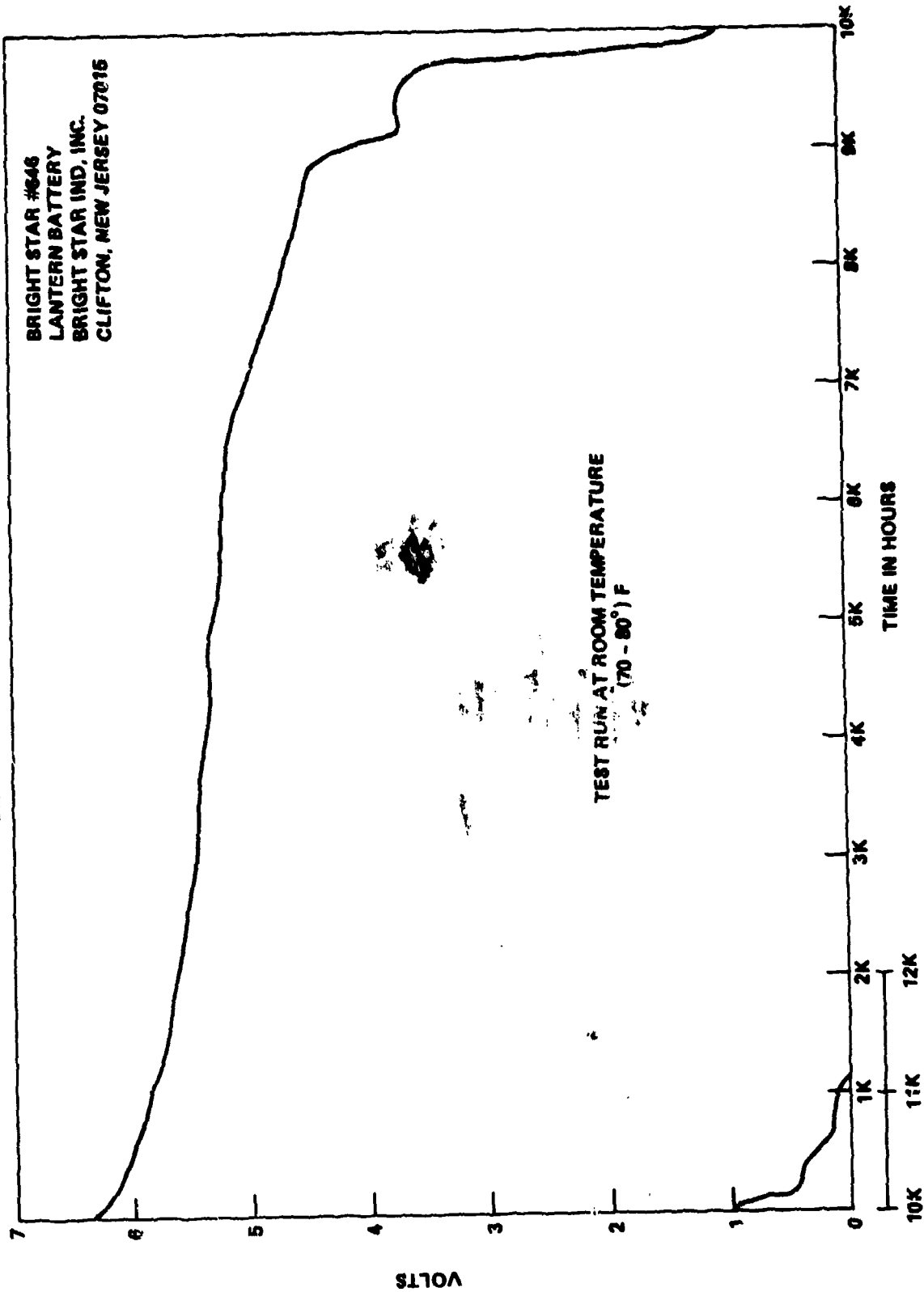
FIGURE 49. BATTERY DISCHARGE CURVE BRIGHT STAR #648.

145
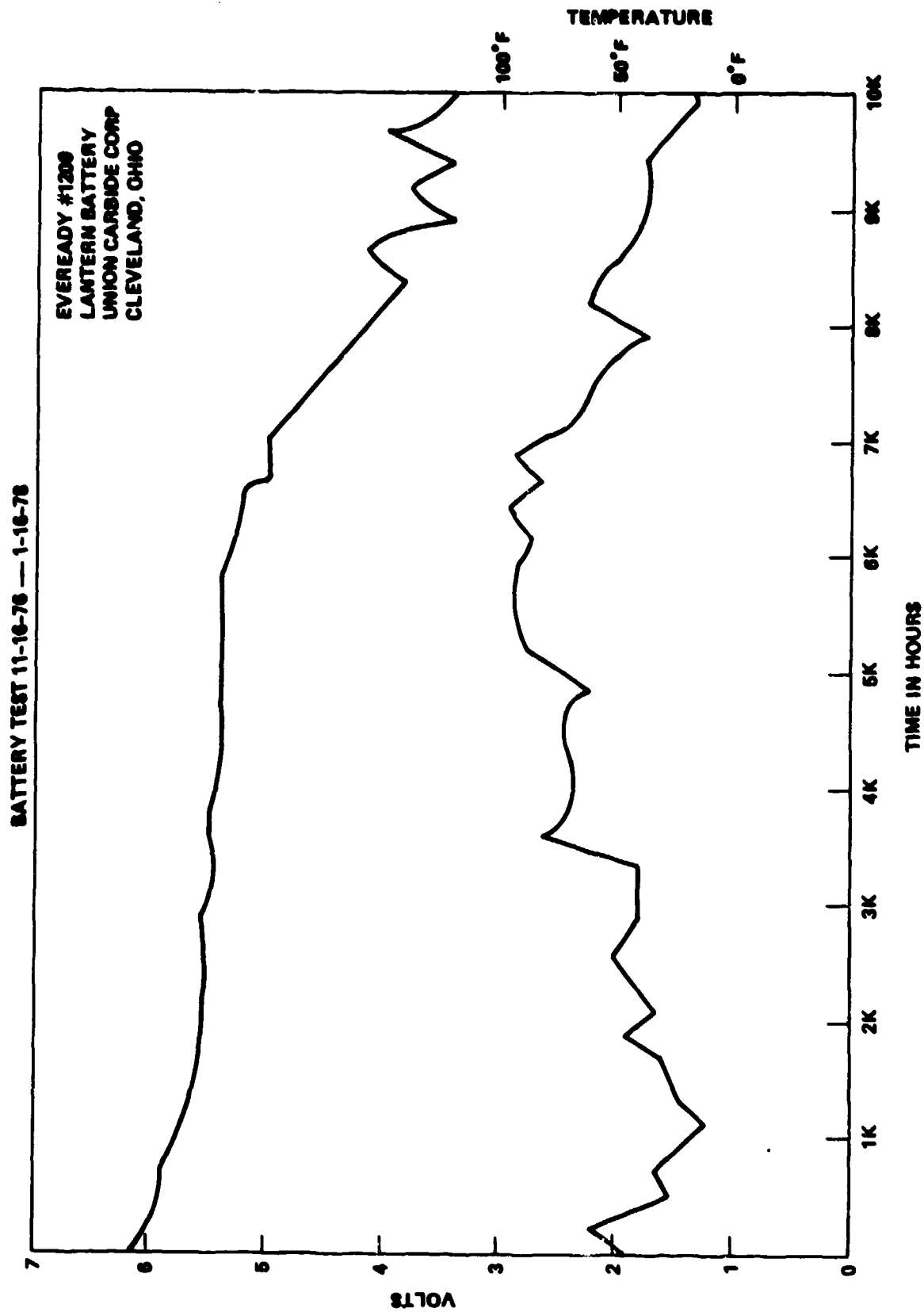
FIGURE 50. BATTERY DISCHARGE CURVE, EVEREADY #1209
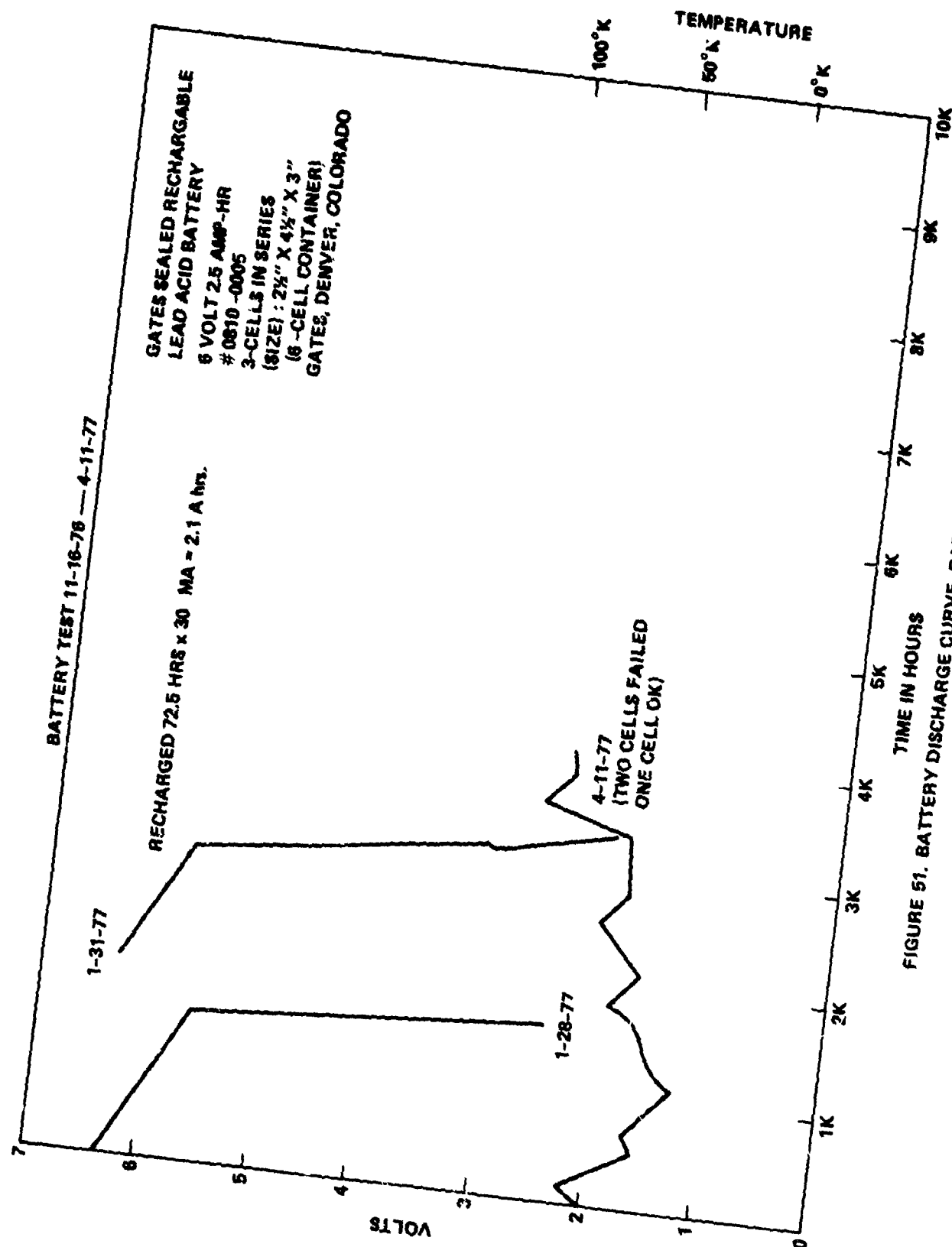
FIGURE 51. BATTERY DISCHARGE CURVE, GATES 0810-0005

147
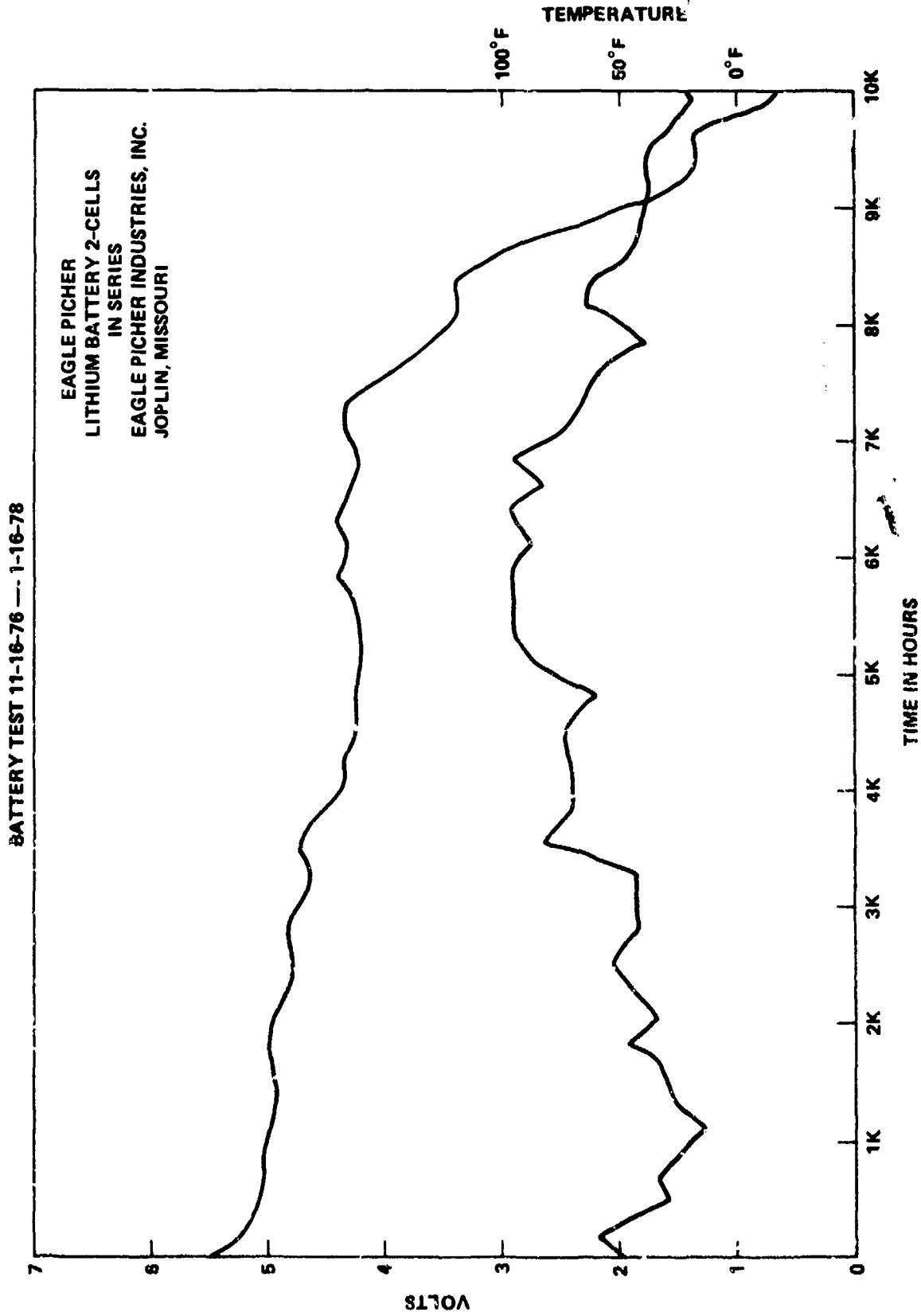
FIGURE 52. BATTERY DISCHARGE CURVE, EAGLE PICHER LITHIUM "C" CELLS.
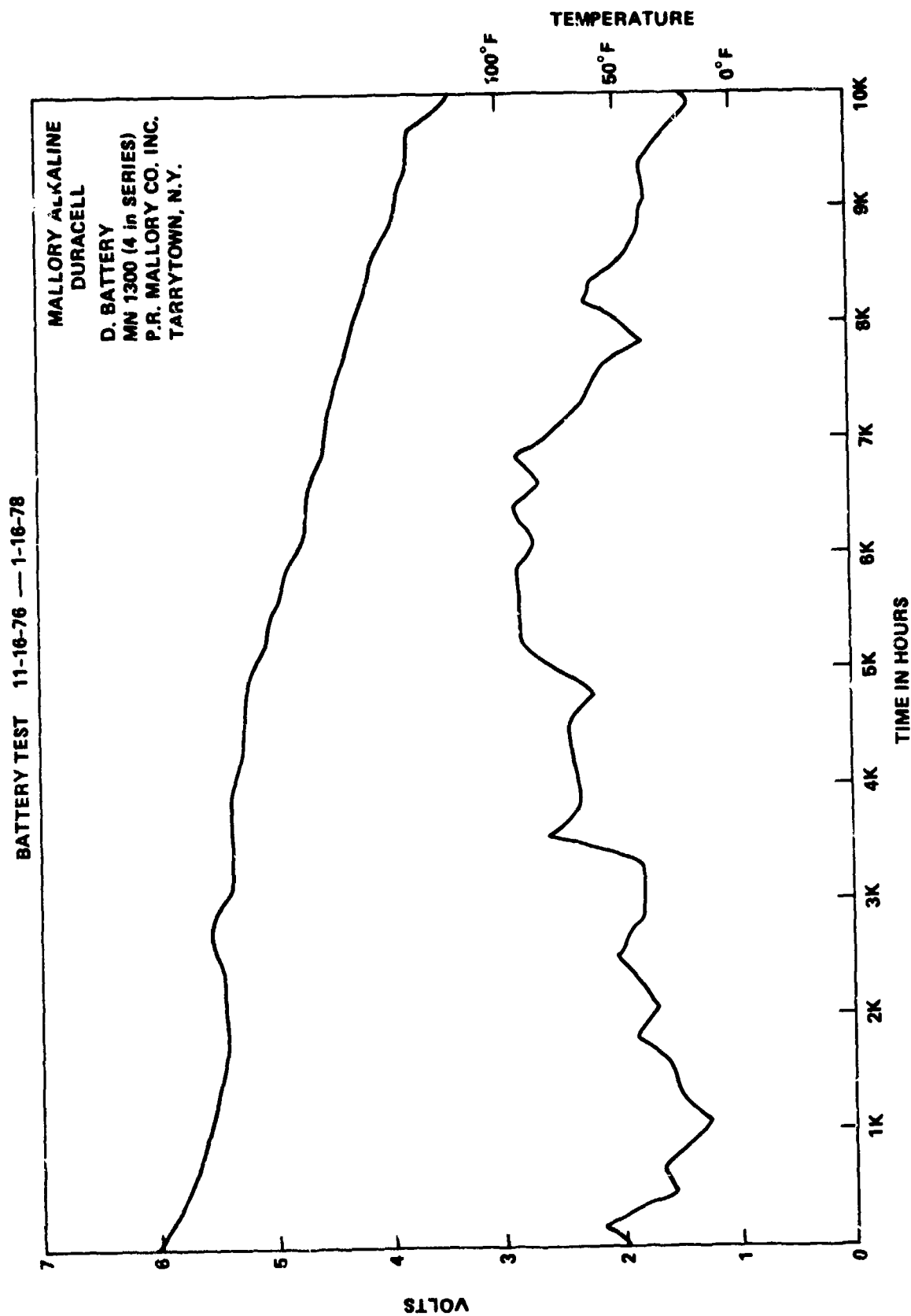
FIGURE 53. BATTERY DISCHARGE CURVE, MALLORY ALKALINE "D" CELLS.
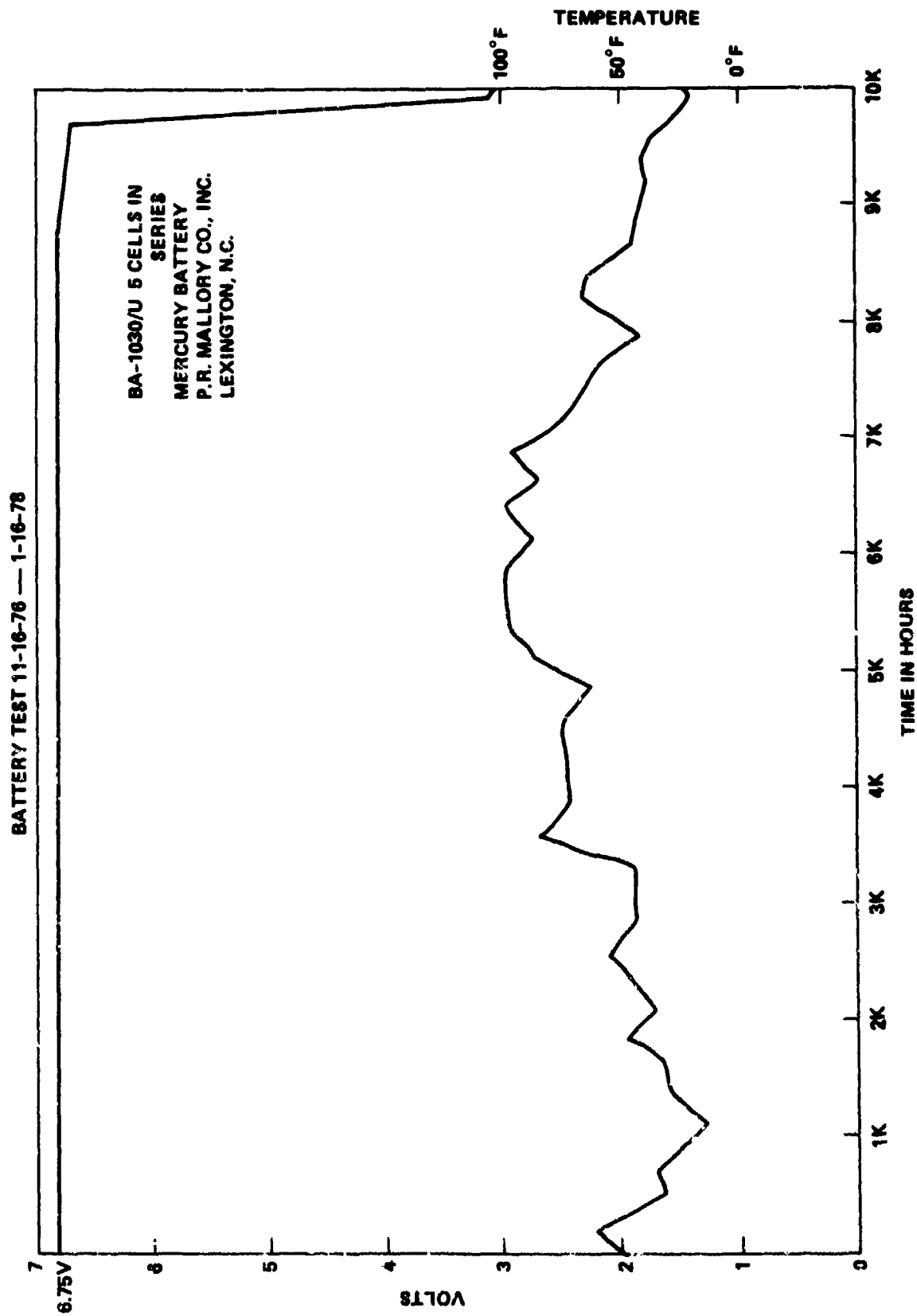
FIGURE 54. BATTERY DISCHARGE CURVE, BA-1030/U.

Figure 54, accelerated discharges and unit temperature tests were conducted.

Each battery terminal voltage was measured under the continuous drain and the simulated pulse drain of the transmitter approximately 6 months and 11 months into the test. In Figure 55(a,b) are some oscilloscope photographs of the battery terminal voltage during the pulsed load. The mercury, alkaline, and lithium cells have very low internal impedance. However, lantern batteries had developed very high internal impedance. Also shown is the effect of putting a 100 µfd capacitor across the terminals in an effort to reduce the impedance. In Figure 56 are oscilloscope photographs of some of the remaining batteries under test approximately eleven months after the test started. The alkaline and mercury cells have extremely low internal resistance considering the lowered terminal voltage.

Since the mercury system seemed to satisfy our system requirements, an inquiry was made to the Mallory Battery Company, Tarrytown, New York. They recommended a Mallory #310856-5 consisting of 5, RM-2550R cells. Because this cell size was more conducive to the SPVD unit, it was selected.

Mercury battery temperature/load tests were performed. Figure 57 is a voltage discharge curve for RM-42R (BA-1030/U) cells which have been discharged at 50ma at room temperature (25°C) and at +76°C, exhibiting a 15.6 A-hour capacity confirming the anticipated 14 A-hour capacity (rated @ 280ma). During a similar test, (i.e., 50ma continuous load) at low temperature, we noted that at -10°C the cell voltage rapidly approached .8 volts. In Figure 58 is plotted the terminal voltage of the mercury battery for a constant 3mw load. Below -20°C, the internal cell impedance rises and at -30°C the cell voltage falls 5% of the normal voltage, certainly within the 20% undervoltage operational limit. The sensor module therefore can operate satisfactorily at low temperature, and this was confirmed in systems tests at -40°C.
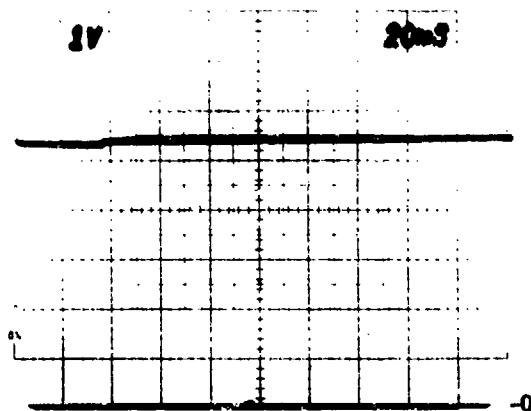
4-MN 1300 2 MAY 77
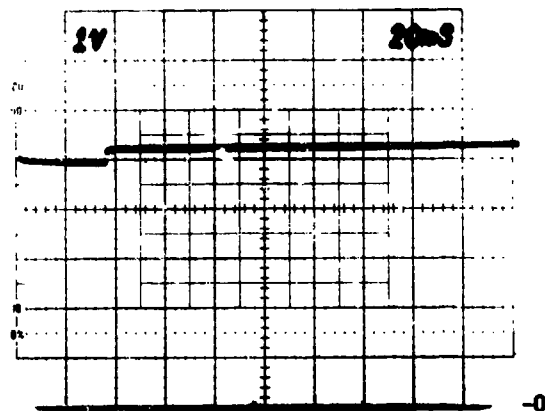
2 MAY 77 LANTERN M-908 5.12V
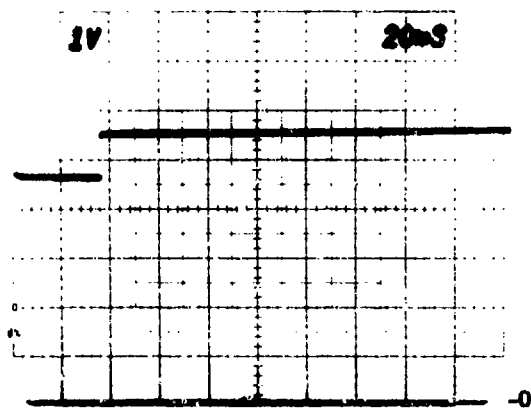
2 MAY 77   EVEREADY   1209   5.40 V
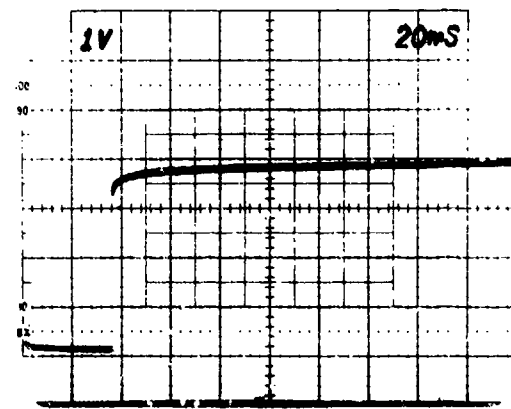
2 MAY 77 RAY-O-VAC 944   4.74V
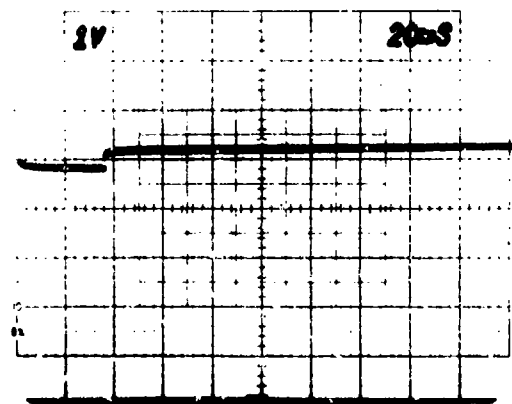
2 MAY 77 BA-200V EVEREADY   5.06 V
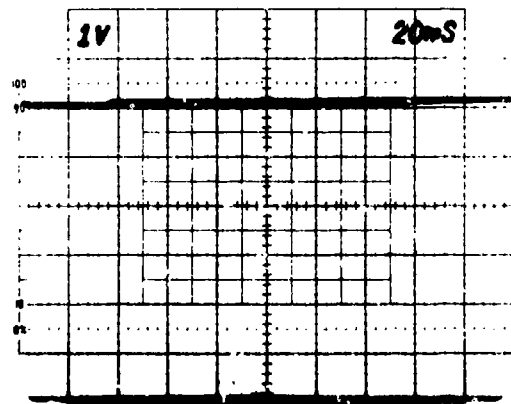
BA-803/V (NEW) 3 2MAY 77   5.92V

FIGURE 55a.   BATTERY TERMINAL VOLTAGE FOR SIMULATED TRANSMITTER LOAD, 2 MAY 77.
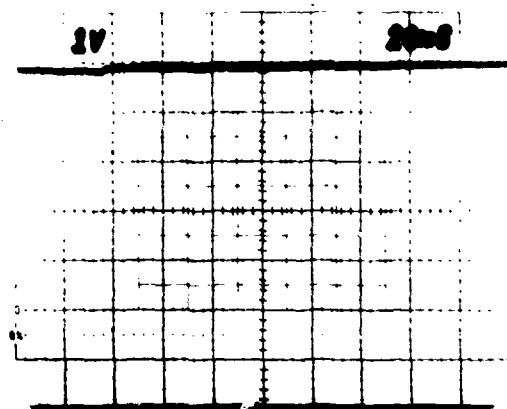
BA-1030/U MERCURY 6.72V 2 MAY 77
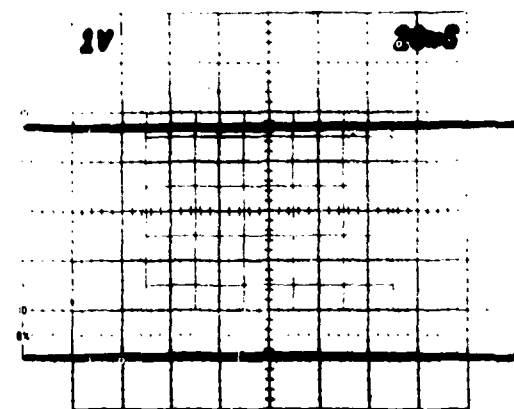
LITHIUM LCF-7.0 4.39V   2 MAY 77
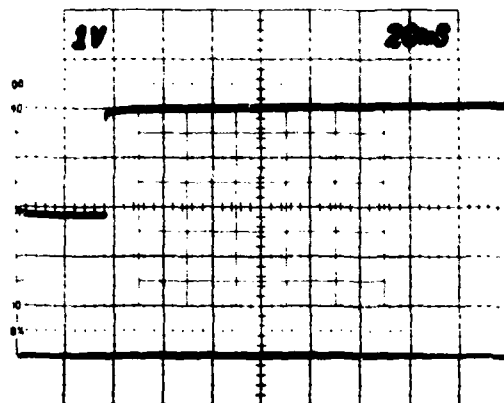
BRIGHT STAR   4.92V   2 MAY 77
                100MF   #4 W CAP
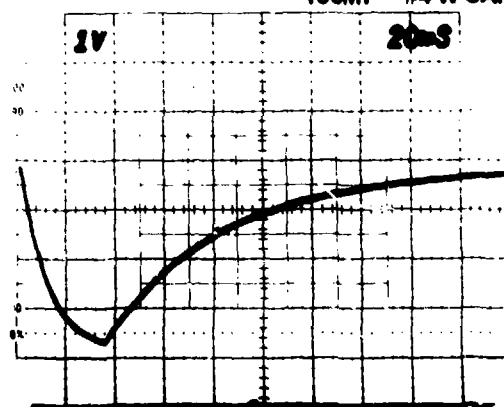
FIGURE 55b.   BATTERY TERMINAL VOLTAGE FOR SIMULATED TRANSMITTER LOAD.
              2 MAY 77.

153

35 msec TRANSMISSION ≈ 38,400 VEHICLES/DAY
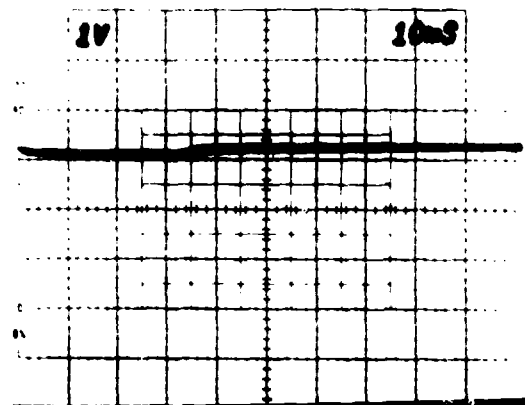
4-MN 1300   20 OCT 77
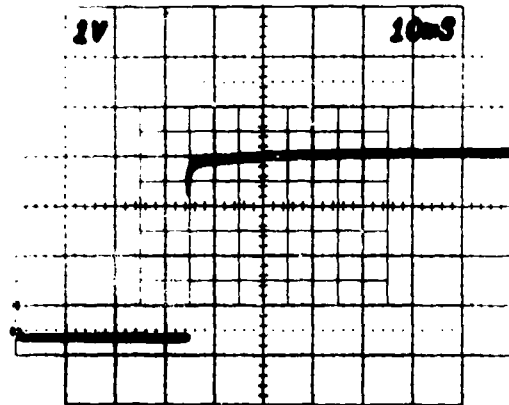
U.V. 1209   20 OCT 77
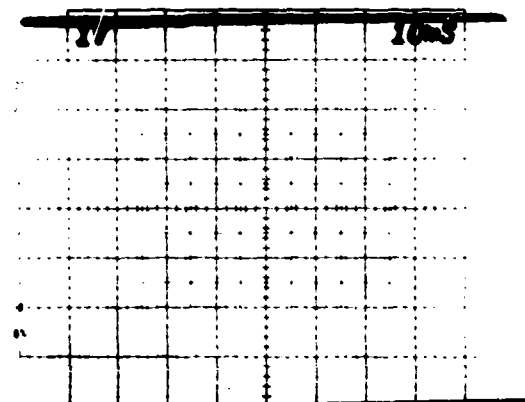
BA-1030/V   20 OCT 77
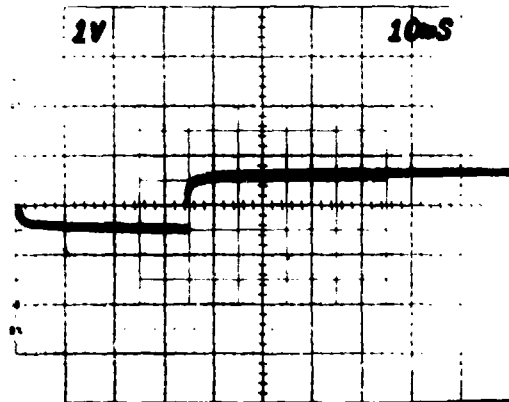
LITHIUM   20 OCT 77
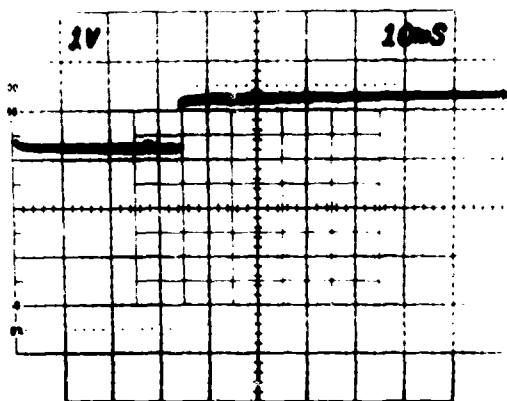
BA-903/V   20 OCT 77
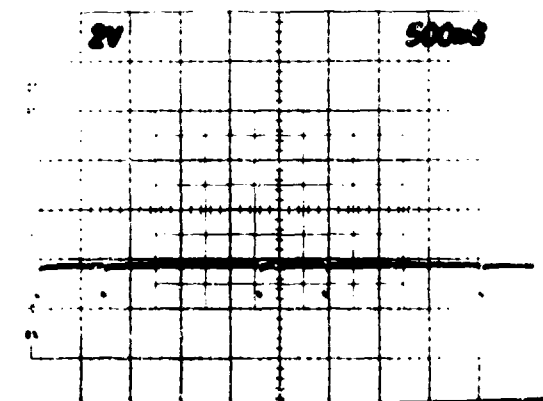
LITHIUM   DUTY CYCLE   20 OCT 77

FIGURE 56.   BATTERY TERMINAL VOLTAGE FOR SIMULATED TRANSMITTER LOAD, 20 OCT 77.
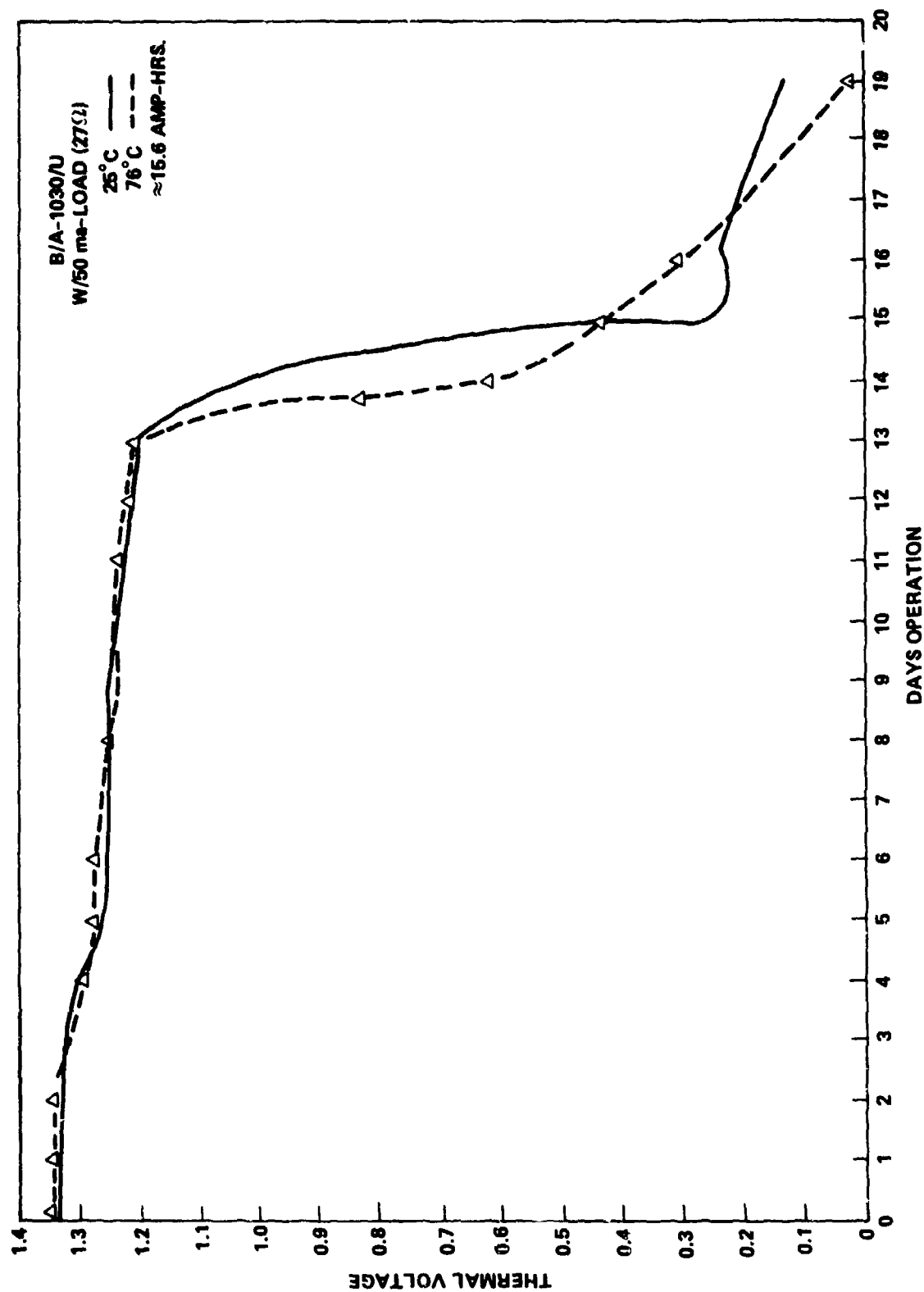
FIGURE 57. MERCURY BATTERY DISCHARGE CURVE (50 MA LOAD-BA-1030/U).
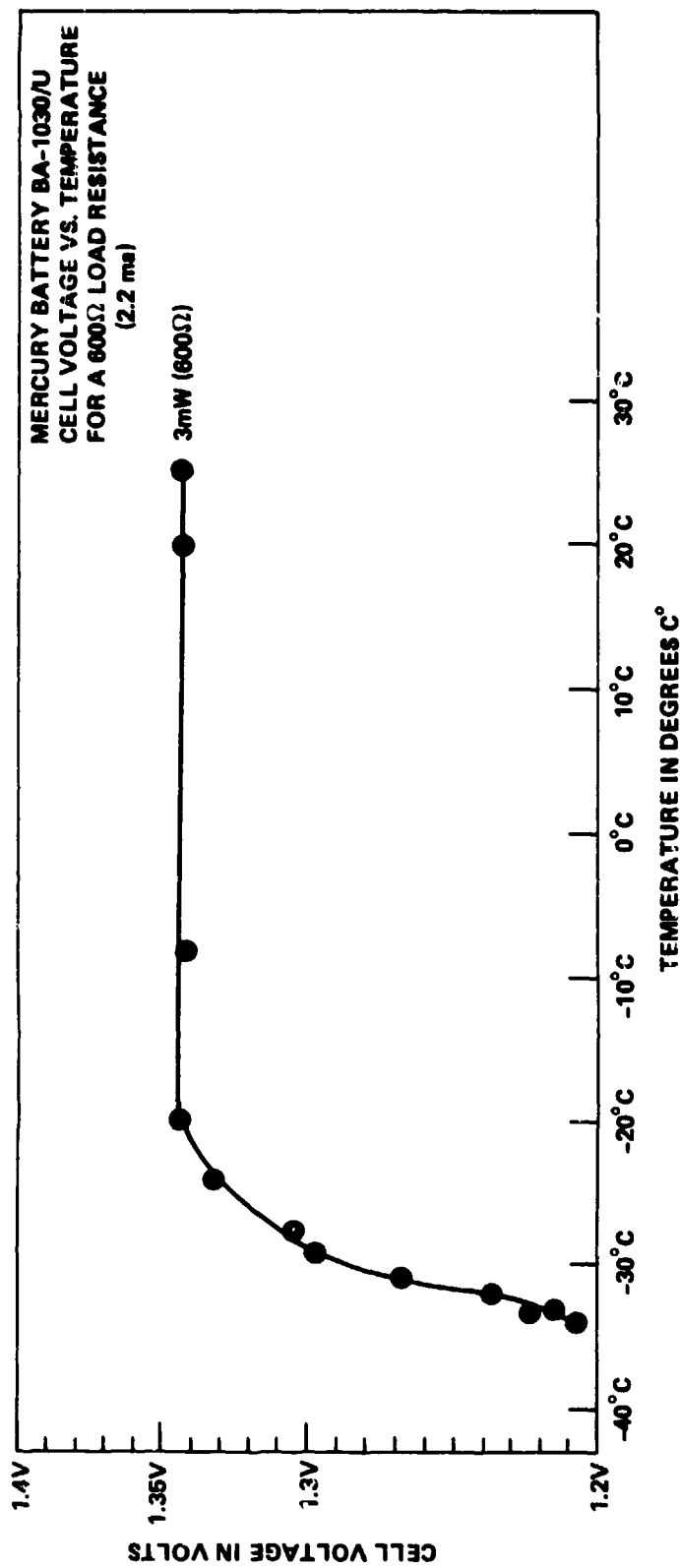
FIGURE 58. MERCURY BATTERY VOLTAGE VS TEMPERATURE FOR A 600 Ω LOAD

The next step was to verify that a pulsed transmitter load could also be accommodated by the mercury battery. A simple test was conducted with the BA-1030/U and is plotted in Figure 59. Notice at -20°C, the cell voltage with a 27Ω load (50ma normal) falls to .84 volts, and after 8.52A-hrs had been discharged, with a more characteristic load of 680Ω (2ma or 13.5mw) it fell to approximately .88 volts. To simulate discharged battery performance, a second, 27Ω load was applied and several voltages measurements are shown in Figure 59. At -40°C, the voltage although adequate to run the sensor module would not sustain the load. But for -20°C the battery performed satisfactorily. Figure 60 is a plot of similar test results on the Mallory #316856-5 battery. Systems tests on the SPVD prototype also confirmed its ability to operate at low temperatures. A photograph of the SPVD battery is shown in Figure 61. Two batteries are connected in parallel for a total battery capacity of 26 ampere-hours at 6.75 volts. The assembled battery compartment is then demagnetized and attached to the SPVD electronic modules.

Critical battery/systems parameters for the selected battery give a measure of projected performance as:

Mission lifetime: ≈ 2 years

Battery Capacity: 26 A-hr @ 6.75v

Battery Noise: < 10mv

Storageability & Maintenance: > 2 years

Ruggedness: 10,000g, drop test

Availability/lead time: Commercial ≈ 2 months

Cost: $27.18 each ($54.36/SPVD)

Safety: No problem

Environmental Impact: Recycled to conserve Mercury

Reliability: 99% desired

Weight: 835 grams/(≈ 2#) unit
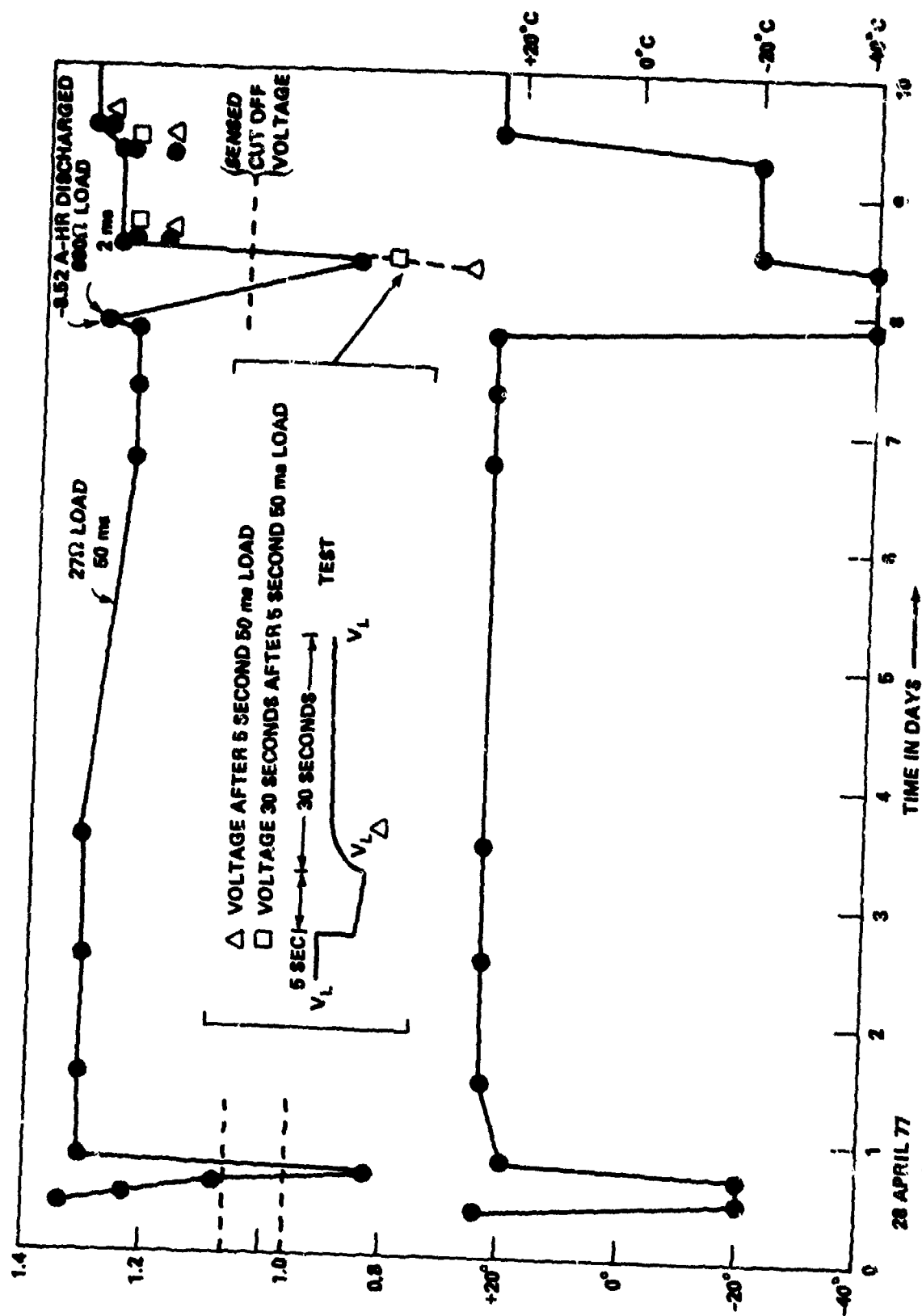
FIGURE 59. BA-1030/U (RM-42R) LOW TEMPERATURE PERFORMANCE.
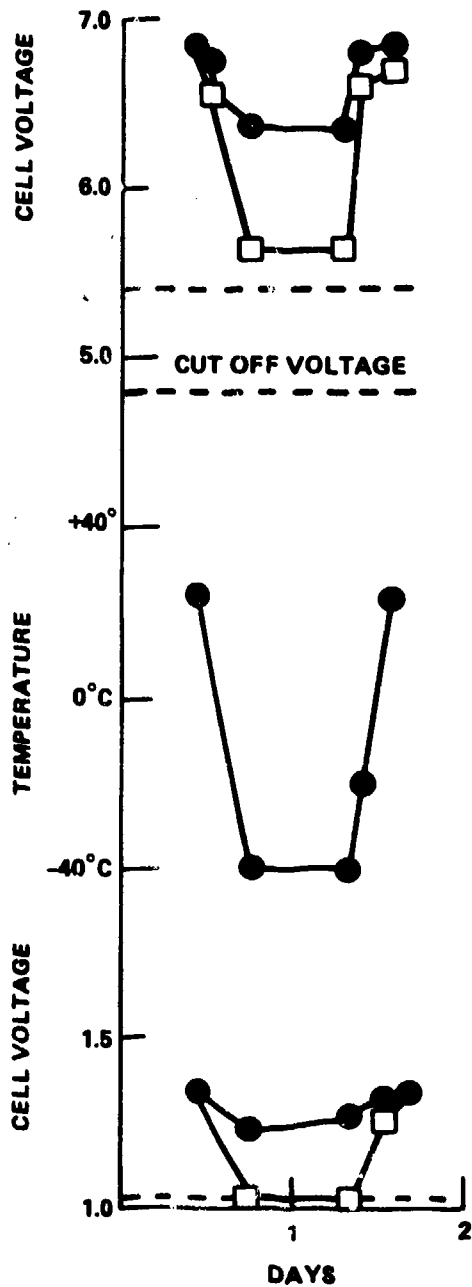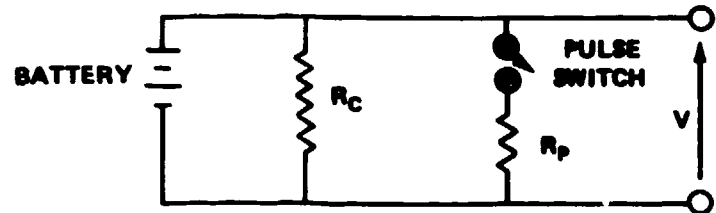
FIGURE 60. LOW TEMPERATURE MERCURY BATTERY PERFORMANCE.
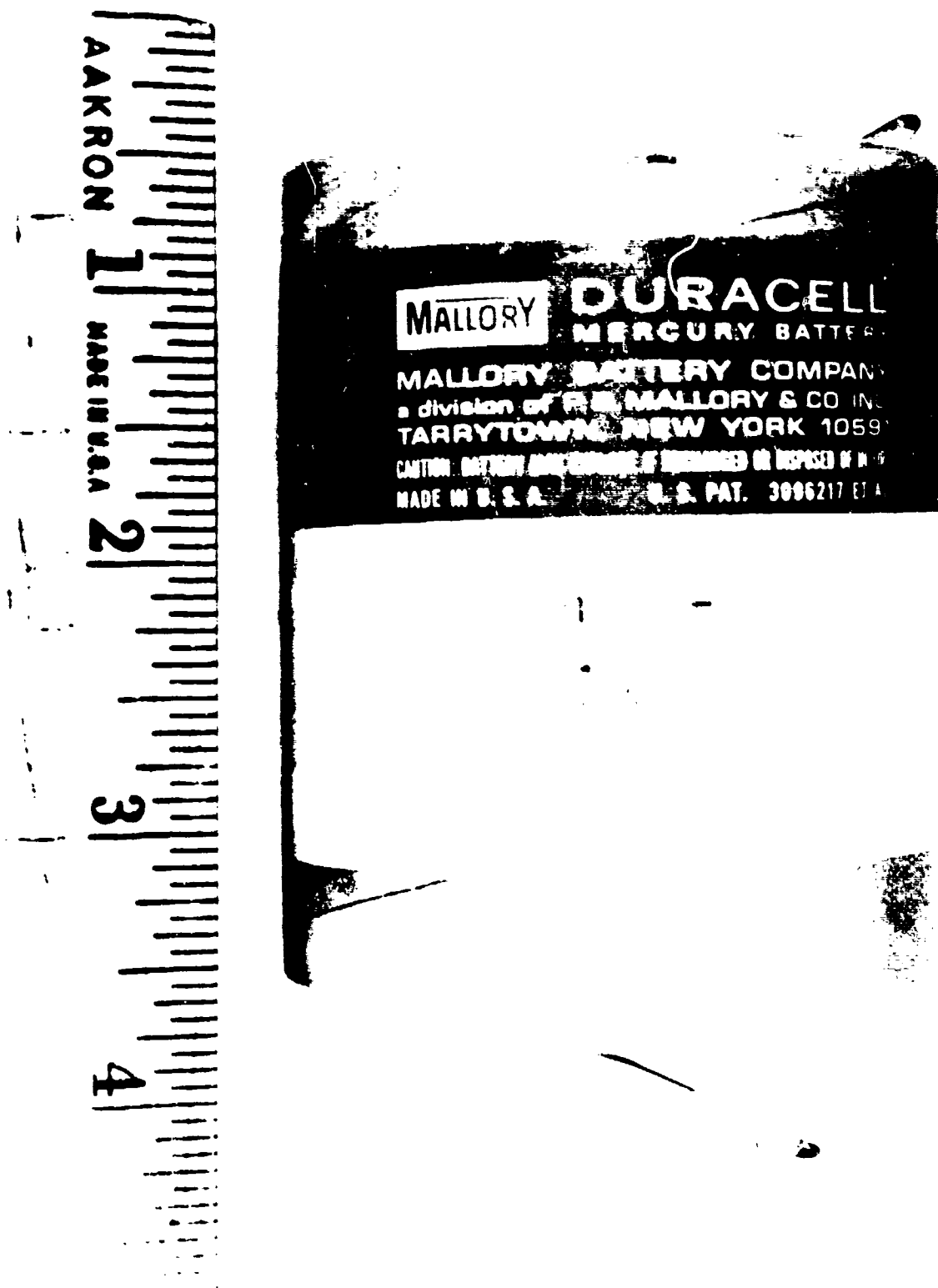
FIGURE 61. PHOTOGRAPH OF THE SPVD BATTERY.

The standby battery selected for the SPVD control unit is a sealed lead acid, 12 volt-4.5 amp-hour Type A (Globe Gel Cell, model GC-1245-1 or similar). The battery will operate the control unit for a minimum of 22 hours and significantly longer if the receiver LED is disconnected.

Solar Cell Array Evaluation

Early in the program techniques of supplying power to a buried SPVD unit were considered. One technique, that of a magnetic induction link similar to an open core transformer, is used in charging heart pacemakers. It would demand a road crew to periodically charge secondary batteries with smaller energy densities for a significant amount of time. It would also require a significant amount of magnetic material near the magnetometer sensor module. This approach was not pursued.

A solar cell array was designed about the SPVD housing and its mechanical design is discussed in that report section. The reason for using solar cell array is that the roadway is relatively unobstructed and a "typical" mid latitude value of solar power flux is $70mw/cm^2$ during the day. Therefore $70mw/cm^2$ x .14 (conversion efficiency) = 9.8 mw/cm^2. For a 20 cell array 2 cm^2 = 80 cm^2 or 9.8 mw/cm^2 x $80cm^2$ = 784 mw. Now derate by 80% for the 1/2" plate glass cover and dirt, resulting in 156.8 mw.

$156.8mw = 6v.I$

$I = 2.61$ ma maximum estimated array current.

After the array was constructed, a current of 14ma was measured. If we assume 1 hour per day sunlight for 365 days at 14ma, then a 5.1 A-hour charge is obtained, almost the entire SPVD system requirement. For 2 hours of sunlight per day, 10.2 A-hr is obtained. Therefore an attempt was made using twenty solar cells (2 x 2 cm) (centralab Semiconductor Solar Cells #N220cG-11) each

rated at 58.2mw @ 430mv were connected in series. A circuit capable of determining its effectiveness is shown in Figure 62. The solar cells are attached to a diode with a low reverse current (<<25µa) and to a filter network to remove any possible RFI/EMI problems with a real system and then to a Nickel Cadmium battery. The nominal system voltage is 6.2 volts where the 5.6Ω resistor simulates the SPVD power requirements (≈9.6 A-hrs/year). A 7.5 volt zener diode is put across the battery so when the solar cell voltage is a maximum, i.e., 10 volts, the additional current will flow through it. An E-Cell coulometric timer (BISSETT Berman #S-163-6843, 150 µa-hr 3860 Centinela Ave., Los Angeles, California) is used as a long term integrator, i.e., to sum the total current delivered by the solar cell array during a desired measurement period. The maximum anticipated charging rate of 20ma will produce a 20mv signal across the 1Ω series resistor. Therefore for a worse case required yearly capacity,

$$\frac{13 \text{ A-hours}}{8760 \text{ hrs/year}} = 1.48\text{ma-hours}$$

and

$$E = 1.5\text{ma} \times 1 \text{ ohm} = 1.5\text{mv}.$$

For a 150µa - hour E-Cell,

$$\frac{150 \text{ µa hours}}{8760 \text{ hrs/year}} = .017\text{µa}$$

Finally 1.5mv = .07µa R

$$R = 38.235\text{k}\Omega.$$

In this way, the circuit in Figure 62 is able to measure the worse case SPVD energy requirements obtained from the solar cell array. The depleted E-cell is a measure of the total ampere hour capacity obtained during the measurement period. Figure 63 is a circuit used to determine the exact condition of the E-cell.

FIGURE 62. SOLAR CELL ARRAY EFFECTIVENESS TEST CIRCUIT.

$$\frac{1.35 \text{ V}}{4.50 \times 10^{-6}} = 3 \times 10^3 \Omega = R$$

REPLATING (RECHARGE)
POLARITY. DO FOR
EXACTLY 20 MINUTES

PROCEDURE:

- DEPLATE E-CELL W/450 ma CURRENT FOR 20 MINUTES
  AS A CHECK ON UNIT CAPACITY

- REVERSE BATTERY AND REPLATE FOR 20 MINUTES

- INSTALL CELL IN CHARGING TEST CIRCUIT-TEST

- AFTER TEST, PUT IN CIRCUIT (DEPLATING POLARITY)
  FOR MEASURED PERIOD OF TIME.
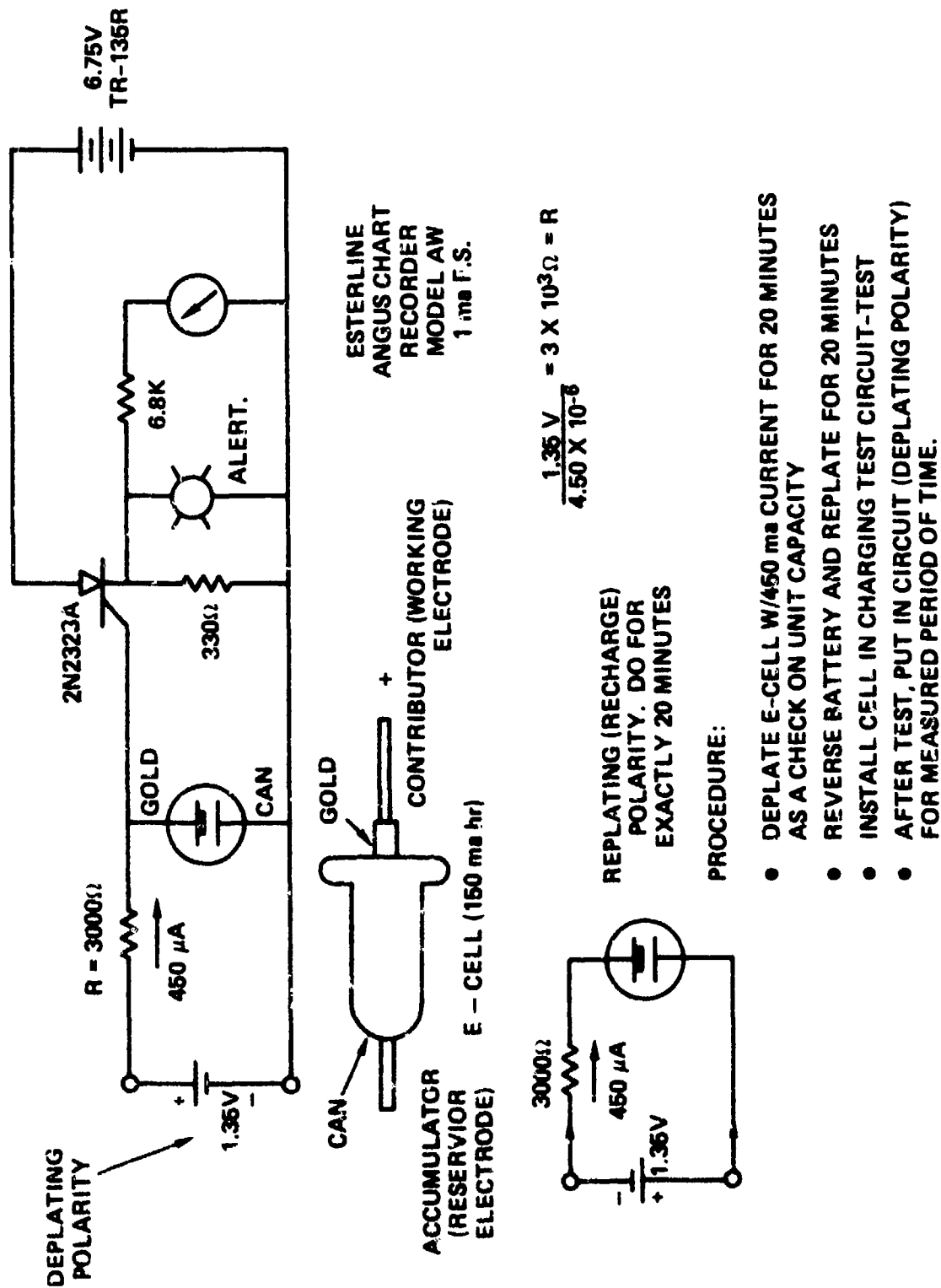
FIGURE 63. SOLAR CELL ARRAY E-CELL PLATING/DEPLATING CIRCUIT.

163

A photograph of the solar cell array/SPVD housing is shown in Figure 64. A small 6.2v-450 ma-hour Nicad battery was used with the array. The solar cell/ SPVD unit was positioned in the NSWC roadway test hole shown in Figures 65 and 66. As indicated, the test hole has a phenolic liner and a phenolic cover plate when SPVD units are being tested.

The array test period extended over one year (24 Sept 76 to 14 Dec 77) with four measurement periods to determine the solar cell array capacity. During the first period 24 Sept 76 to 3 Jan 77, the housing leaked thereby shorting out the E-cell. However, the Nicad battery was at a higher terminal voltage than when installed; therefore a charging capacity greater than 2.7 A-hours was obtained. The second measurement period, 4 Jan 77 to 12 Aprill 77 (98 days) resulted in a 7.72 A-hour charge delivered by the solar cell array, with 2.5 A-hours of it required for SPVD operation. During the third period (12 April 77 → 5 Aug 77) 12.85 Amp-hours were delivered for the 114 day period.

For the last measurement period (5 Aug 77 to 14 Dec 77) the capacity was estimated from a dissassembled E-cell as the unit was completely flooded. By taking dimensions of the E-cell electrode and its plating amount, a 10.2 A-hour charge was delivered during this period.

Using the solar cell array described with a better mechanically designed container, the SPVD system power requirements can be satisfied. For the roadside SPVD receiver control unit (if used for vehicle counting at remote sites) it appears that such a solar power scheme would be even more feasible.

Solar cells cost about $2 each or $40 for the designed unit.

Discussion

The energy density of lithium batteries is very attractive for the SPVD. However, because of the potential explosive safety hazard uncovered in some

FIGURE 84. SOLAR CELL EVALUATION UNIT.

169

FIGURE 65. SOLAR CELL ARRAY IN THE ROADWAY.

FIGURE 66. INSIDE VIEW OF THE NSWC ROADWAY TEST HOLE.

military batteries,[33] it was decided that no additional lithium batteries be evaluated for this program. This most certainly will change in the future, as lithium battery improvements are made.

The Nickel Cadmium battery system was not investigated more thorougly because of its high temperature degradation, low energy density, and lack of a suitable charging system for the secondary cell. If it were possible to charge the Nickel Cadmium batteries, there still is not enough information on "memory" effects (if charged at 1 year intervals) and the associated reliability.[34]

The mercury battery has no recharging capability, has potential electrolyte leakage problem (frequently observed), and is expensive because of the cost of mercury ($\approx$ \$4/lb for Hg). However, its energy density and reliability should insure a 2 year mission lifteime for a 20,000 vehicle/day traffic flux. A battery/systems operation cost tradeoff analysis should be done and include the recycling costs of the mercury battery.

Alkaline cells should also be more fully evaluated in a cost/performance tradeoff. The battery choice was between the alkaline and the mercury, and the energy density/performance (i.e., flat discharge curve) won out over cost.

IX.   MECHANICAL COMPONENT DESIGNS

SPVD MECHANICAL DESIGN AND HOUSINGS

An objective of the SPVD is easy installation of the sensor electronics unit into the roadway. Therefore the SPVD size was designed to be compatible with commonly used roadway core sample drill bits so it could be utilized for unit installation. For this reason, the size of the SPVD could not exceed that of the Phase I unit[1] or 11.43cm diameter and 38.1cm long (4.5" dia x 15"). Other housing problems with the Phase I SPVD were briefly addressed including the aluminum end caps/polyvinyl chloride (PVC) container joint and its reliability over long mission times, more easily opened container to facilitate battery replacement, and general survivability in the roadway environment.

During the early phases of this program, three housings were constructed from standard 4 1/2" dia (11.43cm) PVC Schedule 40 pipe with aluminum end caps sealed with double O rings and 6 screws (6-32) holding the cap to the 1/4" thick pipe wall. This procedure did not provide a reliable long term leakproof housing seal and resulted in the loss of some experimental data in the solar cell unit described in the Battery Section. PVC caps were machined and the bottom cap cemented on with HARVEL PVC heavyweight solvent cement (Harvel Plastics, Inc., P.O. Box 757, Easton, PA). In this way the material expansion coefficients would be more closely matched, i.e., 6.12×10^{-5} in/in/°F for PVC pipe. Some segments of the drawn PVC pipe were out of round which could be minimized by cementing the bottom cap.

The solar cell housing was constructed from a PVC bottom cap cemented to the PVC pipe housing (Figure 67) and an aluminum (6061-T6) array top plate shown in Figure 68. A 1/2" thick 5 7/16" dia. piece of lightly sandblasted plate glass

MATERIAL: P.V.C.
PIPE ALL TOLERANCES: ±0.010"
                     ±10°

#6-32 COUNTERSUNK
HOLES, 120° SPACING
TYP: BOTH ENDS

4" P.V.C.
PIPE, SCHEDULE 40

0.30"

0.30"

13.875"
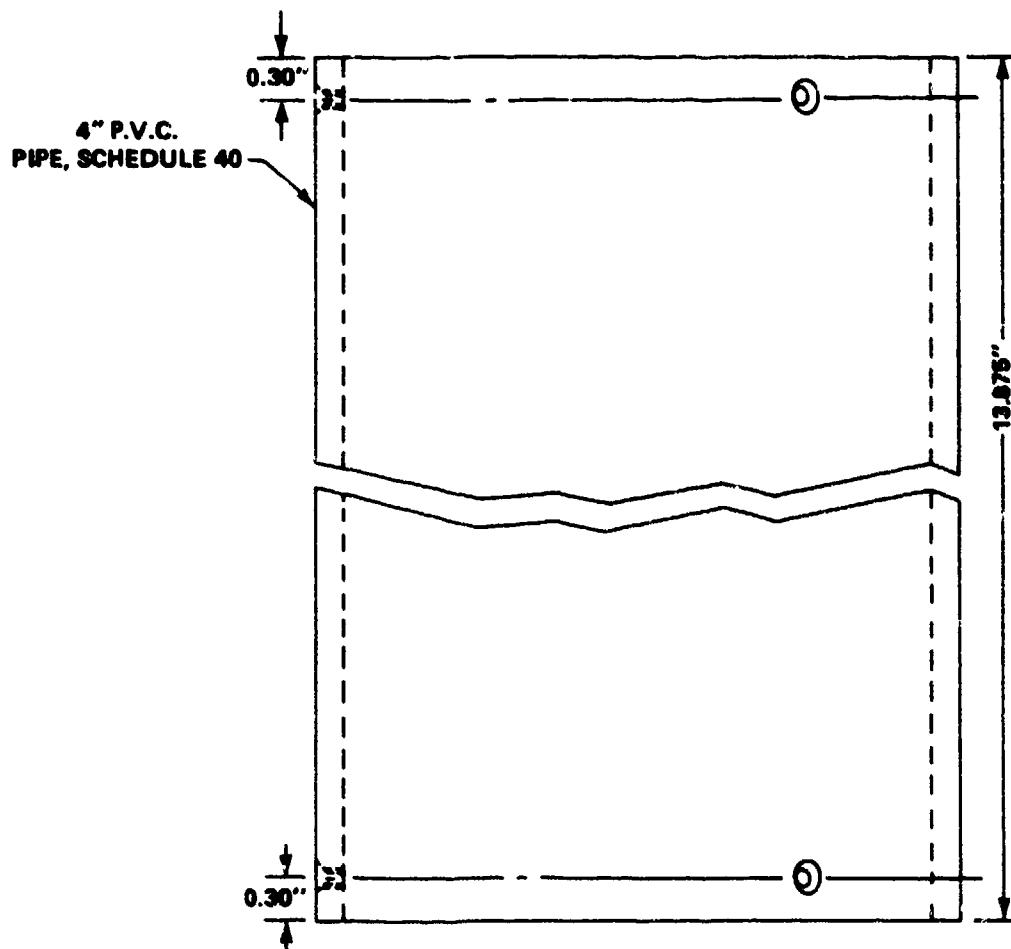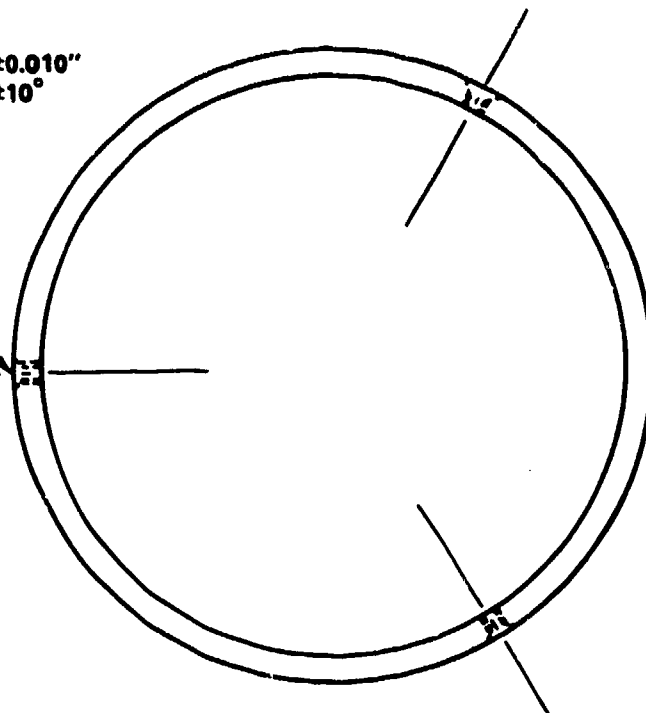
FIGURE 67.   SOLAR CELL UNIT PVC HOUSING.

MATERIAL: ALUMINUM
ALL TOLERANCES ±0.010" UNLESS NOTED.

DRILL & TAP 1/4 X 20,
5/8" DEEP TYP. 2 PLACES

1.37"

#24 DRILL THRU HOLE

A

A

3 9/64"

6.950" ±0.005"
5.60"
5.500" ±0.005"
5.260" ±0.005"

0.65"
0.50"
0.28"
0.20"
0.16"
0.10"

1.00"

0.75"

±.005
0.226"
0.45"
0.40"
0.20"

5.00" ±0.005"
3.925 ±0.005"
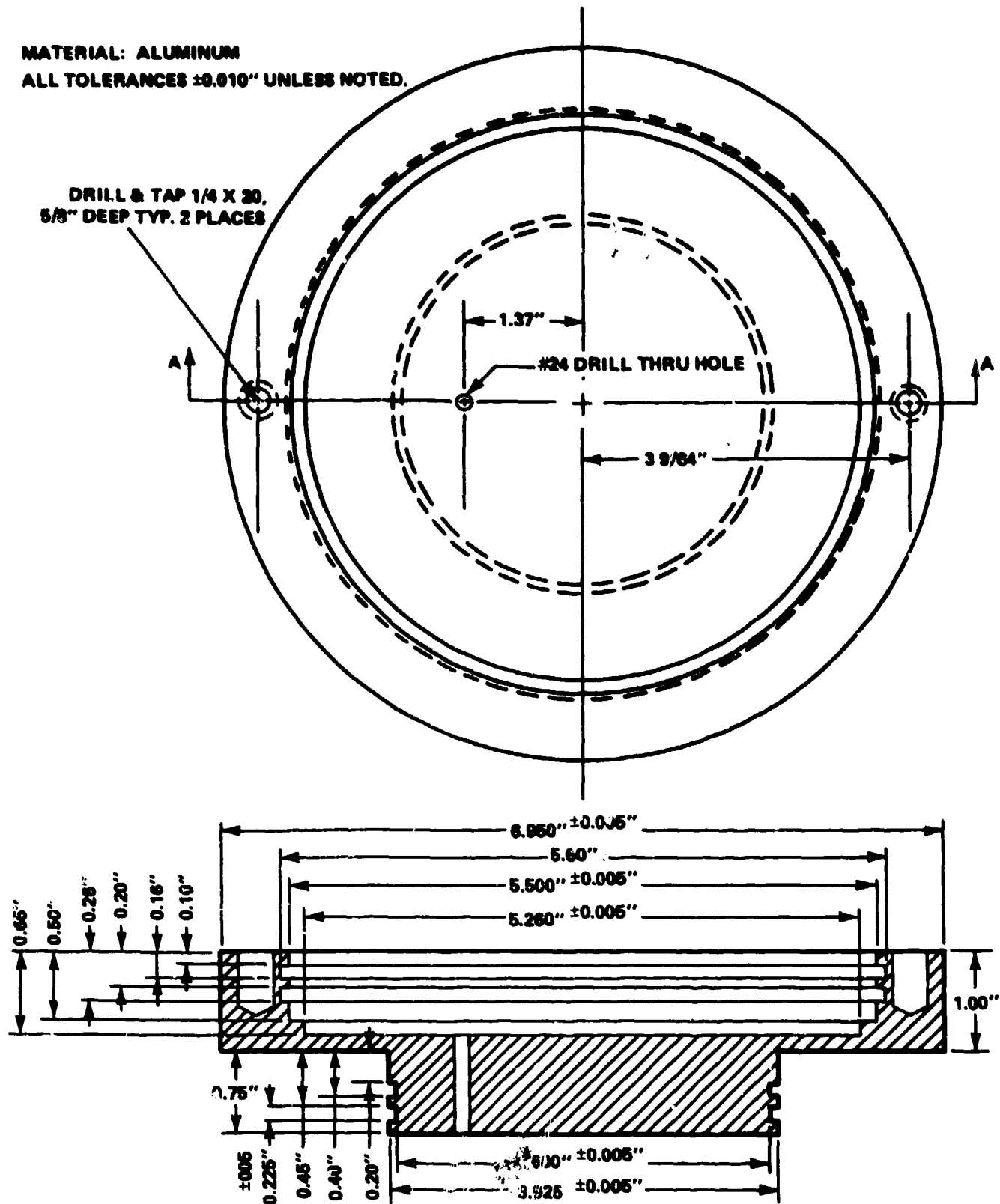
SECTION AA

FIGURE 68. SOLAR CELL ARRAY PLATE.

171

covered the twenty 2 x 2cm series silicon solar cells. The plate glass was slightly sandblasted to diffuse the light, provide a roughed surface for sealing, and make the array less attractive to vandalize. The plate was attached to the aluminum array housing using SCOTCH-WELD STRUCTURAL Adhesive #2216A & B, (7:5 by weight) (Adhesives, Coatings and Sealers Div., 3M Company, St. Paul, Minn.). This joint held up extremely well for the entire length of the test i.e. 24 Sept 1976 to 14 Dec 1977 (see Battery Evaluation Section).

The solar cell array is arranged in a circular pattern which is approximately 5 inches (12.7cm) in diameter and shown in Figure 69. Two O-rings, 3 3/4" I.D., 4" O.D. (FSN 5330-194-3733 are used to seal the array top to the PVC pipe with three 6-32-1/2" stainless screws located to hold the aluminum array housing to the PVC pipe. The experience gained with the above described solar cell array unit was helpful in the design of the final SPVD unit housing.

The SPVD housing design was first completed for an internally housed transmitting antenna, being either orthogonal loops as done in Phase 1, or with a $\lambda/2$ ominidirectional microstrip antenna. The housing consists of PVC pipe, (4" Schedule 40, 4 1/2" OD) as shown in Figure 70 with one end threaded (4 1/8" - 10 RH) for a screw off top cap shown in Figure 71. At the top of the threads is a 45^d sealing surface for an O-Ring (4 1/8" ID x 4 3/8 OD) which is located on the top screw cap. Two holes are drilled in the top cap so a 3" spanner wrench can be used for removal. A third hole is drilled and taped in the top cap's center for a 3/8" - 16 x 1/2" long nylon hex head bolt. This bolt can be screwed into the cap to facilitate SPVD unit recovery from the roadway hole. The bottom housing cap is machined from PVC as shown in Figure 72 and cemented to the bottom end of the PVC pipe of Figure 4 with PVC solvent cement. Both caps have engraved instructions and identification data shown in Figure 73. Arrows are painted on the unit's side to indicate the proper implanting orientation for the SPVD sensor.

172
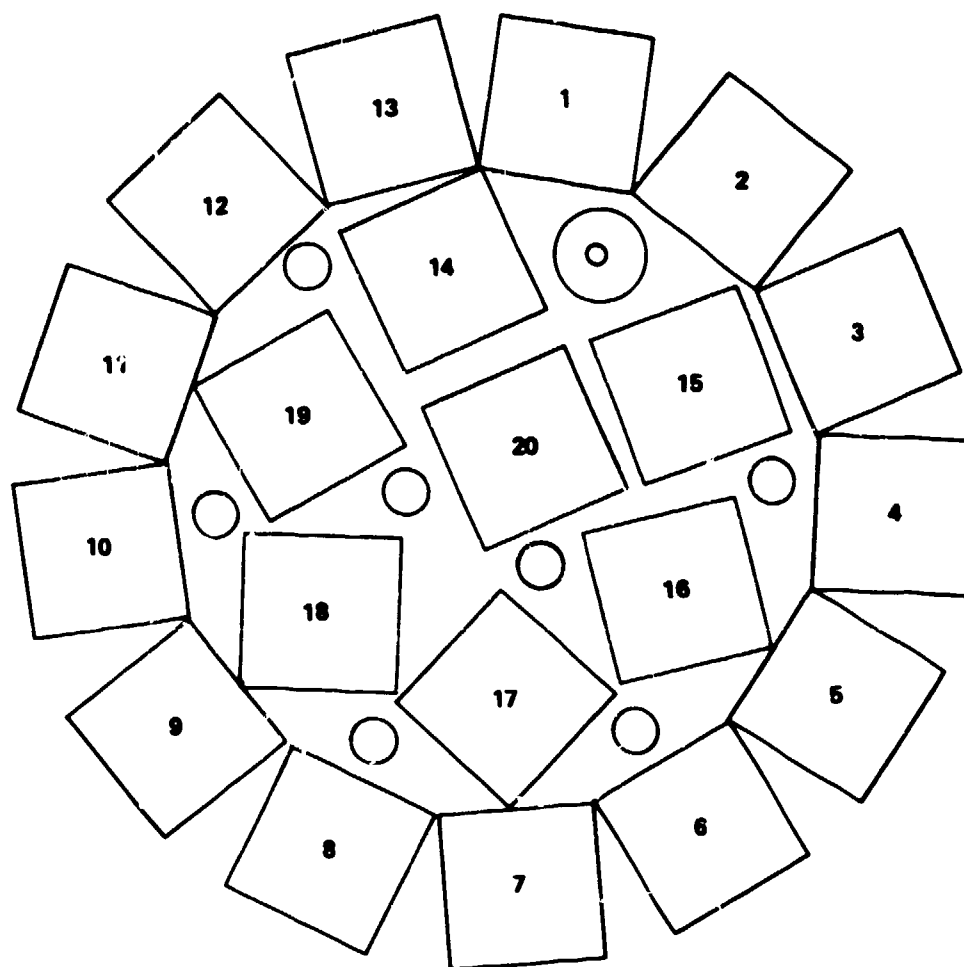
FIGURE 69. SOLAR CELL LAYOUT
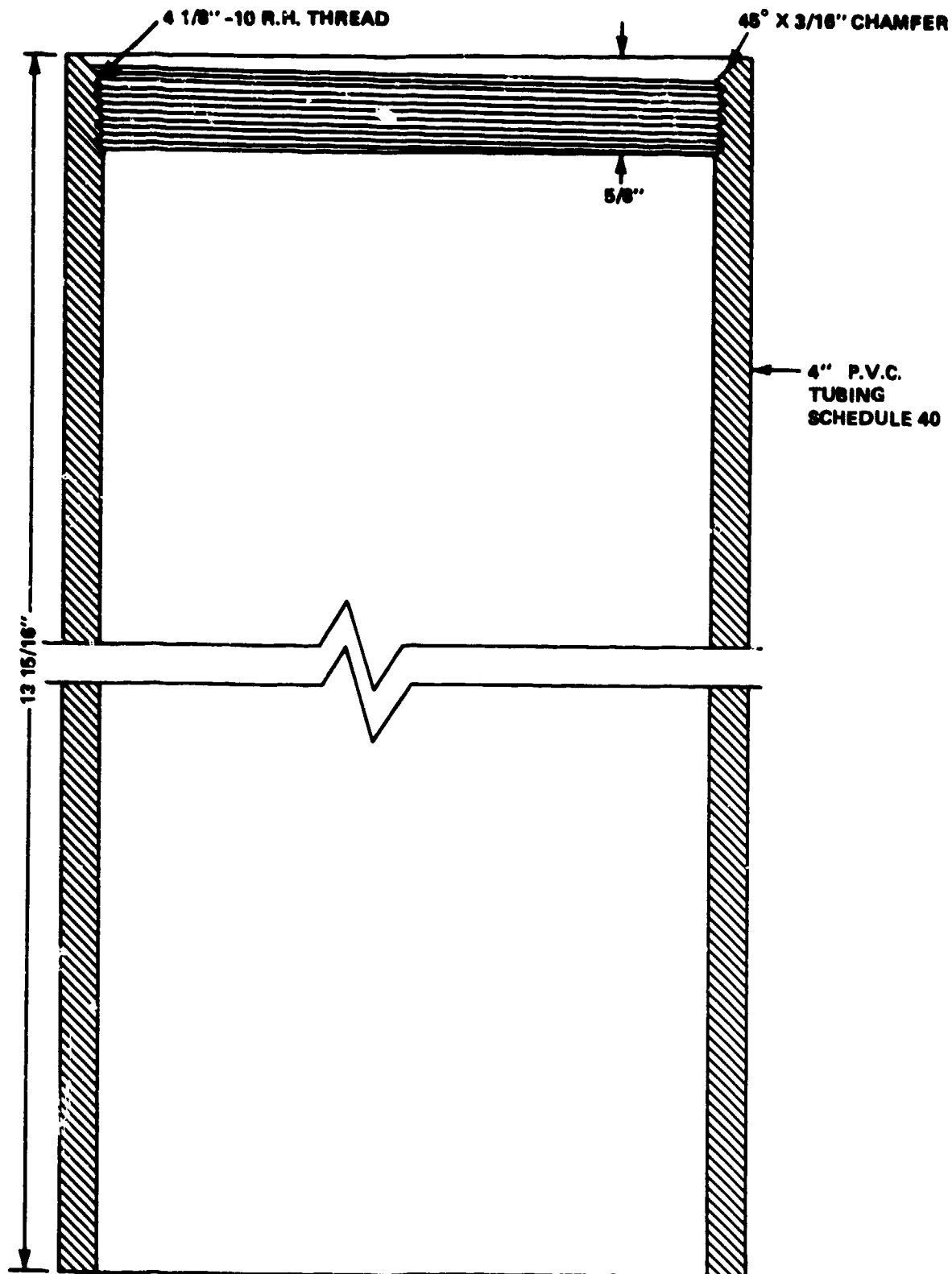
FIGURE 70. DRAWING OF THE SPVD HOUSING.
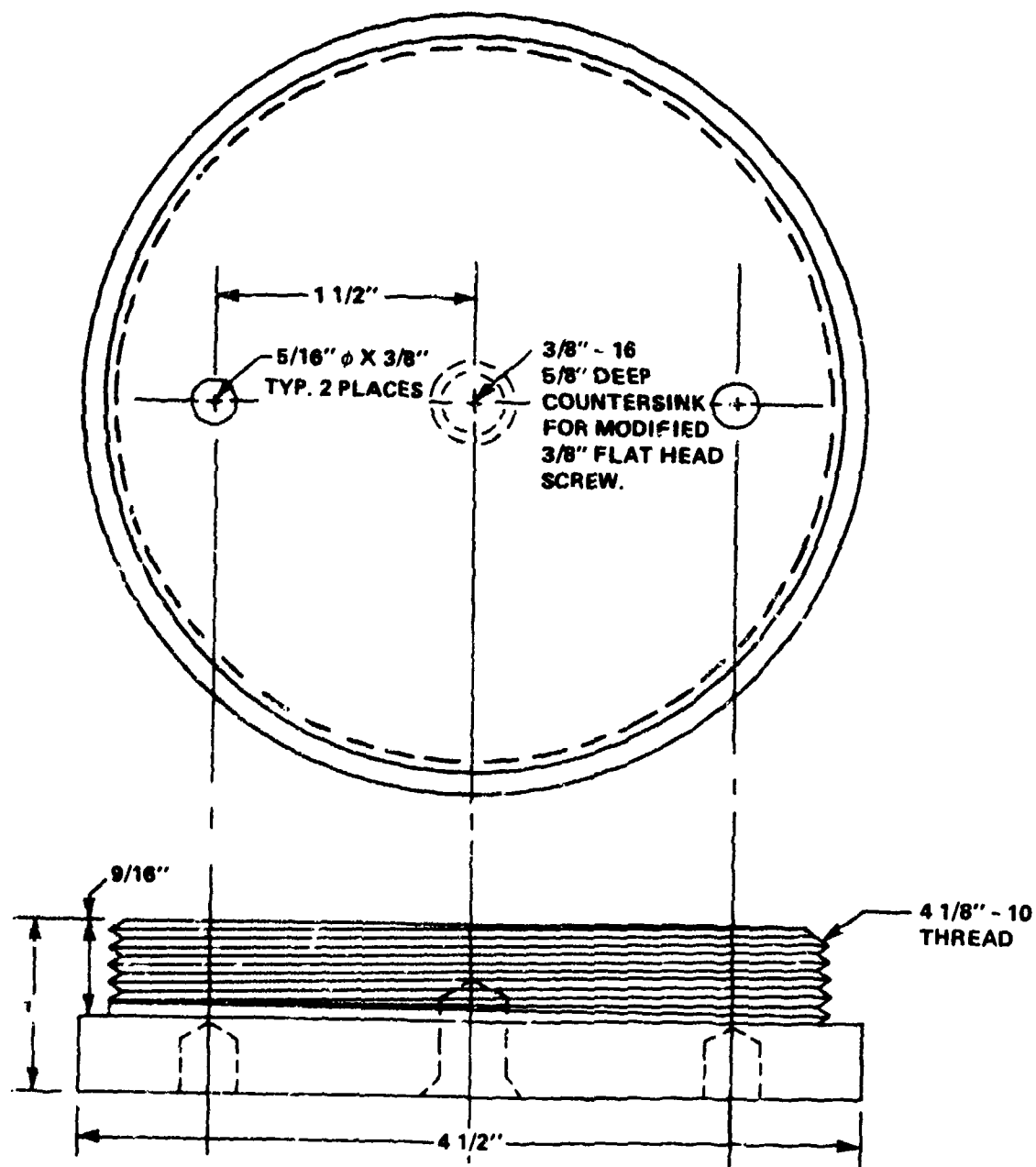
TOP CAP

MATERIAL: P.V.C.

CAP USES 4 1/8" I.D. X 4 3/8" O.D. "O" RING FSN 5330-194-3739

FIGURE 71. DRAWING OF THE SPVD HOUSING TOP CAP.

175

"F" DRILL
3/8" DEEP

4 1/2"

4"

TO FIT INSIDE
4" P.V.C.
TUBING

HOLES FOR
FINAL SPVD
UNIT DESIGN.

1/2"

15/16"

MATERIAL: P.V.C.
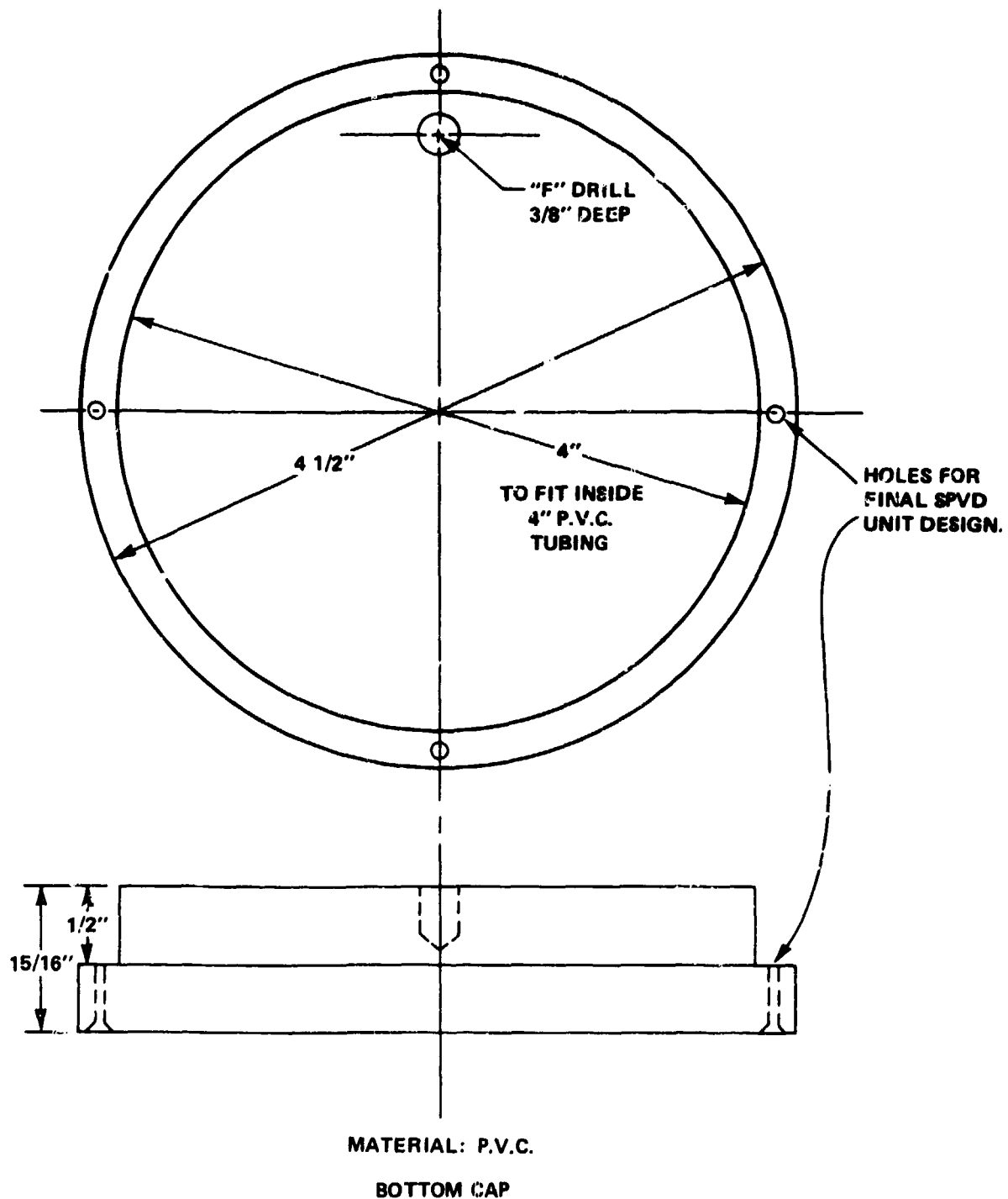
BOTTOM CAP

FIGURE 72. DRAWING OF THE SPVD HOUSING BOTTOM CAP.

176

TOP CAP

BOTTOM CAP

FIGURE 73. ENGRAVED INFORMATION ON SPVD TOP AND BOTTOM CAPS.

This first unit was thoroughly tested for watertight integrity, was temperature cycled (-40°C - +75°C), and subject to a 1000 pound compression test to simulate a worse case load distributed on the top cap (62.9#/sq.") and on the threads (300#/sq."). The unit survived well including several severe and inadvertent drop tests.

The second and final SPVD unit housing design was specifically tailored to the λ/4 omnidirectional microstrip antenna. Dimensions of all three housing component parts were basically unchanged (Figures 70, 71, 72). The bottom cap was modified by drilling four holes for four 6-32-1/2" flat head nylon screws to aid in holding the bottom cap to the PVC pipe. The PVC pipe had been completely plated (except for the threads with a 3 mil copper foil etched antenna. In order to maintain conductor continuity from the inside antenna ground plane to the external antenna, the cap is now sealed with RTV (Silicone Sealant RTV - Dow Corning) rather than the PVC solvent cement.

Before the bottom cap is attached, the outside portion of the copper plated PVC pipe is etched to form the λ/4 omnidirectional microstrip antenna. The antenna is then connected to a coaxial cable from the inside by drilling a hole through the PVC pipe wail at the appropriate location. The center conductor is soldered to the outside foil antenna strip while the inside foil is soldered to the coax shielded braid. A strain relief is installed to rigidly secure the 17" length of cable (RG-58C/V - 50Ω) by drilling a hole through the PVC wall and inserting a nylon screw (6-32-1/4") which holds a cable clamp. The nylon screw is dipped in PVC solvent cement before it is inserted to facilitate sealing. After testing the antenna, it is coated with a gray acrylic lacquer primer (Dupont #100S Multi-Purpose) and then several coats of clear Imron (#500S) polyurethane enamel. The Imron

FIGURE 74. SPVD ELECTRONICS.

2-56 TAPPED HOLES X 5/16" DEEP
(TYP. 6 PLACES)

#26 DRILLED HOLE
1.725" RAD.

12-28 TAPPED HOLES
WITH 0.400" DIA X 0.200"
DEEP COUNTERBORE. 1.700"
RAD. (TYP. 3 PLACES)

#26 DRILLED HOLES
1.675" RAD.
(TYP 2 PLACES)
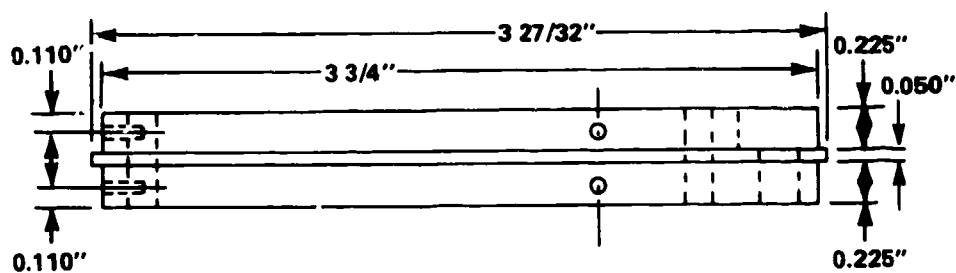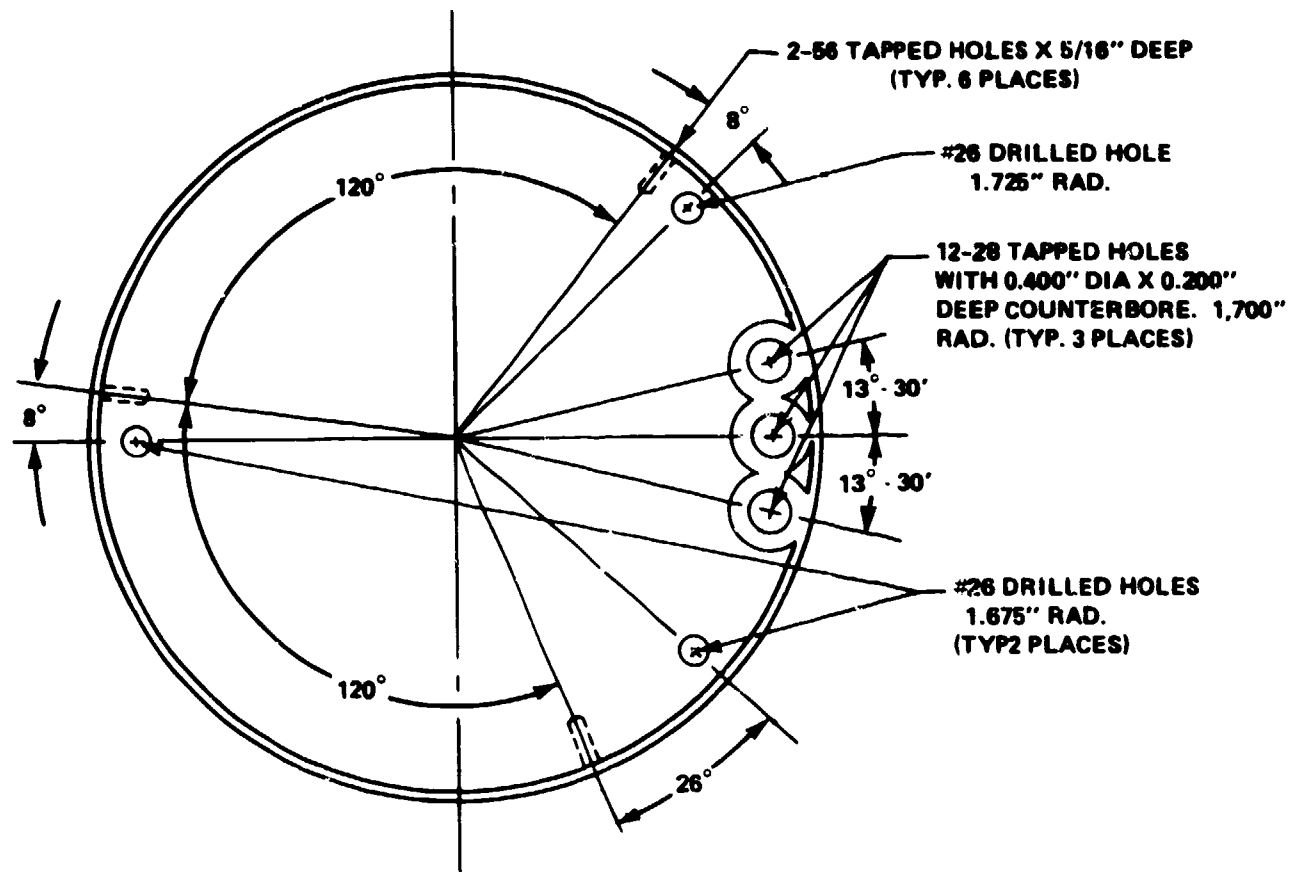
MATERIAL: ALUMINUM 1/2" THICK

FIGURE 75. DRAWING OF THE SENSOR MODULE INTERFACE PLATE.

X = SENSOR MODULE
    TOP - 1½"

X = TRANSMITTER MODULE
    BOTTOM -1 15/16"

0.110"

3 3/4"

3.850"

COUNTERSINK FOR #2 SCREWS
120° SPACING (TYP 3 PLACES)

MATERIAL: ALUMINUM 0.050" THICK.
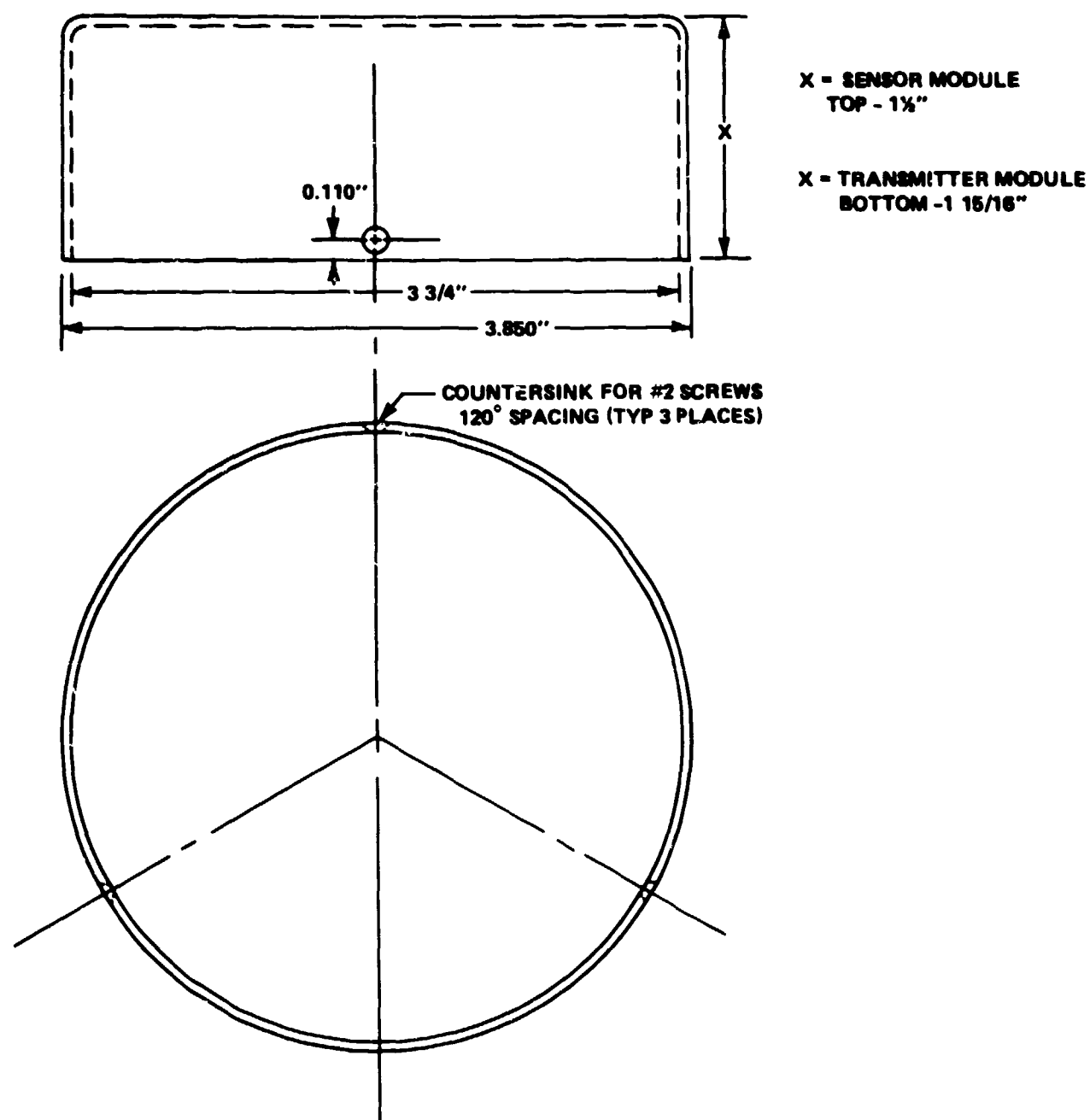
FIGURE 76. DRAWING OF ELECTRONICS MODULE COVERS.

connectors required for unit operation. The rear panel has an opening (2 3/4"
x 1 1/2") in the top right corner for receiver module control access. It is covered
by an aluminum plate 3 1/2" x 1 7/8" which is secured to the box by two self-
tapping screws.

Lettering the front and top panels with identifying nomenclature was done by
a silk-screening technique. Figure 77 is a photograph of the front silk-screened
panel. Before silk screening the front and top panels, all box holes were drilled
and the front panel cleaned and repainted.

All control unit components are rigidly secured to the box by a variety of
steel brackets. Figures 78 and 79 are photographs of the control box, the side view
and rear view showing the power supply battery, electronic boards, and receiver
module mounting and relative positions.

SPVD Battery Housing

After selecting the Mallory Mercury Battery (#316856-5) a suitable housing
was required to protect the SPVD electronics from potential electrolyte leakage over
the long mission time. Although the seals on mercury cells are quite good, it has
been found that at elevated temperatures over long periods of time the potassium
hydroxide (KOH) electrolyte seeps out and is potentially damaging to all non-noble
metals.

ABS (Acrylonitrile - Butadiene - Styrene) plastic material is immune to the
effects of strong alkalies and is quite inexpensive. Three inch ABS extruded pipe,
Schedule 40 (i.e. 3" ID, 3.5" OD) was obtained and machined to form a housing shown
in Figures 80, 81, and 82. The end caps were machined from 4" dia. ABS rod, and
one cap is sealed with ABS solvent cement (Oatey Solvent Cement, Fleck Marshall
Corp., Baltimore, MD). The other end has a removable cap which is threaded
(3 1/8" - 10 thread) and able to be removed with a small spanner wrench. An O-ring
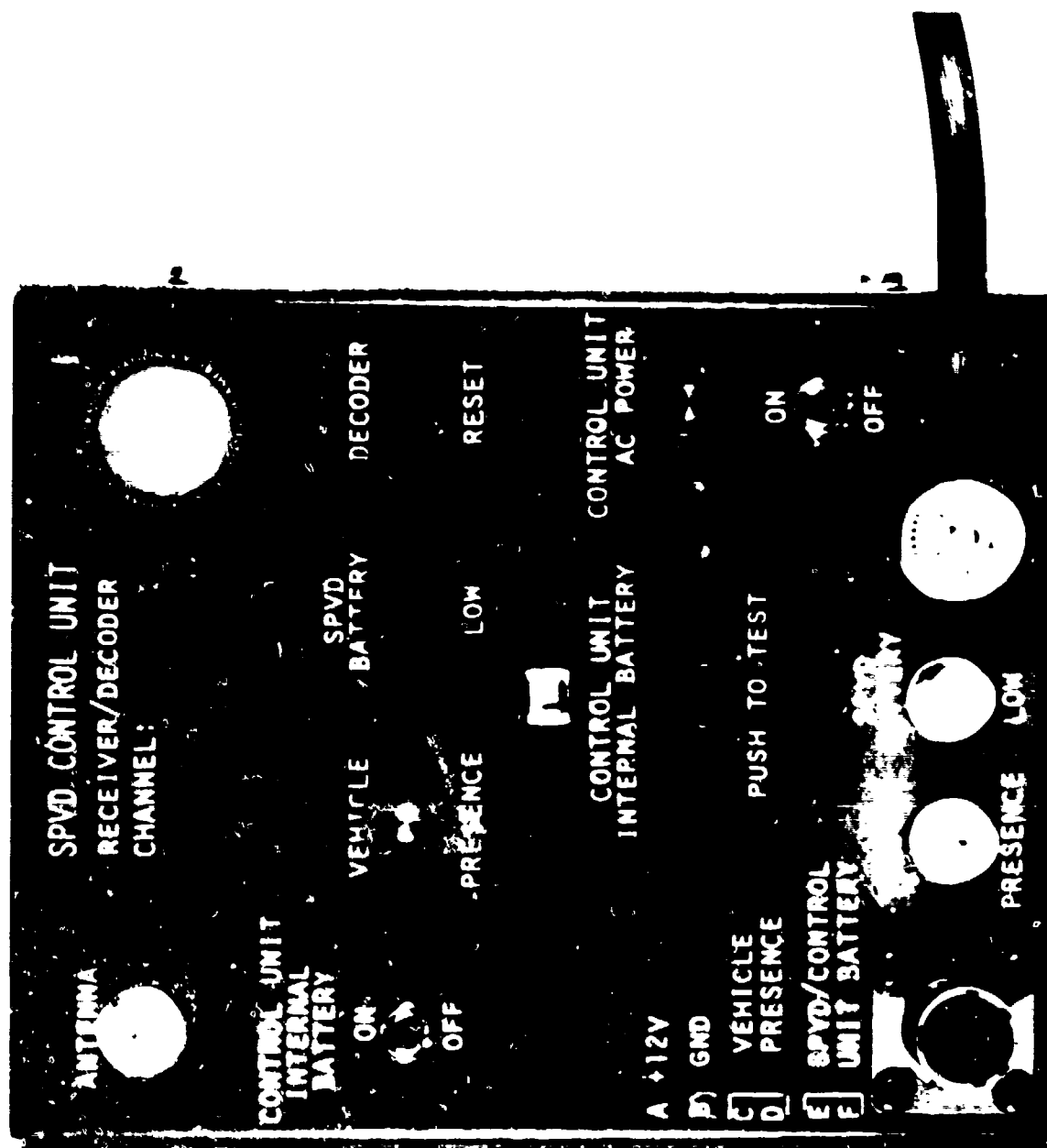
FIGURE 77. SPVD CONTROL UNIT FRONT PANEL LAYOUT.
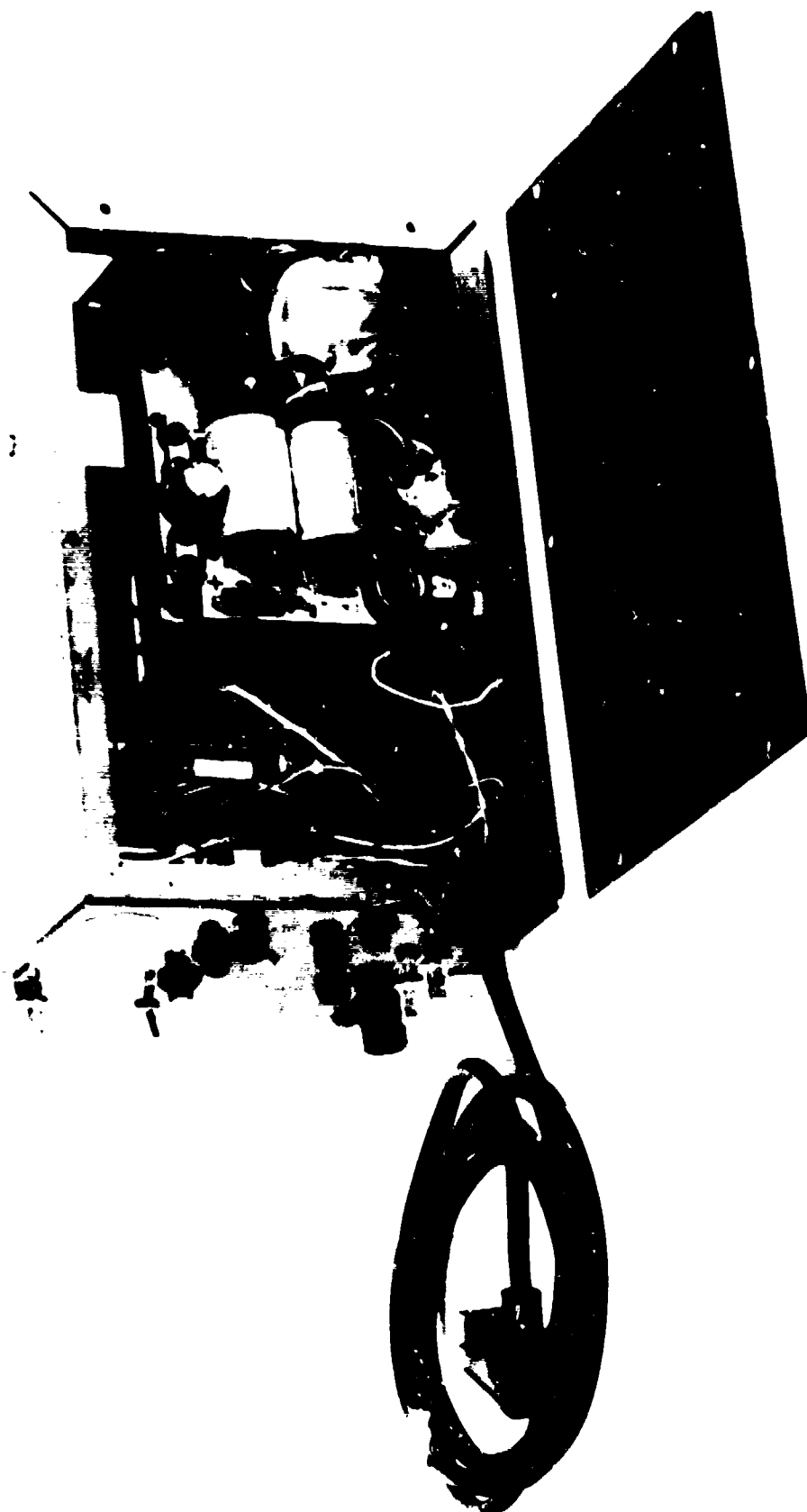
FIGURE 78. SPVD CONTROL UNIT, SIDE VIEW.
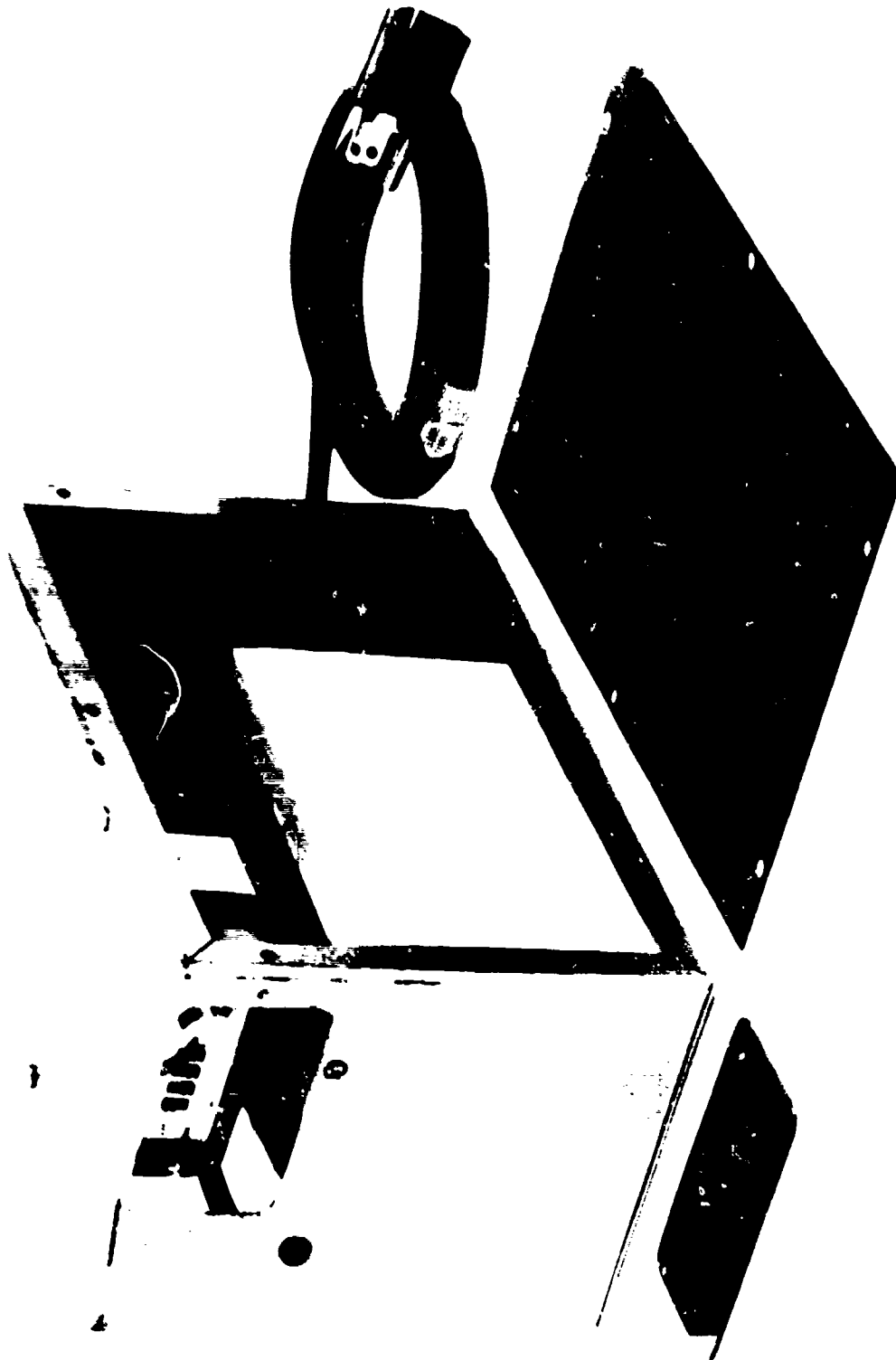
FIGURE 79. SPVD CONTROL UNIT REAR VIEW.

3 1/8" X 10 THREAD

0.080"

5/8"

7/8"

3¼"

3/16" DIA X 3/16" DEEP, 2 PLACES

7/16" DIA X 3/16" DEEP

1"
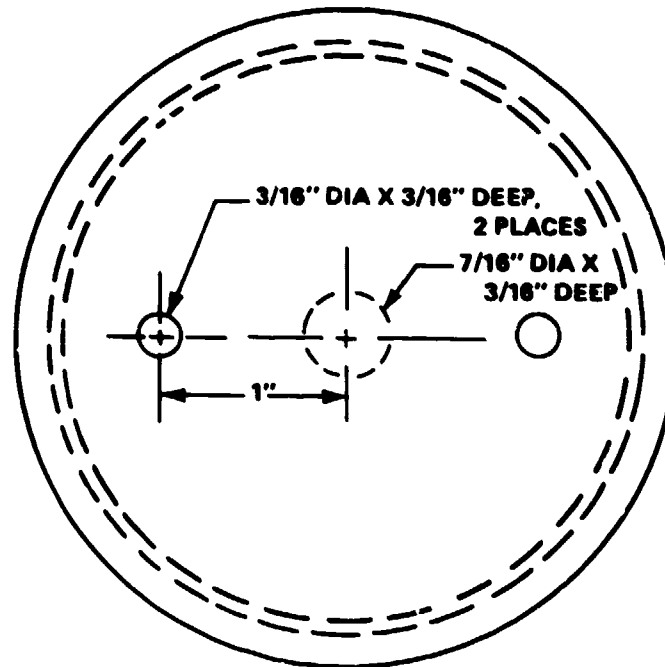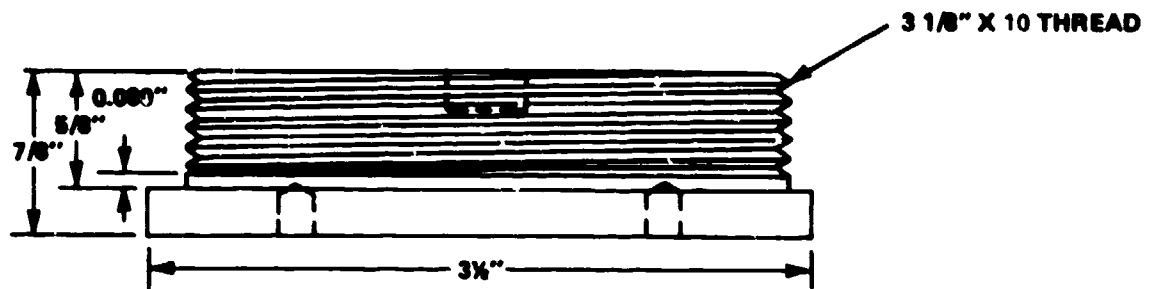
MATERIAL: ABS PLASTIC

FIGURE 80. DRAWING OF BATTERY HOUSING END CAP (BOTTOM).
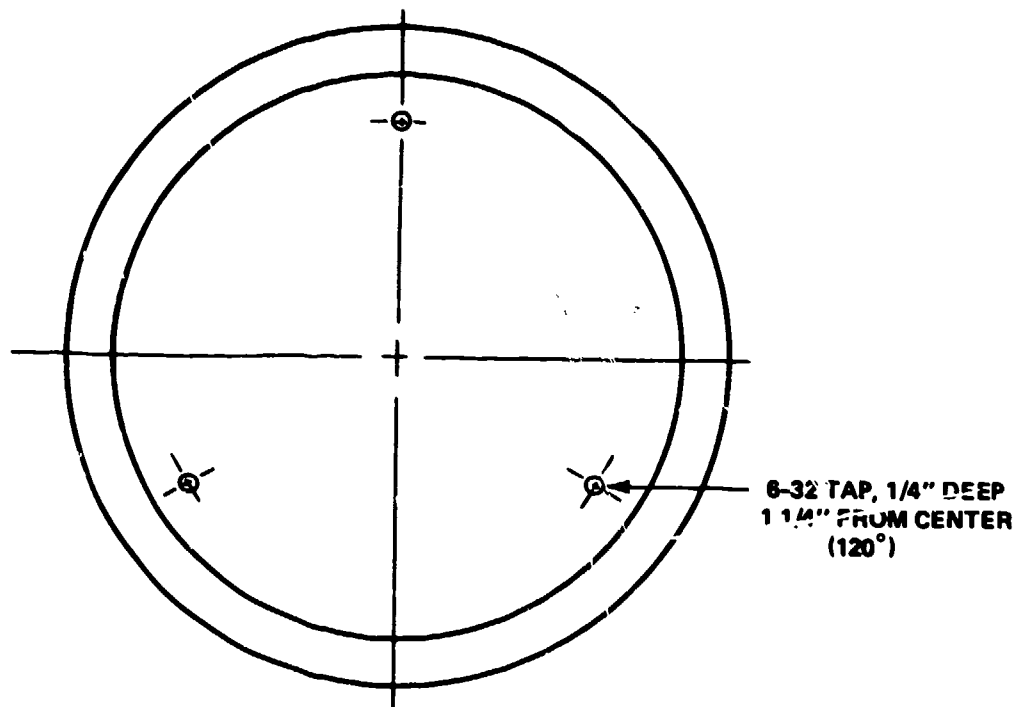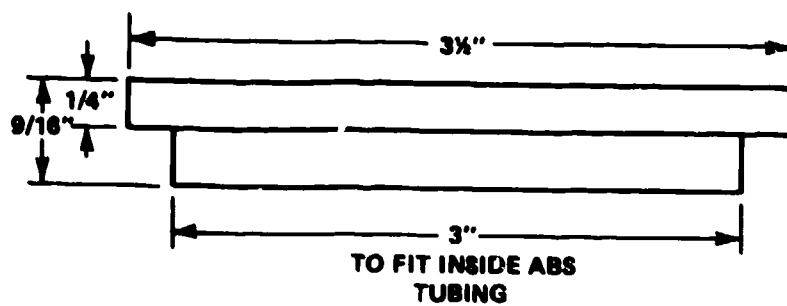
MATERIAL: ABS PLASTIC

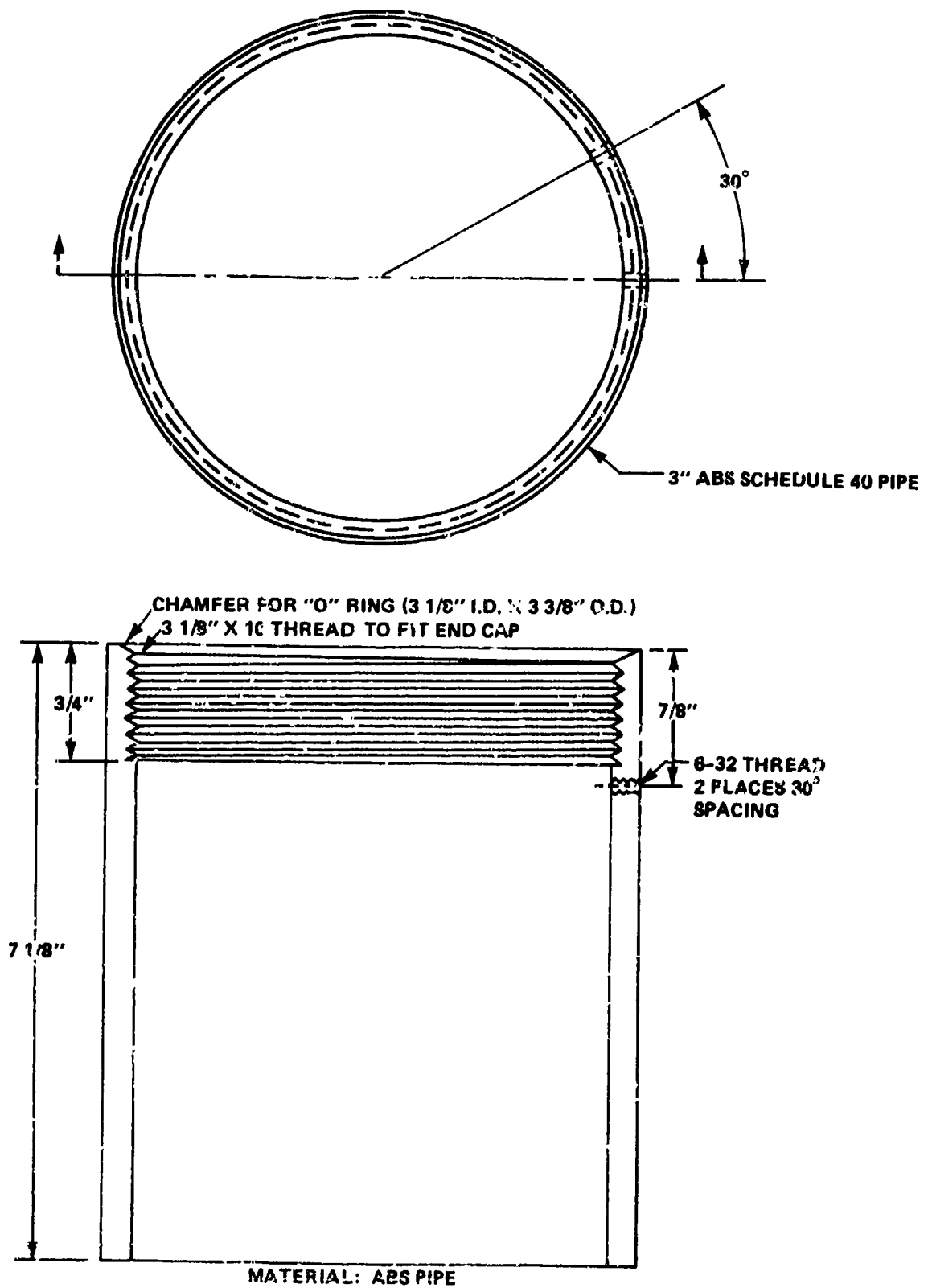**FIGURE 81. DRAWING OF BATTERY HOUSING END CAP (TOP).**

FIGURE 82. DRAWING OF BATTERY HOUSING TUBE.

(3 1/8" ID x 3 3/8" OD) is used to seal the battery housing and is lubricated with silicon grease (GE Silicon Compound G-624, MIL S-8660B).

The housing is 7 1/8" long and contains two paralleled Mallory #316856-5 batteries for a total of 26 amp-hours capacity. The housing terminals consist of two #6-32 stainless steel screws which connect two solder lugs located inside the housing with the two external solder lugs each containing a Cambion (#450-3388-01-03-00) Connector Jack (Cambion Corp., Cambridge, Mass.). One screw terminal is painted red indicating the +6.75 volts.

A stainless steel spring is inserted in the removable cap to reduce battery motion. The batteries are placed end-to-end, and the two positive terminals are soldered directly together; also a #22 teflon red insulated wire is soldered to that junction. The negative terminals are connected with a 6" length of #22 black teflon insulated wire with a longer black wire soldered to a 2A Fuse which connects to the top negative terminal. The two batteries are then taped together and wrapped with several layers of absorbant paper towels and inserted into the housing. The two wires are soldered to the terminals (red to red) and then the container sealed.

To test the battery housing, 105 grams of 40% KOH solution (worse case) was put into a sealed battery housing with its terminal lugs and springs in place. It was put into an oven at 130°F (54°C) for 16 days and then examined. Results were that no KOH absorption was observed, no leakage occurred, nor was the O-ring attacked. The spring was discolored and the tin removed from the solder lug terminals.

Battery Replacement Procedure

1. Check battery voltage at the battery housing terminals (see Figure 74) before proceeding. If 6 volts or greater under load, i.e., with sensor module on, batteries are capable of operating the SPVD.

2. If no voltage at all is measured, the protective fuse inside the housing is probably blown. Check the fuse with an ohmmeter after step (3).

3. With a small spanner wrench (2") remove the battery housing cap.

4. Pull out the batteries and check the fuse with an ohmmeter. If the fuse is CK, check each battery again. Unsolder leads from terminals, if less than 6 volts.

5. Clean terminals and inside battery housing. Discard absorbent paper towels surrounding the batteries, cut the negative wire connecting the two batteries.

6. Put batteries in a sealed plastic bag and return to FHWA, HRS-32, Washington, DC for recycling. Note the date unit was installed and date replaced, and SPVD Serial Number.

7. Connect two new batteries (Mallory #316856-5) in parallel, i.e.,two positive terminal tabs (+) are soldered together with a red wire attached.

8. Tape the two batteries together and solder a black wire to the two negative (exposed) battery terminal tabs. Another longer black wire is then attached to one of the ends. Solder in the 2A fuse in series with the black lead connected to the negative housing terminal.

9. Wrap the batteries with several layers of absorbent paper towels.

10. Insert the batteries into the housing, solder the wires to the appropriate terminal lug (red wire to red terminal, +6.75v).

11. Clean the cap and O-ring and regrease the O-ring with silicone grease and seal the housing.

12. Check the voltage; should be +6.75 volts and mark the date on the housing. The batteries if supplied by NSWC or FHWA are demagnetized. However, if purchased directly from the manufacturer it may be necessary to demagnetize them.

Some battery's permanent magnetic field (PERM) can add an additional 10000γ to the ambient earth's field when measured 3 inches from a magnetometer sensor. A color TV picture tube face demagnetizer may be used to demagnetize the batteries before they are inserted into the battery housing. Each battery weighs 885 grams (≈2#) and costs $27.18. The weight of the total battery housing containing two batteries is 2310 grams (≈5.1#). Because of the high battery cost and mercury being a valuable strategic resource and a poisonous pollutant, each battery should be recycled. A label is put on each battery with the following information:

RECYCLE

RETURN USED BATTERY TO:
FEDERAL HIGHWAY ADMINISTRATION
HRS-32
WASHINGTON, DC 20590

SPVD System's Electronics, Components and Circuit Board Layouts

The SPVD system electronics consists of a commercially available power supply and receiver and six electronics circuit boards. The power supply module is a Power Mate Corporation Model EMA-12/15B, 12 volt/2 amperes with case dimensions shown in Figure 1.

The radio receiver module is a Tandy Corp. (Radio Shack) Realistic Model PRO-6 scanning receiver. Case dimensions are shown in Figure 2. There are four receiver modifications: (a) removal of the battery compartment by milling of the bottom 1 3/8" of the receiver, (b) connecting a coaxial connector to Test Point 2 (TP-2) on the receiver printed circuit board and filing an exit hole on the side of the case, (c) soldering a twisted Red/Black of #22 AWG stranded wire to the receiver power terminals (6v), and (d) soldering a coaxial cable to the earphone plug for use as an external antenna input. Crystals are inserted in the proper

position so that Position 1 is the 41.37 MHz channel and Position 2 is 41.41 MHz.
Two other channels are available if desired.

Circuit Board Layouts

Three of the SPVD systems six circuit boards are double sided boards. The
sensor module consists of a single sided Brown magnetometer circuit board shown
in Figure 83, the two digital nulling loop electronics on a double sided board
of Figure 84, and the double sided signal processing/regulator board shown in
Figure 85. Three 1/2" standoffs (6-32) hold the two sensor module boards together,
and a brass bracket attaches the Brown magnetometer circit board to them. In this
way, the magnetometer can sense the vertical component of the magnetic field.
Sensor module board sizes are 1 7/8" x 1" and two 3 11/16" diameter boards with a
2" x 7/16" chord removed. All circuit boards are 1/16" thick.

Several versions of the transmitter/encoder board were made reflecting
design changes and problems of integrating the transmitter with the system.
Figure 86 shows the transmitter encoder board foil layout which dimensionally is
3 11/16" dia x 1/16" thick.

The receiver decoder interface circuit board component layout is shown in
Figure 87. There are several interconnecting wires to both the front panel,
receiver, and encoder board as indicated in Figure 87.

The tone decoder circuit board component layout is a single-sided board shown
in Figure 88. Board size is 4" x v 7/8" x 1/16" thick and must be positioned
with the potentiometers up so the mercury reed relays will activate properly.
All electronics units in the control box, except for the receiver module, are
connected to this circuit board.

Several control unit brackets were fabricated to hold the two electronic
circuit boards, receiver module, and standby battery securely to the box.

193

CORE ORIENTATION
(TOP VIEW)

SIZE: 1 7/8" X 1" X 1/16" FIBERGLASS
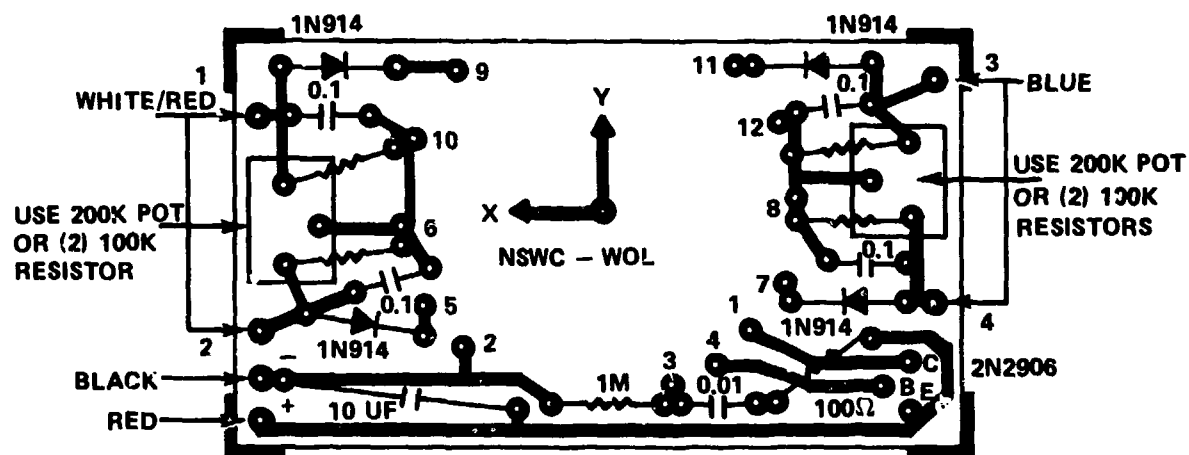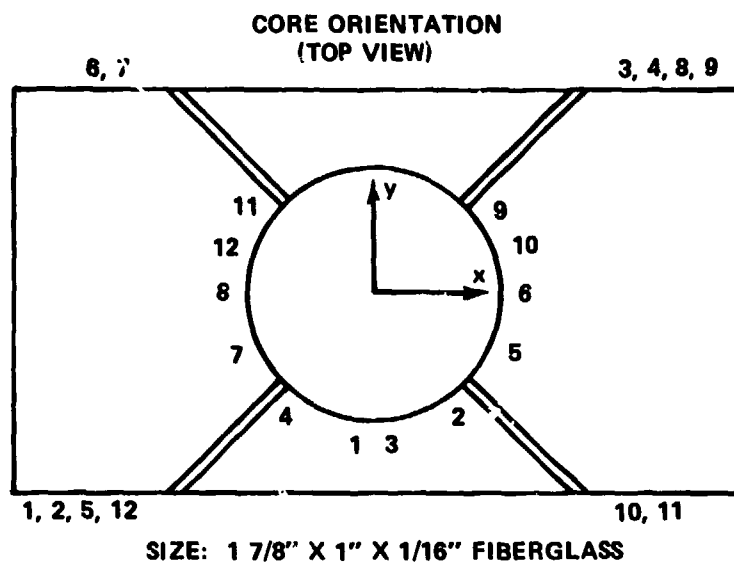
FIGURE 83. BROWN MAGNETOMETER CIRCUIT BOARD LAYOUT.
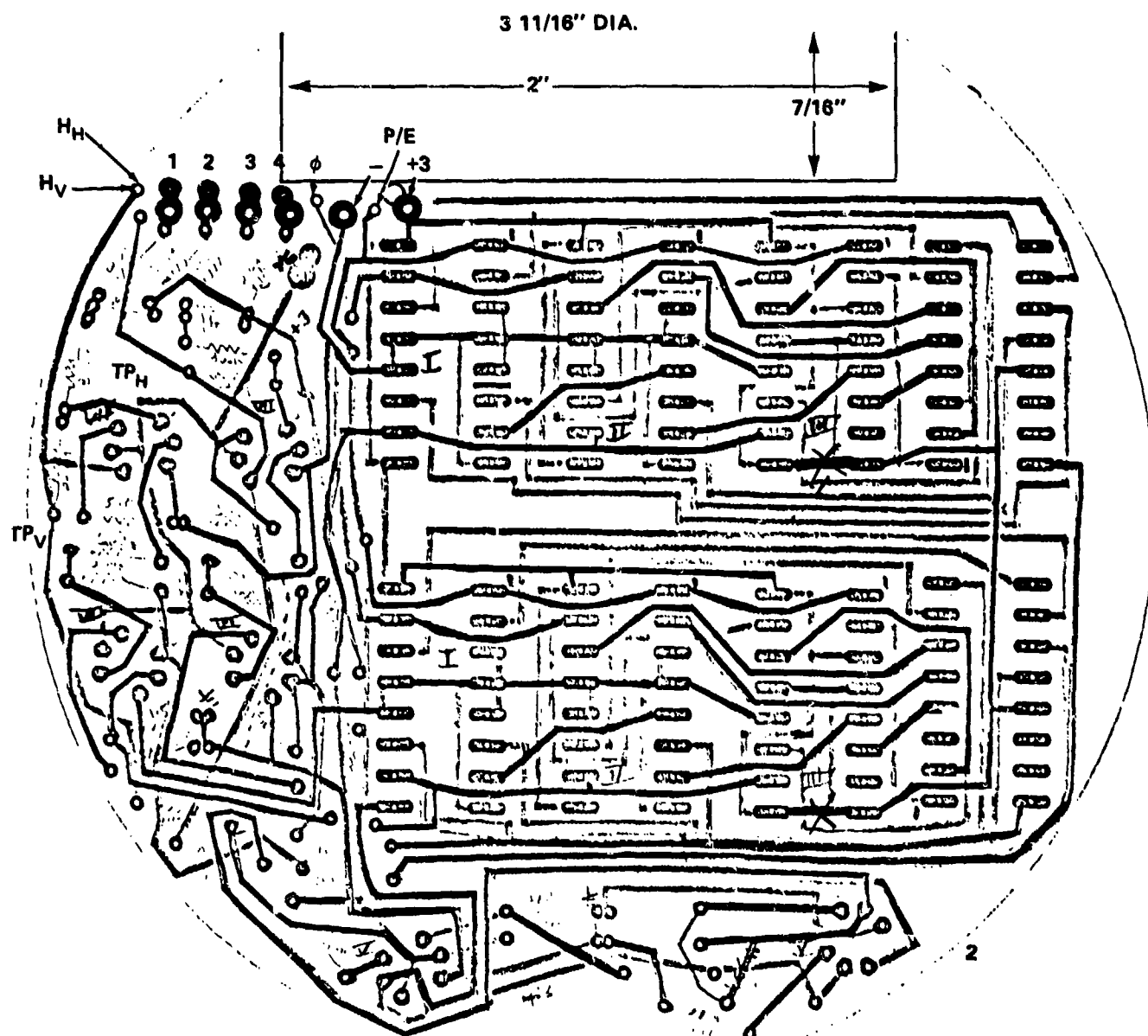
FIGURE 84. LAYOUT OF DIGITAL NULLING BOARD, SPVD SENSOR.

FIGURE 85. LAYOUT OF SIGNAL PROCESSING/REGULATOR BOARD, SPVD SENSOR.
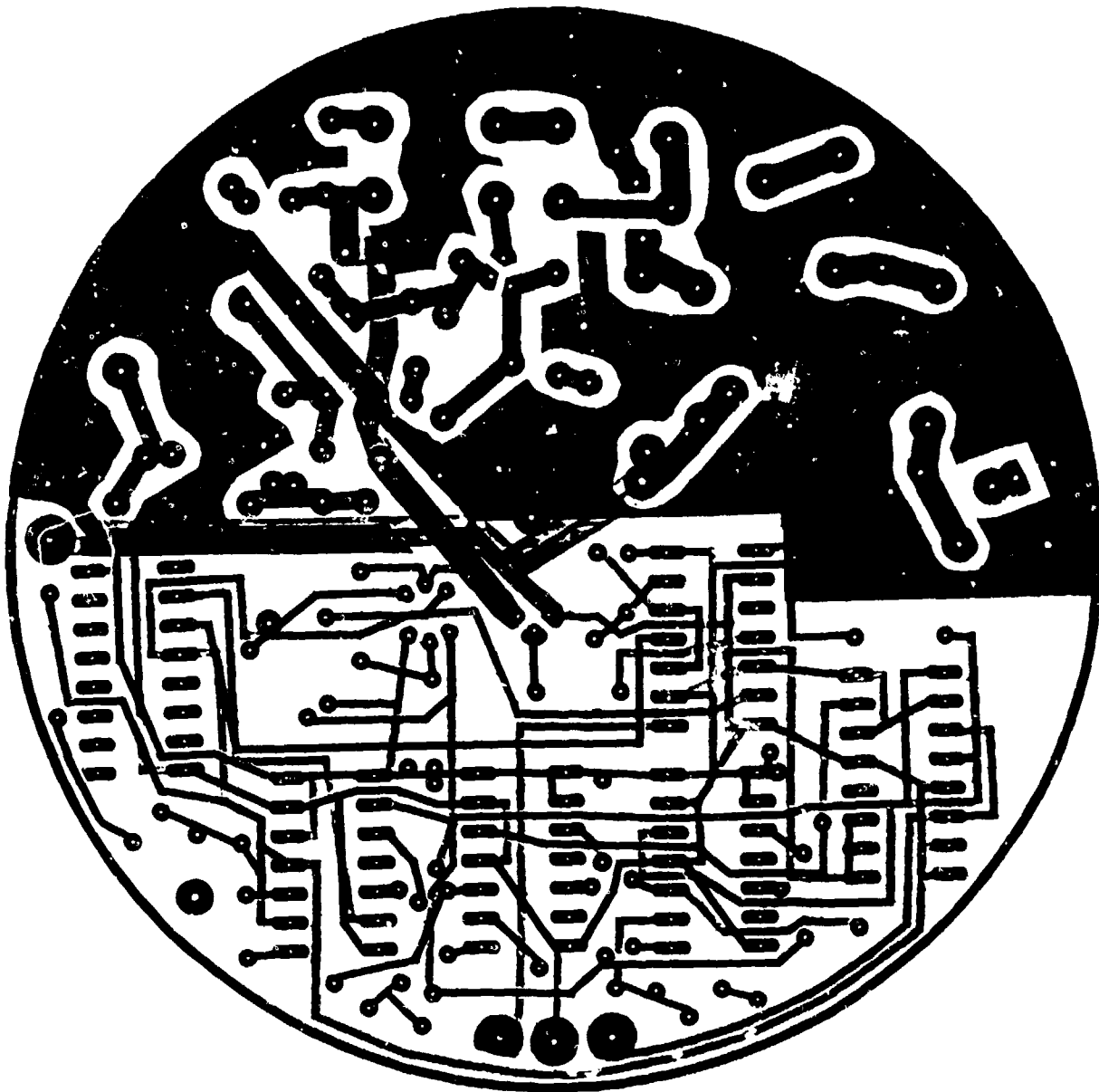
3 11/16" DIA.

FIGURE 86. LAYOUT OF SPVD TRANSMITTER/ENCODER BOARD.

FIGURE 87. RECEIVER DECODER INTERFACE CIRCUIT BOARD LAYOUT.
4 1/2" X 1 3/4" X 1/16"

FIGURE 88. DECODER CIRCUIT BOARD LAYOUT
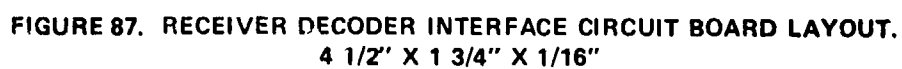
The power supply and several cable straps are screwed into the box and provide cable strain relief. All completed circuit boards are cleaned with Freon TF or trichlorethylene and sprayed with Humiseal Protective Coating Type 1B15 (Humiseal Division, Columbia Technical Corp., Woodside, New York 11377).

To trouble-shoot or adjust the decoder circuit board electronics, remove the right box panel and two bottom 6-32 screws holding the circuit board brackets. There are sufficient lengths of cable for the boards to be removed from the box.

All circuit board layouts (originals) and photographic masters were delivered to the FHWA.

Receiving Antenna

A quarter wave whip antenna is supplied for each SPVD system. It is a commercially available stainless steel whip citizens band antenna (Tandy Corporation, ARCHER,102 inch body mount whip antenna Cat No. 21-1094) which has been cut to a total length of 71.28 inches (1.81 meters). The spring is not required for installation on a traffic control box. Figure 89 outlines the installation procedure. With a simple bracket, it may be pole mounted with an RG-58C/U lead in cable to the control box's antenna input BNC connector. Installation of the receiving antenna relative to the location of the SPVD will be quite important to system performance. Therefore it is suggested that several antenna locations be tried for the optimum location before a standard bracket is made.

WHIP

SPRING (NOT USED WITH THE SPVD RECEIVER)

BALL MOUNT

SOLDER LUGS

71.28"

1-1/16"

1" DIA. HOLE

9/32" DIA. HOLES

TEMPLATE

BODY

GROUNDING PLATE

CENTER STUD   RUBBER PAD

ANGLE NUT

PLASTIC INSULATOR

UPPER HEMISPHERE

ANGLE BOLT

MOUNTING NUTS

LOCKWASHER

MOUNTING BOLTS
LOCKWASHERS

LOWER HEMISPHERE
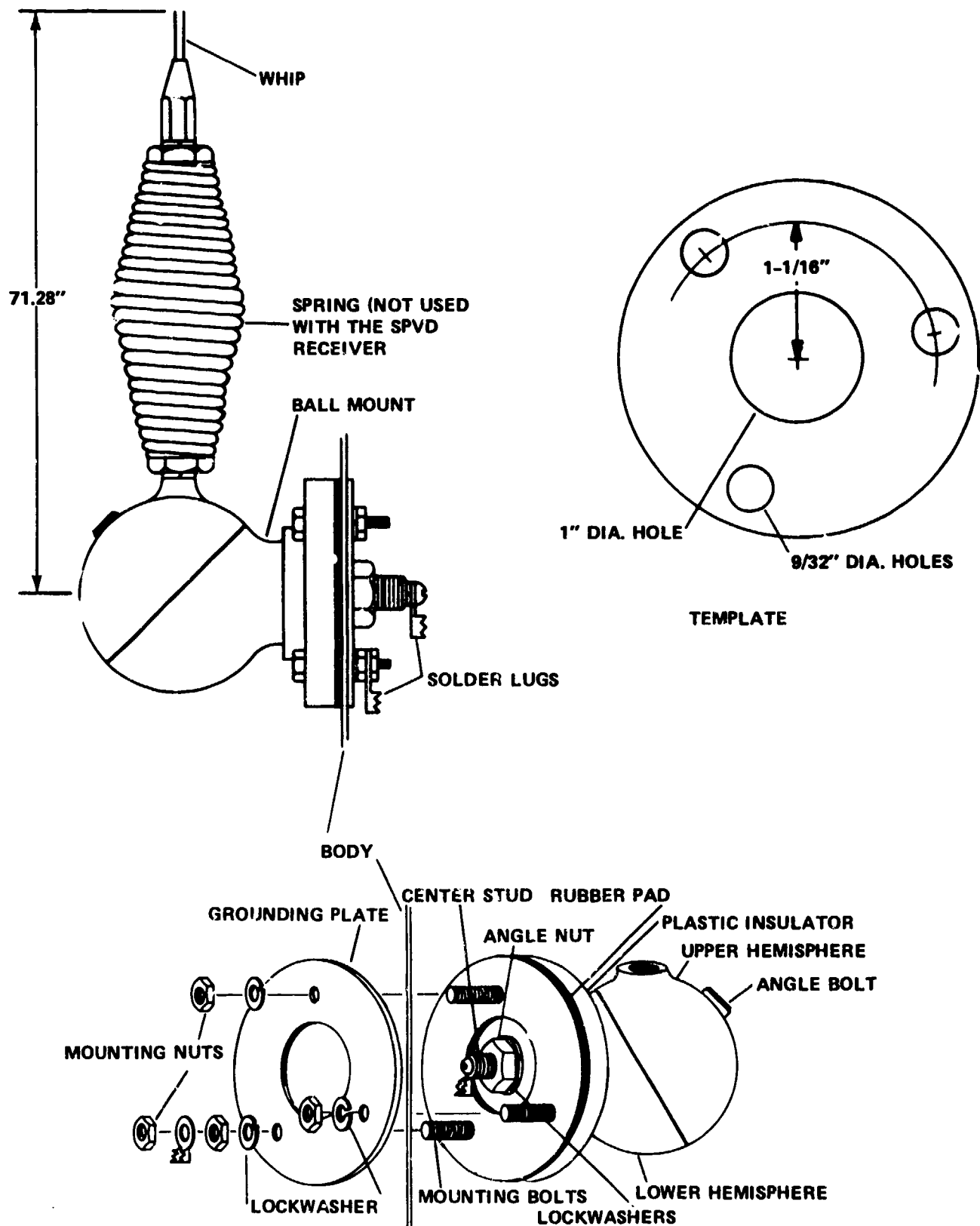
FIGURE 89. RECEIVING ANTENNA MOUNTING INSTRUCTIONS.

X.   SPVD SCHEMATIC DIAGRAMS, DRAWINGS, AND DATA TABLES

The SPVD System is divided into several distinct parts or modules. The SPVD unit contains a sensor module, transmitter/encoder module, battery module, and the omnidirectional microstrip antenna/housing. The SPVD control unit consists of a receiver module, decoder electronics, standby battery, power supply module, and a steel box housing.

In this section five drawings of the complete SPVD system electronics are provided to help give an overall view of the system. Figure 90 is a detailed schematic diagram of the sensor module containing all the magnetometer and sensor electronics associated with the actual vehicle detection functions. Figure 91 is a detailed schematic diagram of the SPVD encoder/transmitter module with summary instructions to set the encoder tones. One should see the text for more detailed instructions. The SPVD housing is drawn in Figure 92 and shows the various component modules assembled inside the SPVD antenna/housing.

The SPVD control unit contains a receiver module consisting of a Radio Shack (Tandy Inc.) Model PRO 6 scanning receiver and an interface board both schematically depicted in Figure 93. Figure 94 is a schematic diagram of the SPVD control units decoder electronics and control box wiring diagram. Figure 95 is the power supply module data sheet containing specifications, parts list, and a schematic diagram of the Power/Mate Corp. Model EMA-12/15B power supply.

Twenty SPVD units were fabricated and tabulated in Tables XVI and XVII are the sensor module and transmitter/encoder module control sheets containing all checkout data on each unit.

All twenty SPVD system control boxes were operated for a minimum 500 hours burn in period and experienced 60,000 programmed activations. The prototype control box and SPVD have been operating for longer than one year.
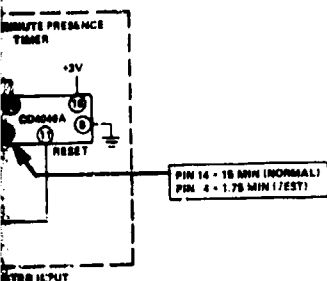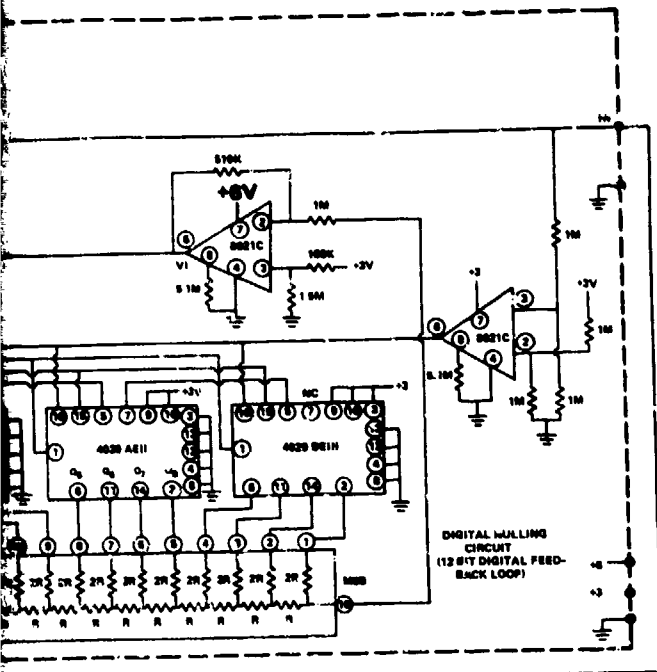
FIGURE 90. SPVD MAGNETIC SENSOR MO

DIGITAL NULLING CIRCUIT
(12 BIT DIGITAL FEED-
BACK LOOP)

MINUTE PRESENCE TIMER

PIN 14 - 15 MIN (NORMAL)
PIN 4 - 1.75 MIN (TEST)

* THRESHOLD VALVE (0.67 - 0.7V)
1M 340.0/365.9 (X36.9)
12M 535.0/33.7 (X17.6)

ERIE
1201-062
SINGLE
SECTION L.P.
EMI FILTERS

VEHICLE PRESENCE

TO +6 REGULATOR BOARD

+6 VOLTS

UNDER-VOLTAGE OUTPUT

SHIELD CAN

TO BPVD TRANSMITTER/DECODER BOARD

MODULE SCHEMATIC DIAGRAM.

204
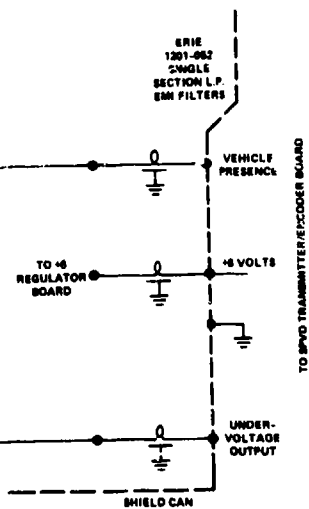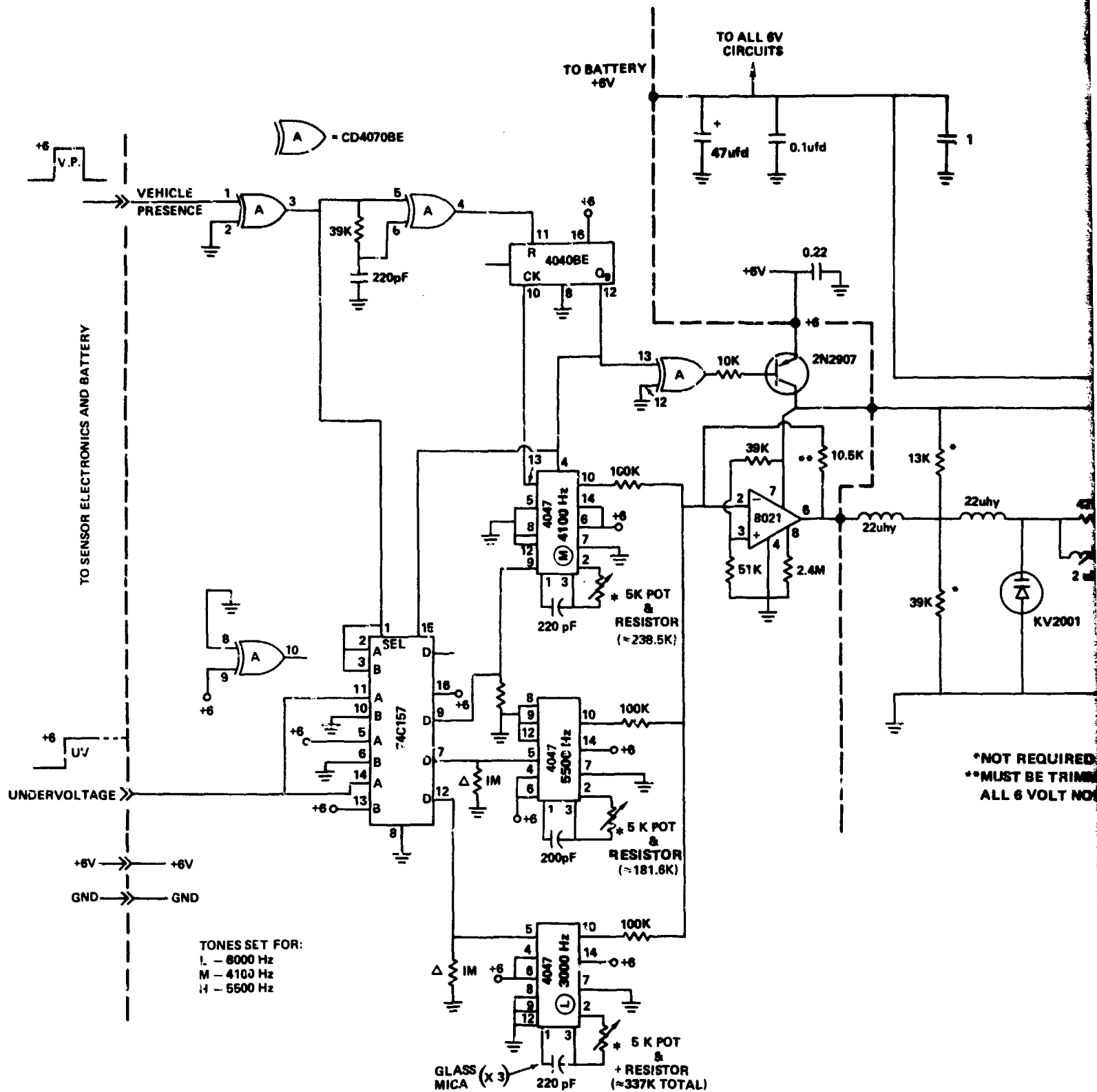
TO SET TONES:

a) MIDDLE TONES — PUT CD 4047 MIDDLE PIN #4 & PIN #9
LOW WITH 250Ω RESISTOR TO GND.
ADJUST RESISTOR & POT., USE PIN
10 TO MONITOR FREQUENCY

b) HIGH TONE — PUT CD 4047(H) HIGH, PIN 5 HIGH TO
6.75V WITH A 250Ω RESISTOR, ADJUST
RESISTOR & POT, OUTPUT READ ON
PIN 10

c) LOW TONE — PUT CD4047(L) LOW, PIN 5, HIGH TO
6.75V WITH A 250Ω RESISTOR, ADJUST
RESISTOR & POT, OUTPUT READ ON
PIN 10.

L1 1/4" DIA OSCILLATOR COIL 22 1/2T #30 2 uhy
SPARTON ELECTRONICS #100-6688

L2 1/4" DIA OSCILLATOR/DOUBLE COILS
SPARTON ELECTRONICS #100-5532

L3 1/4" DIA FORM, 21T #29, 4 uhy

L4 1/4" DIA FORM, 17T #29, 2.8 uhy
WITH EPOXY

A FAIR RITE SHIELD BEAD #2673000101

B FAIR RITE SHIELD BEAD #2673000701

RED
DES = 6.75V BATTERY VOLTAGE

FIGURE 91.   SPVD ENCODER/TRANSMITTER MODULE SCHEMATIC DIAGRAM

IMPLANT
WITH THIS END UP
AND
ARROWS IN DIRECTION
OF TRAFFIC FLOW

ARROW & SERIAL NO.

SENSOR
MODULE

TRANSMITTER/
ENCODER
MODULE

BATTERY
MALLORY # 316856—5
6.75 VOLTS

2A FUSE SOLDERED
IN LINE

NYLON SCREW
FOR RECOVERY
9/16" HEX HEAD
(3/8 — 16 x 1/2)

TO REMOVE CAP USE
3" ADJUSTABLE FACE
SPANNER WRENCH

ARROW ON HOUSING/ANTENNA
EXTERIOR TO LINE UP WITH
ARROW ON TOP OF SENSOR MODULE

ANTENNA COAX (TEFLON, 50Ω & RG-58 C/U)

OTHER SIDE UP
FEDERAL HIGHWAY ADMINISTRATION
HRS—32
WASHINGTON, D.C. 20590
SPVD SERIAL NO.
CHANNEL

BATTERY
MALLORY # 316856—5
6.75 VOLTS

←FOAM→
SPACERS

6—5

(DEMAGNETIZED)

15" OVERALL LENGTH
13" INSIDE LENGTH

ANTENNA

TO REMOVE CAP
USE 2" ADJUSTABLE
FACE SPANNER
WRENCH

FIGURE 92.   DRAWING OF THE SPVD UNIT.
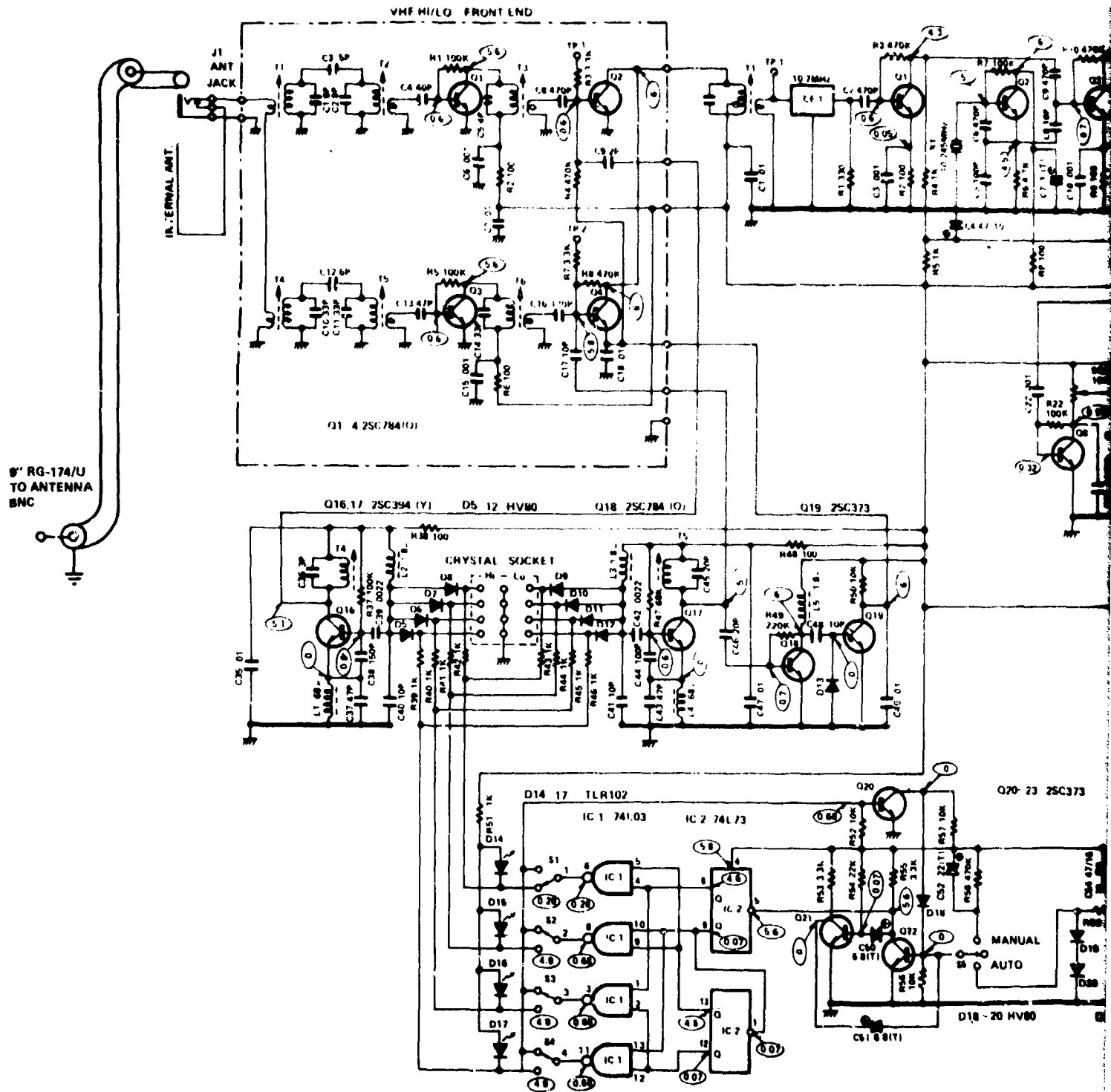
TANDY (RADIO SHACK) PRO 6 SCANNING RECEIVER
XTAL FREQUENCY 52.110C MHz (41.41 MHz)

FIGURE 93. SPVD RECEIVER

100K

+12

7

8021C

.1   10K

2

3   8021C

+12V

7

6

8

.1   T.P.

TO DECODER
BOARD INPUT

2M

1M   2M

+6

3 POLE H.P. 2.7 kHz

+12V

+12V

7806

10 ufd   10 ufd

CONTROL UNIT
BATTERY
CHECK & MONITOR
CIRCUITRY

PUSH
TO CHECK
BATTERY

75Ω
2W

10 VOLTS MIN
@ 160 ma DRAIN

VER MODULE SCHEMATIC DIAGRAM.

/210

1   3

LEADING EDGE = LOW TONE + MIDDLE TONE = 3000Hz + 4100Hz
TRAILING EDGE = HIGH TONE + MIDDLE TONE = 5500Hz + 4100Hz
UNDER VOLTAGE = LOW TONE + HIGH TONE = 3000Hz + 5500Hz

DECODER ELECTRONICS BOARD

FIGURE

ANTENNA (BNC) INPUT

STANBY BATTER ON/OFF SWITCH

FUSE HOLDER, EXTRACTOR FHN26G1
P&N 5920-00-892-8J11 WITH FUSE
CARTRIDGE, TYPE FO 3A 250V

115VAC
POWER SWITCH

115V POWER CORD

AC POWER ON LED - GREEN
DIALCO 10V-20ma #248-7970-3332-504

DECODER RESET

VEHICLE PRESENCE LED - YELLOW
(DIALCO 5V,20ma #248-9088-3333-504

6 PIN CHASSIE
CONNECTOR

(A) +
    12V BATTERY TERMINALS
(B) GND

(C)
    V.P. RELAY TERMINASL
(D)

(E) U.V. RELAY TERMINALS
        MAX RELAY LOAD 35VA,
(F)   (.75A MAX, - 500VDC MAX)

PLUG TO
OTHER
CIRCUITS,
MS 3116E
10-6P

V.P. OUTPUT BNC

U.V. OUTPUT BNC

U.V. INDICATOR LED - RED
DIALCO 5V-20ma #248-7988-3331-504

SPVD CONTROL UNIT PANNEL

MINIMUM UNIT LIFE ON INTERNAL BATTERY IS 20.5 HOURS.
CIRCUIT - 50ma, RELAYS - 60ma, RECEIVER MODULE - 70ma.
LED DISPLAY - 40ma, 220ma MAX DRAIN.

FIGURE 94. SPVD CONTROL UNIT SCHEMATIC DIAGRAM.

211/212

POWER/MATE CORP.
114 S. RIVER STREET, HACKENSACK, N.J. 07601
PHONE: (201) 343-6294 TWX: (710) 990-5373

POWER SUPPLY APPLICATION AND MAINTENANCE DATA EMA "B" CASE

SPECIFICATIONS

INPUT: 105 to 125 VAC or 210 to 250 VAC at 47 to 63 Hz. Derate output current 10% for 50 Hz operation.

DC OUTPUT RATINGS: See Voltage/Current Rating Chart.

REGULATION: Line regulation is rated at 0.05% for a 10% input voltage change and load regulation is rated at 0.1% for a zero to full load change.

OUTPUT RIPPLE: Better than 1 m V RMS; 3 m V peak to peak typical.

OVERLOAD PROTECTION: Self restoring current limiting (foldback type) is standard.

TEMPERATURE COEFFICIENT: ± 0.005%/°C typical. ± 0.02%/°C maximum.

COOLING: Convection cooled. Moving air is recommended when mounting in a confined area.

MOUNTING: The open frame mounts on any one of three surfaces.

OUTPUT VOLTAGE ADJUSTMENT

The output of all EconoMate II power supplies may be adjusted by means of a potentiometer located on the printed circuit board. The potentiometer is labeled 'EO ADJ'. During the adjustment procedure, monitor the DC output voltage by connecting a meter across the output terminals.

INPUT CONNECTIONS

When operating with 115 VAC input, place a jumper between transformer terminals one (1) and two (2) and also between three (3) and four (4). Then connect the AC primary leads to terminals one (1) and four (4) as shown in Fig. 1.

When operating with 230 VAC input, place a jumper between transformer terminals two (2) and three (3) and connect the AC primary leads to terminals one (1) and four (4) as shown in Fig. 2.

SECONDARY TRANSFORMER CONNECTIONS

On certain models it will be necessary to connect the transformer secondary to the PC board before adjusting the output voltage. This is accomplished by soldering the loose wire attached to the PC board to the appropriate tap on the transformer.

LOCAL SENSING

EconoMate II power supplies are factory wired for local sensing. Sensing terminals are located on the PC board. A jumper connecting the DC output and sensing terminals provides local sensing as shown in Fig. 3.

REMOTE SENSING

Remote sensing is a standard feature. To sense the output voltage directly at the load, disconnect the jumpers between the DC output terminals and sensing terminals. Connect the load to the DC output terminals. Then wire the (+) and (−) sensing terminals respectively across the load as shown in Fig. 4. This permits sensing directly at the load.

MODEL	Voltage/current RATING
EMA-5/6 B	5V @ 3.0A
	6V @ 2.5A
EMA-9/10 B	9V @ 1.8A
	10V @ 1.8A
EMA-12/15 B	12V @ 1.6A
	15V @ 1.3A
EMA-18/24 B	18V @ 1.2A
	20V @ 1.0A
	24V @ 1.0A
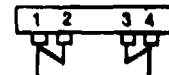
Fig. 1
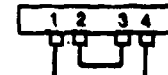
Fig. 2
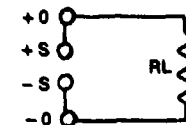
Fig. 3
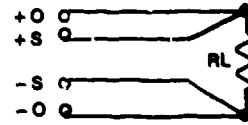
Fig. 4
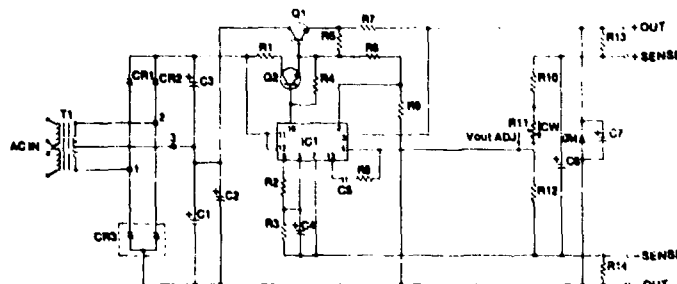
SCHEMATIC# 27817
EMA-5/6 B

SCHEMATIC# 27816
EMA-9/10 B
EMA-12/15 B
EMA-18/24 B

PR-0531

FIGURE 95. POWER SUPPLY MODULE.

Table XVI. SPVD Sensor Module Control Sheet

Sensor Module #	Offset Check & Bias H_v to 25 kγ	Threshold On γ	Threshold Off γ	Rise/Fall Times ≈20 ms/ms	Current (max) ma	Power Consumption @ 6.75V
1	.08 – OK	5850	3656	OK/425	.36	2.43
2	.08 – OK	5362	3250	OK/400	.35	2.36
3	.07 – OK	4875	2762	OK/400	.38	2.56
4	.1 – OK	5687	3250	OK/350	.36	2.43
5	.1 – OK	5525	3087	OK/300	.39	2.63
6	.08 – OK	5687	3412	OK/300	.33	2.22
7	.1 – OK	5687	3575	OK/375	.33	2.22
8	.1 – OK	5362	3575	OK/300	.42	2.83
9	.1 – OK	5362	2762	OK/250	.38	2.56
10	.1 – OK	4875	2437	OK/375	.36	2.43
11	.1 – OK	5850	3656	OK/275	.36	2.43
12	.08 – OK	5037	2762	OK/400	.36	2.43
13	.08 – OK	5362	3250	OK/275	.34	2.29
14	.08 – OK	6000	4225	OK/350	.39	2.63
15	.08 – OK	5850	3900	OK/350	.38	2.55
16	.08 – OK	5525	3087	OK/325	.35	2.36
17	.1 – OK	4387	2925	OK/325	.36	2.43
18	.08 OK	6175	4062	OK/350	.44	2.97
19	.1 OK	5200	3087	OK/350	.37	2.49
20	.1 OK	5200	2925	OK/450	.34	2.29

Table XVII. SPVD Transmitter/Encoder Module Control Sheet

SPVD Unit No.	Idle Current (µA)	Total Deviation (KHz)	Tones (N/M)	Transmitter Power mw/ma*	Frequency of Carrier** (N/M)	Control Unit Receiver Output	V.P. & U.V. Activation	Deviation Limits w/no meter in ckt. High / Low
1	340	10.44	✓	11.9/40	41.3708	1.0	✓	75311 64871
2	320	9.99	✓	12.3/40	41.3709	.96	✓	74911 64924
3	340	10.35	✓	11.3/40	41.3709	.96	✓	75165 64820
4	340	10.2	✓	11.6/40	41.3709	.96	✓	75107 64900
5	380	10.37	✓	12/40	41.3709	.96	✓	75151 64784
6	300	10.12	✓	11.2/40	41.3709	.96	✓	74959 64839
7	330	10.5	✓	11.3/40	41.3709	1.04	✓	75176 64653
8	337	10.13	✓	11.3/40	41.3709	.96	✓	75111 64980
9	360	10.15	✓	11.6/43	41.3709	.93	✓	75093 64963
10	340	10.25	✓	11.1/40	41.3709	.96	✓	75094 64842
11	340	10.53	✓	11/42	41.4109	1.06	✓	15284 04755
12	340	10.45	✓	11/42	41.4109	1.02	✓	15300 04865
13	340	10.26	✓	11.3/42.5	41.4109	.96	✓	15200 04936
14	360	10.32	✓	11.2/42.5	41.4109	.96	✓	15198 04875
15	350	10.03	✓	11.2/42.5	41.4109	1.0	✓	14956 04922
16	330	10.41	✓	11.6/42.5	41.4109	1.04	✓	15227 04817
17	340	10.22	✓	11.6/42.5	41.4109	1.0	✓	15058 04832
18	360	10.48	✓	11.3/42.5	41.4109	.98	✓	15255 04773
19	330	10.17	✓	11.3/42.5	41.4109	.92	✓	15080 04907
20	330	10.24	✓	11/43	41.4109	.96	✓	15157 04913

(Deviation Limits: 41.3 for units 1–10; 41.4 for units 11–20)

* Transmitter power is measured with a 50Ω power meter shunted with a 5.6 Ω resistor.
** Carrier frequency adjustment with modulating tones on and no current meter = (N/M)

215

XI. SENSOR MODULE WITH HARDWIRED SENSOR

The objective of this task is to remotely locate a miniature two axis magnetometer beneath the roadway in the center of the traffic lane and connect it via mulitconductor cable to a small electronics unit. The sensor fuctions like the Inductive Loop Detector (ILD) except both the connecting cable and magnetometer could be installed in the 1/4" wide pavement cutting saw blade width. This would provide easier sensor installation and require no electronics unit field adjustments.

A standard two axis Brown magnetometer was built and encapsulated in epoxy. A 100 foot six-conductor shielded cable with a PVC jacket is used to connect the magnetometer to the 5" x 4" x 3" electronics box. Figure 96 is a photograph of the completed SPVD hardwired sensor system. The unit operates from 110VAC, and contains a relay which can activate existing traffic control equipment.

A simple power supply and integrated circuit voltage regulators are used to separately power the SPVD electronics and magnetometer. Back-to-back 7.1 volt zener diodes are put across all cable leads to protect the unit from large transients caused by lightning or EMI. The lightning problem however, should be much less severe than with the ILD. Sensitivity and offset adjustments can be made to set the desired threshold and compensate for unusually close steel reinforcing rods when installed. The threshold was set a 5200/3000 nT, and the unit was continuously operated for one month.

The FHWA requested NSWC to make a hardwired sensor version of the SPVD in "consideration" for increased costs, mainly associated with fabrication of the SPVD electronics hardware.
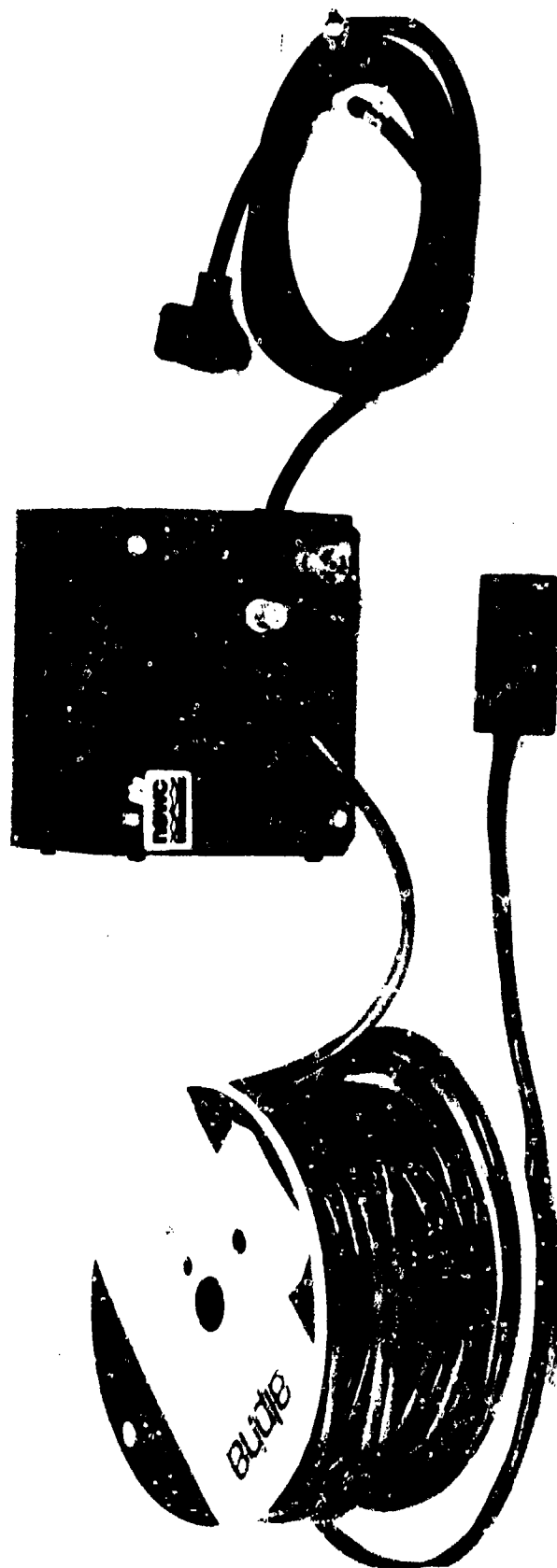
FIGURE 96. PHOTOGRAPH OF SPVD HARDWIRED SENSOR.

XII. DISCUSSION/CONCLUSION

Two main topics are discussed herein, namely, areas of improvement and SPVD cost estimates. Twenty SPVD systems have been fabricated as described previously and throughly tested. From the NSWC/WOL development experience several areas should be investigated further and may require improvement. They include 1) antenna/housing design optimization, 2) power source rexaminat , of lithium cells and solar cells with respect to system cost and operational requirements, 3) expansion of the digital nulling loops dynamic range to 16 bits, 4) remeasuring magnetic field signatures of smaller vehicles and motorcycles which have become more common recently, 5) stabilization of the sensor modules magnetic activation threshold with respect to temperature, 6) examine coding and RF telemetry techniques for simultaneous operation of eight or more SPVD units with one Receiver Control unit.

During the SPVD housing development, the PVC housing was designed to enclose orthogonal loop antennas. However, with the invention of the omnidirectional microstrip antenna (OMA), the choice of PVC was not optimium for a number of reasons. But in all simulated laboratory and roadway tests it appeared adaquate. The first major change suggested is to construct the outside SPVD housing from fiberglass thereby eliminating the relatively large dimensional changes encountered in the PVC. Also the additional mechanical strength obtained from a good grade of fiberglass should satisfy most roadway requirements and provide a better base for construction of the OMA. Antenna redesign for fiberglass can be done using the information of Section VI.

At the time of the SPVD battery evaluation, lithium battery safety was suspect, as documented in several accidents. However, one type of lithium battery was tested with satisfactory results (Section VIII) and within the last two years,

remarkable improvements have been made for such low drain applications. The second recommendation is that before specifying a power source, that the new lithium battery systems (lithium iodide, lithium sulfur dioxide, etc.) be examined and tested. The present mercury batteries used will meet the system requirements, but the cost ($60 per SPVD unit) and the potentially large use of mercury, a stragetic resource, would require costly recycling.

Solar cell arrays have been demonstrated as a feasible power source. However, the problems of vandalism and long term roadway surface durability are unanswered questions and require significant testing to answer. A solar cell array could also power the control box if the high power LED receiver and panel indicators are disconnected. Such a device would be useful for remote unattended vehicle counter/recorder applications. Mercury batteries and other electrochemical battery systems do liberate hydrogen gas from the cells chemical reaction. The rate of released gas depends on the discharge rate. Hydrogen gas diffusion in the PVC/ABS materials used is quite large and could not contain any significant volume of hydrogen. There will be no build-up of hydrogen in the SPVD and no safety threat. The battery is fused inside the battery compartment to prevent any high discharge rates.

The magnetic sensor module digital nulling loops (DNL) should be expanded from 2 bits to 16 bits to extend the nulling loops dynamic range. In this way all roadway ambient magnetic fields could be nulled while providing more sensitivity required to detect smaller motor vehicles. Detection logic could also be improved if provided this added system sensitivity.

Magnetic signatures of small motor vehicles have not been comprehensively measured and should include motorcycles and bicycles as well. Although the magnetic signature amplitude is directly proportional to the amount of magnetic material in the vehicle, the large dynamic range and sensitivity of the detection

219

system could detect a wide variety of vehicle classes. Variation of the sensor modules magnetic actuation threshold with temperature is quite significant, especially at low temperatures. A temperature compensation network is desirable, especially if the DNL is expanded to 16 bits and small motor vehicles are to be detected with very low miss rates.

In addition to the noted telemetry system improvements (Sections IV, V and I), it seems desirable to operate more than one SPVD on one RF channel (thereby conserving spectrum space) and have unique tone codes for specific SPVD roadway locations. The Control Box has several features which could be eliminated to save costs, including the standby battery, panel connectors and lights.

The SPVD System Voltage (6.75 volts) appears satisfactory for the sensor module, particularly the magnetometer, but higher efficiency may be obtained from the RF oscillator and transmitter with a higher system voltage. It is felt that despite the potential gains in transmitter efficiency, they will be offset by losses incurred in the sensor module electronics.

Techniques for implanting the SPVD for long term survival must be optimized for a variety of roadway environments encountered. During the program four test holes were used, 1) the main test hole (5" dia.) located under a black top road with a phenolic liner and cover plate; 2) the dry hole (5" dia.) with a removable metal liner inserted to maintain hole dimensions when the SPVD was not being tested; 3) antenna range test hole with dry earth sides, and 4) the Interstate I-95 test hole located south of the Capital Beltway on an unused section of MD I-95. The main test hole was almost always filled with water or ice and was the test site of the solar cell array and most system testing. For RF System tests the SPVD was required to transmit 400 to 450 feet to the control box in the completely water filled main test hole, and 700 feet minimum at the I-95 test hole using only a $\lambda/4$ whip receiving antenna on the control box approximately 4 feet above the road surface. In an actual

installation the receiving antenna supplied would provide greater signal strength to the control units receiver.

Some vehicle RF telemetry link path shading experiments were performed with little change in detection distance, and in some cases increased it. A grid of 5 foot long 5/8" diameter reinforcing rods were positioned over the SPVD in the main test hole in a number of configurations. No change in either magnetic detection or telemetry link performance was noted.

A phenolic or non-conductive liner may be useful to increase SPVD survivability. However, in the I-95 concrete pavement, adding dirt, foam or plastic insulating styrofoam may be desirable to both center the SPVD and stabilize the sensor from apparent errosion of the base gravel/dirt under the concrete. Addition of non-conductive stabilizing plastics with a one-inch thick black top cover patch should not affect system performance. The suggested SPVD implant procedure is outlined in both section I of this report and in an operating manual supplied with each SPVD system.

Two SPVD systems can be used for an accurate vehicle speed sensor. The time differences between vehicle presence leading edges can be used to determine vehicle speed from two accurately located SPVD sensors.

As a "contingency" for some SPVD development problems, NSWC fabricated a hardwired magnetic vehicle detector (Section XI). This should also ease sensor installation when compared with the inductive loop detectors (ILD). The remote sensor housing could be made somewhat smaller and quality of the cable improved for long term survivability. EMI/Lightning imunity, however, should be evaluated. Presently, 100 feet of cable has been supplied. It appears likely that operation on cable lengths of 1000 feet is possible, even with the high sensor source impedance ($\approx$ 15KΩ). However, a line driving buffer amplifier with low output impedance at the remote sensor is desirable for environmental noise immunity.

221

SPVD Costs

An estimate of SPVD system component and assembly costs has been made for one unit and 1000 units and is tabulated in Table XVIII.

Each component item cost is added up for unit quanties (1 to 20) and for 1000 units, and divided into major component blocks, i.e., sensor module, battery, housing, etc. In this way, trained production engineers could refer to the appropriate report section and estimate costs more accurately for his particular overhead and plant operating environment. The estimates in Table XVIII are based on NSWC rates for FY 77/78 and component costs from local electronics distributors. In single unit quanties (1-20), estimated SPVD system cost per unit is $2540 and for 1000 units estimated at $745 each. Both estimates are based on the present design, excluding test instrumentation costs, but including system adjustments and final performance tests. The SPVD hardwired sensor cost per unit is estimated at $1000 (1 to 20) and probably less than $300 in 100 unit quanties.

Deliverable program items include: 1) 20 complete SPVD systems w/SPVD, SPVD control units, receiving antennas, interface plug and operating manual. 2) All printed circuit board artwork, originals, mylars, and samples. 3) Prototype solar cell array housing and miscellaneous photographs, prototype components and circuits. 4) One SPVD Prototype hardwired sensor with 100 feet of cable, and 5) this report with an advance copy supplied on 1 December 1978.

Conclusion

All twenty SPVD systems were fabricated and met all technical design goals as tested in the laboratory. However, survivability in the roadway environment appears to be the crucial test.

XVIII.   SPVD System Estimated Costs

SPVD	1 Unit	1000 Units
Sensor Electronics	600.	200.
Battery	60.	50.
Battery Housing	10.	5.
Encoder Board	150.	50.
Transmitter	150.	50.
Antenna	200.	20.
Housing	150.	60.
Module Assembly	250. (8 hours)	25. (1 hour)
SUB TOTAL	$1570.	$460.

CONTROL UNIT		
Receiver Module/Interface.	200.	75.
Decoder Board	150.	75.
Standby Battery	30.	20.
AC Power Supply	35.	20.
Housing/Lights/Connectors	150.	10.
Receiving Antenna	30.	10.
Assembly	375. (12 hours)	75.(3 hours)
SUB TOTAL	$ 970.	$285.
TOTAL	$2540. system	$745. system

REFERENCES

1. D. O. Wick, R. A. Lubke, "Vehicle Detection, Phase I: SPVD Development," Federal Highway Administration Report No. FHWA-RD-75-18, Jan 1975.

2. J. F. Scarzello, G. W. Usher, Jr., "SPVD - Magnetic Sensor Development," Report No. FHWA-RD-76-147, June 1976.

3. J. F. Scarzello, G. W. Usher, Jr., "A Low Power Magnetometer for Vehicle Detection," IEEE Transactions on Magnetics, Vol. MAG-13, Vol. 5, Sept 1977.

4. J. F. Scarzello, D. S. Lenko, R. E. Brown, A. D. Krall, "SPVD: A Magnetic Vehicle Detection System Using a Low Power Magnetometer," IEEE Transactions on Magnetics, Vol. MAG 14, Vol. 5, Sept 1978.

5. R. E. Brown, "A Miniature Fluxgate Magnetometer with Subgamma Noise," Presented at IEEE Intermag Conference, Kyoto, Japan, April 1972.

6. R. E. Brown, "Magnetic Field Gradiometer Utilizing a Pair of Cores Driven by a Blocking Oscillator," U.S. Patent 3,649,908, 14 March 1972.

7. R. E. Brown, "Micropower Magnetometer," Invention Disclosure Navy Case No. 62,640   (D- 568), October 1977.

8. J. F. Scarzello, D. S. Lenko, A. D. Krall, R. E. Brown, W. R. Grine, G. W. Usher, Jr., M. K. Mills, "An Improved Self Powered Vehicle Detection System," Invention Disclosure, Navy Case No. 63,028, NSWC D-5707 of 6 April 1978.

9. D. O. Wick, R. A. Lubke, Vehicle Detection - Phase I, SPVD Development, Sensor Design Tradeoff Analysis, FHWA Report No. FHWA-RD-7522, Jan 1975.

10. G. W. Usher, Jr., "Adjustable Micropower Voltage Regulator," Invention Disclosure Navy Case No. 61446 (D-5870), 10 Nov 1976.

11. D. E. Hildreth, "IC Crystal Oscillators", Interdesign: Monochip Application Note APN-4

12. Frank W. Noble, "Need an Adjustable Crystal Oscillator?", Electronic Design, March 29, 1976, pp. 88-90.

13. Stuart J. Lipoff, "Linearity of Direct FM Frequency Modulators," IEEE Transactions on Vehicular Technology, Feb 1978, pp. 7-17

14. Frank Davis, "Matching Network Designs with Computer Solution," Motorola Application Note AN-267.

15. Roy Hejhall, "Systemizing RF Power Amplifier Design, "Motorola Application Note AN-282A.

16a. Frederick H. Raab, "Get Broadband, dual-mode operation with this FET power amplifier," END, October 20, 1978, pp. 117-124.

REFERENCES (Cont.)

16b. Nathan O. Sokal, "Class E can Boost the Efficiency," Electronic Design, Sept 27, 1977, pp. 96-102.

17. L. M. Black, J. W. McCorkle, "Exploratory Development on Micropatch Antennas," NSWC/WOL/TR 75-200, Dec 1975, UNCLASSIFIED.

18. H. A. Wheeler, "Transmission Line Properties of Parallel Strips Separated by a Dielectric Sheet," IEEE Trans. MTT-13, p. 172, March 1965.

19. M. V. Schneider, "Microstrip Lines for Microwave Integrated Circuits," BSTJ Vol. 48, p. 1421, May-June 1969.

20. E. Belohoubek & E. Denlinger, "Loss Considerations for Microstrip Resonators," IEEE Trans. MTT-23, p. 522, June 1975.

21. Assadourian F. & Rimai E., "Simplified Theory of Microstrip Transmission Systems," PROC. IRE, Vol. 40, p. 1651, Dec 1952.

22. J. O. Welch & H. J. Pratt, "Losses in Microstrip Transmission Systems for MIC," NEREM Record IEEE Cat. F-70, p. 100, 1966.

23. L. Lewin, "Radiation from Discontinuities in Strip-Line," IEE Vol. 107, Part C., p. 163, Feb 1960.

24. Leo J. van der Pauw, "The Radiation of Electromagnetic Power by Microstrip Configurations," IEEE Trans. MTT-25, p. 719, Sept 1977.

25. P. Troughton, "High Q Factor Resonators in Microstrip," Electronic Letters, Vol. 4,0p. 520, 29 Nov 1968.

26. A. Presser, "RF Properties of the Microstrip Line," Microwaves, p. 53, March 1978.

27. E. C. Jordan & K. G. Balman, "Electromagnetic Waves and Radiating Systems," 2nd Edition, New Jersey, Prentice-Hall, p. 228, 1968.

28. Harold A. Wheeler, "The Radiansphere around a Small Antenna," PROC. IRE Vol. 47, #9, p. 1325, August 1959.

29. S. A. Schelkunoff & J. T. Friis, "Antennas Theory & Practice," John Wiley & Sons, Inc., New York, 1952.

30. A. D. Krall, J. W. McCorkle, J. F. Scarzello, A. M. Syeles, "Omnidirectional Microstrip Antenna," Navy Case No. 62,800 (D-5691) of 16 Feb 1978.

31. Mallory Technical Data Sheets, Mallory Battery Company, S. Broadway, Tarrytown, New York, 10591.

REFERENCES (Cont.)

32. Eveready Battery Engineering Data Book, Union Carbide Corp., 1976.

33. NSWC Memo WR-33:DLW:mlf, from WR-33 to WR-30, Subject: Lithium Battery Development, 6 August 1976.

34. S. F. Pensabene, J. W. Gould III, "Unwanted Memory Spooks Nickel Cadmium Cells," IEEE Spectrum, Sept 1976, pp. 33.

DISTRIBUTION

Federal Highway Administration   30
  Mr. M. K. Mills
Offices of Research and Development
Traffic Systems Division
HRS-32
Washington, D. C. 20590

U. S. Secret Service
  Mr. T. Allen   1
  Mr. E. Morris   1
1800 G. St., N. W.
Washington, D. C. 20223

Commander, Naval Sea Systems Command
  SEA03 (Blaine)   1
  SEA0342 (W. Welsh)   1
Washington, D. C. 20362
Chief, Office of Naval Research
  Code 463, R. Obrachta   1
800 N. Quincy St.
Arlington, VA 22217

Office of the Chief of Naval Operations
  OP374 (Blouin)   1
Washington, D. C. 20350

Motorola Inc.
Communications Division
  Mr. Wayne C. Roach   1
Suite 350
4710 Auth Place, S. E.
Washington, D. C. 20023

David W. Taylor Naval Ship Research & Development Center
Magnetic Fields Branch
  Mr. D. G. Everstine   1
  Mr. B. R. Hood   1
Annapolis, MD 21404

Infinetics, Inc.
  Mr. J. Jaquet   1
P. O. Box 3330
201 Vander Avenue
Wilmington, DE 19899

Defense Documentation Center
Cameron Station
Alexandria, VA 22314   12

Goddard Space Flight Center
  Dr. M. Acuna
Greenbelt, MD 20770   1

Institute of Geophysics and Planetary Physics
University of California
Space Sciences Center
  Mr. R. Snare
Los Angeles, CA 90024   1

New York State Department of Transportation
  Mr. W. F. Crans
  Mr. L. S. DuBois   1
4 Burnette Blvd   1
Poughkeepsie, NY 12603

U. S. Army Mobility Equipment R&D Center
  Mr. D. Keehan
  Mr. P. Hartman   1
Ft. Belvoir, VA 22060   1

Federal Aviation Administration
NAFEC
  Mr. P. J. Lizzi   1
ANA 310, Bldg. 301
Atlantic City, NJ 08405

Honeywell, Inc.
  Mr. D. O. Wick
  Mr. R. A. Lubke   1
2600 Ridgeway Parkway   1
Minneapolis, Minnesota 55413

Sparton Electronics Corporation
  Mr. L. R. Staszak   1
2400 East Ganson St.
Jackson, MI 49202

EG&G Geometrics, Inc.
  Dr. Sheldon Breiner
  Mr. Neil Hickman   1
395 Java Drive   1
Sunnyvale, CA 94086

Catalyst Research Corporation
  Mr. David Harney   1
1421 Clarkview Road
Baltimore, MD 21209

U. S. Army, Harry Diamond Laboratory
Dr. M. Conner
Dr. F. G. Farrar
Dr. D. H. Schaubert
Adelphi, Maryland 20783   1

NSW-NSWC(W)-2685/1 (Rev. 5-78)

TO AID IN UPDATING THE DISTRIBUTION LIST
FOR NAVAL SURFACE WEAPONS CENTER, WHITE
OAK TECHNICAL REPORTS PLEASE COMPLETE THE
FORM BELOW:

TO ALL HOLDERS OF __NSWC/WOL/TR 78-177__
by J. F. Scarzello, Code R-43
DO NOT RETURN THIS FORM IF ALL INFORMATION IS CURRENT

A. FACILITY NAME AND ADDRESS (OLD) (Show Zip Code)

NEW ADDRESS (Show Zip Code)

B. ATTENTION LINE ADDRESSES:

C.

☐ REMOVE THIS FACILITY FROM THE DISTRIBUTION LIST FOR TECHNICAL REPORTS ON THIS SUBJECT.

D.
NUMBER OF COPIES DESIRED _____

GPO 000-784

DEPARTMENT OF THE NAVY
NAVAL SURFACE WEAPONS CENTER
WHITE OAK, SILVER SPRING, MD. 20910

OFFICIAL BUSINESS
PENALTY FOR PRIVATE USE, $300

COMMANDER
NAVAL SURFACE WEAPONS CENTER
WHITE OAK, SILVER SPRING, MARYLAND 20910

ATTENTION: CODE R-43